uOttawa

L'Université canadienne
Canada's university

FACULTÉ DES ÉTUDES SUPÉRIEURES ET POSTOCTORALES

uOttawa

L'Université canadienne
Canada's university

FACULTY OF GRADUATE AND POSDOCTORAL STUDIES

Juraj Farkas

AUTEUR DE LA THÈSE / AUTHOR OF THESIS

Ph.D. (Earth Sciences)

GRADE / DEGREE

Department of Earth Sciences

FACULTÉ, ÉCOLE, DÉPARTEMENT / FACULTY, SCHOOL, DEPARTMENT

Calcium and Boron Isotope Variations in Marine Biogenic Carbonates: Implications for Chemical Evolution of Seawater during the Phanerozoic

TITRE DE LA THÈSE / TITLE OF THESIS

John Blenkinsop

DIRECTEUR (DIRECTRICE) DE LA THÈSE / THESIS SUPERVISOR

Jan Veizer

CO-DIRECTEUR (CO-DIRECTRICE) DE LA THÈSE / THESIS CO-SUPERVISOR

EXAMINATEURS (EXAMINATRICES) DE LA THÈSE / THESIS EXAMINERS

Ian Clark

James Farquhar

Brian Cousens

Keiko Hattori

Gary W. Slater

Le Doyen de la Faculté des études supérieures et postdoctorales / Dean of the Faculty of Graduate and Postdoctoral Studies

Calcium and boron isotope variations in marine biogenic carbonates: Implications for chemical evolution of seawater during the Phanerozoic

by

Juraj Farkaš

Thesis submitted to the
Faculty of Graduate and Postdoctoral Studies
University of Ottawa
in partial fulfillment of the requirements for the degree of

Doctor of Philosophy (Ph.D.)

in the Earth Sciences

Ottawa-Carleton Geoscience Centre
and
University of Ottawa
Ottawa, Canada

uOttawa

L'Université canadienne
Canada's university

Your file Votre référence
ISBN: 978-0-494-49345-8
Our file Notre référence
ISBN: 978-0-494-49345-8

Contents

List of Tables

List of Figures

Acknowledgements

I would like to acknowledge several people who contributed in many ways to the completion of this thesis. Above all, I would like to thank my wife and soul mate Katarina for all her support and help. I am deeply indebted to Ján Veizer and John Blenkinsop, my thesis advisors who agreed to take me on and offered their supervision. Jan, thank you for being so generous with your time, resources and experience, but especially for being immensely patient with my numerous mistakes I have made over the course of my studies. John, I owe you an enormous debt of gratitude for showing me all the intricacies of mass spectrometry and sharing valuable knowledge, but above all for keeping those stubborn instruments running. I would like to acknowledge Dieter Buhl, at the Ruhr University Bochum, who helped me so much in my pursuit of a high-precision calcium isotope analysis, especially during the initial stages of this thesis. I am also grateful to several people at the IFM-GEOMAR (Leibniz Institute of Marine Sciences), particularly to Florian Böhm and Klaus Wallmann who have provided many inspirational ideas and made significant contribution in the final stages of my work.

I also owe many thanks to several faculty members at the University of Ottawa and Carleton University. Patricia Wickham, Brian Cousens, Sharon Carr, Keiko Hattori, Ian Clark, Keith Bell, Monika Wilk-Alemany, Hélène DeGouffe and Lizzy Ann Spencer; thanks to all of you for being so helpful when it was most needed.

Many thanks go also to my graduate student colleagues at the University of Ottawa. Paul, Kristal, Mike, Martin, Lillian, Fedora, Vigdís, Hossein, Mark and many others. Special thanks must go to my office-mates, Paul and Martin, for giving me everyday lessons on how be behave like a Canadian, which is by the way very appreciated, and also for exposing me to every last detail of NHL games.

Last but certainly not least, I would like to thank my parents and close family for being so supportive and giving me the basic values to be able to function and achieve my goals in this complex global world. Thanks!

Abstract

Calcium and boron isotope variations in marine biogenic carbonates: Implications for chemical evolution of seawater during the Phanerozoic

by

Juraj Farkaš

University of Ottawa, Ottawa, Canada

Thesis supervisors: Dr. Ján Veizer and Dr. John Blenkinsop

The aim of this dissertation, based on three papers, is to utilize novel analytical techniques to examine the potential of non-traditional geochemical proxies, such as calcium and boron isotopes, to address questions related to earth system science.

The first paper presents analytical protocols for high-precision calcium isotope measurements using thermal (TIMS) and plasma ionization mass spectrometry (MC-ICP-MS). These are applied to determine calcium isotope abundances of the Late Mesozoic belemnites that, in turn, are used to reconstruct the isotope composition of paleo-seawater and the evolution of the oceanic calcium cycle.

The second paper discusses in details the history of the oceanic calcium isotope budget during the Phanerozoic (last ~500 Ma), which is based on the analysis of calcium isotope compositions of several hundred marine skeletal carbonates, mostly brachiopods, measured by the TIMS technique. The observed experimental record is simulated using a numerical model of coupled calcium/carbon/magnesium global cycles and the results are discussed in the context of changing fluxes of major cations to the oceans.

The third paper aims to utilize boron isotopes to constrain temporal changes in pH of the Jurassic surface oceans, with the ultimate goal to evaluate the effect of seawater pH on the oxygen isotope ($\delta^{18}O$) composition of coeval belemnites, hence on the $\delta^{18}O$-based paleo-temperature estimates.

Overall, the results of this thesis demonstrate the usefulness and limitations of calcium and boron isotope proxies for studies concerning the evolution of earth system, specifically oceans and the atmosphere, over geological time scales.

1 Introduction

1.1 Framework of current study

Recent advances in analytical instrumentation such as multi-collector inductively-plasma mass spectrometers (MC-ICP-MS) or the latest generation of thermal ionization mass spectrometers (TIMS) open new opportunities to investigate isotope systematics of transition metals or elements such as calcium, magnesium (Johnson et al., 2004) and boron (Grew and Anovitz, 1996).

Of particular interest to earth system science are the isotope studies of calcium and boron as these could provide information on the evolution of past seawater Ca^{2+} concentrations (Zhu and MacDougall, 1998; De La Rocha and DePaolo, 2000) and pH variations of the surface oceans (Spivack et al., 1993; Sandal et al., 1995), respectively. These parameters are important for reconstructions of carbon dioxide system in the oceans and atmosphere (Berner et al., 1983; Millero, 1995; De Paolo, 2004), thus helping to clarify the relationship between atmospheric CO_2 levels and the Earth's climate over time (Kasemann et al., 2005).

In addition, the oceanic calcium cycle is intimately linked to the global carbon cycle via weathering of continental carbonate and silicate rocks, induced by carbonic acid, and the subsequent deposition of dissolved calcium and carbonate ions as $CaCO_3$ in the oceans (Berner et al., 1983). The isotope studies of calcium may therefore provide insights into the functioning of the global carbon cycle in the ocean-atmosphere system.

The first studies of calcium isotope variations in natural samples date back to the early 1950s (Herzog et al., 1954; Backus, 1955) and general interest persisted until the late 1970s (Artemov et al., 1966 and 1967; Corless, 1968; Stahl, 1968; Stahl and Wendt, 1968; Heumann and Lieser, 1973; Russell et al., 1978). Throughout the 1960s and 70s the focus was on cosmochemistry (Hirt and Epstein, 1964; Backus et al., 1964; Russell et al., 1978) and on the application of calcium isotopes for radiometric dating (Coleman, 1971; Heumann et al., 1977 and 1979). This trend lasted until the late 1980s (Marshall and DePaolo, 1982 and 1989; Niederer and Papanastassiou, 1984; Jungck et al., 1984) but the

interest in calcium isotope geochemistry slowly ceased as high-precision measurements posed a considerable challenge.

The last decade, however, has seen a dramatic increase in the number of publications dealing with calcium isotope variations in terrestrial materials, particularly in marine carbonates (Skulan et al., 1997; Zhu and Macdougall, 1998; Skulan and DePaolo, 1999; De La Rocha and DePaolo, 2000; Nägler et al., 2000; Schmitt et al., 2003a,b; Soudry et al., 2004; Fantle and DePaolo, 2005; Heuser et al., 2002 and 2005; Hippler et al., 2002 and 2003; Gussone et al., 2003, 2004 and 2005; Lemarchand et al., 2004; Kasemann et al., 2005; Immenhauser et al., 2005; Steuber and Buhl, 2006). These studies show that calcium isotopes can, in some cases, be used as a paleo-thermometer (Nägler et al., 2000; Hippler et al., 2002) but for the most part they have been applied as a proxy for reconstruction of calcium isotope composition of seawater over geological time (De La Rocha DePaolo, 2000; Fantle and DePaolo, 2005; Heuser et al. 2005; Kasemann et al., 2005). The most recent research also investigates calcium isotope systematics in river systems (Schmitt et al., 2003a; Tipper et al., 2006) and in weathering processes (Wiegand et al., 2005) with the ultimate goal of better understanding the global calcium cycle, its major reservoirs and interrelated fluxes.

Our understanding of boron isotope geochemistry is far more advanced (Grew and Anovitz, 1996). Nevertheless, the utility of boron isotopes as a proxy for seawater pH has been recognized only recently, in the 1990s. This approach is based on the fact that the boron isotope composition of modern marine carbonates is primarily controlled by pH of seawater (Hemming and Hanson, 1992; Sanyal, 1996, Hobbs and Reardon, 1999; Sanyal et al., 2000). As of today, the boron isotope 'paleo-acidimetry' has been used to constrain seawater pH variations during the Pleistocene/Holocene (Sandal et al., 1995; Sanyal et al., 1995 and 1997; Palmer and Pearson 2003; Hönisch and Hemming, 2005), the Cenozoic (Spivack et al., 1993; Palmer et al., 1998; Pearson and Palmer, 1999 and 2000) and the Neoproterozoic (Kasemann et al., 2005).

1.2 Objectives

The primary objective of this thesis, based on three papers, is to develop analytical protocols for high-precision measurements of calcium ($\delta^{44/40}Ca$) and boron ($\delta^{11}B$) isotope

abundances in marine carbonates and natural waters using the new generation of TIMS and MC-ICP-MS and subsequently to determine $\delta^{44/40}Ca$ and $\delta^{11}B$ values of modern and fossil skeletal carbonates in order to: (i) reconstruct the evolution of the calcium isotope composition of seawater during the Phanerozoic (papers 1 and 2); and to (ii) evaluate the effect of seawater pH variations on $\delta^{18}O$-based estimates of past sea surface temperatures during the Mesozoic (paper 3).

Marine skeletal carbonates, brachiopods and belemnites investigated in this work are, for the most part, from the sample collection of Veizer et al. (1999) but some brachiopods are from van Geldern et al. (2006), Samtleben et al. (2000, 2001) and Voigt et al. (2004). These samples were already analyzed for their $^{87}Sr/^{86}Sr$, $\delta^{18}O$, $\delta^{13}C$ (Veizer et al., 1999; van Geldern et al., 2006), $\delta^{34}S$ values (Kampschulte and Strauss, 2004) as well as their Sr contents (Steuber and Veizer, 2002). These isotope datasets, plotted as a function of time (Fig. 1.1), have provided valuable and detailed insight into the dynamic evolution of the Earth's crust-mantle-ocean-atmosphere system.

1.3 Summary

Paper 1:

Farkaš J., Buhl D., Blenkinsop J. and Veizer J., Evolution of the oceanic calcium cycle during the Late Mesozoic: Evidence from $\delta^{44/40}Ca$ of marine skeletal carbonates.
Manuscript published in Earth and Planetary Sciences Letters 253 (2007) 96-11

The objective of this paper is to reconstruct the calcium isotope composition of seawater ($\delta^{44/40}Ca_{SW}$) during the Late Mesozoic (from ~160 to ~125 Ma). We report the results of calcium isotope measurements of Middle Jurassic to Early Cretaceous skeletal carbonates, mostly belemnites, performed by MC-ICP-MS and TIMS techniques. The former technique, established at the Ruhr University Bochum (Germany), is based on the standard-sample bracketing method of Wieser et al. (2004) and the latter, developed at Carleton University (Ottawa, Canada), uses a $^{43}Ca/^{48}Ca$ double spike and the iterative data reduction algorithm of Heuser et al. (2002).

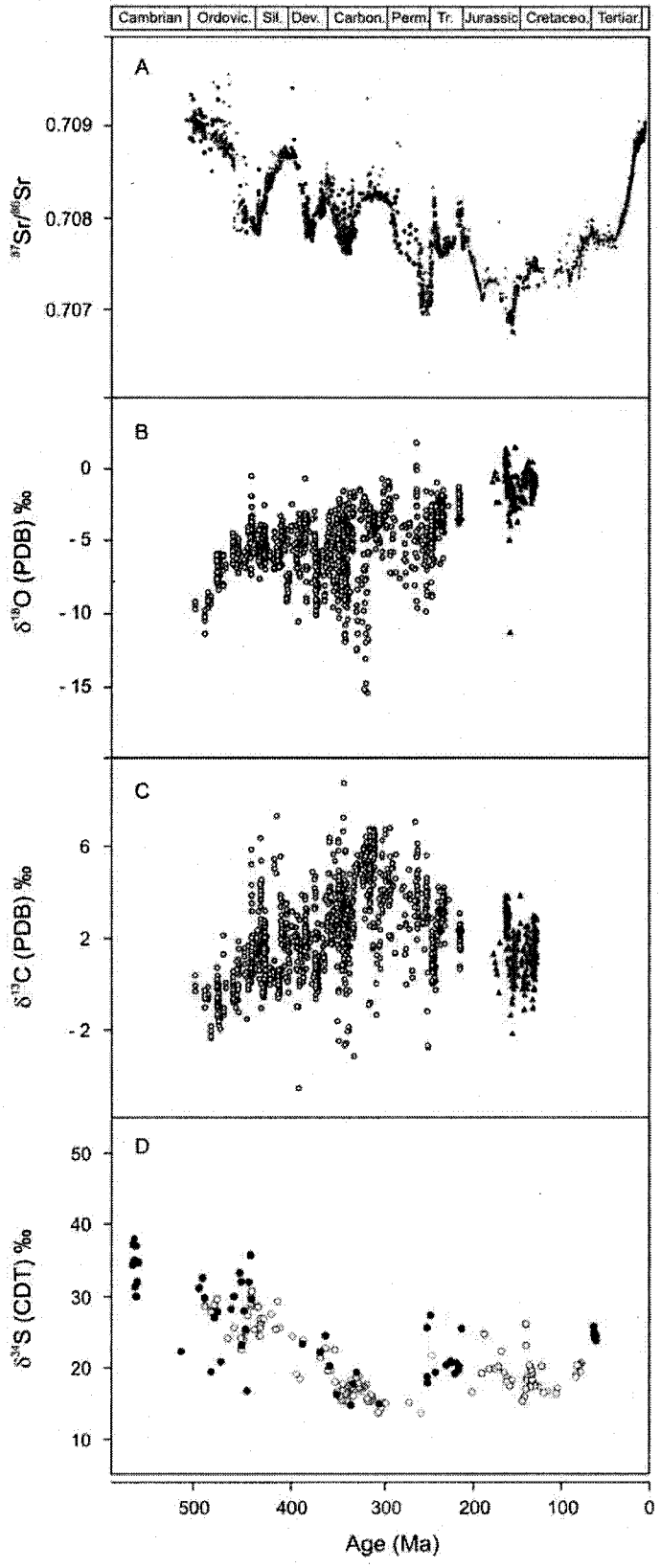

Fig. 1.1. (A) Phanerozoic $^{87}Sr/^{86}Sr$ trend compiled from brachiopod and belemnite data (open circles, n = 1451), supplemented by literature data (crosses, n = 2607) (Veizer et al. 1999). $\delta^{18}O$ (B) and $\delta^{13}C$ (C) trends based on data of brachiopods (open circles, n = 1302) and belemnites (solid triangles, n = 262) (Veizer et al. 1999). $\delta^{34}S$ (D) trend compiled from biogenic (open circles, n = 156) and whole rock (solid circles, n = 96) carbonates (Kampschulte and Strauss, 2004).

The Late Mesozoic $\delta^{44/40}Ca_{SW}$ record is inferred from the measured calcium isotope compositions of belemnites ($\delta^{44/40}Ca$) and the experimentally determined fractionation factor between seawater calcium and belemnite calcite ($\alpha_{CC\text{-}SW}$) of 0.9986. The reconstructed Late Mesozoic $\delta^{44/40}Ca_{SW}$ record shows an increasing trend with time, from the Middle/Late Jurassic minimum of ~1.4‰ to the Early Cretaceous maximum of ~1.9‰.

A simple box model of the oceanic calcium cycle is used to simulate the experimental $\delta^{44/40}Ca_{SW}$ record and the results indicate that the observed trend can be explained by varying intensities of input fluxes of calcium to the oceans, particularly the hydrothermal and/or dolomitization fluxes as these are independent of carbonate ion flux (Heuser et al., 2005). Finally, we propose that the calcium isotope composition of Late Mesozoic seawater was, for the most part, controlled by the changing intensity of the hydrothermal flux of calcium to the oceans, which is justified by a statistically significant correlation between $\delta^{44/40}Ca$ and $^{87}Sr/^{86}Sr$ values of belemnites ($r^2 = 0.58$, $p<0.0001$).

Paper 2:

Farkaš J., Böhm F., Wallmann K., Blenkinsop J., Eisenhauer A., van Geldern R., Munnecke A., Voigt S. and Veizer J., Calcium isotope budget of Phanerozoic oceans: Implications for chemical evolution of seawater and its causative mechanisms.

Manuscript submitted to Geochimica et Cosmochimica Acta

Building on the results of the preceding paper, this contribution aims to reconstruct the evolution of calcium isotope composition of seawater during the Phanerozoic, using brachiopods as carrier phases. The analytical protocol used in this study is based on the multicollector TIMS technique described in Heuser et al. (2002) and Farkaš et al. (2007), however, here we skipped the chromatographic clean-up of carbonate samples and introduced a fully automated routine for calcium isotope measurements. This has significantly increased sample throughput, allowing us to run up to 10 samples per day.

In total, we analyzed $\delta^{44/40}Ca$ values of 280 brachiopod shells of Ordovician to Cretaceous age at the mass spectrometry facilities of Carleton University (Ottawa) and the IFM-GEOMAR (Leibniz Institute of Marine Sciences, Kiel, Germany). This dataset is complemented by 139 literature data from marine carbonates (Heuser et al., 2005; Steuber

and Buhl, 2006; Farkaš et al., 2007) and phosphates (Schmitt et al., 2003b; Soudry et al., 2004). The fractionation factors ($\alpha_{CC\text{-}SW}$) for individual recording phases, used to reconstruct the secular $\delta^{44/40}Ca_{SW}$ trend, are adopted from literature (Gussone et al., 2005; Schmitt et al., 2003b; Heuser et al., 2005; Steuber and Buhl, 2006; Farkaš et al., 2007).

The Phanerozoic $\delta^{44/40}Ca_{SW}$ trend shows an increase from ~1.3‰ at the beginning of the Ordovician to ~2‰ at present. Superimposed on this trend is a major long-term positive excursion from the Early Carboniferous to Early Permian and several short-term, mostly negative, oscillations. The observed $\delta^{44/40}Ca_{SW}$ record is simulated using a high complexity model of coupled calcium/carbon/magnesium global cycles (Hansen and Wallmann, 2003; Wallmann, 2001 and 2004; Heuser et al., 2005). Model simulations show that the observed $\delta^{44/40}Ca_{SW}$ variations cannot be explained only by varying the incoming and outgoing fluxes of calcium to the oceans, suggesting that their isotope signatures must also have changed during the course of the Phanerozoic. Our results indicate that the most likely complementary mechanism to explain the experimental data is the alternating mineralogy of marine skeletal carbonates, i.e. 'calcite-aragonite seas'. Thus, we conclude that the calcium isotope budget of Phanerozoic oceans was ultimately controlled by tectonic processes, specifically via variable rates of oceanic crust production and its hydrothermal alteration. The hydrothermal flux of calcium modulated the oceanic Mg/Ca ratio that, in turn, controlled the dominant mineralogy of marine skeletal carbonates, and hence the $\delta^{44/40}Ca_{SW}$.

Note that the complex geochemical model presented in this paper differs from the more basic box model for the oceanic Ca cycle used in the previous article (Paper 1). This chronological increase in model complexity simply reflects the progress that has been made in our understanding of the global Ca cycle and its role in the evolving earth system.

Paper 3

Farkaš J., Blenkinsop J. and Veizer J., Testing the boron isotope paleo-pH proxy: An example from Middle and Late Jurassic skeletal carbonates.

Manuscript in preparation

The main motivation of this paper is to use the boron isotope composition of belemnite calcite to constrain temporal changes in pH of the Jurassic surface oceans. Knowledge of seawater pH is important for interpretation of the oxygen isotope signal ($\delta^{18}O$) of skeletal carbonates in terms of paleo-temperatures, as $\delta^{18}O$ of calcite reflects not only temperature but also pH of a solution (Spero et al., 1997; Zeebe, 1999).

The heavy $\delta^{18}O$ values of the Middle and Late Jurassic belemnites were originally explained as low sea surface temperatures (SSTs) (Podlaha et al., 1998; Veizer et al., 1999). Others however argued that the ^{18}O enrichment is rather a reflection of lower pH of the contemporary seawater (Royer et al., 2004; Wallmann, 2004). The application of boron isotopes as the pH proxy for past seawater may therefore help to clarify this controversial issue.

The observed $\delta^{11}B$ trend of the Middle and Late Jurassic belemnites exhibits a quasi-systematic variation with an overall magnitute of ~10‰, which is first tentatively explained as a relative seawater pH variability of about 1 unit, assuming a hypothetical value for the boron isotope composition of Jurassic seawater ($\delta^{11}B_{SW}$) of 22 ± 2‰. However, taking into account the results of geochemical modeling (Simon et al., 2006) and/or the published boron isotope data from well-preserved coeval brachiopods (Lécuyer et al., 2002), this interpretation seems unlikely. This is because the above studies suggest that the $\delta^{11}B_{SW}$ value of Jurassic oceans should have been considerably heavier, at least 30‰. Yet, any combination of our boron isotope data with $\delta^{11}B_{SW}$ in excess of ~30‰ yields unreasonable paleo-seawater pH estimates. These results therefore indirectly indicate that the boron isotope systematics of our MLJ belemnites has been compromised by diagenesis.

Consequently, we were unable to utilize the measured $\delta^{11}B$ dataset to evaluate the effect of seawater pH on the $\delta^{18}O$ record of the MLJ belemnites, hence the SSTs estimates. This said, the present study shows that boron isotope geochemistry of fossil skeletal carbonates is much more prone to diagenetic alteration than are the isotope systems of O, C, S, Sr and Ca. Therefore care should be exercised in the use of boron isotopes for the reconstructions of paleo-seawater pH.

1.4 Statement of contributions

Several authors from various institutions have contributed their thoughts and expertise to the papers presented in this thesis and the detailed statement of authorship is presented below. Note, however, that I have been primarily responsible for the study concept and design, analysis and interpretation of experimental data as well as for the drafting of the manuscripts at all stages.

Paper 1:

The measurements of calcium isotope abundances, via MC-ICP-MS, were performed by Dieter Buhl at the Ruhr University Bochum, Germany. I produced the calcium isotope data measured by TIMS, with the assistance of John Blenkinsop, at Carleton University, Ottawa. I wrote the manuscript and was the corresponding author throughout the submission process, although the critical comments of Ján Veizer (University of Ottawa) significantly improved the initial draft. One of the reviewers, Anton Eisenhauer (IFM-GEOMAR, Leibniz Institute of Marine Sciences) contributed to the discussion presented in this paper, by providing an inspiring input regarding the feedback relationship between global calcium and carbon cycles.

Paper 2:

This work represents a joint paper between the two research groups that have been active in the calcium isotope research during the last ca. 5 years. The first group is based in Ottawa (University of Ottawa, Carleton University) and includes myself, Ján Veizer and John Blenkinsop. The second group, based in Kiel (IFM-GEOMAR, Leibniz Institute of Marine Sciences) includes Klaus Wallmann, Anton Eisenhauer, Florian Böhm and Silke Voigt.

I analyzed calcium isotope compositions of 210 brachiopod shells at Carleton University, using the double spike multicollector TIMS technique. A total of 70 brachiopod shells were measured at the IFM-GEOMAR by Florian Böhm, using the identical

technique. John Blenkinsop (Carleton University) helped to design a fully automated routine for the calcium isotope measurements via TIMS.

Klaus Wallmann (IFM-GEOMAR) developed a new numerical model of coupled calcium/carbon/magnesium global cycles that is applied to simulate the experimental $\delta^{44/40}Ca_{SW}$ record. He also wrote one section of the paper, which describes the modeling approach (see auxiliary material, the section A.2.; Simulating Phanerozoic evolution of calcium seawater concentrations and isotopic composition).

I wrote the rest of the manuscript and included a slightly modified version of Klaus Wallmann's contribution into the final draft. Ján Veizer (University of Ottawa), Anton Eisenhauer and Florian Böhm (IFM-GEOMAR) contributed to the discussion and provided helpful editorial advice. Other coauthors, Axel Munnecke (Friedrich-Alexander University, Erlangen), Robert van Geldern (Leibniz Institute for Applied Geosciences, Hannover) and Silke Voigt (IFM-GEOMAR) provided samples of Silurian, Devonian and Cretaceous brachiopods, respectively. These authors also provided useful comments on the discussion.

Paper 3:

I developed, with the assistance of John Blenkinsop, the analytical protocol for measurements of boron isotope abundances and produced all data, $\delta^{11}B$ and B concentrations, at Carleton University. I wrote the paper although the initial draft was significantly improved by inputs and suggestions of Ján Veizer and John Blenkinsop.

References

Artemov Yu. M., Knorre K., Strizhov V.P. and Ustinov V.I. (1966) $^{40}Ca/^{44}Ca$ and $^{16}O/^{18}O$ isotopic ratios in some calcareous rocks. *Geochem. Intern.* **3**, 1082–1086.

Artemov Yu. M., Strizhov V.P., Ustinov V.I. and Yaroshevskiy A.A. (1967) Possible isotope fractionation during dolomitization. *Geokhimiya* **5**, 519–529.

Backus M.M. (1955) Mass spectrometric determination of the relative isotopic abundance of calcium and the determination of geologic age. Doctoral thesis, Massachusetts Institute of Technology.

Backus M.M., Pinson W., Herzog I. and Hurley P. (1964) Calcium isotope ratios in the Homestead and Pasamonte meteorites and Devonian Limestone. *Geochim. Cosmochim. Acta* **28**, 735–742.

Berner R.A., Lasaga A.C. and Garrels R.M. (1983) The carbonate-silicate geochemical cycle and its effect on atmospheric carbon dioxide over the past 100 million years. *Am. J. Sci.* **283**, 641–683.

Coleman M.L. (1971) Potassium-calcium dates from pegmatitic micas. *Earth Planet. Sci. Lett.* **12**, 399–405.

Corless J. (1968) Obsevations on the isotopic geochemistry of calcium. *Earth Planet. Sci. Lett.* **4**, 475–478.

De La Rocha C.L. and DePaolo D.J. (2000) Isotopic evidence for variations in the marine calcium cycle over the Cenozoic. *Science* **289**, 1176–1178.

DePaolo D.J. (2004) Calcium isotopic variations produced by biological, kinetic, radiogenic and nucleosynthetic processes. In: C.M. Johnson, B.L. Beard, F. Albarède (Eds.), Geochemistry of non-traditional stable isotopes, Rev. Mineral. Geochem. Vol. 55, Washington, D.C., 2004, pp. 255–288.

Fantle M.S. and DePaolo D.J. (2005) Variations in marine Ca cycle over the past 20 million years. *Earth Planet. Sci. Lett.* **237**, 102–117.

Farkaš J., Buhl D., Blenkinsop J., and Veizer J. (2007) Evolution of the oceanic calcium cycle during the late Mesozoic: Evidence from $\delta^{44/40}$Ca of marine skeletal carbonates. *Earth Planet. Sci. Lett.* **253**, 96–111.

Grew E.S. and Anovitz L.M., Boron: Mineralogy, Petrology and Geochemistry. Vol 33, Mineralogical Society of America and Geochemical Society, Washington, D.C., Rev. Mineral. Geochem., 1996, pp. 862.

Gussone N., Eisenhauer A., Heuser A., Dietzel M., Bock B., Böhm F., Spero H.J., Lea D.W., Bijma J. and Nägler T. (2003) Model for kinetic effects on calcium isotope fractionation (δ^{44}Ca) in inorganic and cultured planktonic foraminifera. *Geochim. Cosmochim. Acta* **67**, 1375–1382.

Gussone N., Eisenhauer A., Tiedemann R., Haug G.H., Heuser A., Bock B., Nägler T. and Müller A. (2004) Reconstruction of Caribbean sea surface temperature and salinity fluctuations in response to the Pliocene closure of the Central American gateway and radiative forcing, using $\delta^{44/40}$Ca, δ^{18}O and Mg/Ca ratios. *Earth Planet. Sci. Lett.* **227**, 201–214.

Gussone N., Böhm F., Eisenhauer A., Dietzel M., Heuser A., Teichert B.M.A., Reitner J., Wörheide G. and Dullo W.-Ch. (2005) Calcium isotope fractionation in calcite and aragonite. *Geochim. Cosmochim. Acta* **69**, 4485–4494.

Hansen K.W. and Wallmann K. (2003) Cretaceous and Cenozoic evolution of seawater composition, atmospheric O_2 and CO_2: A model perspective. *Am. J. Sci.* **303**, 94-148.

Hemming N.G., Hanson G.N. (1992) Boron isotopic composition and concentration in modern marine carbonates. *Geochim. Cosmochim. Acta* **56**, 537–543.

Herzog L.F., Pinson W.H., Backus M.M., Strickland L. and Hurley P.M. (1954) Variations in isotopic abundances of strontium, calcium, and argon and related topics. Annual Progress Report for 1953-4, NYO 3934-II. Massachusetts Institute of Technology.

Heumann K., Kubassek E., Schwabenbauer W. and Stadler I. (1979) Analytical Method for K/Ca Age Determniantion of Geological Samples. *Fresen. Z. Anal. Chem.* **297**, 35–43.

Heumann K., Schwabenbauer W., Stadler I. and Kubassek E. (1977) K/Ca Altersbestimmungen and Kalifeldspaten. *Z. Naturforsch.* **32a**, 1333–1334.

Heumann K.G. and Lieser K.H. (1973) Isotopic variations of natural calcium in recent carbonates and sulphates. *Geochim. Cosmochim. Acta* **37**, 1463–1471.

Heuser A., Eisenhauer A., Böhm F., Wallmann K., Gussone N., Pearson P.N., Nägler T.F. and Dullo W-Ch. (2005) Calcium isotope ($\delta^{44/40}$Ca) variations of Neogene planktonic foraminifera. *Paleoceanography* **20**, PA2013, doi:10.1029/2004PA001048.

Heuser A., Eisenhauer A., Gussone N., Bock B., Hansen B.T. and Nägler T.F. (2002) Measurement of calcium isotopes ($\delta^{44/40}$Ca) using a multicollector TIMS technique, *Int. J. Mass. Spectrom.* **220**, 387–399.

Hippler D., Gussone N., Darling K., Eisenhauer A. and Nägler T. (2002) δ^{44}Ca in *N. pachy* (left): A new SST-proxy in polar regions. *Geochim. Cosmochim. Acta* **66**, suppl. 1, A331.

Hippler D., Schmitt A.-D., Gussone N., Heuser A., Stille P., Eisenhauer A. and Nägler T. (2003) Ca isotopic composition of various standards and seawater. *Geostandards Newsletter* **27**, 13-19. Gussone N., Böhm F., Eisenhauer A., Dietzel M., Heuser A., Teichert B.M.A., Reitner J., Wörheide G. and Dullo W.-Ch. (2005) Calcium isotope fractionation in calcite and aragonite. *Geochim. Cosmochim. Acta* **69**, 4485–4494.

Hirt B. and Esptein S. (1964) A search for isotopic variations in some terrestrial and meteoric calcium. *Trans. Am. Geophy. Union* **45**, pp. 113.

Hobbs M.Y. and Reardon E.J. (1999) Effect of *p*H on boron coprecipitation by calcite: Further evidence for nonequilibrium partitioning of trace elements. *Geochim. Cosmochim. Acta* **63**, 1013–1021.

Hönisch B. and Hemming N.G. (2005) Surface ocean pH response to variations in pCO_2 through two full glacial cycles. *Earth Planet. Sci. Lett.* **236**, 305–314.

Hönisch B., Hemming N.G. (2005) Surface ocean pH response to variations in pCO_2 through two full glacial cycles. *Earth Planet. Sci. Lett.* **236**, 305–314.

Immenhauser A., Nägler T., Steuber T. and Hippler D. (2005) A critical assessment of mollusk $^{18}O/^{16}O$, Mg/Ca, and $^{44}Ca/^{40}Ca$ ratios as proxies for Cretaceous seawater temperature seasonality. *Palaeogeo. Palaeoclim. Palaeoeco.* **215**, 221–237.

Johnson C.M., Beard B.L. and Albarède F., Geochemistry of non-traditional stable isotopes. Vol. 55, Mineralogical Society of America and Geochemical Society, Washington, D.C., Rev. Mineral. Geochem., 2004, pp. 454.

Jungck M., Shimamura T. and Lugmair G. (1984) Ca isotope variations in Allende. *Geochim. Cosmochim. Acta* **48**, 2651–2658.

Kampschulte A. and Strauss H. (2004) The sulfur isotopic evolution of Phanerozoic seawater based on the analysis of structurally substituted sulfate in carbonates. *Chem. Geol.* **204**, 255–286.

Kasemann S.A., Hawkesworth Ch.J., Pravec A.R., Fallick A.E. and Pearson P.N. (2005) Boron and calcium isotope composition in Neoproterozoic carbonate rocks from Namibia: evidence for extreme environmental change. *Earth Planet. Sci. Lett.* **231**, 73–86.

Lécuyer Ch., Grandjean P., Reynard B., Albarède F. and Telouk P. (2002) $^{11}B/^{10}B$ analysis of geological materials by ICP-MS Plasma 54: Application to the boron fractionation between brachiopod calcite and seawater. *Chem. Geol.* **186** 45–55.

Lemarchand D., Wasserburg G.J. and Papanastassiou D.A. (2004) Rate-controlled calcium isotope fractionation in synthetic calcite. *Geochim. Cosmochim. Acta* **68**, 4665–4678.

Marshall B.D. and DePaolo L.J. (1982) Precise age determination and petrogenetic studies using the K-Ca method. *Geochim. Cosmochim. Acta* **46**, 2537–2545.

Marshall B.D. and DePaolo L.J. (1989) Calcium isotopes in igneous rocks and the origin of granite. *Geochim. Cosmochim. Acta* **53**, 917–922.

Millero F.J. (1995) Thermodynamics of the carbon dioxide system in the oceans. *Geochim. Cosmochim. Acta* **59**, 661–677.

Nägler T., Eisenhauer A., Müller A., Hemleben C. and Kramers J. (2000) The δ^{44}Ca-temperature calibration on fossil and cultured Globigerinoides sacculifer: New tool for reconstruction of past sea surface temperatures, *Geochem. Geophys. Geosyst.* 1, doi: 10.1029/2000GC000091.

Niederer F.R. and Papanastassiou D.A. (1984) Ca isotopes in refractory inclusions. *Geochim. Cosmochim. Acta* **48**, 1279–1293.

Palmer M.R. and Pearson P.N. (2003) A 23,000-Year Record of Surface Water pH and pCO_2 in the Western Equatorial Pacific Ocean. *Science* **300**, 480–482.

Palmer M.R., Pearson P.N. and Cobb S.J. (1998) Reconstructing past ocean *p*H-depth profiles. *Science* **282**, 1468–1471.

Pearson P.N. and Palmer M.R. (1999) Middle Eocene seawater *p*H and atmospheric carbon dioxide concentrations. *Science* **284,** 824–826.

Pearson P.N. and Palmer M.R. (2000) Atmospheric carbon dioxide concentrations over the past 60 million years. *Nature* **406**, 695-699.

Podlaha O.G., Mutterlose J. and Veizer J. (1998) Preservation of δ^{18}O and δ^{13}C in belemnite rostra from the Jurassic/early Cretaceous successions, Am. J. Sci. 298 (1998) 324–347.

Royer D.L., Berner R.A., Montañez I.P., Tabor N.J. and Beerling D.J. (2004) CO_2 as a primary driver of Phanerozoic climate, *GSA Today* **14**, 4–10.

Russell W.A., Papanastassiou D.A. and Tombrello T.A. (1978) Ca isotope fractionation on the Earth and other solar system materials. *Geochim. Cosmochim. Acta* **42**, 1075–1090.

Sandal A., Hemming N.G., Hanson G.N. and Broecker W.S. (1995) Evidence for a higher pH in the glacial ocean from boron isotopes in foraminifera. *Nature* **373**, 234– 236.

Sanyal A., Hemming N.G., Broecker W.S., Lea S.W., Spero H.J. and Hanson G.N. (1996) Oceanic pH control on the boron isotopic composition of foraminifera: evidence from culture experiments. *Paleoceanography* **11**, 513–517.

Sanyal A., Hemming N.G., Broecker W.S. (1997) Changes in *p*H in the eastern equatorial Pacific across stage 5-6 boundary based on boron isotopes in foraminifera. *Global Biogeochem. Cycles* **11**, 125–133.

Sanyal A., Nugent M., Reeder R.J. and Bijma J. (2000) Seawater *p*H control on the boron isotopic composition of calcite: evidence from inorganic calcite precipitation experiments. *Geochim. Cosmochim. Acta* **64**, 1551–1555.

Samtleben C., Munnecke A. and Bickert, T. (2000) Development of facies and C/O-isotopes in transects through the Ludlow of Gotland: Evidence for global and local influences on a shallow-marine environment. *Facies* **43**, 1–38.

Samtleben C., Munnecke A., Bickert, T. and Pätzold, J. (2001) Shell succession, assemblage and species dependent effects on the C/O-isotope composition of brachiopods - examples from the Silurian of Gotland. *Chemical Geology* **175**, 61–107.

Schmitt A.-D., Chabaux F. and Stille P. (2003a) The calcium riverine and hydrothermal isotopic fluxes and the oceanic calcium mass balance, *Earth Planet. Sci. Lett.* **213**, 503–518.

Schmitt A.-D., Stille P. and Vennemann T. (2003b) Variations of $^{44}Ca/^{40}Ca$ ratio in seawater during the past 24 million years: evidence from $\delta^{44}Ca$ and $\delta^{18}O$ values of Miocene phosphates. *Geochim. Cosmochim. Acta* **67**, 2607–2614.

Simon L., Lécuyer Ch., Maréchal Ch. and Coltice N. (2006) Modelling the geochemical cycle of boron: Implications for the long-term $\delta^{11}B$ evolution of seawater and oceanic crust. *Chem. Geol.* **225** 61–76.

Skulan J.L., DePaolo D.J. and Owens T.L. (1997) Biological control of calcium isotopic abundances in the global calcium cycle. *Geochim. Cosmochim. Acta* **61**, 2505–2510.

Skulan J.L. and DePaolo D.J. (1999) Calcium isotope fractionation between soft and mineralized tissues as a monitor of calcium use in vertebrates. *Proc. Natl. Acad. Sci.* **96**, 13709–13713.

Soudry D., Segal I., Nathan Y., Glenn C.R., Halicz L., Lewy Z. and VonderHaar D.L. (2004) $^{44}Ca/^{42}Ca$ and $^{143}Nd/^{144}Nd$ isotope variations in Cretaceous-Eocene Tethyan francolites and their bearings on phosphogenesis in the southern Tethys. *Geology* **32**, 389–392.

Spero H.J., Bijma J., Lea D.W., Bemis B.E., 1997. Effect of seawater carbonate concentration on foraminiferal carbon and oxygen isotopes, Nature 390, 497–500.

Spivack A.J., You C.F. and Smith H.J. (1993) Foraminiferal boron isotope ratios as a proxy for surface ocean pH over the past 21 Myr. *Nature* **363**, 149–151.

Stahl W. (1968) Search for natural variations in calcium isotope abundances. *Earth Planet. Sci. Lett.* **5**, 171–174.

Stahl W. and Wendt L. (1968) Fractionation of calcium isotopes in carbonate precipitation. *Earth Planet. Sci. Lett.* **5**, 184–186.

Steuber T. and Veizer J. (2002) Phanerozoic record of plate tectonic control of seawater chemistry and carbonate sedimentation. *Geology* **30**, 1123-1126.

Steuber T. and Buhl D. (2006) Calcium-isotope fractionation in selected modern and ancient marine carbonates. *Geochim. Cosmochim. Acta* **70**, 5507-5521.

Tipper E.T., Galy A. and Bickle M.J. (2006) Riverine evidence for a fractionated reservoir of Ca and Mg on the continents: Implications for the oceanic Ca cycle. *Earth Planet. Sci. Lett.* **247**, 267–279.

van Geldern R., Joachimski M.M., Daly J., Jansen U., Alvarez F., Yolkin E.A. and Ma X.-P. (2006) Carbon, oxygen and strontium isotope records of Devonian brachiopod shell calcite. *Paleogeo. Paleoclim. Paleoeco.* **240**, 47-67.

Veizer J., Ala D., Azmy K., Bruckschen P., Buhl D., Bruhn F., Carden G.A.F., Diener A., Ebneth S., Godderis Y., Jasper T., Korte Ch., Pawellek F., Podlaha O. and Strauss H. (1999) $^{87}Sr/^{86}Sr$, $\delta^{13}C$ and $\delta^{18}O$ evolution of Phanerozoic seawater, *Chem. Geol.* **161** 59–88.

Voigt S., Gale A.S., Flögel S. (2004) Midlatitude shelf seas in the Cenomanian-Turonian greenhouse world: Temperature evolution and North Atlantic circulation. *Paleoceanography* **19**, PA4020, doi:10.1029/2004PA001015.

Wallmann K. (2001) Controls on the Cretaceous and Cenozoic evolution of seawater composition, atmospheric CO_2 and climate. *Geochim. Cosmochim. Acta* **65**, 3005-3025.

Wallmann K. (2004) Impact of atmospheric CO_2 and galactic cosmic radiation on Phanerozoic climate change and the marine $\delta^{18}O$ record. *Geochem. Geophys. Geosyst.* **5** Q06004, doi: 10.1029/2003GC000683.

Wiegand B.A., Chadwick O.A., Vitousek P.M. and Wooden J.L. (2005) Ca cycling and isotopic fluxes in forested ecosystems in Hawaii. *Geophys. Res. Lett.* **32**, L11404, doi: 10.1029/2005GL022746.

Wieser M. E., Buhl D., Bouman C. and Schwieters J. (2004) High precision calcium isotope ratio measurements using a magnetic sector multiple collector inductively coupled plasma mass spectrometer, *J. Anal. At. Spectrom.* **19**, 844–851.

Zeebe R.E., 1999. An explanation of the effect of seawater carbonate concentration on foraminiferal oxygen isotopes, Geochim. Cosmochim. Acta 63, 2001–2007.

Zhu P. and MacDougall J.D. (1998) Calcium isotopes in the marine environment and the oceanic calcium cycle. *Geochim. Cosmochim. Acta* **62**, 1691–1698.

2 Evolution of the oceanic calcium cycle during the Late Mesozoic: Evidence from $\delta^{44/40}Ca$ of marine skeletal carbonates

by

Juraj Farkaš [a], Dieter Buhl [b], John Blenkinsop [c] and Ján Veizer [a]

[a] *University of Ottawa and Ottawa-Carleton Geoscience Centre, Ottawa, K1N 6N5,ON, Canada*

[b] *Institut für Geologie, Mineralogie und Geophysik, Ruhr Universität, 44801, Bochum, Germany*

[c] *Carleton University and Ottawa-Carleton Geoscience Centre, Ottawa, K1S 5B6,ON, Canada*

Published in:

Earth and Planetary Science Letters **253** 96 – 111 (2007)

Presented at:

The 2nd Earth System Processes (ESP2) Meeting, Calgary, Canada (2005);

The 6th International Symposium on Applied Isotope Geochemistry (AIG-6), Prague, Czech Republic (2005).

Abstract

The Ca isotope compositions of 37 late Mesozoic skeletal carbonates, belemnites and brachiopods, from the Tethyan realm were analyzed by thermal (TIMS) and plasma (MC-ICP-MS) ionization mass spectrometry. A poor correlation between $\delta^{44/40}$Ca and δ^{18}O values of belemnites suggests only a weak temperature dependency for the Ca isotope composition of belemnites, likely less than 0.02‰ °C^{-1}. The $\delta^{44/40}$Ca record of belemnites was therefore used to reconstruct the Ca isotope composition of paleo-seawater ($\delta^{44/40}Ca_{SW}$), based on an experimentally determined fractionation factor between seawater Ca and belemnite calcite ($\alpha_{CC\text{-}SW}$) of ~0.9986. The inferred $\delta^{44/40}Ca_{SW}$ record, with an average stratigraphic resolution of 1 Ma, shows systematic temporal variation of ~0.5‰ with the Middle/Late Jurassic (~154 Ma) minimum of ~1.4‰ and a subsequent general increase to the Early Cretaceous (~124 Ma) maximum of ~1.9‰. The global nature of the $\delta^{44/40}Ca_{SW}$ record is supported by identical Ca isotope compositions of coeval (Kimmeridgian) belemnites collected from two distinct paleogeographic regions, the southern (New Zealand) and northern (Germany) margin of the Tethys Ocean. The observed late Mesozoic $\delta^{44/40}Ca_{SW}$ record was simulated using a simple Ca isotope mass balance model, and the results indicate that the variation in $\delta^{44/40}Ca_{SW}$ record can be explained by changes in oceanic input fluxes of Ca that were independent of the carbonate ion fluxes, such as the hydrothermal Ca flux or the release of Ca to the oceans via dolomitization of marine carbonates.

Keywords: calcium isotopes; belemnites; brachiopods; late Mesozoic, marine calcium cycle; seawater chemistry

2.1 Introduction

Belemnite rostra and brachiopod shells, primarily composed of low-Mg calcite, are frequently used as carrier phases of proxies that record the physical and chemical attributes of the Mesozoic and Paleozoic oceans, such as their chemistry or isotope composition. Calcium, together with carbon and oxygen is the major component of $CaCO_3$ and has six

naturally occurring isotopes ^{40}Ca, ^{42}Ca, ^{43}Ca, ^{44}Ca, ^{46}Ca and ^{48}Ca. Due to its numerous isotopes, and being the fifth most abundant element in the Earth's crust and a major constituent of biological and geological systems, it promises to be a geological tracer with a considerable potential. In terrestrial and marine environments Ca isotopes are fractionated by biological and inorganic processes that discriminate against heavy Ca isotopes (Skulan et al., 1997; Zhu et al., 1998). Biological and inorganic calcification also controls the Ca removal from the ocean (Zhu et al., 1998) that is balanced mostly by riverine and hydrothermal Ca input (Schmitt et al., 2003a). Due to the long residence time of Ca in seawater ($\tau_{Ca} \approx$ 1 to 2 Ma; Holland, 1978; Fantle and DePaolo, 2005) relative to the short mixing time of global ocean (~1000 yr), the Ca isotope composition of modern seawater is globally homogeneous (Zhu et al., 1998; Schmitt et al., 2001), and this likely was the case also in the geological past.

Modern marine carbonates are isotopically lighter and variably enriched in ^{40}Ca relative to present-day seawater (Skulan et al., 1997; Zhu et al., 1998), depending on their mineralogy and precipitation kinetics such as temperature or calcification rates (Gussone et al., 2005; Nägler et al., 2000; Lemarchand et al., 2004; Sime et al., 2005). Nevertheless, the Ca isotope composition, $\delta^{44/40}Ca$, of fossil marine carbonates can potentially record secular changes in $\delta^{44/40}Ca$ of paleo-seawater, providing that the fractionation factor between seawater Ca and a carbonate phase ($\alpha_{cc/sw}$) is known. So far, only a few reconnaissance studies aimed to reconstruct the Ca isotope evolution of seawater ($\delta^{44/40}Ca_{SW}$) based on the $\delta^{44/40}Ca$ of marine carbonates or phosphates. Fantle and DePaolo (2005) and De La Rocha and DePaolo (2000) analyzed the Neogene and Cenozoic nannofossil ooze, respectively; Heuser et al. (2005) the Neogene planktonic foraminifera, Steuber and Buhl (2006) the mid-Cretaceous and the Late Carboniferous marine carbonates, Böhm et al. (2004) the Devonian brachiopods, and Kasemann et al. (2005) the Neoproterozoic whole-rock carbonates. Two studies, Schmitt et al. (2003b) and Soudry et al. (2004) investigated the Ca isotope composition of authigenic marine phosphates from the Miocene and the Cretaceous-Eocene period, respectively. Our study of the Middle Jurassic to Early Cretaceous marine skeletal carbonates expands the existing $\delta^{44/40}Ca$ record, covering a sparsely investigated late Mesozoic (~124 to 159 Ma) period.

2.2 Samples

In this project we analyzed only well preserved Middle Jurassic to Early Cretaceous belemnites and brachiopods. The belemnite samples (Table 2.1 and 2.2) were previously investigated for O, C, Sr and S isotope compositions, screened by cathodoluminescence (CL), SEM, and analyzed for major (Ca, Mg) and trace (Sr, Mn, Fe) element composition. The Kimmeridgian brachiopods and belemnites (Table 2.3), collected in southern Germany from the same stratigraphic horizons, were analyzed only for trace elements (Sr, Mn, Fe). Comprehensive descriptions of ultrastructure, chemistry, location, and stratigraphy of the belemnite samples (Table 2.1 and 2.2) are given in Podlaha et al. (1995, 1998), Veizer et al. (1999), Kampschulte and Strauss (2004) and Kampschulte, (2001); and key information on elemental/isotope composition and stratigraphic age is accessible at http://www.science.uottawa.ca/geology/isotope_data.

The time scale used in this study is from Harland et al. (1990) because some of the experimental data, e.g. $^{87}Sr/^{86}Sr$, used in our model simulation refer to this scale (cf. Veizer et al., 1999). A direct comparison of the numerical ages of Harland et al. (1990) with the most up-to-date geological time scale of Gradstein et al. (2004) is available in Gradstein et al. (1994).

Most of the Middle and Late Jurassic belemnites (Table 2.1, 2.2 and 2.3) are from the northern margin of the Tethys Ocean now exposed on the Russian platform (Rybinsk, Peski and Voskresjensk) and in the southern part of Germany (Geisingen, Ursental), however some Late Jurassic (Kimmeridgian) belemnites were collected in New Zealand (Kawhia Harbour), representing a high-latitude southern margin of the Tethys Ocean. The Early Cretaceous (Valanginian/Aptian) belemnites were sampled in Germany (Sarstedt) and England (Speeton), both corresponding to the northwestern margin of the Tethys Ocean. The belemnite samples thus cover a substantial paleolatitudinal range, from ~40°N to 80°S (Podlaha et al., 1998), (Fig. 2.1), and a total of at least 12 different species.

Table 2.1.

Measured $\delta^{44/40}Ca_{NIST}$ (TIMS) values of Middle Jurassic to Early Cretaceous belemnites

Sample	Location	Fossil Name	Period[a]	Stage	Age (Ma)	$\delta^{44/40}Ca$[b] (NIST)
J138	Russia	*Pachyteuthis russiensis*	MJ	Callovian	158.4	0.35
J132	Russia	*Cylindroteuthis purosiana*	MJ	Callovian	157.7	0.28
J125	Russia	*Cylindroteuthis purosiana*	MJ	Callovian	157.4	0.12
J114	Russia	*Cylindroteuthis beaumonti*	LJ	Oxfordian	156.7	0.09
J94	Russia	*Pachyteuthis russiensis*	LJ	Oxfordian	155.7	0.11
J77	New Zealand	*Belemnopsis keari*	LJ	Kimmeridgian	153.6	0.17
J67	New Zealand	*Hibolites marwicki*	LJ	Kimmeridgian	151.1	0.26
J53	Russia	*Cylindroteuthis volgensis*	LJ	Tithonian	149.4	0.28
J16	Russia	*Cylindroteuthis volgensis*	LJ	Tithonian	147.8	0.31
K112	Germany	Species unidentified	EC	Valanginian	140.0	0.33
K111	Germany	Species unidentified	EC	Valanginian	138.6	0.29
K110	Germany	Species unidentified	EC	Valanginian	138.1	0.35
K98	Germany	Species unidentified	EC	Valanginian	136.2	0.34
K92	Germany	Species unidentified	EC	Hauterivian	135.2	0.46
K75	Germany	*Hibolites jaculoides*	EC	Hauterivian	133.1	0.47
K67	Great Britain	*Praeoxyteuthis pugio*	EC	Barremian	130.5	0.49
K45	Great Britain	*Aulacotheuthis species*	EC	Barremian	128.2	0.46
K41	Germany	*Aulacotheuthis descendens*	EC	Barremian	127.8	0.37
K35	Great Britain	*Oxyteuthis brunsvicensis*	EC	Barremian	127.4	0.42
K20	Germany	Species unidentified	EC	Barremian	126.6	0.37
K15	Great Britain	*Oxyteuthis pseudogermanica*	EC	Barremian	126.3	0.61
K11	Great Britain	*Oxyteuthis pseudogermanica*	EC	Barremian	126.2	0.48
K2	Germany	*Species unidentified*	EC	Aptian	124.5	0.52

[a] The following abbreviations are used: MJ = Middle Jurassic; LJ = Late Jurassic; EC = Early Cretaceous.

[b] The mean long-term external reproducibility (2σ) of the $\delta^{44/40}Ca_{NIST}$ is ± 0.15‰.

Table 2.2.

Measured $\delta^{44/42}Ca_{IAPSO}$ (MC-ICP-MS) values and the recalculated $\delta^{44/40}Ca_{NIST}$ data of the Middle Jurassic to Early Cretaceous belemnites

Sample	Location	Fossil Name	Period[a]	Stage	Age (Ma)	$\delta^{44/42}Ca$[b] IAPSO	$\delta^{44/40}Ca$[c] NIST
J143	Russia	*Pachyteuthis russiensis*	MJ	Callovian	158.7	-0.92	0.27
J138	Russia	*Pachyteuthis russiensis*	MJ	Callovian	158.4	-0.90	0.31
J132	Russia	*Cylindroteuthis purosiana*	MJ	Callovian	157.7	-0.93	0.24
J125	Russia	*Cylindroteuthis purosiana*	MJ	Callovian	157.4	-0.93	0.24
J119	Russia	*Pachyteuthis russiensis*	MJ/LJ	Call/Oxford.	157.3	-0.98	0.16
J114	Russia	*Cylindroteuthis beaumonti*	LJ	Oxfordian	156.7	-1.00	0.11
J109	Russia	*Pachyteuthis russiensis*	LJ	Oxfordian	155.9	-0.97	0.18
J94	Russia	*Pachyteuthis russiensis*	LJ	Oxfordian	155.7	-0.97	0.17
J77	New Zeal.	*Belemnopsis keari*	LJ	Kimmeridgian	153.6	-0.88	0.35
K75	Germany	*Hibolites jaculoides*	EC	Hauterivian	133.1	-0.84	0.44
K67	Great Brit.	*Praeoxyteuthis pugio*	EC	Barremian	130.5	-0.85	0.40
K51	Germany	*Aulacotheuthis absolutiform.*	EC	Barremian	128.3	-0.83	0.45
K45	Great Brit.	*Aulacotheuthis species*	EC	Barremian	128.2	-0.83	0.45
K41	Germany	*Aulacotheuthis descendens*	EC	Barremian	127.8	-0.91	0.29
K35	Great Brit.	*Oxyteuthis brunsvicensis*	EC	Barremian	127.4	-0.91	0.28
K30	Germany	*Oxyteuthis brunsvicensis*	EC	Barremian	127.1	-0.89	0.33
K25	Germany	Species unidentified	EC	Barremian	126.7	-0.89	0.33
K20	Germany	Species unidentified	EC	Barremian	126.6	-0.86	0.39

[a] The following abbreviations are used: MJ = Middle Jurassic; LJ = Late Jurassic; EC = Early Cretaceous.

[b] The mean long-term external reproducibility (2σ) of the $\delta^{44/42}Ca_{IAPSO}$ is ± 0.1‰.

[c] The $\delta^{44/40}Ca_{NIST}$ values were calculated from the measured $\delta^{44/42}Ca_{IAPSO}$ values using the following relationship: $\delta^{44/40}Ca_{NIST} = [(\delta^{44/42}Ca_{IAPSO} + 0.12‰ \text{ (offset-correction)})\cdot 2] + 1.88‰$.

Table 2.3.

The $\delta^{44/40}Ca_{NIST}$ (TIMS) values of modern brachiopods and present-day seawater and the chemical (Sr, Mn, Fe) and isotope ($\delta^{44/40}Ca_{NIST}$) composition of the Kimmeridgian belemnites and brachiopods collected from the same stratigraphic horizons (southern Germany)

Sample	Period[a]	Location	Horizon	Material	Species	Sr (ppm)	Mn (ppm)	Fe (ppm)	$\delta^{44/40}Ca$[b] (‰)
IAPSO	Modern	Atlantic Ocean	NA	seawater	NA	_	_	_	1.86
Y342L	Modern	San Juan Island	NA	brachiopod	*Terebratalia*	1085	16	6	1.07
D519L	Modern	San Juan Island	NA	brachiopod	*Terebratalia*	1120	13	10	1.09
G3-br. 45	Early K.	Geisingen	G3	brachiopod	*Lacunosella*	378	3	21	0.67
G3-be.	Early K.	Geisingen	G3	belemnite	unidentified	1140	5	35	0.14
G5-br 27	Early K.	Geisingen	G5	brachiopod	*Lacunosella*	1318	2	11	0.59
G5-br 39	Early K.	Geisingen	G5	brachiopod	*Lacunosella*	1280	3	19	0.66
G5-be 1	Early K.	Geisingen	G5	belemnite	unidentified	344	4	18	0.08
U2/3-br 17	Late K.	Ursental	U2-3	brachiopod	*Lacunosella*	412	9	303	0.69
U2/3-br 25	Late K.	Ursental	U2-3	brachiopod	*Lacunosella*	392	33	268	0.68
U2/3-be	Late K.	Ursental	U2-3	belemnite	unidentified	1279	9	18	0.23

[a] The following abbreviations are used: Early K. = Early Kimmeridgian; Late K. = Late Kimmeridgian; NA = Not Applicable

[b] The mean long-term external reproducibility (2σ) of the $\delta^{44/40}Ca_{NIST}$ is ± 0.15‰.

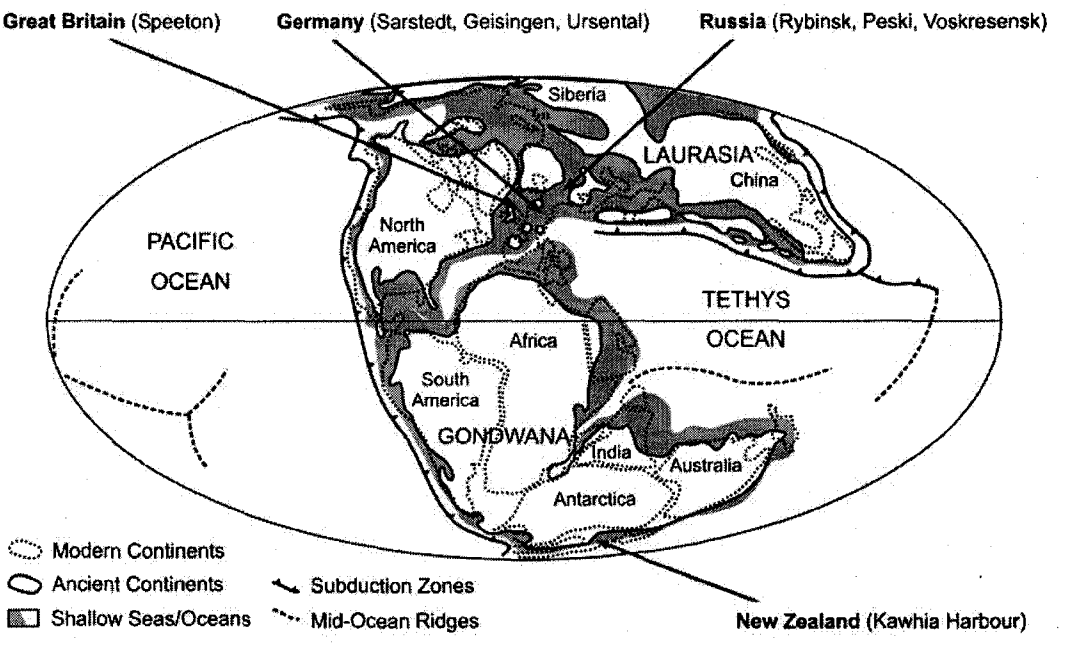

Fig. 2.1. Locations of the sampling areas placed into the paleogeographic settings of the Late Jurassic period (~150 Ma), modified after Scotese, 2002, http://www.scotese.com, PALEOMAP website.

2.3 Methods

2.3.1 Sample Preparation

Calcite powders, frequently from a single lamina of a belemnite rostrum or an interior 'secondary' layer of a brachiopod shell, were ultrasonically cleaned with nanopure water (>18 Mohm/cm), followed by a sonication in 30% H_2O_2 to remove organic matter potentially causing isobaric interferences during the Ca isotope analysis (Heuser et al., 2005). The cleaned powders were dried and weighed into Teflon PFA (perfluoroalkoxy) vials. Sample size permitting, two aliquots of each sample were prepared, one for TIMS and the other for MC-ICP-MS. For small samples, the Ca isotope composition was determined only by one technique, mostly TIMS. The chemical separation of Ca from a sample matrix was done by cation exchange chromatography (see the sections 2.3.2 and

2.3.3). All chemicals used in this study were of high purity to minimize the impact of Ca blank on the measured Ca isotope abundances.

2.3.2 TIMS Technique: Double Spiking, Chemical Separation and Measurement/Correction Routine

The Ca isotope analyses were performed on a Thermo Electron Triton TIMS thermal ionization mass spectrometer at Carleton University, at the Isotope Geochemistry and Geochronology Research Centre (IGGRC). The Ca isotope compositions were determined by conventional double spiking technique (Russell et al., 1978; Heuser et al., 2002) and expressed as $\delta^{44/40}Ca$ values in a permil (‰) relative to the NIST SRM 915a $CaCO_3$ standard, ($\delta^{44/40}Ca_{NIST} = [(^{44}Ca/^{40}Ca)_{sample}/(^{44}Ca/^{40}Ca)_{NIST} - 1] * 1000$), following the proposal of Eisenhauer et al. (2004). We also analyzed natural seawater (IAPSO seawater standard from Ocean Scientific International) as an additional in-house Ca isotope standard.

The weighed samples (~1000 μg $CaCO_3$) were dissolved in ~1000 μL of 2.5 M HCl so the Ca concentration in a solution would be 0.4 μg/μL. From this solution 25 μL (~10 μg of Ca) was pipetted into a PFA vial and mixed with 80 μL of the $^{43}Ca/^{48}Ca$ double spike (~0.2 μg of ^{48}Ca and ~0.15 μg of ^{43}Ca). As a result, the $^{40}Ca/^{48}Ca$ ratio in the mixture was close to 50. The $^{43}Ca/^{48}Ca$ double spike was added to the sample prior to the chemical separation of Ca enabling correction for a possible isotope fractionation associated with an incomplete recovery of the Ca fraction (Russell and Papanastassiou, 1978).

The $^{43}Ca/^{48}Ca$ double spike was prepared from two individual single spike solutions made from isotopically enriched carbonates Ca43-NX and Ca48-RT (Oak Ridge National Laboratory). The ^{43}Ca and ^{48}Ca single spike solutions were mixed in such a way that the $^{43}Ca/^{48}Ca$ ratio in the double spike (0.7221 ± 0.0004, 2σ, n = 8) would be close to that of terrestrial materials, between 0.7215 and 0.7310 (Russell et al., 1978; Coplen et al. 2002; DePaolo, 2004). The Ca isotope composition of the single and double spike solutions were determined by TIMS (no double spike added or data correction applied) using a nitrate loading technique (see below) that yielded a minimal in-run mass fractionation and a typical external reproducibility for $^{43}Ca/^{48}Ca$ of ± 0.6‰ (2σ, n = 8).

The reproducibility of the Ca isotope measurements was, however, significantly improved to less than ± 0.15‰ (2σ), for $^{44}Ca/^{40}Ca$, after the application of the $^{43}Ca/^{48}Ca$ double spike and an iterative double spike correction (Heuser et al., 2002).

After the double spiking, the sample-spike mixtures were dried and redissolved in 10 µL of 2.5 M HCl. These solutions (~10.5 µg Ca) were loaded onto PFA micro-columns, filled with 250 µL of pre-washed cation exchange resin (BioRad AG50W-X12), and washed into the resin with 1600 µL of 2.5 M HCl. Following the elution of the 1600 µL (Mg, Na and K), the Ca fraction was collected in a new PFA vial with additional 1500 µL of 2.5 M HCl. The initial pre-washing of the resin with 7.2 M HCl and 1 M ammonium acetate (Nägler and Villa, 2000) was an important step that enabled the total procedural Ca blank to be consistently below 15 ng, almost three orders of magnitude less than the amount of Ca supplied from a sample.

The collected Ca fraction was evaporated to dryness and redissolved in 10 µL of 5% HNO_3. From this solution 3 µL (3 µg Ca) were loaded as a nitrate on zone-refined Re in double filament assembly. The reaction of $Ca(NO_3)_2$ with Re and O_2 must lead to a precipitation of high-mass Ca compounds on the filament. As a result the in-run fractionation for $^{44}Ca/^{40}Ca$ was minimal, typically bellow ± 0.03‰ (2σ). The loaded sample was dried at a filament current of 0.5 ampere (A), heated at 1.5 A for about 60 seconds and finally taken to dull red at about 2.2 A for 30 seconds (Tuttas and Schwieters, 2002).

In the mass spectrometer, the evaporation filament current was brought to 0.25 A and simultaneously the ionization filament current was raised stepwise to ~2.9 A, resulting in an ionization temperature of ~1400°C and a target ion beam intensity of about 100 pA (^{40}Ca). The Ca isotope peaks were measured in two steps. In the first step, masses 40 to 44 were measured including ^{41}K to monitor possible isobaric interferences of ^{40}K on ^{40}Ca, however, in all cases such interference was negligible. In the second step, masses 44 to 48 were collected. An individual measurement consisted of 100 cycles (10 blocks of 10 cycles each), with each step comprising a 3-second waiting time, followed by a 16-second integration. Defocused baseline measurements collected for 30 seconds were carried out at the beginning of each block. Checks of the baselines and peaks showed that there were no

reflected ions or electrons perturbing measurements, especially during the second step when the large ^{40}Ca signal is not directed into a Faraday cup. A total analytical time including a 25-minute heating routine was approximately 110 minutes.

The measured ratios of interest were $^{40}Ca/^{48}Ca$, $^{43}Ca/^{48}Ca$ and $^{44}Ca/^{48}Ca$. The original $^{44}Ca/^{40}Ca$ ratio of the sample was calculated applying an iterative data reduction algorithm of Heuser et al. (2002) and using the Ca isotope composition of our $^{43}Ca/^{48}Ca$ double spike and 'Russell values' for a pure sample as starting parameters for the calculation (Russell et al., 1978; Heuser et al., 2002).

The external reproducibility of $^{44}Ca/^{40}Ca$ (double spike and data reduction applied) for replicates of same solution was approximately ± 0.15‰ (2σ), generally between ± 0.1‰ and ± 0.2‰. The cited $^{40}Ca/^{44}Ca$ ratio of 46.46 ± 0.08 (Coplen et al., 2002) for the NIST SRM 915a was reproduced within ± 0.13‰ (2σ, n = 30), over a period of six months. The $\delta^{44/40}Ca_{NIST}$ value for the IAPSO seawater showed heavy isotope enrichment of 1.86 ± 0.2‰ (2σ, n = 5), in agreement with the published value of 1.88 ± 0.04‰ (Hippler et al., 2003).

2.3.3 MC-ICP-MS Technique: Sample Preparation/Introduction and Standard-Sample Bracketing

The Ca isotope abundances of standards (NIST SRM 915a, IAPSO seawater) and selected samples (Table 2.2) were also determined on a multi-collector Thermo Electron Neptune inductively plasma mass spectrometer (MC-ICP-MS) at the Ruhr University Bochum, following the standard-sample bracketing technique of Wieser et al. (2004). Briefly, ~500 μg of $CaCO_3$ were loaded with 2.5 M HCl onto quartz-glass columns filled with 3500 μL of resin (BioRad AG50W-X12). Typically Ca was eluted with 25 mL of 2.5 M HCl, after the first 20 mL washed out Mg, Na and K. The Ca fraction (recovery >95%) was collected into PFA vial, evaporated to dryness and redissolved in adjusted volume of 3.5% HNO_3 resulting in the Ca concentration of 10 μg/mL. The standard solution (IAPSO seawater) had the Ca concentration close to 10 μg/mL and comparable matrix properties (3.5% HNO_3) as the sample-solution. All solutions were introduced in the 'hot' (1200 W) plasma passing through a combined Apex-IR and Aridus desolvating system. Due to a high

intensity of the $^{40}Ar^{+}$ ion beam (> 8000 V), interfering on mass 40, the Ca isotope measurements cannot be normalized to ^{40}Ca, as done for TIMS. Instead, the measured ^{44}Ca abundances were normalized to ^{42}Ca and expressed as the $\delta^{44/42}Ca$ notation (‰), ($\delta^{44/42}Ca_{IAPSO} = [(^{44}Ca/^{42}Ca)_{sample}/(^{44}Ca/^{42}Ca)_{IAPSO} - 1] * 1000$). The $\delta^{44/42}Ca$ measurements can be transformed to $\delta^{44/40}Ca$ and compared with the $\delta^{44/40}Ca_{NIST}$ (TIMS) values using the following relationships: $\delta^{44/40}Ca = 2 * \delta^{44/42}Ca$ and $\delta^{44/40}Ca_{NIST} = \delta^{44/40}Ca_{IAPSO} + 1.88‰$ (Eisenhauer et al., 2004). We used an approximate conversion factor of 2, for the calculation of $\delta^{44/40}Ca$, instead of a more accurate 1.9995 (Eisenhauer et al., 2004) or 1.9095 (Criss, 1999), as the uncertainty in $\delta^{44/42}Ca$ due to the analytical error (± 0.15‰, 2σ) exceeded the variations caused by different conversion factors (~0.05‰).

Each $\delta^{44/42}Ca$ value represents an average of three measurements. A single measurement consists of 30 integrations, each consisting of one sample measurement bracketed by two standards (IAPSO seawater). The Ca isotope composition of a sample was calculated relative to the averaged standard. Blanks (pure 3.5% HNO_3) were registered prior to and after each sample and standard measurement.

The external reproducibility for $\delta^{44/42}Ca$ was ± 0.15‰ (2σ). The long-term $\delta^{44/42}Ca_{IAPSO}$ of the NIST SRM 915a showed a relative isotope depletion of –0.88 ± 0.11‰ (2σ, n = 54), (Wieser et al., 2004). Recalculated to $\delta^{44/40}Ca$, the NIST SRM 915a is on average 1.76 ± 0.15‰ lighter than the IAPSO seawater, in agreement with the TIMS measurements (Hippler et al., 2003).

Nevertheless, throughout the analytical period of this project the difference between the $\delta^{44/42}Ca$ of NIST SRM 915a and IAPSO seawater was slightly (~0.12‰), but consistently, lower than the above ~0.88‰ difference (Wieser et al., 2004). As realized later, Ca isotope measurements on MC-ICP-MS are very sensitive to instrumental settings such as the type of cones and gas flow rates. These instrument parameters generate significant but stable and reproducible offsets that are poorly understood. However, long-term tests with samples and standards proved that these differences could be rectified applying a constant offset-correction to all measured $\delta^{44/42}Ca$ values, in our case +0.12‰.

2.4 Results

The analytical results of the Ca isotope measurements are presented in Tables 2.1, 2.2 and 2.3. In total 52 measurements (32 belemnites, 7 brachiopods and IAPSO seawater) were made, 34 by TIMS and 18 by MC-ICP-MS. The combined late Mesozoic Ca isotope record, expressed as the $\delta^{44/40}$Ca (NIST 915a), is plotted against geological time in Fig. 2.2.

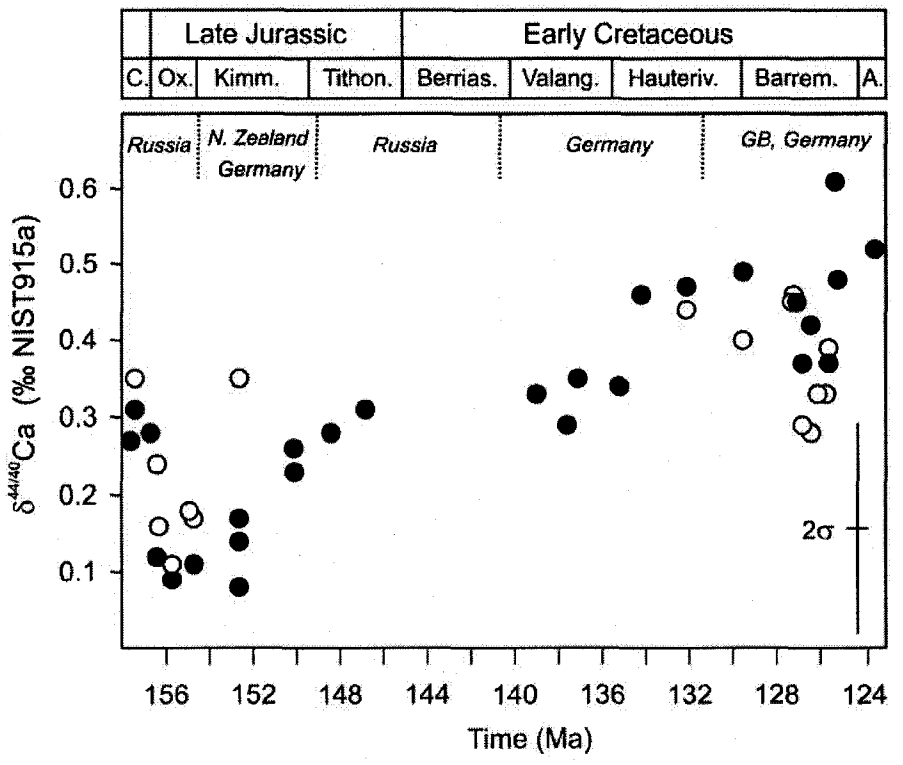

Fig. 2.2. The Ca isotope composition ($\delta^{44/40}Ca_{NIST}$) of the Middle Jurassic to Early Cretaceous belemnites as determined by TIMS (filled circles) and MC-ICP-MS (open circles) technique. The vertical error bar represents the external reproducibility for $\delta^{44/40}$Ca of about ± 0.15‰. The numerical ages on the geological time scale are from Harland et al. (1990). The following abbreviations are used: C. = Callovian; Ox. = Oxfordian; Kimm. = Kimmeridgian; Tithon. = Tithonian; Berrias. = Berriasian; Valang. = Valanginian; Hauteriv. = Hauterivian; Barrem = Barremian; A. = Aptian.

The belemnite $\delta^{44/40}$Ca record reveals a systematic long-term variation of ~0.5‰. Overall, the $\delta^{44/40}$Ca values show a rapid decrease from ~0.3‰ at ~158 Ma to a minimum of ~0.1‰ at ~156 Ma, followed by a gradual increase to ~0.3‰, from ~152 to 146 Ma. We

had no Berriasian (~146 to 141 Ma) samples, but the Valanginian (~140 to 135 Ma) $\delta^{44/40}$Ca values are still holding the earlier Tithonian (~146 Ma) signatures of ~0.3‰, rising steadily to a Hauterivian (~134 to 130 Ma) plateau of ~0.5‰. An abrupt decline to ~0.3‰ is recorded during the Middle Barremian (~126 Ma), followed by a ~0.55‰ maximum at the Barremian-Aptian boundary (~124 Ma).

Table 2.3 and Fig. 2.3 show the $\delta^{44/40}$Ca values of belemnites and brachiopods collected from the same stratigraphic horizons (the Early and Late Kimmeridgian), together with the Ca isotope composition of modern brachiopods and present-day seawater (IAPSO). These data were used to calculate the Ca isotope fractionation factors ($\alpha_{CC\text{-}SW}$) between dissolved Ca in seawater and a brachiopod or belemnite calcite.

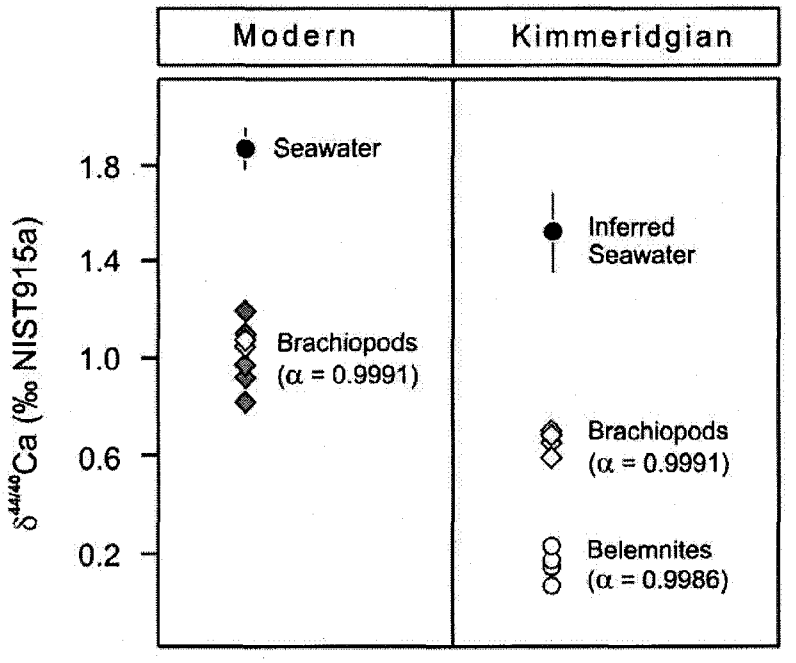

Fig. 2.3. The $\delta^{44/40}Ca_{NIST}$ values of modern brachiopods and present-day seawater (IAPSO) and the calculated Ca isotope fractionation factor between seawater Ca and the brachiopod calcite ($\alpha_{CC\text{-}SW}$) of 0.9991 (Table 2.3, plus data from Gussone et al., 2005); and the Ca isotope composition of the Kimmeridgian brachiopods, belemnites (Table 2.3) and inferred Kimmeridgian seawater together with the calculated $\alpha_{CC\text{-}SW}$ value for a belemnite calcite of 0.9986.

2.5 Discussion

2.5.1 Evaluation of suitability of TIMS and MC-ICP-MS for Ca isotope analysis

High precision Ca isotope measurements were achieved with both techniques and the long-term external reproducibilities (2σ) for TIMS and MC-ICP-MS are comparable, ~0.15‰ for 4 atomic mass units. The Ca isotope abundances of belemnites measured by TIMS and MC-ICP-MS agree within ± 0.15‰ (2σ) analytical error (Fig. 2.3), both techniques reproducing the Oxfordian minimum of ~0.1‰ and the Hauterivian/Barremian maximum of ~0.5‰ ($r^2 = 0.65$, $p < 0.002$, $n = 12$).

Closer inspection of the MC-ICP-MS data revealed a statistically significant correlation ($r^2 = 0.44$, $p < 0.003$, $n = 18$) between the $\delta^{44/42}Ca$ values and Sr concentrations (Podlaha et al., 1995; Podlaha et al., 1998), which was not the case for TIMS data ($r^2 = 0.05$, $p = 0.3$, $n = 23$). The higher correlation coefficient for MC-ICP-MS is likely caused by isobaric interferences of double charged Sr ($^{88}Sr^{2+}$) on mass 44 (^{44}Ca) that can be generated in the high-energy plasma (Wieser et al., 2004). Therefore a complete quantitative separation of Sr from Ca is critical for a reliable determination of Ca isotope abundances via MC-ICP-MS. Nevertheless, the good agreement between the TIMS and MC-ICP-MS data ($r^2 = 0.65$, $p < 0.002$) indicates that the net effect of Sr interferences on the measured Ca isotope abundances was minor.

The significant correlation between $\delta^{44/40}Ca$ (TIMS) and $\delta^{44/42}Ca$ (MC-ICP-MS) values also proves that the documented ~0.5‰ variation in the belemnite $\delta^{44/40}Ca$ record is a result of mass-dependent fractionation and not due to an excess of radiogenic ^{40}Ca produced by ^{40}K decay (DePaolo, 2004; Marshall and DePaolo, 1989).

2.5.2 Diagenesis and $\delta^{44/40}Ca$

Only a few data are available on Ca isotope systematics during post-depositional alteration of marine carbonates. Nevertheless, laboratory experiments showed that diffusive transport of Ca under elevated temperatures and pressures driven by concentration gradients can generate a significant isotope fractionation (DePaolo, 2004; Richter et al., 2003). In addition, the preliminary data of Steuber and Buhl (2006) suggest

that the marine diagenetic alteration of skeletal carbonates tends to shift the $\delta^{44/40}Ca$ signatures of altered calcite towards heavier values. Therefore, diagenetic history and possible isotope resetting should be carefully evaluated when interpreting Ca isotope data from fossil materials.

The internal structure of belemnites is characterized by a complex architecture of concentrically oriented calcite prisms with a high degree, up to 10 vol.%, of internal porosity (Veizer, 1974). Pore spaces and domains enriched in organic matter are commonly filled with diagenetic calcite easily discernible by CL screening (Podlaha et al., 1998). Therefore, only areas with a bluish luminescence were sampled for the isotope investigations (Podlaha et al., 1995; 1998). According to generally accepted textural (SEM, CL) and chemical (Sr, Mn, Fe) parameters, the sampled material was considered well preserved, ruling out diagenetic resetting of the Ca isotope system. Brachiopod samples, modern and the Kimmeridgian, were drilled from interior layers of the shells that had trace element contents indicating a good preservation (Table 2.3).

2.5.3 Temperature effect on $\delta^{44/40}Ca$ of belemnite

Several recent studies (Skulan et al., 1997; Zhu et al., 1998; De La Rocha and DePaolo, 2000; Deyhle et al., 2002; Gussone et al., 2003; Bullen et al., 2003; Marriott et al., 2004; Immenhauser et al., 2005) proposed a temperature dependent Ca isotope fractionation in biogenic and inorganic carbonates, precipitated in natural marine environments and/or cultured under laboratory conditions, with a slope of about 0.02‰ ($\delta^{44/40}Ca$) $°C^{-1}$. This slope is identical for aragonite and calcite, however an offset of about 0.6‰ was documented for the two polymorphs, aragonite being isotopically lighter ($\delta^{44/40}Ca \approx 0.4‰$) than calcite ($\delta^{44/40}Ca \approx 1‰$), (Gussone et al., 2005).

The observed ~0.02‰ $°C^{-1}$ temperature dependency is, however, not consistent in all modern and fossil carbonates and may vary from ~0.001‰ $°C^{-1}$ (Sime et al., 2005) up to ~0.24‰ $°C^{-1}$ (Nägler et al., 2000), suggesting contribution of parameters other than temperature to the Ca isotope fractionation.

We tested the impact of temperature on the Ca isotope composition of belemnites by comparing their $\delta^{18}O$ and $\delta^{44/40}Ca$ values. The late Mesozoic $\delta^{18}O$ belemnite record (Podlaha et al., 1998) spans a range of ~4‰, suggesting approximately 10°C difference between the coolest and warmest sea-surface temperatures, but the $\delta^{18}O$ values showed a statistically insignificant correlation with $\delta^{44/40}Ca$ ($r^2 = 0.001$, $p = 0.86$, $n = 28$). Clearly, temperature did not have a major influence on the Ca isotope composition of belemnites, and processes other than temperature must be responsible for the documented ~0.5‰ variation in the belemnite $\delta^{44/40}Ca$ record.

The weak temperature dependency of the Ca isotope composition of belemnites, likely <0.02‰ $°C^{-1}$, makes their skeletal calcite a suitable recording phase to monitor secular changes in $\delta^{44/40}Ca_{SW}$.

2.5.4 *Determination of Ca isotope fractionation factor between seawater Ca and brachiopod/belemnite calcite*

In order to reconstruct the Ca isotope composition of the oceans from $\delta^{44/40}Ca$ of marine carbonates, one needs to know the fractionation factor between seawater Ca and a carbonate recording phase, assuming that the latter exhibits only weak temperature sensitivity. The Ca isotope fractionation factor $\alpha_{CC\text{-}SW}$ can be determined from:

$$\alpha_{CC\text{-}SW} = (\delta^{44/40}Ca_{CC} + 1000) / (\delta^{44/40}Ca_{SW} + 1000) \quad (2.1)$$

where $\delta^{44/40}Ca_{CC}$ and $\delta^{44/40}Ca_{SW}$ represent the Ca isotope compositions of the carbonate phase and seawater, respectively (cf. Heuser et al., 2005).

In our study, belemnite calcite was used as the recording phase for the $\delta^{44/40}Ca_{SW}$ evolution of the late Mesozoic oceans. Since belemnites are extinct organism, the $\alpha_{CC\text{-}SW}$ value needs to be determined indirectly. One approach is to compare the Ca isotope composition of fossil belemnites with other coeval skeletal carbonates, e.g. brachiopods, which are still present in the modern environment and thus can be used as a 'proxy' to determine the $\alpha_{CC\text{-}SW}$ value of extinct belemnites.

Firstly, the $\alpha_{CC\text{-}SW}$ value of the brachiopod calcite was determined from $\delta^{44/40}$Ca of modern East Pacific brachiopod, *Terebratalia transversa*, and present-day seawater (IAPSO), assuming a homogeneous Ca isotope composition of the oceans (Schmitt et al., 2001) and a weak 0.02‰ $°C^{-1}$ temperature dependence of brachiopods (Gussone et al., 2005). The calculated fractionation factor between seawater Ca and a brachiopod calcite ($\alpha_{CC\text{-}SW}$) is ~0.9991 (Table 2.3 and Fig. 2.3).

Secondly, the $\alpha_{CC\text{-}SW}$ value for the belemnite calcite was calculated from the Ca isotope composition of the Kimmeridgian belemnites and brachiopods that were collected from the same stratigraphic horizon (Table 2.3) and the $\alpha_{CC\text{-}SW}$ value of the brachiopod calcite, assuming that the latter has remained constant through time. The calculated fractionation factor between seawater Ca and a belemnite calcite ($\alpha_{CC\text{-}SW}$) is ~0.9986 (Fig. 2.3). Translated into $\delta^{44/40}$Ca values, the belemnite calcite is ~0.5‰ lighter than the brachiopod calcite, and ~1.4‰ lighter than ambient seawater.

Interestingly, the belemnite $\alpha_{CC\text{-}SW}$ value of ~0.9986 is identical with an 'equilibrium' fractionation factor determined by Lemarchand et al. (2004) in a laboratory experiment, ($\alpha_{CC\text{-}SW}$ = 0.9985 ± 0.0002). There is a disagreement, however, whether the latter value represents a kinetic or an equilibrium fractionation factor (Fantle, 2005; Steuber and Buhl, 2006). Regardless of its nature, the calculated $\alpha_{CC\text{-}SW}$ value of ~0.9986 can be used to reconstruct the Ca isotope evolution of the late Mesozoic oceans from the $\delta^{44/40}$Ca belemnite record.

2.5.5 Reconstruction of seawater Ca isotope variations during the late Mesozoic

The Ca isotope composition of the late Mesozoic seawater ($\delta^{44/40}Ca_{SW}$) was calculated based on Eq. 2.1 and the results are shown in Fig. 2.4. The $\delta^{44/40}Ca_{SW}$ was determined from the Ca isotope composition of belemnites using the $\alpha_{CC\text{-}SW}$ value of ~0.9986.

The reconstructed $\delta^{44/40}Ca_{SW}$ record indicates that the late Mesozoic oceanic Ca cycle was dynamic and experienced significant changes. The data imply that the Ca isotope composition of the Late Jurassic seawater was significantly, up to 0.4‰, lighter than

modern seawater (Fig. 2.4). The situation, however, changed through the Jurassic/Cretaceous transition when the reconstructed $\delta^{44/40}Ca_{SW}$ values show an increase from the Oxfordian/Kimmeridgian minimum of ~1.5‰ to the Hauterivian/Aptian maximum of ~1.9‰, interrupted by a single and relatively abrupt decline to ~1.7‰ during the Middle Barremian (Fig. 2.4). The resemblance between the $\delta^{44/40}Ca_{SW}$ values of modern and the inferred Hauterivian/Aptian seawater might suggest that the oceanic Ca budget during the latter period was similar to present-day one.

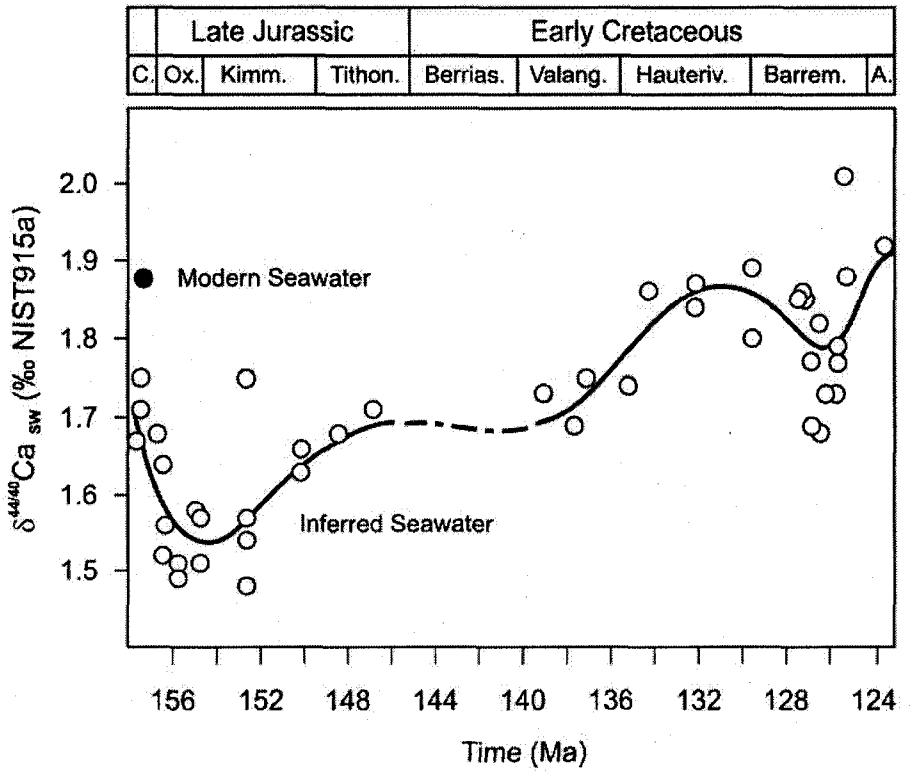

Fig. 2.4. The reconstructed Ca isotope composition of the Middle Jurassic to Early Cretaceous seawater ($\delta^{44/40}Ca_{SW}$) that was calculated from the belemnite $\delta^{44/40}$Ca record (open circles: TIMS and MC-ICP-MS) and using the Ca isotope fractionation factor between seawater Ca and the belemnite calcite ($\alpha_{CC\text{-}SW}$) of 0.9986 (Eq. 2.1). The solid line represents a smoothed moving average with a window of 3 Ma, and a filled circle represents the $\delta^{44/40}Ca_{SW}$ value of modern seawater.

2.5.6 Global Ca cycle from isotope perspective

The concentration and isotope composition of dissolved Ca in modern seawater is uniform and regulated mostly by the balance between incoming and outgoing Ca fluxes to the oceans and their isotope signatures (Schmitt et al., 2003a; De La Rocha and DePaolo, 2000; DePaolo, 2004). The Ca mass balance of the oceans can be simplistically defined as:

$$\frac{dCa}{dt} = F_{RIV} + F_{HY} + F_{DOLO} - F_{BC} - F_{ALT} \tag{2.2}$$

where F_{RIV} is the continental riverine and groundwater Ca flux, F_{HY} represents the hydrothermal Ca flux from mid-ocean ridges (MOR) as well as off-ridge centers, F_{DOLO} corresponds to the flux of Ca from dolomitization of marine carbonates, F_{BC} is the carbonate burial flux dominated by biogenic accumulation of marine carbonates, and F_{ALT} represents an uptake of Ca associated with inorganic carbonate precipitation during low-temperature alteration of oceanic crust (Heuser et al., 2005; DePaolo, 2004; Wallmann, 2001). The actual values of the above Ca fluxes (in Tmol/yr), as estimated for the Quaternary and modern marine Ca cycle, are presented in Table 2.4.

An isotope mass balance of the oceanic Ca cycle, where specific $\delta^{44/40}$Ca signatures are assigned to the individual fluxes, is represented by the following equation (Schmitt, 2003a; DePaolo, 2004):

$$N_{Ca}\frac{d\delta^{44/40}Ca_{SW}}{dt} =$$
$$F_{RIV}(\delta^{44}Ca_{RIV} - \delta^{44/40}Ca_{SW}) + F_{HY}(\delta^{44}Ca_{HY} - \delta^{44/40}Ca_{SW}) + F_{DOLO}(\delta^{44}Ca_{DOLO} - \delta^{44/40}Ca_{SW})$$
$$- F_{BC}(\delta^{44}Ca_{BC} - \delta^{44/40}Ca_{SW}) - F_{ALT}(\delta^{44}Ca_{ALT} - \delta^{44/40}Ca_{SW}) \tag{2.3}$$

where N_{Ca} is the number of moles of Ca in the oceans, and $\delta^{44}Ca_{RIV}$, $\delta^{44}Ca_{HY}$, $\delta^{44}Ca_{DOLO}$, $\delta^{44}Ca_{BC}$, $\delta^{44}Ca_{ALT}$ refer to the Ca isotope composition of the riverine,

hydrothermal, dolomitization, carbonate-burial and alteration flux, respectively (Table 2.4).

The secular variation in the Ca isotope composition of marine carbonates, reflecting the evolution of $\delta^{44/40}Ca_{SW}$, can be related to variations in the oceanic Ca cycle and used to quantify the oceanic Ca fluxes through geological time. This, however, requires not only detail characterization of the Ca isotope compositions and magnitudes of modern sources and sinks of Ca to the oceans (DePaolo, 2004), but also a good understanding of relationships between the global C and Ca cycles and their chemical interactions in marine and continental settings (Heuser et al., 2005).

Table 2.4.
Modern and the Quaternary oceanic Ca budget with major input and output fluxes (in Tmol/yr) and their isotope signatures ($\delta^{44/40}$Ca)

Description	Symbol	Ca flux	Ca flux		Ca isotope signature	Ca isotope signature
		Value (Tmol/yr) Wallmann (2001) [a]	Value (Tmol/yr) DePaolo (2004) [b]	Symbol	$\delta^{44/40}$Ca (‰) Heuser et al. (2005)	$\delta^{44/40}$Ca (‰) DePaolo (2004)
Oceanic Ca input						
Continental riverine weathering	F_{RIV}	11.7 – 13.6	20 – 36	$\delta^{44/40}Ca_{RIV}$	0.8 ± 0.2	0.65 ± 0.2
Hydrothermal release into oceans	F_{HY}	4.5 – 4.8	2 – 3	$\delta^{44/40}Ca_{HY}$	0.9 ± 0.2	0.9 ± 0.2
Release via dolomitization	F_{DOLO}	No data	No data	$\delta^{44/40}Ca_{DOLO}$	~0.3	No data
Total Ca input		16.2 – 18.4	22 – 39			
Oceanic Ca output						
Carbonate burial flux	F_{BC}	16 – 20	32	$\delta^{44/40}Ca_{BC}$	0.9 ± 0.3 (calcite) 0.5 ± 0.2 (aragonite)	0.5 ± 0.2 (nannofossil ooze)
Uptake via oceanic crust alteration	F_{ALT}	1.5 – 2.4	No data	$\delta^{44/40}Ca_{ALT}$	~0.9	No data
Total Ca output		17.5 – 22.4	~32			
Oceanic Ca balance (input –output)		-0.9 to -6.2	-7 to -10	$\delta^{44/40}Ca_{SW}$	1.88 ± 0.1	1.90 ± 0.1

[a] The Quaternary values of Ca fluxes from Wallmann (2001).
[b] Modern values of Ca fluxes from DePaolo (2004); the continental riverine flux (F_{RIV}) includes also diagenetic and groundwater flux of 3–5 and 5–16 Tmol/yr, respectively.

The $\delta^{44/40}$Ca signatures of modern continental-riverine and hydrothermal-marine Ca input fluxes are almost identical, within the analytical error, with mean values of ~0.7 ± 0.2‰ (Heuser et al., 2005; DePaolo, 2004) and 0.9 ± 0.2‰ (Schmitt et al., 2003a; Amini et al., 2006), respectively, and are not expected to change significantly through time. The average $\delta^{44/40}$Ca value of modern marine carbonates that represent a major sink of oceanic Ca is uniform at ~0.9 ± 0.3‰ for calcite, and at ~0.4 ± 0.2‰ for aragonite (Gussone et al., 2005; Heuser et al., 2005; DePaolo, 2004). With these isotope and flux constraints, and a classical box model for oceanic Ca cycle, Schmitt et al. (2003a) concluded that the modern oceanic Ca budget is at or close to steady state with respect to Ca concentrations and isotopes.

As a consequence of the isotope uniformity of modern oceanic Ca fluxes and reservoirs, any change in $\delta^{44/40}Ca_{SW}$ exceeding ~0.2‰ likely results from changes in the intensity of Ca fluxes, rather than from shifts in their $\delta^{44/40}$Ca signatures. For example, an enhanced intensity of the hydrothermal Ca flux to modern oceans, lasting at least ~1.5 Ma (τ_{Ca}), would eventually shift $\delta^{44/40}Ca_{SW}$ to lower values, as the Ca isotope composition of hydrothermal fluids is significantly (~1‰) lighter than that of present-day seawater (Amini et al., 2006). Higher F_{HY} would also increase the concentration of Ca in seawater, since typical hydrothermal fluids have Ca levels of ~30 mmol/kg H_2O (Amini et al., 2006) compared to 10.24 mmol/kg H_2O in modern seawater (de Villiers and Nelson, 1999).

The Ca mass balance modeling of Berner (2004) that was extended to marine Ca isotope system by Heuser et al. (2005) implies, however, that an analogous increase in Ca flux to the oceans from continental weathering (F_{RIV}) would cause no significant changes to the oceanic Ca inventory and its isotope composition. This is because the riverine Ca flux, unlike F_{HY}, is closely coupled to carbonate ion (HCO_3^-, CO_3^{2-}) flux, which is supplied primarily from continental weathering of carbonate rocks. Rivers discharge Ca and carbonate ions to the oceans in approximately equal proportions, with the mean Ca^{2+}/HCO_3^- ratio of ~0.45 ± 0.4‰ (2σ), (Gaillardet et al., 1999). Local anomalies in the riverine Ca^{2+}/HCO_3^- ratio, resulting from a specific lithology of a drainage area, are expected and may range from ~0.2 for silicate-dominated terrains to more than ~0.5 for volcanic areas (Heuser et al., 2005; Gaillardet et al., 1999).

A direct consequence of the Ca^{2+}/HCO_3^- coupling in F_{RIV} would be that an increase in F_{RIV} would also temporarily (within ~0.1Ma, the residence time of carbonate ions in seawater; Broecker, 2003) increase the $CaCO_3$ saturation state of the oceans (Ω), as this is primarily controlled by the concentration of Ca^{2+} and CO_3^{2-} in seawater. Higher Ω facilitates $CaCO_3$ precipitation and accumulation, and thus removal of Ca from the oceans (F_{BC}). Therefore, an increase in the Ca flux to the oceans from F_{RIV} is eventually being balanced by an enhanced removal of Ca from the oceans via F_{BC}.

A prolonged increase in F_{BC} would, however, gradually lower Ω and the oceans would eventually become undersaturated with respect to $CaCO_3$, leading to dissolution of marine carbonates and reduction of F_{BC}. This is partly because the formation of $CaCO_3$ also releases CO_2 into seawater, based on the following equation:

$$Ca^{2+} + 2HCO_3^- = CaCO_3 + H_2O + CO_2 \tag{2.4}$$

The dissolved CO_2 reacts with H_2O producing H_2CO_3, carbonic acid, which dissociates into H^+ and HCO_3^- ions. The H^+ combines with available CO_3^{2-} forming HCO_3^- (cf. Zeebe and Wolf-Gladrow, 2001). Hence, the net effect of $CaCO_3$ precipitation is to increase concentrations of H^+ and HCO_3^- while decreasing the concentration of CO_3^{2-} in seawater, which lowers Ω and eventually promotes $CaCO_3$ dissolution and reduction of F_{BC}.

As a result, the Ca concentration and isotope composition of the oceans can only be changed significantly by altering the Ca input fluxes that are decoupled from the carbonate ion fluxes, such as the hydrothermal flux (F_{HY}) or the dolomite formation (F_{DOLO}), (Heuser et al., 2005; Berner, 2004). In contrast, variations in the continental weathering (F_{RIV}) or carbonate burial (F_{BC}) fluxes would, on a longer time-scale, produce no significant changes to the marine Ca inventory and to its isotope composition, as F_{RIV} and F_{BC} have a profound effect on the $CaCO_3$ saturation state of the oceans. Consequently, any

long-term changes in Ca flux intensity of F_{RIV} and/or F_{BC} are effectively compensated by precipitation and dissolution of $CaCO_3$ in the oceans (cf. Heuser et al., 2005; Berner, 2004). In principle, however, it is also possible to alter the seawater Ca concentrations and $\delta^{44/40}Ca_{SW}$ by changing the Ca^{2+}/HCO_3^- ratio of global riverine discharge (Heuser et al., 2005).

The majority of published studies (Skulan et al., 1997; Zhu et al., 1998; De La Rocha and DePaolo, 2000; Schmitt et al., 2003a, b; Kasemann et al., 2005; Fantle and DePaolo, 2005), however, advocates a simple model of oceanic Ca cycle (cf. DePaolo, 2004), without considering the close coupling of the oceanic Ca and C cycles. In this approach, variations in $\delta^{44/40}Ca_{SW}$ are attributed to imbalances between oceanic Ca input and output fluxes (F_{IN}/F_{OUT}), these usually linked to carbonate ion fluxes, as Ca input is frequently represented by F_{RIV} and Ca removal by F_{BC}.

2.5.7 Model simulation of late Mesozoic Ca isotope ($\delta^{44/40}Ca_{SW}$) record

We used a slightly modified Ca isotope-mass balance approach of Heuser et al. (2005) to simulate the evolution of $\delta^{44/40}Ca_{SW}$ during the late Mesozoic. The model input data are the oceanic Ca fluxes: $F_{RIV}, F_{HY}, F_{DOLO}, F_{BC}$ and F_{ALT} associated with $\delta^{44/40}$Ca signatures (Table 2.4). The model output data, simulated $\delta^{44/40}Ca_{SW}$ values, were calculated using Eq. 2.3 and the above input data. The best fit between the experimental data and a model simulation was achieved by exploring multiple scenarios for the past oceanic Ca budget with variable flux intensities. Two scenarios are presented in this study, and both were generated via altering the oceanic Ca fluxes that are decoupled from carbonate ion fluxes (Heuser et al., 2005), while the $\delta^{44/40}$Ca signatures of individual fluxes were prescribed to match the modern values (see auxiliary material, Tables A.2.1 and A.2.2).

Scenario 1: The $\delta^{44/40}Ca_{SW}$ controlled via hydrothermal Ca flux

In the first scenario, it is assumed that the Ca isotope variation in the belemnite record was produced exclusively due to changes in the hydrothermal Ca flux, while the

remaining fluxes were kept constant at modern levels (see auxiliary material, Table A.2.1). The late Mesozoic flux of Ca to the oceans derived from F_{HY} experienced an almost threefold decrease, from the Late Jurassic maximum of 13.5 Tmol (10^{+12} mol) of Ca per year to the Early Cretaceous value of 4.8 Tmol/yr to (Fig. 2.5c, dashed line).

The input of Ca to the oceans via F_{HY} is controlled by the following basalt-seawater exchange reaction (Berner, 2004):

$$Mg^{2+} + Ca\text{-}basalt \Rightarrow Ca^{2+} + Mg\text{-}basalt \quad (2.5)$$

where MOR-hydrothermal fluids exchange Ca from basalts for Mg in seawater, a process that would eventually increase marine Ca concentrations, simultaneously lowering the $\delta^{44/40}Ca_{SW}$ (Fig. 2.5a, dashed line).

Scenario 2: The $\delta^{44/40}Ca_{SW}$ controlled by dolomitization and hydrothermal Ca flux

In the second scenario, the model considers a combined flux of Ca to the oceans supplied from two distinct sources: dolomite formation (F_{DOLO}) and basalt-seawater reactions (F_{HY}), (Eq. 2.5). The intensities of remaining oceanic Ca fluxes were kept constant and close to modern values (see auxiliary material). The flux of Ca supplied from F_{DOLO} is produced via cation-exchange processes during dolomitization of marine carbonates (cf. Berner, 2004):

$$2CaCO_3 + Mg^{2+} \Rightarrow MgCa(CO_3)_2 + Ca^{2+} \quad (2.6)$$

where diffusion and dissolution-precipitation reactions exchange Ca in carbonates for Mg in seawater. The net effect of dolomitization would therefore be an increase in marine Ca concentrations, likely accompanied by a decrease in $\delta^{44/40}Ca_{SW}$ (Heuser et al., 2005). The latter is expected, as preliminary data suggest that Ca released from F_{DOLO} should have light $\delta^{44/40}$Ca signatures of ~0.3‰ (Table 2.4) (Heuser et al., 2005).

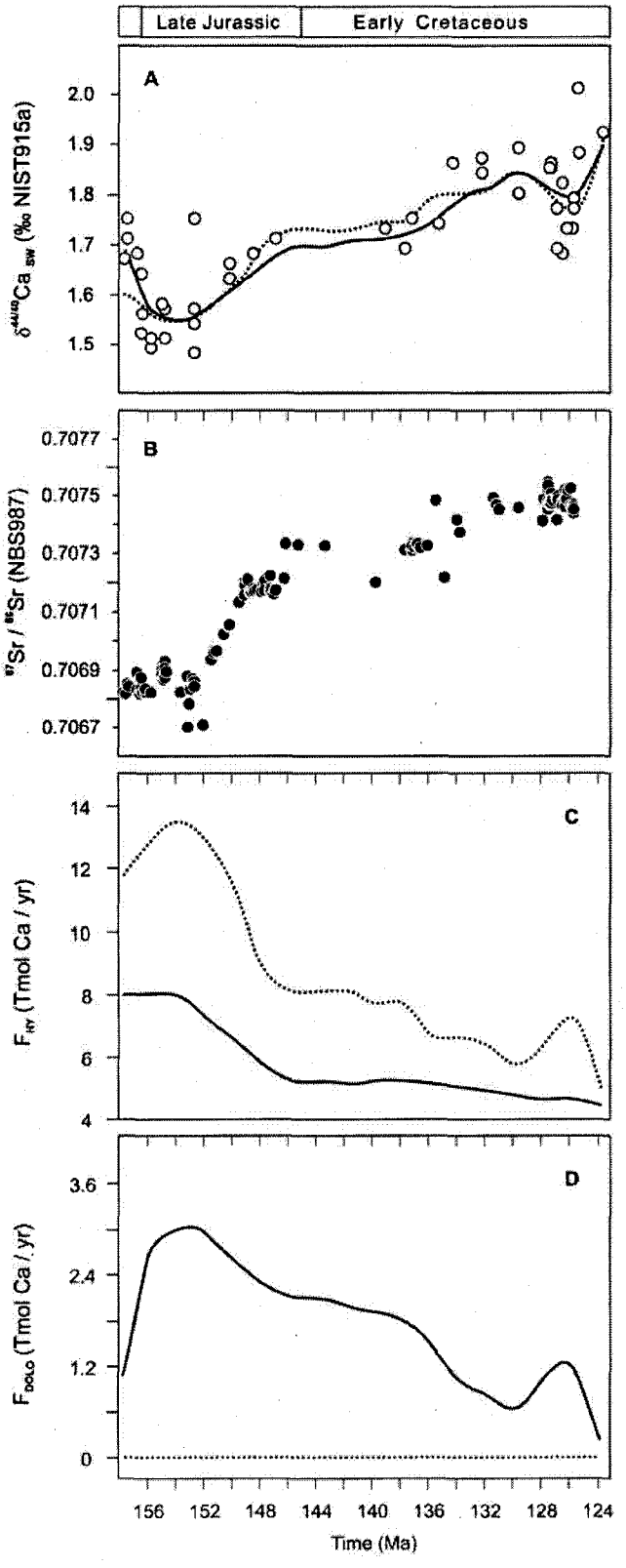

Fig. 2.5. Summary of model simulation results with the Ca isotope experimental data. (A) Evolution of Ca isotope composition of the late Mesozoic seawater ($\delta^{44/40}Ca_{SW}$) as determined from Ca isotope experimental data (open circles: calculated from $\delta^{44/40}$Ca of belemnites and $\alpha_{CC\text{-}SW}$) and reconstructed by model simulations (dashed and solid lines). The dashed line (also in C and D) represents model simulation for the first scenario, where variations in $\delta^{44/40}Ca_{SW}$ were produced exclusively by altering the hydrothermal Ca flux, F_{HY}. The solid line shows results for the second scenario (also in C and D), where changes in $\delta^{44/40}Ca_{SW}$ were simulated via combined variations in F_{HY} and dolomite formation, F_{DOLO}. (B) The secular evolution of marine $^{87}Sr/^{86}Sr$ record during the late Mesozoic; data from Veizer et al. (1999). (C) The rate of Ca release to the oceans supplied by MOR-hydrothermal flux. (D) The intensity of Ca flux to the oceans produced via dolomitization of marine carbonates.

During the model simulation, the intensity of F_{HY} was decreased approximately twofold, from the Middle/Late Jurassic levels of 8 Tmol of Ca/yr to the Early Cretaceous value of 4.4 Tmol/yr (Fig. 2.5c, solid line). The intensity of F_{HY} was parameterized based on a coeval marine $^{87}Sr/^{86}Sr$ record (Fig. 2.5b; Veizer et al., 1999), so that F_{HY} would be a mirror image of the $^{87}Sr/^{86}Sr$ trend.

This approach was adopted as the $^{87}Sr/^{86}Sr$ proxy is expected to be sensitive to changes in the MOR-hydrothermal activity, reflecting a balance between essentially two Sr fluxes: the continental-riverine and hydrothermal-marine flux (e.g. Faure, 1986; Ravizza and Zachos, 2003). Simultaneously, the intensity of F_{DOLO} was also adjusted (Fig. 2.5d, solid line) to generate a best fit between the simulated $\delta^{44/40}Ca_{SW}$ values and the experimental Ca isotope data (Fig. 2.5a, solid line vs. open circles). The amount of Ca released from F_{DOLO} was variable, but in general showed a decrease from the Late Jurassic maximum of 3 Tmol/yr to the Early Cretaceous value of 0.2 Tmol/yr.

2.5.8 The $\delta^{44/40}Ca_{SW}$ record compared to other geochemical proxies

If the Ca isotope variations in the late Mesozoic belemnites indeed reflect the evolution of oceanic Ca cycle, hence changes in seawater Ca concentrations, then other proxies sensitive to perturbations in major-ion seawater chemistry, such as Mg/Ca or Sr/Ca ratios of marine halite fluid inclusions and skeletal carbonates should show patterns coherent with the $\delta^{44/40}Ca_{SW}$ record.

2.5.8.1 Marine halite fluid inclusion data compared to $\delta^{44/40}Ca_{SW}$ record

Our data suggest that the $\delta^{44/40}Ca_{SW}$ value of the Middle/Late Jurassic seawater was up to 0.4% lighter than modern seawater, most likely due to an increased flux of isotopically lighter Ca to the oceans supplied by F_{HY}, and possibly F_{DOLO}. This scenario of elevated marine Ca concentrations during the Middle/Late Jurassic is in agreement with a single available fluid inclusion data representing the Late Jurassic period (~150 Ma), (Fig. 2.6a), which also indicates high seawater Ca concentration of ~23 ± 3 mmol/kg H_2O

(Horita et al., 2002). The inferred Early Cretaceous $\delta^{44/40}Ca_{SW}$ record, suggesting oceanic Ca budget and marine Ca concentrations close to modern ones are, however, at odds with some of the model simulations that indicate seawater Ca concentrations up to ~45 mmol/kg H_2O (Fig. 2.6a), (cf. Hardie, 1996; Wallmann, 2001). Considering that no high-quality fluid inclusion data exist for the investigated Early Cretaceous period (~145 to 125 Ma), these high model estimates may be viewed as tentative, unless validated by empirical observations. Note that the stratigraphically closest fluid inclusion data are dated at ~118 ± 6 Ma and these show seawater Ca concentrations of ~35 ± 4 mmol/kg H_2O (Lowenstein et al., 2003), (Fig. 2.6a).

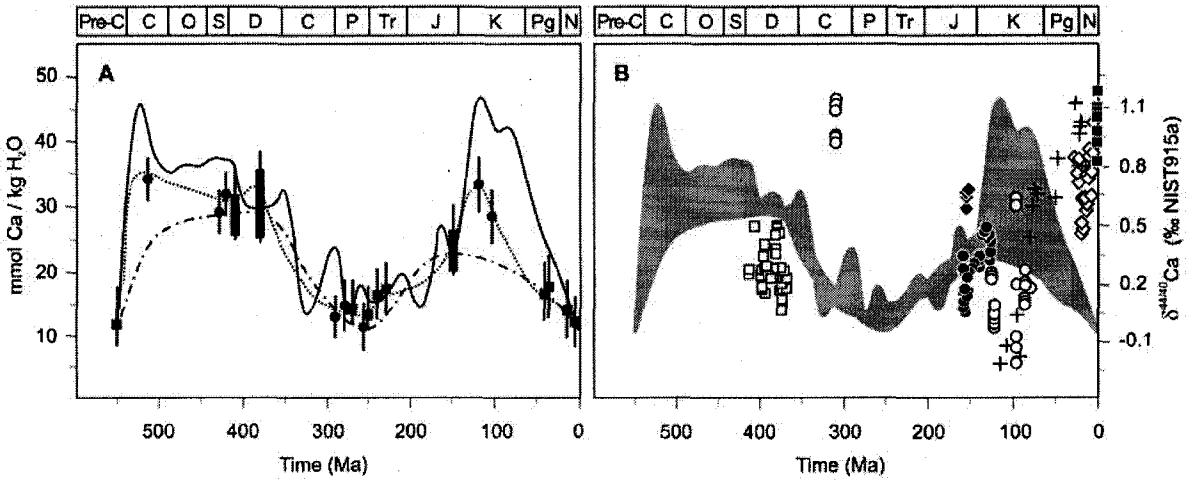

Fig. 2.6. (A) Compilation of model simulations (solid line: Hardie, 1996) and experimental fluid inclusion data (dotted line/filled circles: Lowenstein et al., 2003; dashed-dotted line/filled rectangles: Horita et al., 2002) of seawater Ca concentrations during the Phanerozoic. These are compared to contemporary $\delta^{44/40}$Ca record (B) based on marine skeletal carbonates (filled squares: Gussone et al., 2005; open diamonds: Heuser et al., 2005; open circles: Steuber and Buhl, 2006; filled circles/diamonds: this study; open squares: Böhm et al., 2004) and authigenic marine phosphates (crosses: Soudry et al., 2004). The shaded area (B) reflects the variation in seawater Ca concentrations as showed in part A of the Fig. 2.6. The following abbreviations are used (in left-right order): Pre-C = Precambrian; C = Cambrian; O = Ordovician; S = Silurian; D = Devonian; C = Carboniferous; P = Permian; Tr = Triassic; J = Jurassic; K = Cretaceous; Pg = Paleogene; N = Neogene.

In order to evaluate the potential of Ca isotopes as a proxy for secular variations of seawater Ca concentration, we compiled the available Phanerozoic Ca isotope data measured in marine carbonates and phosphates (Fig. 2.6b) and compared them to seawater Ca concentrations estimated from Phanerozoic marine halite fluid inclusions and from model simulations (Fig. 2.6a,b). Over the Phanerozoic, there is an obvious pattern of inverse covariance between marine $\delta^{44/40}Ca$ record and estimated seawater Ca concentrations (Fig. 2.6), suggesting that Ca isotopes could indeed become a valuable tool for constraining secular changes in marine Ca concentrations during geological history.

2.5.8.2 Elemental (Mg/Ca and Sr/Ca) ratios of marine carbonates and $\delta^{44/40}Ca_{SW}$

The Mg/Ca (mol/mol) ratio of the Middle/Late Jurassic (~160 Ma) seawater of ~1.3 ± 0.3 that was reconstructed from fossil echinoderms (Dickson, 2002 and 2004) is slightly lower than the Early Cretaceous (~130 Ma) value of ~1.8 ± 0.2. This most likely reflects higher seawater Ca concentrations, relative to Mg, during the Middle/Late Jurassic period. Similarly, the late Mesozoic Sr/Ca (mmol/mol) ratio of seawater, estimated from the elemental abundances in belemnites and rudists, shows a gradual increase from the Late Jurassic (~155 Ma) Sr/Ca minimum of ~8 ± 1 to the Early Cretaceous (~130 Ma) values of ~10 ± 1.5 (Steuber and Veizer, 2002). This secular shift in marine Sr/Ca ratio can also be explained by higher seawater Ca concentration, relative to Sr, during the Middle/Late Jurassic and its gradual decline through the Early Cretaceous.

2.6 Summary and Conclusions

This study investigated the magnitude and systematics of Ca isotope variation in the late Mesozoic skeletal carbonates with an intention to test the potential of Ca isotopes as a proxy for paleoceanographic studies. The outcome can be summarized as follows:

1. The statistically insignificant correlation between $\delta^{18}O$ and $\delta^{44/40}Ca$ values of belemnites ($r^2 = 0.001$, $p = 0.86$) suggests that the temperature dependency of Ca isotope composition of belemnites is weak, likely < 0.02‰ $°C^{-1}$. This makes their

skeletal $CaCO_3$ a suitable recording phase for monitoring secular changes in the isotope composition of paleo-seawater.

2. The $\delta^{44/40}$Ca record of the Middle Jurassic to Early Cretaceous belemnites (Fig. 2.2) coupled with an empirically determined fractionation factor ($\alpha_{CC\text{-}SW}$) of ~0.9986 (Fig. 2.3), was used to reconstruct the evolution of Ca isotope composition of the late Mesozoic seawater ($\delta^{44/40}Ca_{SW}$).
3. The inferred $\delta^{44/40}Ca_{SW}$ record (Fig. 2.4) shows a systematic long-term variation of ~0.5‰ magnitude with the Middle/Late Jurassic (~154 Ma) minimum of ~1.4‰ followed by a gradual increase to the Early Cretaceous (~124 Ma) maximum of ~1.9‰, the latter being similar to Ca isotope composition of present-day seawater.
4. The global nature of the $\delta^{44/40}Ca_{SW}$ record is supported by an identical Ca isotope composition of the Kimmeridgian belemnites ($\delta^{44/40}$Ca = 0.15 ± 0.14‰, n = 4) collected from two distinct paleogeographic regions, the southern (New Zealand) and the northern (Germany) margins of the Tethys Ocean (Fig. 2.1).
5. Model simulations of the oceanic Ca cycle clearly show that the observed variation in the $\delta^{44/40}$Ca belemnite record can be produced by varying the input fluxes of Ca to the oceans that are independent of carbonate ion fluxes, such as the hydrothermal flux of Ca and/or the release of Ca via dolomitization (Fig. 2.5a,c,d).
6. The importance of hydrothermal control on the late Mesozoic $\delta^{44/40}Ca_{SW}$ record is, to a degree, corroborated by the statistically significant positive correlation between the $\delta^{44/40}$Ca and $^{87}Sr/^{86}Sr$ values of the late Mesozoic belemnites (r^2 = 0.58, $p < 0.0001$, n = 29; Fig. 2.5a,b), the latter a proxy of MOR-volcanic activity and of the hydrothermal flux of Sr to the oceans.
7. A covariance pattern of Phanerozoic marine $\delta^{44/40}$Ca record and seawater Ca concentrations (Fig. 2.6a,b), as estimated from marine halite fluid inclusions and/or geochemical models, implies that Ca isotopes have the potential to become a valuable tool for constraining the intensity of oceanic Ca fluxes during geological history.

Acknowledgements

This research was funded by the Natural Sciences and Engineering Research Council of Canada and the German Research Foundation (NSERC and DFG research grants to J. Veizer), and partially supported by the Geological Society of America (2003/2004 GSA graduate student research grants to J. Farkaš). The technical laboratory assistance of M. Wilk, S. Carr and B. Cousens from Ottawa (OCGC-IGGRC) is greatly acknowledged. Many thanks to A. Tomašovych (University of Wuerzburg) who promptly provided the Kimmeridgian (brachiopod/belemnite) and modern (brachiopod) samples. We also thanks to A. Paytan (Standford, CA) and particularly to A. Eisenhauer (Kiel, IFM-GEOMAR), who provided detailed and constructive comments that helped to improve the manuscript and our understanding of the marine Ca and C cycle. This study is IGGRC contribution No. 43.

References

Amini M., Eisenhauer A., Böhm F., Fietzke J., Bock B., Grabe-Schönberg D., Lackschewitz K.S. and Hauff F. (2006) Calcium isotope variations along the hydrothermal pathway, *Geoph. Res. Abstr.* **8**, 08864, SRef-ID: 1607-7962/gra/EGU06-A-08864.

Berner R.A. (2004) A model for Calcium, Magnesium and Sulfate in seawater over Phanerozoic, *Am. J. Sci.* **304**, 438–453.

Böhm F., van Geldern R., Gussone N. and Eisenhauer A. (2004) Calcium isotope variation in Devonian brachiopods, 2.7.P08, *Geochim. Cosmochim. Acta* **68/11** Suppl.1, A213, Copenhagen.

Broecker W.S., The oceanic $CaCO_3$ cycle, In: The oceans and marine geochemistry (ed. H. Elderfield) Vol. 6, Treatise on geochemistry (eds. H.D. Holland and K.K. Turkenian), Elsevier-Pergamon, Oxford, 2003, pp. 529–547.

Bullen T.D., Kim S.-T., Paytan A. (2003) Ca isotope fractionation during Ca-carbonate precipitation: There's more to it than temperature, *Geochim. Cosmochim. Acta* **67,** Suppl. 1, A049.

Coplen T.B., Böhlke J.K., De Bièvre P., Ding T., Holden N.E., Hopple J.A., Krouse H.R., Lamberty A., Peiser H.S., Révész K., Rieder S.E., Rosman K.J.R., Roth E., Taylor

P.D.P., Vocke R.D.Jr. and Xiao Y.K. (2002) Isotope-abundance variations of selected elements (IUPAC Technical Report), *Pure Appl. Chem.* **74**, 1987–2017.

Criss R.E., Principles of stable isotope distribution, Oxford University Press, New York, 1999.

De La Rocha C.L. and DePaolo D.J. (2000) Isotopic evidence for variations in the marine calcium cycle over the Cenozoic, *Science* **289**, 1176–1178.

de Villiers S. and Nelson B.K. (1999) Detection of low-temperature hydrothermal fluxes by seawater Mg and Ca anomalies, *Science* **285**, 721–723.

DePaolo D.J. (2004) Calcium isotopic variations produced by biological, kinetic, radiogenic and nucleosynthetic processes, in: C.M. Johnson, B.L. Beard, F. Albarede (Eds.), Geochemistry of non-traditional stable isotopes, Rev. Mineral. Geochem. 55, Washington, D.C., 2004, pp. 255–288.

Deyhle A., MacDougall J.D., Macissac C. and Paytan A. (2002) Temperature dependence of Ca isotope fractionation in marine carbonates. *Geochim. Cosmochim. Acta* **66,** 15A, A181.

Dickson J.A.D. (2002) Fossil echinoderms as a monitor of the Mg/Ca ratio of Phanerozoic oceans, *Science* **298**, 1222–1224.

Dickson J.A.D. (2004) Echinoderm skeletal preservation: calcite-aragonite seas and the Mg/Ca ratio of Phanerozoic oceans, *J. Sedim. Res.* **74**, 355–365.

Eisenhauer A., Nägler T.F., Stille P., Kramers J., Gussone N., Bock B., Fietzke J., Hippler D. and Schmitt A.-D. (2004) Proposal for international agreement on Ca notation resulting from discussion at workshops on stable isotope measurements held in Davos (Goldschmidt 2002) and Nice (EGS-AGU-EUG 2003), *Geostand. Newsl.* **28**, 149–151.

Fantle M.S. (2005) The global geochemical cycles of iron and calcium: using novel isotope systems to understand weathering, global mass budgets, natural reaction rates, and paleoclimate, Doctoral dissertation, University of California.

Fantle M.S. and DePaolo D.J. (2005) Variations in the marine Ca cycle over the past 20 million years, *Earth Planet. Sci. Lett.* **237**, 102–117.

Faure G., Principles of isotope geology, Second edition, John Wiley & Sons, 1986, pp. 589

Gaillardet J., Dupré B., Louvat P. and Allègre C.J. (1999) Global silicate weathering and CO_2 consumption rates deduced from the chemistry of large rivers, *Chem. Geol.* **159**, 3–30.

Gradstein F. M., Agterberg F. P., Ogg J. G., Hardenbol J., van Veen P., Thierry T. and Huang Z. (1994) A Mesozoic time scale. *J. Geophys. Res.* **99**, 24051–24074.

Gradstein F.M., Ogg J.G., Smith A.G., Agterberg F.P., Bleeker W., Cooper R.A., Davydov V., Gibbard P., Hinnov L., House M.R., Lourens L., Luterbacher H-P., McArthur J., Melchin M.J., Robb L.J., Shergold J., Villeneuve M., Wardlaw B.R., Ali J., Brinkhuis H., Hilgen F.J., Hooker J., Howarth R.J., Knoll A.H., Laskar J., Monechi S., Powell J., Plumb K.A., Raffi I., Röhl U., Sanfilippo A., Schmitz B., Shackleton N.J., Shields G.A., Strauss H., Van Dam J., Veizer J., van Kolfschoten Th. and Wilson D.. A Geologic time scale, Cambridge Univ. Press, Cambridge, 2004.

Gussone N., Böhm F., Eisenhauer A., Dietzel M., Heuser A., Teichert B.M.A., Reitner J., Wörheide G. and W.-Ch. Dullo (2005) Calcium isotope fractionation in calcite and aragonite, *Geochim. Cosmochim. Acta* **69**, 4485–4494.

Gussone N., Eisenhauer A., Heuser A., Dietzel M., Bock B., Böhm F., Spero H.J., Lea D.W., Bijma J. and Nägler T.F. (2003) Model for kinetic effects on calcium isotope fractionation ($\delta^{44}Ca$) in inorganic aragonite and cultured planktonic foraminifera, *Geochim. Cosmochim. Acta* **67**, 1375–1382.

Hardie L.A. (1996) Secular variation in seawater chemistry: an explanation for the coupled secular variation in the mineralogies of marine limestones and potash evaporites over the past 600 m.y., *Geology* **24**, 279–283.

Harland W.B., Armstrong R.L., Cox A.V., Craig L.E., Smith A.G. and Smith D.G., A Geologic Time Scale, Cambridge Univ. Press, Cambridge, 1990.

Heuser A., Eisenhauer A., Böhm F., Wallmann K., Gussone N., Pearson P.N., Nägler T.F. amd Dullo W.-Ch. (2005) Calcium isotope ($\delta^{44/40}Ca$) variations of Neogene planktonic foraminifera, *Paleoceanography* **20** PA2013, doi:10.1029/2004PA001048.

Heuser A., Eisenhauer A., Gussone N., Bock B., Hansen B.T. and Nägler T.F. (2002) Measurement of calcium isotopes ($\delta^{44/40}Ca$) using a multicollector TIMS technique, *Int. J. Mass. Spectrom.* **220**, 387–399.

Hippler D., Schmitt A.-D., Gussone N., Heuser A., Stille P., Eisenhauer A. and Nägler T.F. (2003) Ca isotopic composition of various standards and seawater, *Geostand. Newslett.* **27**, 13–19.

Holland H.D., The Chemistry of the Atmosphere and Oceans, Wiley, New York. 1978.

Horita J., Zimmermann H. and Holland H.D. (2002) Chemical evolution of seawater during the Phanerozoic: Implications from the record of marine evaporates, *Geochim. Cosmochim. Acta* **66**, 3733–3756.

Immenhauser A., Nägler T.F., Steuber T. and Hippler D. (2005) A critical assessment of mollusk $^{18}O/^{16}O$, Mg/Ca, and $^{44}Ca/^{40}Ca$ ratios as proxies for Cretaceous seawater temperature seasonality, *Palaeogeogr. Palaeoclimatol. Palaeoecol.* **215**, 221–237.

Kampschulte A. (2001) Sulfur isotope investigations of structurally substituted sulfate of Phanerozoic carbonates: Implications for chemical evolution of seawater, Doctoral dissertation (in German), Ruhr University Bochum.

Kampschulte A. and Strauss H. (2004) The sulfur isotopic evolution of Phanerozoic seawater based on the analysis of structurally substituted sulfate in carbonates, *Chem. Geol.* **204**, 255–286.

Kasemann S.A., Hawkesworth Ch.J., Pravec A.R., Fallick A.E. and Pearson P.N. (2005) Boron and calcium isotope composition in Neoproterozoic carbonate rocks from Namibia: evidence for extreme environmental change, *Earth Planet. Sci. Lett.* **231**, 73–86.

Lemarchand D., Wasserburg G.J. and Papanastassiou D.A. (2004) Rate-controlled calcium isotope fractionation in synthetic calcite, *Geochim. Cosmochim. Acta* **68**, 4665–4678.

Lowenstein T.K., Hardie L.A., Timofeeff M.N. and Demicco R.V. (2003) Secular variations in seawater chemistry and the origin of calcium chloride basinal brines, *Geology* **31**, 857–860.

Marriott C.S., Henderson G.M., Belshaw N.S. and Tudhope A.W. (2004) Temperature dependence of δ^7Li, δ^{44}Ca and Li/Ca during growth of calcium carbonate, *Earth Planet. Sci. Lett.* **222**, 615–624.

Marshall B.D. and DePaolo D.J. (1989) Calcium isotopes in igneous rocks and the origin of granite, *Geochim. Cosmochim. Acta* **53**, 917–922.

Nägler T.F. and Villa I.M. (2000) In pursuit of the ^{40}K branching ratios: K-Ca and ^{39}Ar–^{40}Ar dating of gem silicates, *Chem. Geol.* **169**, 5–16.

Nägler T.F., Eisenhauer A., Müller A., Hemleben C. and Kramers J. (2000) δ^{44}Ca-temperature calibration on fossil and cultured *Globigerinoides sacculifer:* New tool for reconstruction of past sea surface temperatures, *Geochem. Geophys. Geosyst.* **1** doi:10.1029/2000GC000091.

Podlaha O.G. (1995) Model calculations on the basis of high-resolution isotope stratigraphy (Sr, C, O) of the Jurassic and Lower Cretaceous (Bajoc-Apt.) period, Doctoral dissertation (in German), Ruhr University Bochum.

Podlaha O.G., Mutterlose J. and Veizer J. (1998) Preservation of δ^{18}O and δ^{13}C in belemnite rostra from the Jurassic/early Cretaceous successions, *Am. J. Sci.* **298**, 324–347.

Ravizza G.E. and Zachos J.C., Records of Cenozoic ocean chemistry, In: The oceans and marine geochemistry (ed. H. Elderfield) Vol. 6, Treatise on geochemistry (eds. H.D. Holland and K.K. Turkenian), Elsevier-Pergamon, Oxford, 2003, pp. 551–577.

Richter F.M., Davis A.M., DePaolo D.J. and Watson E.B. (2003) Isotope fractionation by chemical diffusion between molten basalt and rhyolite, *Geochim. Cosmochim. Acta* **67**, 3905–3923.

Russell W.A. and Papanastassiou D.A. (1978) Isotope fractionation in ion exchange columns, *Anal. Chem.* **50**, 1151–1154.

Russell W.A., Papanastassiou D.A. and Tombrello T.A. (1978) Ca isotope fractionation on the Earth and other solar system materials, *Geochim. Cosmochim. Acta* **42**, 1075–1090.

Schmitt A.-D., Bracke G., Stille P. and Kiefel B. (2001) The calcium isotope composition of modern seawater determined by thermal ionization mass spectrometry, *Geostand. Newslett.* **25**, 267–275.

Schmitt A.-D., Chabaux F. and Stille P. (2003a) The calcium riverine and hydrothermal isotopic fluxes and the oceanic calcium mass balance, *Earth Planet. Sci. Lett.* **213**, 503–518.

Schmitt A.-D., Stille P. and Vennemann T. (2003b) Variations of the $^{44}Ca/^{40}Ca$ ratio in seawater during the past 24 million years: Evidence from $\delta^{44}Ca$ and $\delta^{18}O$ values of Miocene phosphates, *Geochim. Cosmochim. Acta* **67**, 2607–2614.

Sime N.G., De La Rocha C.L. and Galy A. (2005) Negligible temperature dependence of calcium isotope fractionation in 12 species of planktonic foraminifera, *Earth Planet. Sci. Lett.* **232**, 51–66.

Skulan J.L., DePaolo D.J. and Owens T.L. (1997) Biological control of calcium isotopic abundances in the global calcium cycle, *Geochim. Cosmochim. Acta* **61**, 2505–2510.

Soudry D., Segal I., Nathan Y., Glenn C.R., Halicz L., Lewy Z. and VonderHaar D.L. (2004) $^{44}Ca/^{42}Ca$ and $^{143}Nd/^{144}Nd$ isotope variations in Cretaceous-Eocene Tethyan francolites and their bearing on phosphogenesis in the southern Tethys, *Geology* **32**, 389–392.

Steuber T. and Buhl D. (2006) Calcium-isotope fractionation in modern and ancient marine carbonates, *Geochim. Cosmochim. Acta* **70**, 5507–5521.

Steuber T. and Veizer J. (2002) Phanerozoic record of plate tectonic control of seawater chemistry and carbonate sedimentation, *Geology* **30**, 1123–1126.

Tuttas D. and Schwieters J., Advances in high precision isotope ratio measurements of calcium using TIMS, Triton – Thermo Electron Application Flash Report No. T4. 2002.

Veizer J. (1974) Chemical diagenesis of belemnite shell and possible consequences for paleotemperature determinations, *Neu. Jahrb. Geol. Paleont.* **147**, 91–111.

Veizer J., Ala D., Azmy K., Bruckschen P., Buhl D., Bruhn F., Carden G.A.F., Diener A., Ebneth S., Godderis Y., Jasper T., Korte Ch., Pawellek F., Podlaha O. and Strauss H. (1999) $^{87}Sr/^{86}Sr$, $\delta^{13}C$ and $\delta^{18}O$ evolution of Phanerozoic seawater, *Chem. Geol.* **161** 59–88.

Wallmann K. (2001) Controls on the Cretaceous and Cenozoic evolution of seawater composition, atmospheric CO2 and climate, *Geochim. Cosmochim. Acta* **65**, 3005–3025.

Wieser M. E., Buhl D., Bouman C. and Schwieters J. (2004) High precision calcium isotope ratio measurements using a magnetic sector multiple collector inductively coupled plasma mass spectrometer, *J. Anal. At. Spectrom.* **19**, 844–851.

Zeebe R.E. and Wolf-Gladrow D.A., CO_2 in seawater: Equilibrium, kinetics, isotopes, Elsevier Oceanography Series, 65, Elsevier, Amsterdam, 2001, pp. 346

Zhu P. and Macdougall J.D. (1998) Calcium isotopes in the marine environment and the oceanic calcium cycle, *Geochim. Cosmochim. Acta* **62**, 1691–1698.

Auxiliary material for the 'Paper 1'

Supplementary data: Ca isotope mass balance model

Table A.2.1. Scenario 1 (hydrothermal control)

Age	F_{HY}	$\delta^{44}Ca_{HY}$	F_{RIV}	$\delta^{44}Ca_{RIV}$	F_{DOLO}	$\delta^{44}Ca_{DOLO}$	F_{BC}	$\delta^{44}Ca_{BC}$	F_{ALT}	$\delta^{44}Ca_{ALT}$	$\delta^{44}Ca_{SW}$ (MODEL)
158	11.7	0.90	11.7	0.70	0	0.30	17.2	0.90	2.0	0.90	**1.60**
156	12.8	0.90	11.7	0.70	0	0.30	17.2	0.90	2.0	0.90	**1.57**
154	13.5	0.90	11.7	0.70	0	0.30	17.2	0.90	2.0	0.90	**1.55**
152	12.8	0.90	11.7	0.70	0	0.30	17.2	0.90	2.0	0.90	**1.57**
150	11.2	0.90	11.7	0.70	0	0.30	17.2	0.90	2.0	0.90	**1.62**
148	8.8	0.90	11.7	0.70	0	0.30	17.2	0.90	2.0	0.90	**1.70**
146	8.1	0.90	11.7	0.70	0	0.30	17.2	0.90	2.0	0.90	**1.73**
144	8.1	0.90	11.7	0.70	0	0.30	17.2	0.90	2.0	0.90	**1.73**
142	8.1	0.90	11.7	0.70	0	0.30	17.2	0.90	2.0	0.90	**1.73**
140	7.7	0.90	11.7	0.70	0	0.30	17.2	0.90	2.0	0.90	**1.75**
138	7.7	0.90	11.7	0.70	0	0.30	17.2	0.90	2.0	0.90	**1.75**
136	6.6	0.90	11.7	0.70	0	0.30	17.2	0.90	2.0	0.90	**1.80**
134	6.6	0.90	11.7	0.70	0	0.30	17.2	0.90	2.0	0.90	**1.80**
132	6.3	0.90	11.7	0.70	0	0.30	17.2	0.90	2.0	0.90	**1.82**
130	5.7	0.90	11.7	0.70	0	0.30	17.2	0.90	2.0	0.90	**1.85**
128	6.2	0.90	11.7	0.70	0	0.30	17.2	0.90	2.0	0.90	**1.82**
126	6.6	0.90	11.7	0.70	0	0.30	17.2	0.90	2.0	0.90	**1.80**
124	4.8	0.90	11.7	0.70	0	0.30	17.2	0.90	2.0	0.90	**1.90**
0	4.8	0.90	11.8	0.70	0	0.30	17.2	0.90	2.0	0.90	**1.88**

The Ca fluxes (F) are in Tmol (10^{+12} mol) of Ca per year and the isotopic signatures ($\delta^{44/40}Ca_{NIST}$) are expressed in per mil (‰).

Note: The simulation of $\delta^{44/40}Ca_{SW}$, in the scenario 1 and 2, started from the Early Cretaceous, 124 Ma, and was calculated backward to the Middle Jurassic, 158 Ma. This approach was adopted due to apparent similarity between the $\delta^{44/40}Ca_{SW}$ values of modern and the inferred Barremian/Aptian seawater (Fig. 2.2). The Barremian/Aptian oceanic Ca budget was, therefore, parameterized to closely resemble the modern, and the $\delta^{44/40}Ca$ signatures of the individual fluxes were also prescribed to match to the present-day values.

Table A.2.2. Scenario 2 (hydrothermal control coupled with dolomite formation)

Age	F_{HY}	$\delta^{44}Ca_{HY}$	F_{RIV}	$\delta^{44}Ca_{RIV}$	F_{DOLO}	$\delta^{44}Ca_{DOLO}$	F_{BC}	$\delta^{44}Ca_{BC}$	F_{ALT}	$\delta^{44}Ca_{ALT}$	$\delta^{44}Ca_{SW}$ (MODEL)
158	8.0	0.90	11.7	0.70	0.5	0.30	17.2	0.90	2.0	0.90	**1.70**
156	8.0	0.90	11.7	0.70	2.6	0.30	17.2	0.90	2.0	0.90	**1.57**
154	8.0	0.90	11.7	0.70	3.0	0.30	17.2	0.90	2.0	0.90	**1.55**
152	7.2	0.90	11.7	0.70	3.0	0.30	17.2	0.90	2.0	0.90	**1.57**
150	6.5	0.90	11.7	0.70	2.6	0.30	17.2	0.90	2.0	0.90	**1.62**
148	5.7	0.90	11.7	0.70	2.3	0.30	17.2	0.90	2.0	0.90	**1.67**
146	5.2	0.90	11.7	0.70	2.1	0.30	17.2	0.90	2.0	0.90	**1.70**
144	5.2	0.90	11.7	0.70	2.1	0.30	17.2	0.90	2.0	0.90	**1.70**
142	5.1	0.90	11.7	0.70	2.0	0.30	17.2	0.90	2.0	0.90	**1.71**
140	5.2	0.90	11.7	0.70	1.9	0.30	17.2	0.90	2.0	0.90	**1.72**
138	5.2	0.90	11.7	0.70	1.8	0.30	17.2	0.90	2.0	0.90	**1.72**
136	5.1	0.90	11.7	0.70	1.5	0.30	17.2	0.90	2.0	0.90	**1.75**
134	5.0	0.90	11.7	0.70	1.0	0.30	17.2	0.90	2.0	0.90	**1.80**
132	4.9	0.90	11.7	0.70	0.8	0.30	17.2	0.90	2.0	0.90	**1.82**
130	4.7	0.90	11.7	0.70	0.6	0.30	17.2	0.90	2.0	0.90	**1.85**
128	4.6	0.90	11.7	0.70	1.0	0.30	17.2	0.90	2.0	0.90	**1.82**
126	4.6	0.90	11.7	0.70	1.2	0.30	17.2	0.90	2.0	0.90	**1.80**
124	4.4	0.90	11.7	0.70	0.2	0.30	17.2	0.90	2.0	0.90	**1.90**
0	4.8	0.90	11.8	0.70	0.0	0.30	17.2	0.90	2.0	0.90	**1.88**

The Ca fluxes (F) are in Tmol (10^{+12} mol) of Ca per year and the isotopic signatures ($\delta^{44/40}Ca_{NIST}$) are expressed in per mil (‰).

3 Calcium isotope budget of Phanerozoic oceans: Implications for chemical evolution of seawater and its causative mechanisms

by

Juraj Farkaš [a], Florian Böhm [b], Klaus Wallmann [b], John Blenkinsop [c], Anton Eisenhauer [b], Robert van Geldern [d], Axel Munnecke [e], Silke Voigt [b] and Ján Veizer [a]

[a] *University of Ottawa and Ottawa-Carleton Geoscience Centre, Ottawa, K1N 6N5,ON, Canada*

[b] *Leibniz Institute of Marine Sciences, IFM-GEOMAR, D-24148 Kiel, Germany*

[c] *Carleton University and Ottawa-Carleton Geoscience Centre, Ottawa, K1S 5B6,ON, Canada*

[d] *Leibniz Institute for Applied Geosciences, Stilleweg 2, 30655 Hannover, Germany*

[e] *Palaeontological Institute of the Friedrich-Alexander University, D-91054, Erlangen, Germany*

Presented at:

The 5th Calcium Isotope Workshop, Ruhr University Bochum, Germany (2007),

Abstract

A total of 280 brachiopods of Ordovician to Cretaceous age, complemented by 139 literature data, are used to reconstruct the evolution of calcium isotope composition of seawater ($\delta^{44/40}Ca_{SW}$) over the Phanerozoic. The compiled $\delta^{44/40}Ca_{SW}$ record shows a general increase from ~1.3‰ at the beginning of the Ordovician to ~2‰ at present. Superimposed on this trend is a major long-term positive excursion from the Early Carboniferous to Early Permian as well as several short-term, mostly negative, oscillations.

A model simulation of global calcium/carbon/magnesium cycles indicates that the observed $\delta^{44/40}Ca_{SW}$ variations during the Phanerozoic cannot be explained solely by varying magnitudes of input and output fluxes of calcium to the oceans, indicating that their isotope signatures must also have changed, most likely as a consequence of alternating mineralogy of marine carbonates, i.e. 'calcite-aragonite seas'. The ultimate control of the calcium isotope budget of Phanerozoic oceans appears to have been tectonic processes, specifically variable rates of oceanic crust production that modulated the hydrothermal calcium flux and the oceanic Mg/Ca ratio, which in turn controlled the dominant mineralogy of marine carbonates, hence the $\delta^{44/40}Ca_{SW}$.

As to the causes of the short-term oscillations recorded in the secular $\delta^{44/40}Ca_{SW}$ trend, we tentatively propose that these are related to variable rates of dolomite formation and/or changing chemical composition of the riverine flux, in particular Ca/HCO_3^- and Ca/SO_4^{2-} ratios, induced by changing proportions of silicate vs. carbonate weathering rates on continents.

Keywords: calcium isotopes; Phanerozoic; global calcium cycle; seawater chemistry

3.1 Introduction

One of the primary research interests of earth system sciences is to constrain the chemical and isotope evolution of the oceans over geological time, as processes that control seawater chemistry also affect the composition of the atmosphere that, in turn, modulates the

Earth's climate. The major ion and isotope composition of seawater varied significantly over the Phanerozoic, as suggested by the fluid inclusion data of primary marine halite (Horita et al., 2002; Lowenstein et al., 2001 and 2003), by the elemental and isotope compositions of marine skeletal carbonates (Veizer et al., 1999; Dickson, 2002; Steuber and Veizer, 2002; Kampschulte and Strauss, 2004), and by changing mineralogy of marine carbonates and potash evaporites (Sandberg, 1983; Hardie, 1996).

The synchronous nature of these temporal trends indicates that they may have been controlled by a common causative mechanism (Horita et al., 2002), but as yet there is no consensus as to the identity of this underlying mechanism (Veizer and Mackenzie, 2003; Holland, 2005).

Two main contenders have been advocated as principal drivers of chemical and isotope evolution of seawater during the Phanerozoic. One group of explanations (Spencer and Hardie, 1990; Hardie, 1996; Steuber and Veizer, 2002) regards plate tectonics as the ultimate driving force. In this alternative, ocean chemistry varied mostly due to variable seawater cycling rates via submarine hydrothermal systems, which in turn are controlled by seafloor spreading rates and by the total volume of mid-ocean ridges. An alternative, or complementary, hypothesis (Zimmermann, 2000; Holland and Zimmermann, 2000; Berner, 2004; Holland, 2005) argues that seawater chemistry was largely controlled by sedimentological factors, such as variable rates of dolomite and/or gypsum (anhydrite) deposition, with a possible although relatively minor contribution from the submarine hydrothermal systems.

The relative importance of these causative factors can potentially be resolved by novel analytical techniques, such as the non-traditional isotope systems of calcium and magnesium. The calcium isotope record, based on marine skeletal carbonates, has already proved to be a useful indicator of changing intensity of oceanic calcium fluxes (Heuser et al., 2005), particularly of their hydrothermal component (Farkaš et al., 2007).

In this study we reconstruct the calcium isotope evolution of seawater ($\delta^{44/40}Ca_{SW}$) during the Phanerozoic, based on brachiopods as carrier phases and supplemented by literature data from marine carbonates (Heuser et al., 2005; Steuber and Buhl, 2006; Farkaš et al., 2007) and phosphates (Schmitt et al., 2003b; Soudry et al., 2004 and 2006). This empirical Phanerozoic $\delta^{44/40}Ca_{SW}$ record is subsequently simulated by an expanded version

of the numerical model for coupled calcium/carbon/magnesium global cycles (Hansen and Wallmann 2003; Wallmann, 2004; Heuser et al., 2005).

Our calcium isotope data represent the first continuous $\delta^{44/40}Ca_{SW}$ record for the Paleozoic and complemented by literature data (De La Rocha and DePaolo, 2000; Schmitt et al., 2003b; Soudry et al., 2004, 2006; Fantle and DePaolo, 2005 and 2007; Heuser et al., 2005; Kasemann et al., 2005; Steuber and Buhl, 2006; Farkaš et al., 2007), this study presents the first $\delta^{44/40}Ca_{SW}$ record across the entire Phanerozoic.

3.2 Samples

We analyzed calcium isotope composition of 280 brachiopod shells of Ordovician to modern ages, thus covering most of the Phanerozoic time span. The $\delta^{44/40}Ca_{SW}$ record is based for the most part (~87%) on our brachiopod samples, but the Cenozoic, Cretaceous, and Middle/Late Jurassic portions are mostly constrained by literature data (n = 139).

Specifically, we measured $\delta^{44/40}Ca$ values of low-Mg calcite that was sampled from the interior 'secondary' layer of brachiopod shells. This layer is fairly resistant to post-depositional alteration (Veizer et al., 1999; Samtleben et al., 2001). Most of these shells were previously analyzed for their trace element (Sr, Mn, Fe) and isotope ($^{87}Sr/^{86}Sr$, $\delta^{18}O$, $\delta^{13}C$ and $\delta^{34}S$) compositions and were also screened by cathodoluminescence (CL) and scanning electron microscopy (SEM) in order to evaluate their state of preservation (Veizer et al., 1999; Samtleben et al., 2000, 2001; Kampschulte and Strauss, 2004; van Geldern et al., 2006).

The samples for the present study were selected utilizing the following textural and geochemical criteria: (i) the calcite was non-luminescent and retained its original ultrastructure; (ii) had high Sr/Mn ratio (Veizer, 1983); and (iii) the lowest $^{87}Sr/^{86}Sr$ among the coeval or stratigraphically close samples (Veizer et al., 1999). We adopted this approach because diagenetic alteration of marine carbonates tends to increase their $^{87}Sr/^{86}Sr$ ratios while decreasing Sr/Mn and induces typical yellow/orange luminescence (Veizer, 1983; Veizer et al., 1999).

Brachiopods were collected in the USA (including San Juan Island), Canada (including Anticosti Island), Great Britain, Ireland, Germany, Sweden (including Gotland),

Belgium, Austria, Italy, Spain, Morocco, Lithuania, Latvia, Hungary, Ukraine, Russia, China and Australia. Further details on location, stratigraphy and the additional geochemical data are available from: http://www.science.uottawa.ca/geology/isotope_data; and also in Veizer et al. (1999), Samtleben et al. (2000, 2001), Calner et al. (2004), Jeppsson et al. (2006) and van Geldern et al. (2006). Based on the paleogeographic reconstructions of Scotese et al. (1994) and Scotese (1997) most of the samples originated from tropical to subtropical regions, representing a paleolatitudinal range from 30°N to 30°S.

The time scale used in our figures is from Harland et al. (1990) to enable correlation with the previously published datasets (Veizer et al., 1999) that were used as controlling variables for our geochemical modeling. For ease of comparison, we converted the numerical ages of Harland et al. (1990) also into the time scale of Gradstein et al. (2004), using simple linear interpolation between the stage boundaries (see auxiliary material, Tables A.3.4 and A.3.5).

3.3 Methods

3.3.1 Sample Preparation

Powders composed of low-Mg calcite were sampled using a micro-drill then weighed into a Teflon PFA (perfluoroaloxy) vial and ultrasonically cleaned in ultrapure water (>18 MΩ cm) for about 30 minutes. The cleaning procedure was repeated at least twice. To remove the organic matter causing isobaric interferences during the calcium isotope analysis (Hippler at al., 2004; Böhm et al., 2006) the powders were also ultrasonically cleaned with 30% H_2O_2 at Ottawa-Carleton. A mixture of HNO_3-H_2O_2 was added to the sample solution at IFM-GEOMAR, as described in Böhm et al. (2006). These solutions were evaporated to dryness at 80 °C and dissolved in adjusted volume of 2 N HCl. All chemicals used in this study were of high purity with sub-ppb levels of metal concentrations.

3.3.2 Mass Spectrometry and Data Reduction

The calcium isotope measurements were performed on a Thermo Electron Triton TIMS thermal ionization mass spectrometer in Ottawa, Canada (Carleton University) as well as in Kiel, Germany (IFM-GEOMAR). The isotope composition was determined by a conventional double spiking technique (Russell et al., 1978) using a $^{43}Ca/^{48}Ca$ double spike (Heuser et al., 2002). For the data reduction we used an iterative algorithm of Heuser et al. (2002) with an exponential term for the fractionation correction. This approach allowed us to calculate the original $^{44}Ca/^{40}Ca$ ratio of a sample from the measured $^{40}Ca/^{48}Ca$, $^{43}Ca/^{48}Ca$ and $^{44}Ca/^{48}Ca$ ratios in a sample/spike mixture and the isotope composition of our $^{43}Ca/^{48}Ca$ double spike.

Analytical results are expressed as $\delta^{44/40}Ca$ values in permil (‰) relative to the NIST SRM 915a $CaCO_3$ standard, using the following relation (Eisenhauer et al., 2004): $\delta^{44/40}Ca = [(^{44}Ca/^{40}Ca)_{sample}/(^{44}Ca/^{40}Ca)_{standard} -1]*1000$. The external precision for $\delta^{44/40}Ca$ is expressed as two standard deviations ($\pm 2\sigma$) determined by repeat measurements from the same sample solution. The potential influence of radiogenic ^{40}Ca on measured $\delta^{44/40}Ca$ was tested on selected Devonian brachiopod samples and was found to be negligible at the level of our analytical uncertainty, ± 0.15‰ (for details see the section 3.3.2.2).

3.3.2.1 Ottawa/Carleton: Calcium isotope experimental procedures

A total of 210 brachiopods (Ordovician, Silurian, Devonian, Carboniferous, Permian, Triassic and modern) were analyzed for their $\delta^{44/40}Ca$ at Carleton University in the Isotope Geochemistry and Geochronology Research Centre (IGGRC). The analytical technique is based on the method described in Farkaš et al. (2007) with a few modifications adopted for the chemical preparation and data acquisition. Specifically, we skipped the chromatographic clean-up (see below), except for seawater, and introduced a fully automated routine for the calcium isotope analysis (see auxiliary material, section A.3.1), which significantly increased the sample throughput allowing us to analyze up to 10 samples over the course of 24 hours.

Experimental testing on brachiopods with variable trace element contents showed that chromatographic clean-up on cation-exchange columns is not necessary for relatively pure biogenic carbonates. The influence of carbonate matrix on measured $\delta^{44/40}Ca$ was investigated on two aliquots of the same sample, one prepared by direct dissolution and the other passed through a cation-exchange column filled with BioRad AG50W resin (Farkaš et al., 2007). The measured $\delta^{44/40}Ca$ values of two aliquots were identical, within ± 0.15‰, for all the cases (Table 3.1), suggesting only a negligible or no influence of carbonate matrix on measured $\delta^{44/40}Ca$.

Table 3.1.
The effect of chromatographic clean-up on measured $\delta^{44/40}Ca$ of modern (Y342L) and fossil (Devonian: D176; Silurian: G68) brachiopods

Sample	Material	Mg (wt %)	Sr (ppm)	Fe (ppm)	Direct dissolution (Ca fraction + matrix) $\delta^{44/40}Ca$ (‰), (2σ) [b]	Chromatography [a] (Ca fraction only) $\delta^{44/40}Ca$ (‰), (2σ) [b]
Y342L	Brachiopod	0.15	1085	6	1.05 ±0.01	1.07 ±0.01
D176	Brachiopod	0.58	592	1954	0.73 ±0.07	0.75 ±0.04
G68	Brachiopod	0.20	2042	-	0.48 ±0.03	0.54 ±0.08

[a] Samples were passed through cation-exchange micro-columns filled with BioRad AG50W resin.
[b] External precision was determined as 2σ from two measurements of the same sample solution.

A brief description of the modified method is presented below. Weighed samples (~1000 μg of powdered $CaCO_3$) were dissolved in 1000 μL of 2 M HCl in a PFA Teflon vial. From this solution 25 μL (~10 μg Ca) were pipetted into a new vial and mixed with 65 μL of a Ca-isotope double spike solution with $^{43}Ca/^{48}Ca$ of 0.7221 ± 0.0004 (2σ, n = 8) (Farkaš et al. (2007). As a result, the $^{40}Ca/^{48}Ca$ ratio of a mixture was approximately 60, usually somewhere between 55 and 65. After the double spiking, the mixture was evaporated to dryness and redissolved in 10 μL of 5% HNO_3. From this solution 3 μL (3 μg Ca) were loaded as a nitrate on a zone-refined Re ribbon of a double filament assembly. The sample solution was dried at a filament current of 0.5 ampere (A), heated at 1.5 A for 60 s and finally brought to dull red at about 2.2 A for 30 s.

In the mass spectrometer, the samples were heated to an ionization temperature of about 1400 °C using an automatic sequence with a built-in program for sample heating (see auxiliary material, Table A.3.1).

The target ion beam intensity for ^{40}Ca signal was 130 pA (13000 mV) and this was usually reached within ~30 min. The sample heating sequence was followed by an automated data acquisition routine. The calcium isotope peaks (masses 40 to 48) were measured in two steps, including ^{41}K that was monitored for possible isobaric interferences of ^{40}K on ^{40}Ca. An individual measurement consisted of 108 cycles, 9 blocks of 12 cycles each, with an integration time of 16-s per cycle followed by a 3-s waiting time. Defocused baselines measurements were collected for 30 s at the beginning of each block. A total analytical time of this fully automated routine was about 150 min per sample (30 min for the heating plus 120 min for the data acquisition).

The external precision of $\delta^{44/40}Ca$, as determined by the repeat analysis of NIST SRM 915a over a period of six months, was ± 0.13‰ (2σ, n = 30) with a mean $^{44}Ca/^{40}Ca$ ratio of 0.021538 ± 0.000003 (2σ), the latter value was also used as a normalizing ratio for $\delta^{44/40}Ca$. The measured $\delta^{44/40}Ca$ (NIST SRM 915a) value of IAPSO seawater yielded 1.86 ± 0.20‰ (2σ, n = 5), in agreement with the published value of 1.88 ± 0.04‰ (Hippler et al., 2003).

3.3.2.2 IFM-GEOMAR: Calcium isotope experimental procedures

The calcium isotope analyses of 70 brachiopods (Silurian, Devonian and Cretaceous) were performed at the mass spectrometer facilities of the IFM-GEOMAR (Leibniz Institute of Marine Sciences) in Kiel, Germany, following the method described in Heuser et al. (2002) and Böhm et al. (2006).

Briefly, washed powders were dissolved in 2 N HCl, evaporated and redissolved so the concentration of calcium in a solution would be ~0.15 µg per µL. From this solution, ~0.3 µg of Ca was spiked with 10 µL of a $^{43}Ca/^{48}Ca$ double spike, evaporated to dryness, and loaded with 2 N HCl and a $TaCl_5$ activator on a single zone-refined Re filament. Sample filaments were heated to a temperature of ~1500 °C, corresponding to a current of 3 A and a

^{40}Ca signal intensity of about 40 pA (4000 mV). The heating procedure typically lasted 40 min. Data were collected in dynamic mode with ^{40}Ca, ^{42}Ca, ^{43}Ca and ^{44}Ca peaks measured in the first cycle, and ^{43}Ca, ^{44}Ca and ^{48}Ca in the second cycle. The intensity of ^{40}Ca during the measurement was 40 to 50 pA (4000-5000 mV). Data were acquired for about 50 min. (7 blocks of 22 cycles each).

Typical external precision for $\delta^{44/40}Ca$ was ± 0.1‰ (2σ) and the long-term (4 years) mean for $^{44}Ca/^{40}Ca$ of SRM 915a is 0.021182 ± 0.000006 (2σ, n = 289). The $\delta^{44/40}Ca$ value of IAPSO seawater, normalized to SRM 915a, showed heavy isotope enrichment of 1.89 ± 0.1‰ (2σ, n = 20). The long-term (2 years) mean $^{44}Ca/^{40}Ca$ ratio of IAPSO was measured as 0.021222 ± 0.000008 (2σ, n = 20). Total Ca blanks were less than 2 ng of the loaded 300 ng, i.e. less than 1%.

We observed minor but consistent inter-laboratory bias where the $\delta^{44/40}Ca$ values measured at IFM-GEOMAR are about 0.15‰ lighter compared to data acquired at Ottawa/Carleron (Fig. 3.1), thus all data measured at IFM-GEOMAR were adjusted by adding 0.15‰. This offset is most likely a consequence of different loading techniques used in the above laboratories (double filament and HNO_3 at Ottawa-Carleton vs. single filament and $TaCl_5$ at IFM-GEOMAR).

For the determination of radiogenic ^{40}Ca about 1 μg of Ca was prepared and loaded on a single zone-refined Re filament as described above, however without addition of a double spike. Sample filaments were heated to about 1550°C corresponding to a ^{40}Ca signal intensity of about 100 pA (10 000 mV). Data for masses ^{40}Ca, ^{42}Ca and ^{44}Ca were collected in static mode. The measured $^{40}Ca/^{44}Ca$ ratios were corrected for mass fractionation to a $^{42}Ca/^{44}Ca$ value of 0.31221 (DePaolo, 2004) using an exponential fractionation law. Data were acquired for up to 75 minutes (20 blocks of 20 cycles each). In some runs acquisition was stopped when the standard error of the $^{40}Ca/^{44}Ca$ ratios became smaller than 0.002.

We found an average $^{40}Ca/^{44}Ca$ for modern marine skeletal carbonates (corals and sclerosponges) of 47.163 ± 0.01 (2σ, n = 7). This value is not significantly different (ANOVA, p=0.15) from the average Devonian/Silurian ratio of 47.159 ± 0.01 (2σ, n = 9), measured on brachiopods from the Wenlock, Ludlow, Lochkovian, Emsian, Eifelian, Givetian, Frasnian (2 specimens), and Famennian.

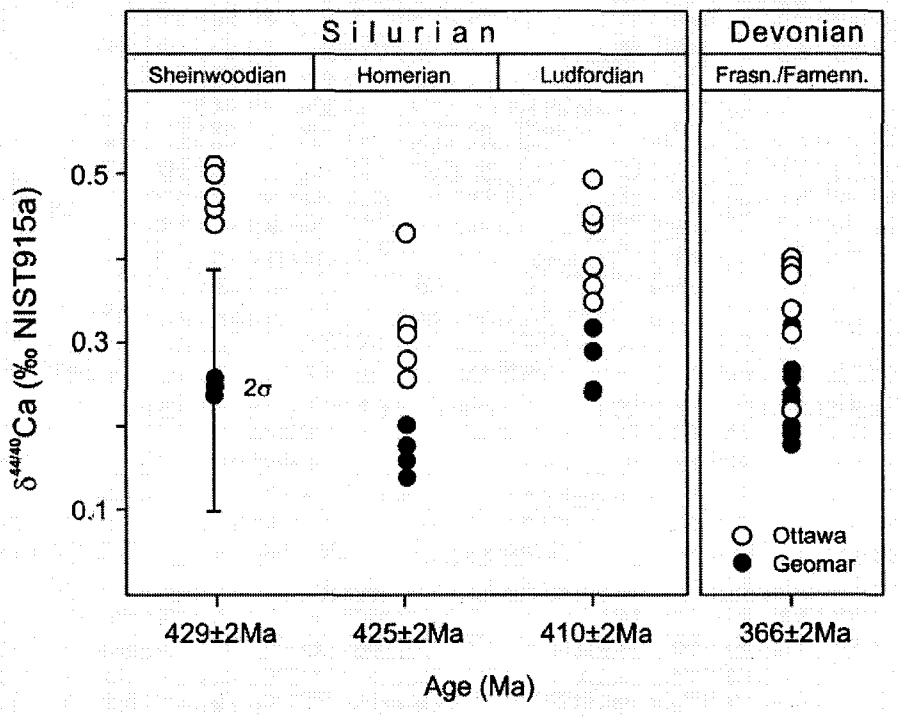

Fig. 3.1. Measured $\delta^{44/40}Ca$ values of coeval, Silurian and Devonian, brachiopods as determined at Ottawa/Carleton (open circles) and IFM-GEOMAR (black circles) laboratories. Error bar represents the average 2σ of ± 0.15‰.

Both $^{40}Ca/^{44}Ca$ values agree with the modern marine carbonate (*Tridacna*) value of 47.168 ± 0.01 determined by Nelson & McCulloch (1989), and the MORB ratios of 47.155 ± 0.001 and 47.168 ± 0.009 of Kreissig & Elliott (2005) and Nelson & McCulloch (1989), respectively. This confirms the conclusion of the latter study, that modern seawater has a radiogenic Ca excess that is indistinguishable from the mantle (MORB) signature. Our Early Paleozoic $^{40}Ca/^{44}Ca$ ratio indicates that this was also the case in the early Phanerozoic.

3.4 Results

The measured $\delta^{44/40}$Ca values of brachiopods (see auxiliary material, Table A.3.4), complemented by literature data (Table A.3.5), are plotted as a function of time in Fig. 3.2. The Phanerozoic $\delta^{44/40}$Ca record of marine carbonates and phosphates (n = 419) exhibits a temporal variation with a magnitude of about 2‰, from -0.5‰ to 1.5‰.

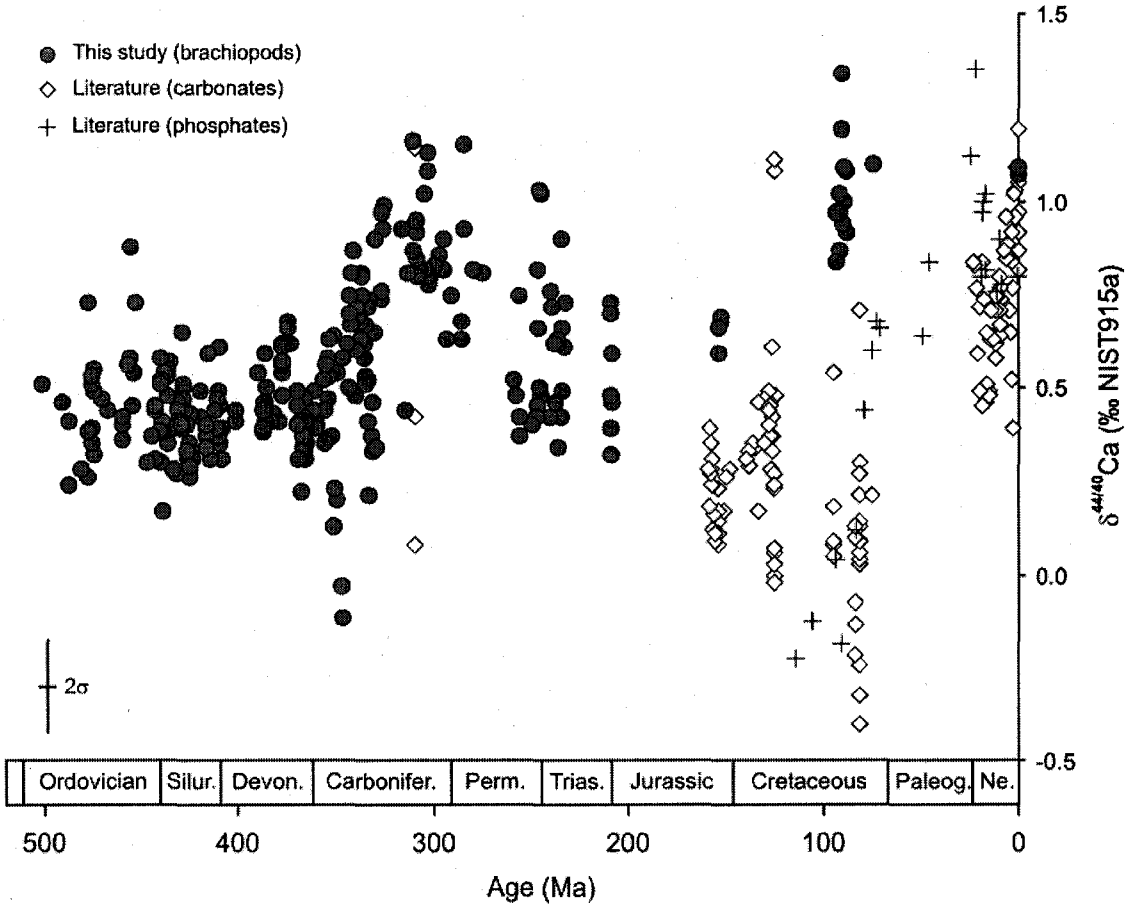

Fig. 3.2. Measured $\delta^{44/40}$Ca values of Phanerozoic brachiopods (grey circles, n = 280; this study), complemented by literature data from marine carbonates (open diamonds, n = 139) and authigenic phosphates (black crosses, n = 22). The literature data are from the following sources: Heuser et al. (2005), Steuber and Buhl (2006), Farkaš et al. (2007), Schmitt et al. (2003b) and Soudry et al. (2004). Time scale from Harland et al. (1990).

Overall, the compiled $\delta^{44/40}$Ca dataset defines a rising trend, from ~0.4‰ at the beginning of the Ordovician to ~1‰ at present, with a major positive excursion at the Carboniferous/Permian transition and a substantial scatter, up to ~2‰, during the Cretaceous. In addition, there are indications of several, mostly negative, short-term oscillation superimposed on the general rising trend.

3.5 Discussion

While the $\delta^{44/40}$Ca of marine carbonates and phosphates reflects primarily the isotope composition of seawater (De La Rocha and DePaolo, 2000; Heuser et al., 2005; Schmitt et al., 2003b), ambient temperature (Nägler et al., 2000; Gussone et al., 2003, 2004; Hippler 2002), mineralogy of precipitates (Gussone et al. 2005) and kinetics (Gussone et al., 2005; Lemarchand et al., 2004) also play a role. In order to reconstruct the calcium isotope composition of Phanerozoic seawater it is essential to know the isotope fractionation factor ($\alpha_{cc/sw}$) between seawater and the recording phase (e.g. brachiopod calcite) as well as its dependence on temperature.

3.5.1 Fractionation factors ($\alpha_{cc/sw}$) and their sensitivity to temperature

The compiled $\delta^{44/40}$Ca data set comprises samples with either calcitic or phosphatic mineralogies, the former includes brachiopods, belemnites, foraminifera and rudists, and the latter marine authigenic phosphates.

The $\alpha_{cc/sw}$ can be calculated from the calcium isotope composition of seawater and the corresponding recording phase using the following relation:

$$\alpha_{CC/SW} = \left(\delta^{44/40}Ca_{CC} + 1000\right)/\left(\delta^{44/40}Ca_{SW} + 1000\right) \qquad (3.1)$$

where $\delta^{44/40}Ca_{CC}$ and $\delta^{44/40}Ca_{SW}$ represent the calcium isotope compositions of the recording phase and seawater, respectively (Heuser et al., 2005).

For brachiopods, the fractionation factor was determined on modern specimens (*Terebratalia*, *Thecidellina*, *Waltonia* sp.) and these yielded the mean $\alpha_{cc/sw}$ of ~0.99915 and a weak temperature dependency of ~0.014‰ °C^{-1} (Fig. 3.3) (Gussone et al., 2005; Farkaš et al., 2007).

For belemnites, we used $\alpha_{cc/sw}$ of ~0.99860 (Fig. 3.3) inferred from samples of coeval Late Jurassic belemnites (*Hibolites* sp.) and brachiopods (*Lacunosella* sp.) that were collected from the same stratigraphic horizons (cf. Farkaš et al., 2007). The temperature sensitivity of belemnite $\delta^{44/40}$Ca is assumed to be weak, likely <0.02‰ °C^{-1}, judging from the statistically insignificant correlation between $\delta^{44/40}$Ca and δ^{18}O (Farkaš et al., 2007).

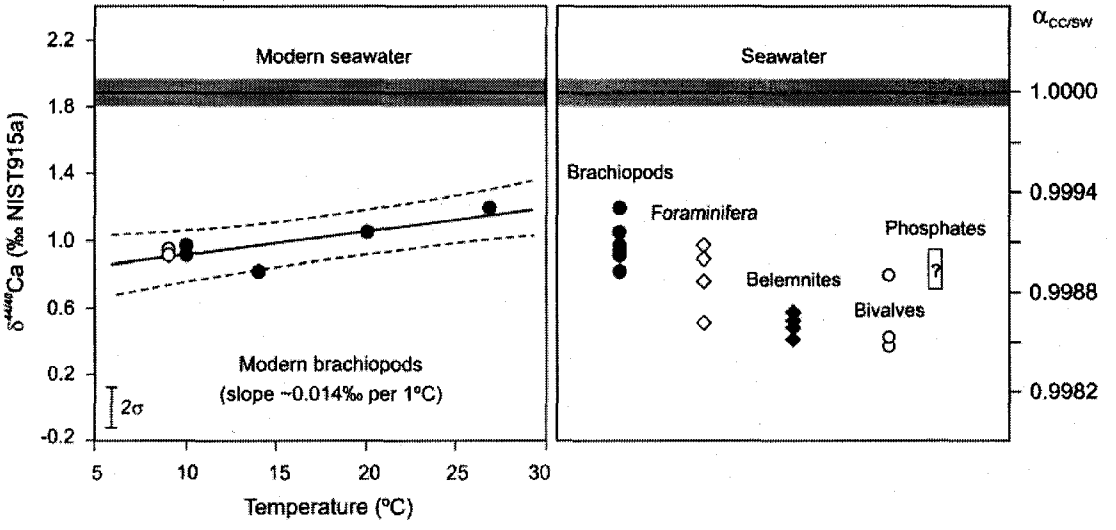

Fig. 3.3. Left panel: $\delta^{44/40}$Ca of modern brachiopod calcite as a function of seawater temperature (black circles = data from Gussone et al., 2005; gray circles = data from Farkaš et al., 2007; solid/dashed lines with a gray band represent the isotope composition of modern seawater). Right panel: calcium isotope fractionation factors ($\alpha_{cc\text{-}sw}$) between seawater (sw) and the following solid phases (cc): skeletal calcite of brachiopods, foraminifera (Heuser et al., 2005), belemnites (Farkaš et al., 2007) and bivalves (Steuber and Buhl, 2006) as well as marine phosphates (Schmitt et al., 2003b).

For foraminifera, the $\alpha_{cc/sw}$ was calculated from modern, or the most recent, planktonic foraminifers (*Globigerinoides tribolus, Globigerina bulloides*) that yielded the mean $\alpha_{cc/sw}$ of ~0.99905 and a weak $\delta^{44/40}$Ca-temperature gradient of <0.02‰ °C^{-1} (Heuser

et al., 2005; Gussone et al., 2003). For rudist bivalves, the fractionation factor has not yet been constrained experimentally and we therefore adopted $\alpha_{cc/sw}$ of modern oysters (*Ostrea* sp.) of ~0.99850 (Steuber and Buhl, 2006). The sensitivity of rudist $\delta^{44/40}Ca$ to temperature is expected to be high, possibly up to 0.25‰ $°C^{-1}$ (Immenhauser et al., 2005; see, however, discussion in Steuber and Buhl, 2006), which may result in significantly larger scatter and uncertainty for the reconstructed calcium isotope composition of Cretaceous seawater.

For marine phosphates, the $\alpha_{cc/sw}$ is assumed to be close to 0.9991 based on the analysis of a Pleistocene (0.5 Ma) sample (Schmitt et al., 2003b). This value, however, should be taken with caution because marine authigenic phosphates are products of early diagenesis, and thus calcium used for their formation originates not only from seawater but also from the dissolution of carbonates in the sediment (Soudry et al., 2004 and 2006). The latter have significantly lighter $\delta^{44/40}Ca$ compared to seawater. The $\delta^{44/40}Ca$-temperature gradient of phosphates is considered to be weak, likely less than 0.02‰ $°C^{-1}$, as indicated by poor correlation between $\delta^{44/40}Ca$ and $\delta^{18}O$ of Miocene phosphates (Schmitt et al., 2003b).

A summary showing the calcium isotope fractionation factors, $\alpha_{cc/sw}$, for the above mentioned recording phases, with the corresponding $\delta^{44/40}Ca$-temperature gradients, is presented in Fig. 3.3 and Table 3.2.

Table 3.2.
The calcium isotope fractionation factors between seawater and skeletal calcite ($\alpha_{cc/sw}$) of brachiopods, belemnites, foraminifera and bivalves as well as marine authigenic phosphates

Material / Recording phase	$\alpha_{cc/sw}$	$1000\ln(\alpha_{cc/sw})$	$\delta^{44/40}Ca$-temperature gradient
Brachiopods	0.99915 [a]	-0.85 ‰	< 0.015‰ $°C^{-1}$
Belemnites	0.99860 [b]	-1.40 ‰	< 0.020‰ $°C^{-1}$
Foraminifera (*G. trilobus*)	0.99906 [c]	-0.94 ‰	< 0.020‰ $°C^{-1}$
Bivalves: oysters, (rudists)	0.99850 [d]	-1.50 ‰	~ 0.250 ‰ $°C^{-1}$ [f]
Authigenic phosphates	0.99910 [e]	-0.90 ‰	< 0.020‰ $°C^{-1}$

[a] Gussone et al. (2005) and Farkaš et al. (2007).
[b] Farkaš et al. (2007).
[c] Heuser et al. (2005).
[d] Steuber and Buhl (2006).
[e] Schmidt et al. (2003).
[f] Based on data of rudist bivalve (*Vaccinites* sp.) of Immenhauser et al. (2005).

3.5.2 Reconstruction of calcium isotope composition of Phanerozoic seawater

The calcium isotope composition of paleo-seawater was calculated from the compiled $\delta^{44/40}Ca$ data set of marine carbonates and phosphates (Fig. 3.2) and the corresponding fractionation factors $\alpha_{cc/sw}$ (Table 3.2), using Eq. 3.1. The reconstructed Phanerozoic $\delta^{44/40}Ca_{SW}$ curve (Fig. 3.4) exhibits an increasing trend from about 1.3‰ at the beginning of the Ordovician to about 2‰ at present.

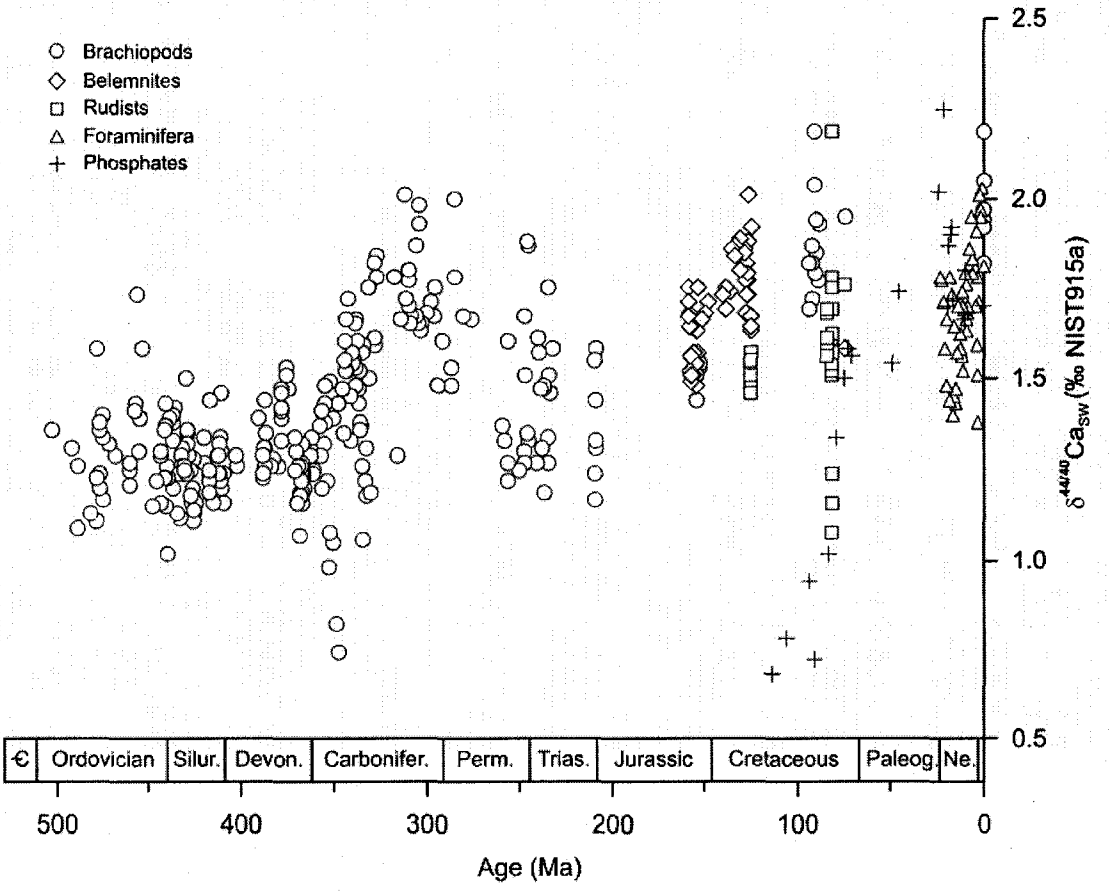

Fig. 3.4. The compilation of our and literature data (n = 419) showing the reconstructed calcium isotope evolution of Phanerozoic seawater ($\delta^{44/40}Ca_{SW}$) based on data of brachiopods (open circles), belemnites (open diamonds), rudists (open squares), foraminifera (open triangles) and marine phosphates (crosses). The $\delta^{44/40}Ca_{SW}$ trend was calculated using the following fractionation factors ($\alpha_{cc/sw}$): brachiopods = 0.99915; belemnites = 0.99860; rudists = 0.99850; foraminifera = 0.99905; and phosphates = 0.99910. Time scale from Harland et al. (1990).

Superimposed on this overall trend is a major long-term (~70 Ma) positive excursion, from the Early Carboniferous to Early Permian, and several, mostly negative, short-term excursions with a typical duration on the order of 5 to 10 Ma.

In general, the secular $\delta^{44/40}Ca_{SW}$ trend exhibits a rather uniform scatter of ± 0.15‰, except for the Late Cretaceous where $\delta^{44/40}Ca_{SW}$ data spread is from ~0.7 to 2.2‰. The predominant scatter of ± 0.15‰ is consistent with $\delta^{44/40}Ca$ variability observed in modern skeletal carbonates that show the weak temperature dependency of <0.02‰ $°C^{-1}$ (Fig. 3.3) (Gussone et al., 2005), which may suggest that the scatter reflects variability in the past sea surface temperatures of about ± 10 °C. This temperature range is, however, too large considering that most of fossil skeletal carbonates originated from tropical to subtropical settings, from 30°N to 30°S. Therefore, the uniform scatter of ± 0.15‰ is most likely due to the external reproducibility of our calcium isotope measurements.

To smooth natural fluctuations observed in the experimental $\delta^{44/40}Ca_{SW}$ record we applied a moving-average filter with a 10 point window to illustrate the secular $\delta^{44/40}Ca_{SW}$ trend for most of the Paleozoic and parts of the Mesozoic and Cenozoic (Fig. 3.5). Note that the phosphate data were excluded from this exercise, as the inclusion of the phosphate data generates a significantly different $\delta^{44/40}Ca_{SW}$ record during the Cretaceous which will be discussed below.

The statistical filtering confirmed a presence of several higher-order oscillations with a typical magnitude of about 0.4‰ and duration of 5 to 10 Ma that are superimposed on the overall $\delta^{44/40}Ca_{SW}$ trend. There are indications of several short-term positive peaks, the most apparent in the Middle Ordovician, Middle/Late Devonian and Late Permian (Fig. 3.5). The negative excursions are however much more common and the most pronounced are documented in the Middle Silurian, Late Devonian, Early Carboniferous, Late Jurassic, Early/Late Cretaceous and Neogene (Fig. 3.5).

The magnitudes of these short-term excursions vary from less than ~0.2, (e.g. Middle Silurian) up to more than ~0.5‰ (e.g. Early Carboniferous). Note that these values represent minimal estimates as they are derived from the smoothed dataset (Fig. 3.5).

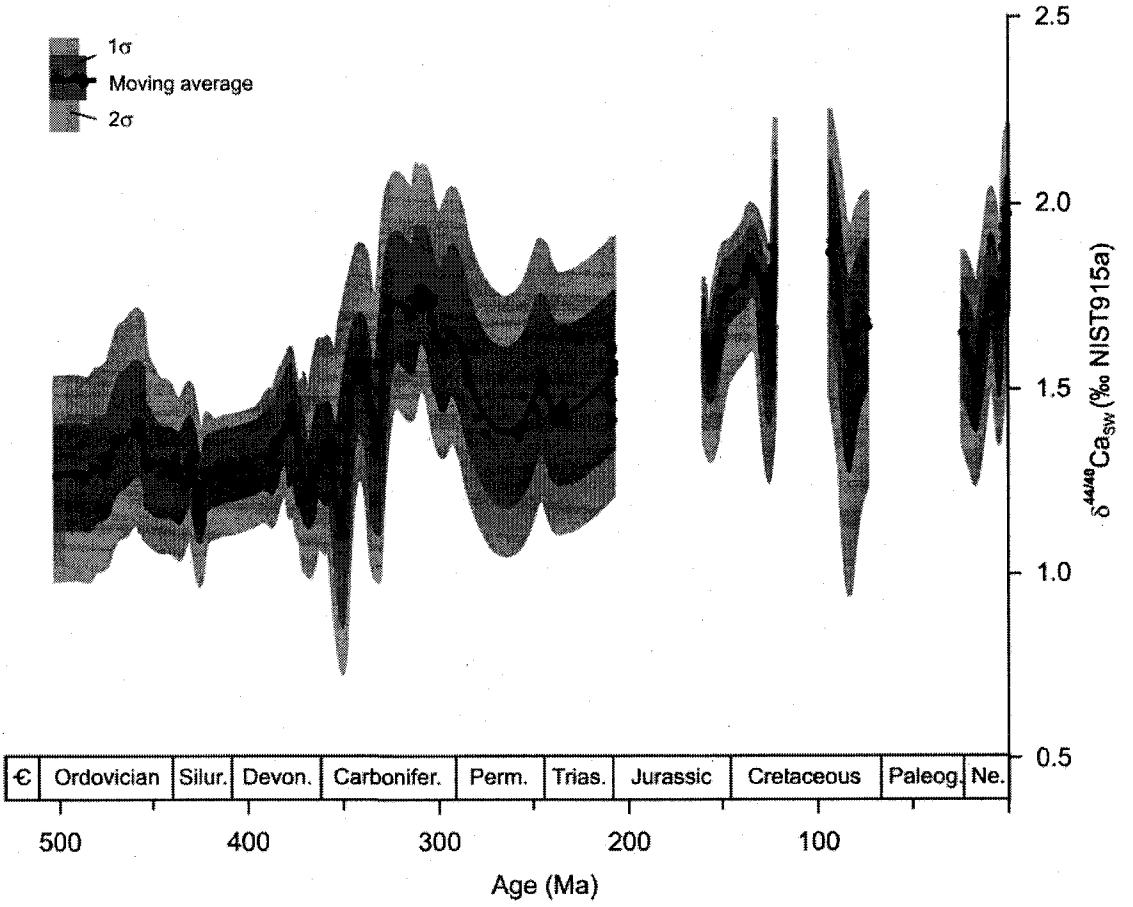

Fig. 3.5. Smoothed Phanerozoic $\delta^{44/40}Ca_{SW}$ trend based only on data of marine skeletal carbonates (n = 397). The moving average (solid line, black circles) is calculated using a 10-point smoothing window. The dark and light bands around the moving average trend represent 68% (±1σ) and 95% (±2σ) confidence intervals, respectively. Time scale from Harland et al. (1990).

Taking the Carboniferous $\delta^{44/40}Ca_{SW}$ trend as an example, the approximate duration and magnitude of the short-term excursions can be constrained (Fig. 3.6). The calcium isotope composition of Early Carboniferous (Mississippian) seawater, based on 60 brachiopod samples, exhibits a gradually increasing trend from the Early Tournaisian $\delta^{44/40}Ca_{SW}$ of ~1.3‰ to Late Serpukhovian values of ~1.75‰. Superimposed on this trend are two pronounced short-term negative excursions with $\delta^{44/40}Ca_{SW}$ minima dated

at ~352 Ma (Tournaisian/Visean) and ~334 Ma (Visean/Serpukhovian). The approximate duration of these excursions is about 10 ± 2 Ma and the magnitudes are close to 0.7 ‰, the latter based on the original (non-smoothed) $\delta^{44/40}Ca_{SW}$ dataset. The calcium isotope composition of the Late Carboniferous (Pennsylvanian) seawater is based on a much smaller data set (n = 23) and it shows a rather constant $\delta^{44/40}Ca_{SW}$ trend with a mean of ~1.7‰.

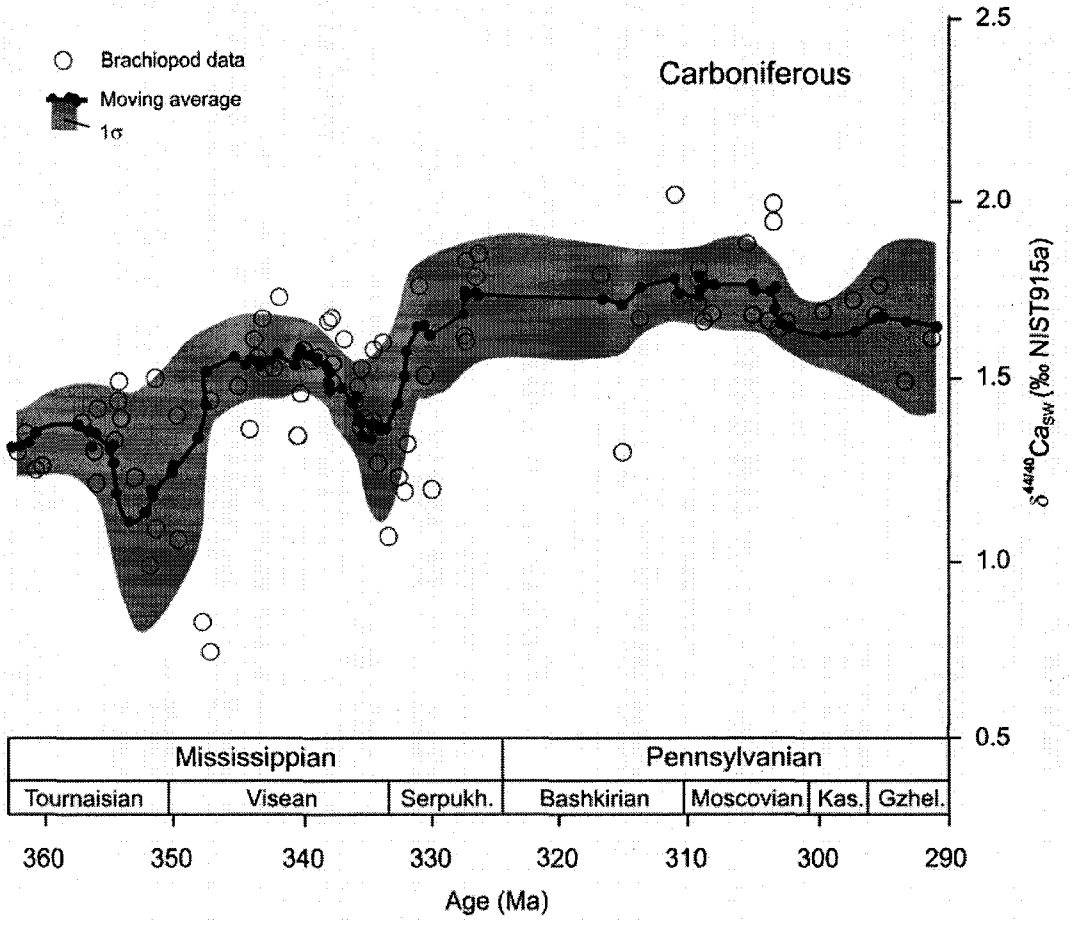

Fig. 3.6. The Carboniferous $\delta^{44/40}Ca_{SW}$ trend, based on brachiopod data (n = 83), showing two short-term negative excursions during the Mississippian. The smoothed trend (solid line + shaded area (±1σ)) is calculated from the original $\delta^{44/40}Ca_{SW}$ data set (open circles) using a 10-point moving average. Time scale from Harland et al. (1990).

3.5.3 Causes and implications of secular variations in Phanerozoic $\delta^{44/40}Ca_{SW}$ record

The $\delta^{44/40}Ca_{SW}$ value of the modern ocean of 1.88 ± 0.1‰ is globally homogeneous and independent of depth (Hippler at al., 2003; Schmitt et al., 2001), as expected from the long residence time of calcium in seawater, ~1 Ma, compared to the average mixing time of the ocean of ~1500 years (Broecker and Peng, 1982).

The average $\delta^{44/40}Ca$ of the primary source of calcium to the ocean, the continental river flux, is not accurately known but it is assumed to be close to 0.8 ± 0.2‰ (Zhu and Macdougall, 1998; Schmitt et al., 2003a; Heuser et al., 2005; Tipper et al., 2006). For smaller catchments, however, this value may vary significantly, from 0.5 to 1‰ (Schmitt et al., 2003a; Wiegand et al., 2005), depending on the net effect of biogeochemical processes, such as downstream precipitation of carbonates (Tipper et al., 2006) and/or recycling of soil calcium by vegetation (Schmitt et al., 2003a; Wiegand et al., 2005).

The isotope signature of calcium supplied to the ocean by high-temperature hydrothermal solutions at mid-ocean ridges is estimated to be close to ~0.9 ± 0.2‰ (Schmitt et al., 2003a; Amini et al., 2006) and is not expected to change with time. The low-temperature diffuse calcium flux at mid-ocean ridges is likely more depleted in ^{44}Ca than the discrete high-temperature flux, due to redissolution of isotopically light hydrothermal anhydrite. Mass balance considerations point to a general hydrothermal $\delta^{44/40}Ca$ of about 0.7‰ (Amini et al., submitted; Berner and Berner, 1996). Calcium released to the ocean during the dolomitization of marine carbonates is expected to be significantly lighter, with the mean $\delta^{44/40}Ca$ of about 0.3 ± 0.2‰ (Artemov et al., 1967; Heuser et al., 2005; Böhm et al., 2005).

The major sink for the oceanic calcium, neritic and pelagic carbonate sedimentation, has $\delta^{44/40}Ca$ uniform at ~0.95 ± 0.3‰ for calcite (Gussone et al., 2005; Heuser et al., 2005; De Paolo, 2004), at ~0.4 ± 0.2‰ for aragonite (Gussone et al., 2003 and 2005; Böhm et al., 2002), and around ~0.7 ± 0.2‰ for mineralization characterized by biological fractionation, e.g. in coccoliths and corals (Gussone et al., 2006; Böhm et al., 2006).

The $\delta^{44/40}Ca$ of marine carbonates is also dependent on temperature (Nägler et al. 2000; Hippler et al., 2002) and carbonate ion concentration in the surface ocean

(Lemarchand et al., 2004; Gussone et al., 2005). Nevertheless, modern biogenic carbonates exhibit only a weak sensitivity to these variables (Gussone et al., 2003 and 2005; De Paolo, 2004; Heuser et al., 2005).

The isotope composition of marine evaporites, specifically gypsum and anhydrite, is very variable with values ranging from 0.2 to 1.7 ‰, which is mostly due to Rayleigh fractionation associated with rapid precipitation (Hensley, 2006). Yet gypsum formed in marginal marine basins or salt-pans shows only little isotope fractionation with respect to the dissolved calcium in seawater (1.88‰) (Yang et al., 2006; F. Böhm, unpublished data) and therefore we assume the upper limit of the measured values (1.7 ‰) to be the most representative for marine evaporites. Anhydrites formed during the hydrothermal alteration of oceanic crust have generally lighter signatures of -0.5 to 0.7‰, because they are precipitated from hydrothermal fluids with low $\delta^{44/40}$Ca values (Hensley, 2006; Amini et al., submitted).

Based on the above isotope compositions of the major sources and sinks of calcium to the modern ocean, and also their corresponding fluxes (cf. Wallmann, 2001; De Paolo, 2004), the present-day seawater is close to steady state with respect to calcium isotopes and concentrations (Skulan et al., 1997; De La Rocha and DePaolo, 2000; Schmitt et al., 2003a), which however was not always the case in geological history.

3.5.4 Simulating Phanerozoic evolution of $\delta^{44/40}$Ca and seawater calcium concentrations

To simulate the Phanerozoic evolution of calcium seawater concentrations and isotope composition we used a model of coupled calcium/carbon/magnesium global cycles (Hansen and Wallmann, 2003; Wallmann, 2001, 2004; Heuser et al., 2005). The model uses the Phanerozoic $^{87}Sr/^{86}Sr$ record of Veizer et al. (1999) to calculate seafloor spreading and subduction rates (Wallmann, 2004). Dolomite formation rates are calculated from the record of oceanic Mg/Ca ratios (Horita et al., 2002; Ries, 2004; Lowenstein et al., 2001; Steuber and Rauch, 2005). The model is described in detail in the auxiliary material (see Appendix A.3.2).

For the mass balance of the oceanic calcium cycle the model considers release of calcium into the oceans through hydrothermal circulation at mid-ocean ridges (F_{HY}^{Ca}), dolomitization of carbonates deposited on the continental shelf (F_{DOLO}^{Ca}) and via continental weathering of carbonate (F_{WC}^{Ca}), silicate (F_{WS}^{Ca}) and evaporite (F_{WE}^{Ca}) rocks. Calcium is removed from seawater through carbonate burial on the continental shelf (F_{BCS}^{Ca}), pelagic carbonate deposition at the deep-sea floor (F_{BCP}^{Ca}), evaporite accumulation (F_{BE}^{Ca}) and the low-temperature alteration of oceanic crust (F_{ALT}^{Ca}). All of these fluxes are considered in the model:

$$\frac{dCa}{dt} = F_{HY}^{Ca} + F_{DOLO}^{Ca} + F_{WC}^{Ca} + F_{WS}^{Ca} + F_{WE}^{Ca} - F_{BCP}^{Ca} - F_{BCS}^{Ca} - F_{BE}^{Ca} - F_{ALT}^{Ca} \quad (3.2)$$

The magnitudes (in Tmol of Ca yr^{-1}) of input and output fluxes of calcium to the ocean applied in the model are presented in Fig. 3.7. The corresponding equations for the calculation of individual calcium fluxes are available in the auxiliary material (section A.3.2, Table A.3.2) (see also Wallmann, 2001).

For the isotope model of the oceanic calcium cycle a characteristic $\delta^{44/40}Ca$ signature is assigned to each flux (auxiliary material, section A.2, Table A.3.3) to simulate the experimental $\delta^{44/40}Ca_{SW}$ record. Briefly, the isotope signatures of the calcium input fluxes from weathering of silicates (F_{WS}^{Ca}) and evaporites (F_{WE}^{Ca}) as well as the hydrothermal flux (F_{HY}^{Ca}) were all kept constant at their modern $\delta^{44/40}Ca$ levels.

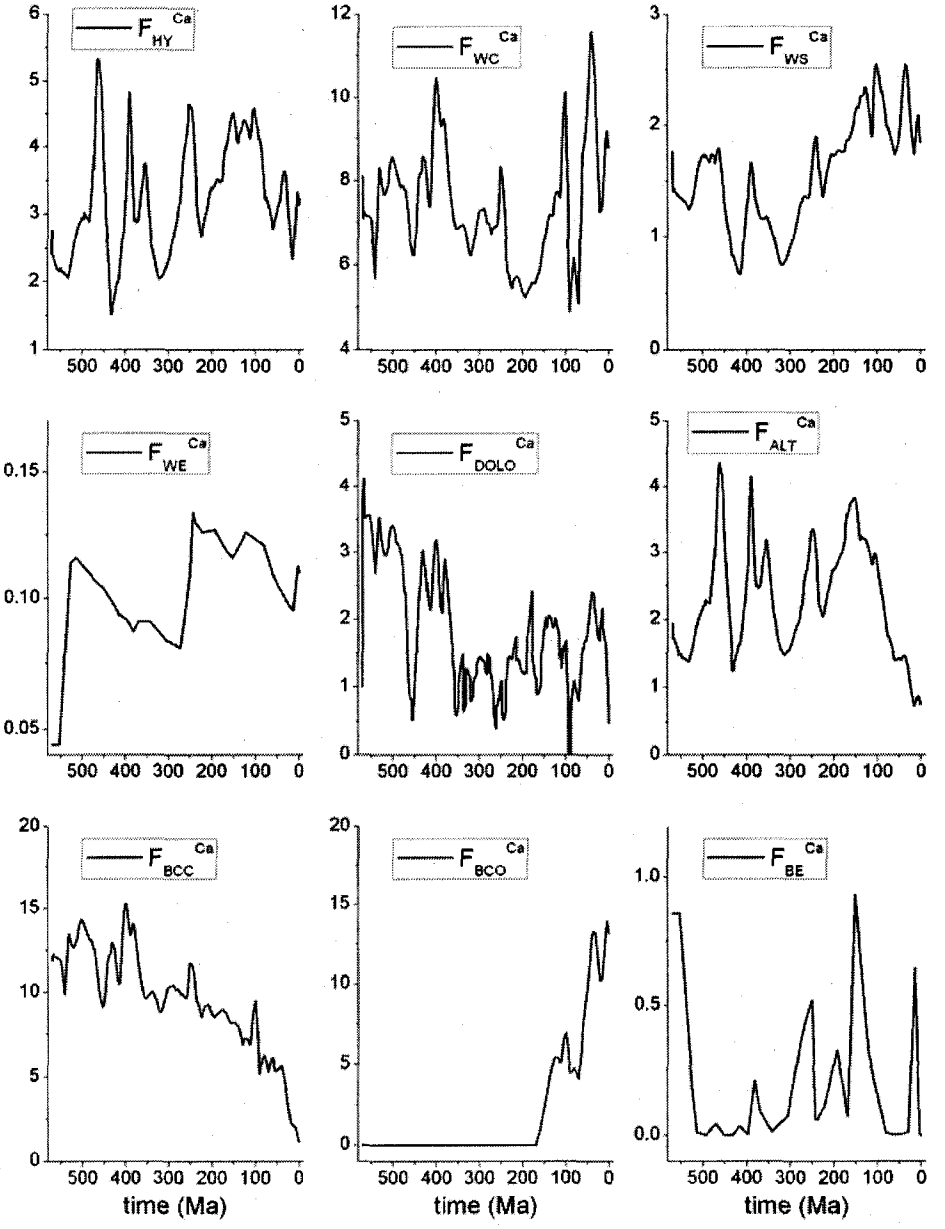

Fig. 3.7. Calcium fluxes applied in the model (in Tmol Ca yr^{-1}). F_{HY}^{Ca}: hydrothermal Ca input into the ocean; F_{WC}^{Ca}: Ca released during carbonate weathering; F_{WS}^{Ca}: Ca released via silicate weathering; F_{WE}^{Ca}: Ca released during evaporite weathering; F_{DOLO}^{Ca}: Ca released during dolomitization of marine carbonates; F_{ALT}^{Ca}: seawater Ca removed from the ocean during the alteration of oceanic crust; F_{BCC}^{Ca}: seawater Ca fixed in carbonates deposited on the continental shelf; F_{BCO}^{Ca}: seawater Ca fixed in pelagic carbonates; F_{BE}^{Ca}: seawater Ca fixed in marine evaporites. The corresponding equations for individual fluxes of calcium are available in the auxiliary material (Table A.3.2).

However, since the calcium isotope composition of marine carbonates changes with time, we applied a time dependent $\delta^{44/40}Ca$ signature for the continental river flux derived from weathering of carbonate rocks (F_{WC}^{Ca}) (Fig. 3.8), as well as for the dolomitization flux (F_{DOLO}^{Ca}) as the isotope composition of the latter is dependent on the source rock, i.e. marine carbonates.

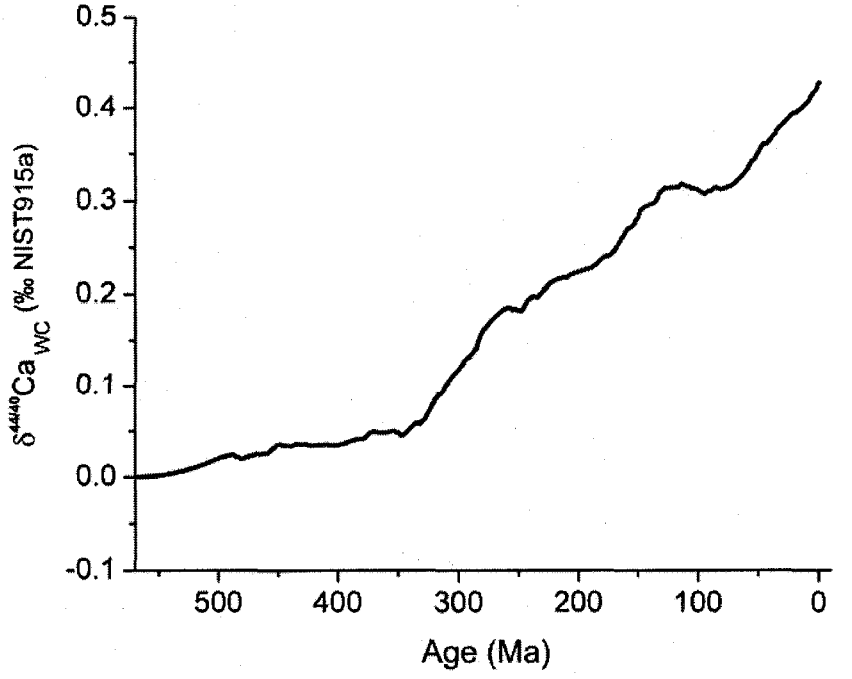

Fig. 3.8. Time dependent $\delta^{44/40}Ca$ signature of carbonates subjected to weathering. Following Garrels and Mackenzie (1971), we assumed that the carbonate rocks have an average renewal time of 200 Ma, which was used to calculate the isotopic composition of weathering carbonates by a corresponding running mean through the carbonate fossils dataset presented in this paper.

The calcium isotope composition of the oceanic carbonate burial flux (F_{BCS}^{Ca}, F_{BCP}^{Ca} and F_{ALT}^{Ca}) is related to the composition of seawater, temperature, mineralogy (aragonite vs. calcite) and the carbonate ion concentration in the surface ocean as well as the metabolic mechanisms of a calcifying organism (Böhm et al., 2002 and 2006; Gussone et al., 2003 and 2005; Lemarchand et al., 2004). Since the fractionation mechanisms involved in the formation of marine carbonates are poorly known, we used an inverse approach to determine

the fractionation factor (α_{CARB}) of the oceanic carbonate burial flux needed to simulate the $\delta^{44/40}Ca_{SW}$ database presented in this paper, when the relevant calcium fluxes varied as shown in Figs. 3.7 and 3.8.

$$\alpha_{CARB} = \frac{\left(\delta^{44/40}Ca_{CC} + 1000\right)}{\left(\delta^{44/40}Ca_{SW} + 1000\right)} = k_{CARB} \cdot \left(\delta^{44/40}Ca^{SW}{}_{MOD} - \delta^{44/40}Ca^{SW}{}_{DAT}\right) \quad (3.3)$$

The fractionation factor is proportional to the difference between the modeled and observed $\delta^{44/40}Ca_{SW}$ values. With this parameterization, α_{CARB} is automatically adjusted to minimize the difference between the two values for each time step. The kinetic constant k_{CARB} is set to a large value (50) so that the $\delta^{44/40}Ca_{SW}$ values calculated in the model (MOD) closely track the values documented in the geological record (DAT).

We explored two scenarios for the calculated α_{CARB} parameter to reconcile a large variability documented in Cretaceous $\delta^{44/40}Ca_{SW}$ values (Fig. 3.4). In the first scenario, α_{CARB} was varied to simulate the $\delta^{44/40}Ca_{SW}$ record based on skeletal carbonates, whereas in the second scenario it was adjusted to match $\delta^{44/40}Ca_{SW}$ reconstructed from the phosphate data. The results of the modeling: concentrations of dissolved calcium and magnesium in seawater, partial pressures of CO_2 in the atmosphere, pH and total dissolved inorganic carbon in surface waters and the deep ocean, are presented in Fig. 3.9.

Fig. 3.10 shows a comparison between modeled and measured $\delta^{44/40}Ca_{SW}$ as well as comparisons between model results and independent data from the geological record, such as, seawater calcium and magnesium concentrations (Horita et al., 2002; Lowenstein et al., 2001), the oceanic Mg/Ca ratios (Horita et al., 2002; Lowenstein et al., 2001; Ries, 2004; Steuber and Rauch, 2005) and the dominant mineralogy of marine skeletal carbonates in reefs (Kiessling, 2002).

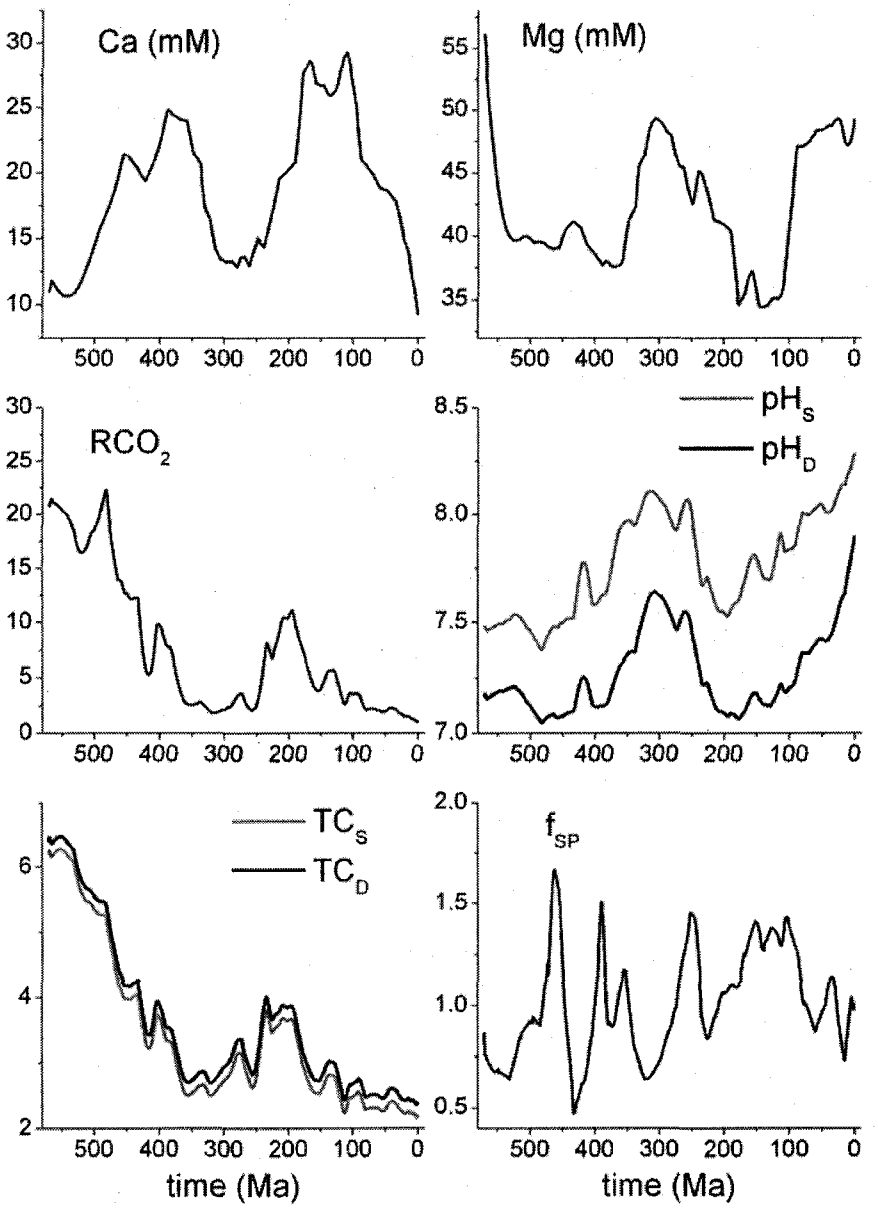

Fig. 3.9. Model results: concentrations of dissolved calcium and magnesium in seawater, partial pressures of CO_2 in the atmosphere normalized to the Quaternary value (RCO_2), pH in surface and deep waters, total dissolved inorganic carbon (TC) in surface and deep waters, spreading/subduction rate normalized to the modern value (f_{SP}).

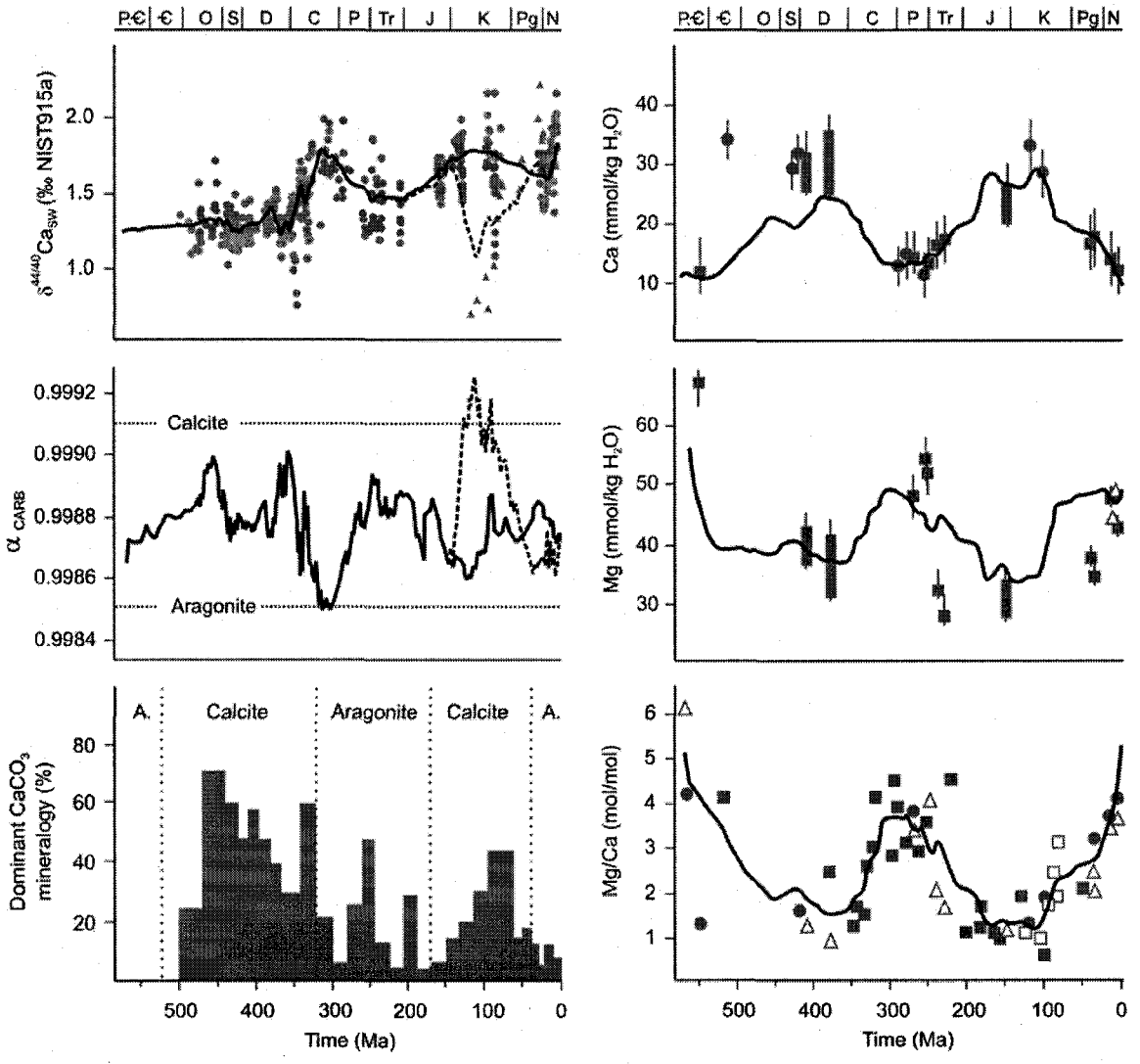

Fig. 3.10. Model results compared to independent data. Upper left panel: Phanerozoic $\delta^{44/40}Ca_{SW}$ trend as documented in the geological record (circles = carbonate data; triangles = phosphate data) and calculated in the model (solid line = scenario 1; dashed line = scenario 2). Middle left panel: Fractionation factor, α_{CARB}, for the formation of marine carbonates (shelf + pelagic + ocean crust) from seawater as calculated in the model (solid line = scenario 1; dashed line = scenario 2); dotted lines represent $\alpha_{cc/sw}$ of calcite and aragonite (Gussone et al., 2005). Lower left panel: Dominant mineralogy of marine skeletal carbonates in reefs; shaded = calcite, white = aragonite + high-Mg calcite (Kiessling, 2002). Upper right panel: Concentration of dissolved calcium in seawater documented in geological record (circles: Lowenstein et al., 2001; rectangles/squares: Horita et al., 2002) and calculated in the model. Middle right panel: Concentration of dissolved magnesium in seawater documented in geological record (rectangles/squares: Horita et al., 2002; triangles: Zimmermann, 2000) and calculated in the model. Lower right panel: Mg/Ca ratio in seawater as documented in the geological record and calculated in the model. Solid circles: (Horita et al., 2002); solid squares: (Ries, 2004); open triangles: (Lowenstein et al., 2001), open squares: (Steuber and Rauch, 2005); solid line: model result.

3.5.5 Implications for chemical evolution of Phanerozoic seawater and the concept of 'calcite-aragonite seas'

Experimental data from fluid inclusions of primary marine halite (Horita et al., 2002; Lowenstein et al., 2001 and 2003) indicate that the major ion composition of seawater has changed significantly over the Phanerozoic. Specifically, the concentrations of dissolved calcium and magnesium in seawater fluctuated in two long-term cycles and as mirror images of each other (Fig. 3.10). Consequently, the Mg/Ca ratio of Phanerozoic seawater also changed being mimicked by variations in mineral composition of marine skeletal and inorganic carbonates, so called 'calcite-aragonite seas' (Sandberg, 1983) (Fig. 3.10). These phenomena appear to be in phase with the stand of global sea level (Vail et al., 1977; Haq et al., 1987; Haq and Al-Qahtani, 2005), suggesting that the secular variations in chemical composition of seawater and the oscillating mineralogy of marine carbonates were primarily controlled by tectonic processes, specifically by changes in the rate of oceanic crust production and its hydrothermal alteration (Spencer and Hardie, 1990; Hardie 1996; Stanley and Hardie, 1998; Steuber and Veizer, 2002).

The newly formed oceanic crust reacts with seawater exchanging dissolved magnesium for the igneous derived calcium that modifies the oceanic Mg/Ca ratio (Edmond et al., 1979), which in turn affects the mineralogy of marine carbonates (Sandberg, 1975; Hardie, 1996; Morse et al. 1997; Stanley and Hardie, 1998). At low Mg/Ca ratio (<2) the dominant mineralogy of marine carbonates is low-Mg calcite, whereas during period of high oceanic Mg/Ca ratio the preference is given to aragonite and hig-Mg calcite, as higher levels of magnesium in seawater inhibit the formation of low-Mg calcite (Berner, 1975; Morse et al. 1997).

The Paleozoic, Early Mesozoic and Neogene $\delta^{44/40}Ca_{SW}$ trends, and also the calculated α_{CARB}, are in phase with the variation in the oceanic Mg/Ca ratio and the alternating 'calcite-aragonite seas' (Fig. 3.10). In general, 'calcite seas' correspond to periods of light $\delta^{44/40}Ca_{SW}$ and high α_{CARB} values, whereas the trends are opposite for 'aragonite seas'. This correlation, however, does not hold true for the Late Mesozoic and Cenozoic $\delta^{44/40}Ca_{SW}$ and α_{CARB} trends reconstructed from data of skeletal carbonates (Fig. 3.10; scenario 1), but it holds quite well for the coeval phosphate-based data (scenario 2).

This inconsistency in the correlation pattern may be partly due to the poorly constrained calcium isotope composition of Mesozoic seawater compared to the much better defined Paleozoic and Neogene $\delta^{44/40}Ca_{SW}$ trends, the latter two based exclusively on brachiopod and foraminifera data, respectively.

With these qualifications, the major features of the trend can be explained by taking into account the difference between the calcium isotope composition of calcite vs. aragonite burial fluxes of the oceanic calcium, the former uniform at ~0.95 ± 0.3‰ ($\alpha_{cc/sw} \approx 0.9991$) and the latter at ~0.4 ± 0.2‰ ($\alpha_{cc/sw} \approx 0.9985$) (Fig. 3.10). Therefore, an increase in aragonite formation, i.e. 'aragonite seas', would preferentially remove light ^{40}Ca from seawater leaving the residual calcium in the ocean reservoir isotopically heavier, whereas an enhanced calcite formation, i.e. 'calcite seas', would shift $\delta^{44/40}Ca_{SW}$ towards isotopically lighter values. Thus, the long-term excursions in Phanerozoic $\delta^{44/40}Ca_{SW}$ record most likely reflect variable rates of aragonite vs. calcite production and deposition in the oceans over time.

In this point of view the above mentioned correlation breakdown in the Mesozoic and Cenozoic may be due to the expansion of coccolithophorids and modern scleractinian corals as major calcium carbonate producers (Falkowski et al., 2004; Kiessling, 2002). Calcification in both groups has been shown to produce a distinct Ca isotope signal that is independent of the skeletal mineralogy (Gussone et al., 2006; Böhm et al., 2006). Dominant marine $CaCO_3$ production by these organisms would therefore decouple biogenic Ca isotope fractionation from the 'aragonite-calcite sea' oscillations.

The results of the modeling exercise further support our interpretation as they show that the observed variation in Phanerozoic $\delta^{44/40}Ca_{SW}$ record cannot be explained solely by changing the magnitudes of input and output fluxes of calcium to the oceans. Other factors, such as the changing calcium isotope composition of the oceanic carbonate burial flux, i.e. 'calcite-aragonite seas', must be taken into account.

In agreement with this explanation is the study of Steuber and Veizer (2002) that investigated the strontium contents of Phanerozoic skeletal carbonates (the same samples as in this study) and concluded that changes in mineralogy of marine carbonates and their

effect on burial rates of strontium in the oceans provide the most consistent explanation for their experimental data.

An alternative, or complementary, explanation for the long-term excursions in the Phanerozoic $\delta^{44/40}Ca_{SW}$ trend may be, at least in part, based on the effect of carbonate ion concentration, i.e. $[CO_3^{2-}]$, on calcium isotope fractionation of inorganic calcite (Lemarchand et al., 2004). These authors showed that $\delta^{44/40}Ca$ of inorganic calcite precipitated from a solution with a high Ca/CO_3^{2-} ratio, such as seawater, is a linear function of dissolved $[CO_3^{2-}]$, which in turn controls the saturation state of the solution with respect to calcite and aragonite (Ω).

In theory, large shifts in $[CO_3^{2-}]$ of Phanerozoic surface oceans by up to a factor of 5, as proposed by the geochemical models of Tyrell and Zeebe (2004) and Locklair and Lerman (2005), could have shifted the calcium isotope composition of marine carbonates by up to 0.7‰ (Gussone et al., 2005). Therefore the heavy $\delta^{44/40}Ca$ signatures of Late Carboniferous/Early Permian and Late Cenozoic brachiopods and foraminifera could be due to the higher $[CO_3^{2-}]$ of the contemporary surface oceans.

On the other hand, a generally weaker fractionation of the marine calcium carbonate production during these periods of higher seawater $[CO_3^{2-}]$ would have enriched seawater in light calcium, thus compensating for the carbonate ion effect on our $\delta^{44/40}Ca_{SW}$ recorders. In this case the seawater isotope shift would only be visible in $\delta^{44/40}Ca$ recorders that are not influenced by $[CO_3^{2-}]$, e.g. planktonic foraminifera (Gussone et al., 2003).

At this stage, we are not able to quantify the effect of carbonate ions on the reconstructed Phanerozoic $\delta^{44/40}Ca_{SW}$ trend as data constraining the $\delta^{44/40}Ca/CO_3^{2-}$ relationship for the individual recording phases and calcium carbonate producers are lacking. The only exceptions are the studies of Gussone et al. (2003) that showed no dependency of foraminiferal $\delta^{44/40}Ca$ (*Orbulina universa*) on ambient $[CO_3^{2-}]$, and of Gussone et al. (2006) who found a very weak negative dependency in the coccolithophorid *Emiliania huxleyi*. In addition, Langer (2005) found no dependency in another coccolithophorid, *Calcidiscus leptoporus*. These studies suggest that the effect of seawater

carbonate ion concentration on the $\delta^{44/40}Ca$ of skeletal carbonates may be negligible, at least for calcifiers that use photosynthesis and control the carbonate chemistry in their calcifying fluids.

Finally, one of the most striking features of Phanerozoic $\delta^{44/40}Ca_{SW}$ trend are the short-term oscillations superimposed on the overall trend (Figs. 3.5 and 3.6). We speculate that these are related to periods of enhanced dolomite formation and/or to changes in the chemical composition of the continental weathering flux, specifically short-term changes in Ca/HCO_3^- and Ca/SO_4^{2-} ratios of the global riverine flux, induced by variable rates of silicate vs. carbonate weathering on continents (Heuser et al., 2005).

A short-term negative excursion in $\delta^{44/40}Ca_{SW}$ record could be produced by enhanced rates of silicate weathering by sulphuric acid, e.g. during a period of enhanced volcanism. This would supply isotopically light calcium to the ocean without a proportional change in the carbonate ion flux, which would eventually shift $\delta^{44/40}Ca_{SW}$ to more negative values. Periods of increased sulfuric acid weathering should produce excursions in the marine sulfur isotope record, providing a possible test for the volcanic event hypothesis.

As to the explanation that is based on variable rates of dolomite formation, the resolution of the Mg/Ca record used to drive dolomitization in our model is unfortunately not sufficient to quantify events on a million year time-scale. Future work on magnesium isotopes may provide high-resolution records of marine $\delta^{26}Mg$ to test whether dolomitization episodes influenced the calcium concentration and isotope composition of the oceans.

3.6 Summary and Conclusions

The reconstructed Phanerozoic $\delta^{44/40}Ca_{SW}$ trend, based on the analysis of 397 marine skeletal carbonates and 22 phosphates, shows a generally increasing trend from ~1.3‰ at the beginning of the Ordovician to ~2‰ at present. Superimposed on this trend is a major long-term positive excursion from the Late Carboniferous to Early Permian as well as several short-term, mostly negative, oscillations during the Middle Silurian, Late Devonian, Early Carboniferous, Late Jurassic, Early/Late Cretaceous and Neogene.

The secular $\delta^{44/40}Ca_{SW}$ trend defines a rather consistent band of about ± 0.15‰ width, in agreement with our external reproducibility. This indicates that the isotope trends observed in this study are not caused by local factors like temperature variations or diagenesis. An exception is found in the Late Cretaceous where the scatter is much larger, possibly due to a higher sensitivity of rudist $\delta^{44/40}Ca$ to temperature and/or because the phosphate data may not faithfully reflect $\delta^{44/40}Ca_{SW}$. It is desirable that the calcium isotope composition of paleo-seawater should be based on comparable carrier phases, such as brachiopod and foraminiferal calcite that have only a weak $\delta^{44/40}Ca$-temperature gradient, <0.02‰ $°C^{-1}$.

Model simulations show that the observed variation in Phanerozoic $\delta^{44/40}Ca_{SW}$ record cannot be explained solely by varying the magnitudes of input and output fluxes of calcium to the ocean. The most likely complementary mechanism is the alternating mineralogy of marine skeletal carbonates, i.e. 'calcite-aragonite seas'.

Our results indicate that the calcium isotope budget of Phanerozoic oceans was ultimately controlled by tectonic processes, most likely via variable rates of oceanic crust production and its hydrothermal alteration. This modulated the oceanic Mg/Ca ratio that, in turn, controlled the dominant mineralogy of marine skeletal carbonates and thus the $\delta^{44/40}Ca_{SW}$. This interpretation is in accord with the proposition of Steuber and Veizer (2002) who concluded, from strontium concentrations in biological calcites, that the chemical composition of Phanerozoic seawater has been ultimately tectonically controlled.

As to the possible causes of the short-term, mostly negative, oscillations that are superimposed on the long-term $\delta^{44/40}Ca_{SW}$ trend, we tentatively suggest that these are related to periods of enhanced dolomite formation and/or to temporal changes in the chemical composition of the continental riverine flux, specifically Ca/HCO_3^- and Ca/SO_4^{2-} ratios, induced by variable proportions of silicate vs. carbonate and CO_2 vs. SO_2 weathering rates.

Acknowledgements

This study was supported by the Natural Science and Engineering Research Council of Canada and the Canadian Institute for Advanced Research (NSERC and CIAR research

grants to J. Veizer). J. Farkaš was supported by the International Graduate Admission Scholarship of the University of Ottawa (2003-2007) and partially supported by Geological Society of America (2003 and 2004 GSA graduate student research grant). The contribution of F. Böhm and A. Eisenhauer was supported by the European Science Foundation (ESF) as part of the EUROclimate project (08) CASIOPEIA. Further support was provided by the 'Deutsche Forschungsgemeinschaft, DFG' grant Ei272/13-1 (CATO) and Mu2352/1. Assistance with mass spectrometry and laboratory work of M. Wilk, L.A. Spencer, B. Cousens and S. Carr from Ottawa-Carleton Geoscience Centre (OCGC) and the Isotope Geochemistry and Geochronology Research Centre (IGGRC) is greatly acknowledged. M. Amini and B. Kisakürek kindly helped with measuring the IAPSO seawater standard at IFM-GEOMAR, and with discussions about hydrothermal calcium pathways and biogenic calcium fractionation. This work is the IGGRC contribution No. 48.

References

Alt J.C., Teagle D.A.H., Laverne C., Vanko D.A., Bach W., Honnorez J., Becker K., Ayadi M. and Pezard P.A. (1996) Ridge flank alteration of upper ocean crust in the eastern Pacific: Synthesis of results for volcanic rocks of Holes 504B and 896A. *Proceedings of the Ocean Drilling Program, Scientific Results* **148**, 435-450.

Amini M., Eisenhauer A., Böhm F., Fietzke J., Bock B., Garbe-Schönberg D., Lackschewitz K.S. and Hauff F. (2006) Calcium isotope variations along the hydrothermal pathway, *Geophys. Res. Abstr.* **8,** Sref-ID: 1607-7962/gra/EGU06-A-08864.

Amini M., Eisenhauer A., Böhm F., Fietzke J., Bach W., Garbe-Schönberg D.,Rosner M., Bock B., Lackschewitz K.S. and Hauff F. (2007) Calcium Isotope ($\delta^{44/40}$Ca) Fractionation along Hydrothermal Pathways, Logatchev Field (Mid-Atlantic Ridge, 14°45' N). Submitted to *Geochim. Cosmochim. Acta.*

Artemov Yu. M., Strizhov V.P., Ustinov V.I. and Yaroshevskiy A.A. (1967) Possible isotope fractionation during dolomitization. *Geokhimiya* **5**, 519-529.

Berner R.A. (1975) The role of magnesium in the crystal growth of calcite and aragonite from seawater. *Geochim. Cosmochim. Acta* **39**, 489–504.

Berner E.K., Berner R.A. (1996) Global Environment: Water, Air, and Geochemical Cycles. Prentice Hall, Upper Saddle River, N.J.

Berner R.A. (2004) A model for calcium, magnesium and sulfate in seawater over Phanerozoic time. *Am. J. Sci.* **304**, 438-453.

Böhm F., Eisenhauer A., Gussone N., Heuser A., Haase-Schramm A., Dietzel M., Reitner J. and Vacelet J. (2002) Fractionation of $^{44}Ca/^{40}Ca$ between aragonite and calcite. *Geochim. Cosmochim. Acta* **66**, suppl. 1, A87.

Böhm F., van Geldern R., Gussone N. and Eisenhauer A. (2004) Calcium isotope variation in Devonian brachiopods, 2.7.P08, *Geochim. Cosmochim. Acta* **68/11**, suppl. 1, A213.

Böhm F., Eisenhauer A., Heuser A., Kiessling W. and Wallmann K. (2005) Calcium isotope fractionation during dolomitization. *Schriftenreihe Deutsch. Ges. Geowissensch.* **39**, pp. 39.

Böhm F., Gussone N., Eisenhauer A., Dullo W-Ch., Reynaud S. and Paytan A. (2006) Calcium isotope fractionation in modern scleractinian corals. *Geochim. Cosmochim. Acta* **70**, 4452–4462.

Broecker W.S. and Peng T.-H. Tracers in the Sea, Eldigo Press, New York, 1982, pp. 690.

Calner M., Jeppsson L. and Munnecke A. (2004) The Silurian of Gotland - Part I: Review of the stratigraphic framework, event stratigraphy, and stable carbon and oxygen isotope development.- Erlanger geologische Abhandlungen, Sb**5**, 113-131.

De La Rocha C.L. and DePaolo D.J. (2000) Isotopic evidence for variations in the marine calcium cycle over the Cenozoic. *Science* **289**, 1176–1178.

DePaolo D.J. (2004) Calcium isotopic variations produced by biological, kinetic, radiogenic and nucleosynthetic processes, in: C.M. Johnson, B.L. Beard, F. Albarede (Eds.), Geochemistry of Non-traditional Stable Isotopes, vol. 55, Mineralogical Society of America and Geochemical Society, Washington, D.C., Rev. Mineral. Geochem., 2004, pp. 255–288.

Dickson J.A.D. (2002) Fossil echinoderms as a monitor of the Mg/Ca ratio of Phanerozoic oceans. *Science* **298**, 1222-1224.

Edmond J.M., Measures C., McDuff R.E., Chan L.H., Collier R., Grant B., Gordon L.I. and Corliss J.B. (1979) Ridge crest hydrothermal activity and the balances of the major and minor elements in the ocean: The Galapagos data. *Earth Planet. Sci. Lett.* **46**, 1–18.

Eisenhauer A., Nägler T., Stille P., Kramers J., Gussone N., Bock B., Fietzke J., Hippler D. and Schmitt A-D. (2004) Proposal for an International Agreement on Ca Notation as a result of the Discussion from the workshop on Stable Isotope Measurements in Davos (Goldschmidt 2002) and Nice (EGS-AGU-EUG 2003). *Geostandards Geoanal. Res.* **28**, 149-151.

Falkowski P.G., Katz M.E., Knoll A.H., Quigg A., Raven J.A., Schofield O., Taylor F.J.R. (2004) The Evolution of Modern Eukaryotic Phytoplankton. *Science*, **305**, 354-360.

Fantle M.S. and DePaolo D.J. (2005) Variations in marine Ca cycle over the past 20 million years. *Earth Planet. Sci. Lett.* **237**, 102–117.

Fantle M.S. and DePaolo D.J. (2007) Ca isotopes in carbonate sediment and pore fluid from ODP Site 807A: The Ca^{2+}(aq)-calcite equilibrium fractionation factor and calcite recrystallization rates in Pleistocene sediments. *Geochim. Cosmochim. Acta*, **71**, 2524-2546.

Farkaš J., Buhl D., Blenkinsop J., and Veizer J. (2007) Evolution of the oceanic calcium cycle during the late Mesozoic: Evidence from $\delta^{44/40}$Ca of marine skeletal carbonates. *Earth Planet. Sci. Lett.* **253**, 96–111.

Garrels R.M. and Mackenzie F.T. (1971) Evolution of Sedimentary Rocks. W.W. Norton and Company, New York, 397 pp.

Gradstein F.M., Ogg J.G., Smith A.G., Agterberg F.P., Bleeker W., Cooper R.A., Davydov V., Gibbard P., Hinnov L., House M.R., Lourens L., Luterbacher H.-P., McArthur J., Melchin M.J., Robb L.J., Shergold J., Villeneuve M., Wardlaw B.R., Ali J., Brinkhuis H., Hilgen F.J., Hooker J., Howarth R.J., Knoll A.H., Laskar J., Monechi S., Powell J., Plumb K.A., Raffi I., Röhl U., Sanfilippo A., Schmitz B., Shackleton N.J., Shields G.A., Strauss H., Van Dam J., Veizer J., van Kolfschoten Th. and Wilson D. (2004) A Geologic Time Scale, Cambridge Univ. Press, Cambridge.

Gussone N., Eisenhauer A., Heuser A., Dietzel M., Bock B., Böhm F., Spero H.J., Lea D.W., Bijma J. and Nägler T. (2003) Model for kinetic effects on calcium isotope fractionation (δ^{44}Ca) in inorganic and cultured planktonic foraminifera. *Geochim. Cosmochim. Acta* **67**, 1375–1382.

Gussone N., Eisenhauer A., Tiedemann R., Haug G.H., Heuser A., Bock B., Nägler T. and Müller A. (2004) Reconstruction of Caribbean sea surface temperature and salinity fluctuations in response to the Pliocene closure of the Central American gateway and radiative forcing, using $\delta^{44/40}$Ca, δ^{18}O and Mg/Ca ratios. *Earth Planet. Sci. Lett.* **227**, 201–214.

Gussone N., Böhm F., Eisenhauer A., Dietzel M., Heuser A., Teichert B.M.A., Reitner J., Wörheide G. and Dullo W.-Ch. (2005) Calcium isotope fractionation in calcite and aragonite. *Geochim. Cosmochim. Acta* **69**, 4485–4494.

Gussone N., Langer G., Thoms S., Nehrke G., Eisenhauer A., Riebesell U., Wefer G. (2006) Cellular calcium pathways and isotope fractionation in *Emiliania huxleyi*. *Geology*, **34**, 625-628.

Hansen K.W. and Wallmann K. (2003) Cretaceous and Cenozoic evolution of seawater composition, atmospheric O_2 and CO_2: A model perspective. *Am. J. Sci.* **303**, 94-148.

Haq, B.U. and Al-Qahtani, A.M. (2005) Phanerozoic cycles of sea-level change on the Arabian Platform. *GeoArabia*, **10**, 127-160.

Haq, B.U., Hardenbol, J. and Vail, P.R. (1987) Chronology of fluctuating sea-levels since the Triassic. *Science* **235**, 1156-1167.

Hardie L.A. (1996) Secular variations in seawater chemistry: An explanation for the coupled secular variation in the mineralogies of marine limestones and potash evaporites over the past 600 My. *Geology* **24**, 279-283.

Harland W.B., Armstrong R.L., Cox A.V., Craig L.E., Smith A.G. and Smith D.G., A Geologic Time Scale, Cambridge Univ. Press, Cambridge, 1990.

Hay W.W., Migdisov A., Balukhovsky A.N., Wold C.N., Flögel S. and Söding E. (2006) The decline in salinity of the ocean during the Phanerozoic: implications for climate, ocean circulation and life. *Palaeogeo. Palaeoclimat. Palaeoeco.* **240**, 3-46.

Hensley T.M. (2006) Calcium isotope variation in marine evaporites and carbonates: Applications to Late Miocene Mediterranean brine chemistry and Late Cenozoic calcium cycling in the oceans, Doctoral dissertation, University of Californian, San Diego.

Heuser A., Eisenhauer A., Böhm F., Wallmann K., Gussone N., Pearson P.N., Nägler T.F. and Dullo W-Ch. (2005) Calcium isotope ($\delta^{44/40}$Ca) variations of Neogene planktonic foraminifera. *Paleoceanography* **20**, PA2013, doi:10.1029/2004PA001048.

Heuser A., Eisenhauer A., Gussone N., Bock B., Hansen B.T. and Nägler T.F. (2002) Measurement of calcium isotopes ($\delta^{44/40}$Ca) using a multicollector TIMS technique. *Int. J. Mass Spectrom.* **220**, 387-399.

Hippler D., Gussone N., Darling K., Eisenhauer A. and Nägler T. (2002) δ^{44}Ca in *N. pachy* (left): A new SST-proxy in polar regions. *Geochim. Cosmochim. Acta* **66**, suppl. 1, A331.

Hippler D., Schmitt A.-D., Gussone N., Heuser A., Stille P., Eisenhauer A. and Nägler T. (2003) Ca isotopic composition of various standards and seawater. *Geostandards Newsletter* **27**, 13-19.

Hippler D., Villa I., Nägler Th.F. and Kramers J. (2004) A ghost haunts mass spectrometry: Real isotope fractionation or analytical paradox? *Geochim. Cosmochim. Acta* **68/11** (Suppl. 1), A215.

Holland H.D. (2005) Sea level, sediments and the composition of seawater. *Am. J. Sci.* **305**, 220-239.

Holland H.D. and Zimmermann H. (2000) The dolomite problem revisited. *Int. Geol. Rev.* **42**, 481–490.

Horita J., Zimmermann H. and Holland H.D. (2002) Chemical evolution of seawater during the Phanerozoic: Implications from the record of marine evaporites. *Geochim. Cosmochim. Acta* **66**, 3733–3756.

Immenhauser A., Nägler T., Steuber T. and Hippler D. (2005) A critical assessment of mollusk $^{18}O/^{16}O$, Mg/Ca, and $^{44}Ca/^{40}Ca$ ratios as proxies for Cretaceous seawater temperature seasonality. *Palaeogeo. Palaeoclim. Palaeoeco.* **215**, 221–237.

Jeppsson L., Eriksson M.E. and Calner M. (2006) A latest Llandovery to latest Ludlow high-resolution biostratigraphy based on the Silurian of Gotland – a summary. *GFF* **128**, 109–114.

Kampschulte A. and Strauss H. (2004) The sulfur isotopic evolution of Phanerozoic seawater based on the analysis of structurally substituted sulfate in carbonates. *Chem. Geol.* **204**, 255–286.

Kasemann S.A., Hawkesworth Ch.J., Pravec A.R., Fallick P.N. and Pearson P.N. (2005) Boron and calcium isotope composition in Neoproterozoic carbonate rocks from Namibia: evidence for extreme environmental change. *Earth Planet. Sci. Lett.* **231**, 73–86.

Kiessling W. (2002) Secular variations in the Phanerozoic reef ecosystem, in: *Phanerozoic Reef Patterns* (Kiessling W., Flügel E. and Golonka J., eds.) Soc. Econ. Paleontologists Mineralogists Spec. Pub. No. 72, Tulsa, Okla. pp. 625–690.

Kreissig K., Elliott T. (2005) Ca isotope fingerprints of early crust-mantle evolution. *Geochim. Cosmochim. Acta*, **69**, 165-176.

Langer G. (2005) Calcification of selected coccolithophore species: strontium partitioning, calcium isotope fractionation and dependence on seawater carbonate chemistry. Ph.D. thesis, University of Bremen, 169 pp.

Lemarchand D., Wasserburg G.J. and Papanastassiou D.A. (2004) Rate-controlled calcium isotope fractionation in synthetic calcite. *Geochim. Cosmochim. Acta* **68**, 4665–4678.

Locklair R.E. and Lerman A. (2005) A model of the Phanerozoic cycles of carbon and calcium in the global ocean: evaluation and constraints on ocean chemistry and input fluxes. *Chem. Geol.* **217**, 113–126.

Lowenstein T.K., Hardie M.N., Timofeeff R.V. and Demicco R.V. (2003) Secular variations in seawater chemistry and the origin of calcium chloride basinal brines, *Geology* **31**, 857–860.

Lowenstein T.K., Timofeeff R.V., Brennan S.T., Hardie M.N. and Demicco R.V. (2001) Oscillations in Phanerozoic seawater chemistry: Evidence from fluid inclusions, *Science* **294**, 1086–1088.

Morse J.W., Wang Q. and Tsio M.Y. (1997) Influences of temperature and Mg:Ca ratio on $CaCO_3$ precipitates from seawater. *Geology* **25**, 85–87.

Nelson D.R., McCulloch M.T. (1989) Petrogenetic applications of the ^{40}K-^{40}Ca radiogenic decay scheme - A reconnaissance study. *Chem. Geol.*, **79**, 275-293.

Nägler T., Eisenhauer A., Müller A., Hemleben C. and Kramers J. (2000) The $\delta^{44}Ca$-temperature calibration on fossil and cultured Globigerinoides sacculifer: New tool for reconstruction of past sea surface temperatures, *Geochem. Geophys. Geosyst.* 1, doi: 10.1029/2000GC000091.

Ridgwell A. and Zeebe R. E. (2005) The role of the global carbonate cycle in the regulation and evolution of the Earth system. *Earth Planet. Sci. Lett.* **234**, 299-315.

Ries J.B. (2004) Effect of ambient Mg/Ca ratio on Mg fractionation in calcareous marine invertebrates: A record of the oceanic Mg/Ca ratio over the Phanerozoic. *Geology* **32**, 981–984.

Russell W.A., Papanastassiou D.A. and Tomberllo T.A. (1978) Ca isotope fractionation on the Earth and other solar system materials. *Geochim. Cosmochim. Acta* **42**, 1075–1090.

Samtleben C., Munnecke A. and Bickert, T. (2000) Development of facies and C/O-isotopes in transects through the Ludlow of Gotland: Evidence for global and local influences on a shallow-marine environment. *Facies* **43**, 1–38.

Samtleben C., Munnecke A., Bickert, T. and Pätzold, J. (2001) Shell succession, assemblage and species dependent effects on the C/O-isotope composition of brachiopods - examples from the Silurian of Gotland. *Chemical Geology* **175**, 61–107.

Sandberg P.A. (1975) New interpretations of Great Salt Lake ooids and of ancient nonskeletal carbonates mineralogy. *Sedimentology* **22**, 497–537.

Sandberg P.A. (1983) An oscillating trend in Phanerozoic non-skeletal carbonate mineralogy. *Nature* **305**, 19-22.

Schmitt A.-D., Bracke G., Stille P. and Kiefel B. (2001) The calcium isotope composition of modern seawater determined by Thermal Ionization Mass Spectrometry. *Geostand. Newslett.* **25**, 267-275.

Schmitt A.-D., Chabaux F. and Stille P. (2003a) The calcium riverine and hydrothermal isotopic fluxes and the oceanic calcium mass balance, *Earth Planet. Sci. Lett.* **213**, 503–518.

Schmitt A.-D., Stille P. and Vennemann T. (2003b) Variations of the $^{44}Ca/^{40}Ca$ ratio in seawater during the past 24 million years: Evidence from $\delta^{44}Ca$ and $\delta^{18}O$ values of Miocene phosphates, *Geochim. Cosmochim. Acta* **67**, 2607–2614.

Scotese C.R. (1997) Paleogeographic Atlas, PALEOMAP Progress Report 90-0497. Department of Geology, University of Texas at Arlington, Arlington, TX. 37 pp.

Scotese C.R., MacKinnon D.I., Marlatt J.R., Reilly W.J., Smith A.G. and Stanford B.D. (1994) Continental Drift, edn. 6. The PALEOMAP Project.

Skulan J. L., D.J. DePaolo and T.L. Owens (1997), Biological control of calcium isotopic abundances in the global calcium cycle, *Geochim. Cosmochim. Acta,* **61**, 2505-2510.

Soudry D., Segal I., Nathan Y., Glenn C.R., Halicz L., Lewy Z. and VonderHaar D.L. (2004) $^{44}Ca/^{42}Ca$ and $^{143}Nd/^{144}Nd$ isotope variations in Cretaceous-Eocene Tethyan francolites and their bearings on phosphogenesis in the southern Tethys. *Geology* **32**, 389–392.

Soudry D., Glenn C.R., Nathan Y., Segal I., VonderHaar D.L. (2006) Evolution of Tethyan phosphogenesis along the northern edges of the Arabian-African shield during the Cretaceous-Eocene as deduced from temporal variations of Ca and Nd isotopes and rates of P accumulation. *Earth-Science Rev.*, **78**, 27-57.

Spencer R.J. and Hardie L.A. (1990) Control of seawater composition by mixing of river waters and mid-ocean ridge hydrothermal brines. In *Fluid-Mineral Interactions: A Tribute to H.P. Eugster* (eds. R.J. Spencer and I.-M. Chou), pp. 409-419. Special Publication 2. Geochemical Society.

Stanley S.M. and Hardie L.A. (1998) Secular oscillations in the carbonate mineralogy of reef-building and sediment-producing organisms driven by tectonically forced shifts in seawater chemistry. *Paleogeo. Paleoclim. Paleoeco.* **144**, 3-19.

Steuber T. and Buhl D. (2006) Calcium-isotope fractionation in selected modern and ancient marine carbonates. *Geochim. Cosmochim. Acta* **70**, 5507-5521.

Steuber T. and Rauch M. (2005) Evolution of the Mg/Ca ratio of Cretaceous seawater: Implications from the composition of biological low-Mg calcite. *Mar. Geol.* **217**, 199-213.

Steuber T. and Veizer J. (2002) Phanerozoic record of plate tectonic control of seawater chemistry and carbonate sedimentation. *Geology* **30**, 1123-1126.

Teagle D.A.H., Alt J.C., Bach W., Halliday A.N. and Erzinger J. (1996) Alteration of upper ocean crust in a ridge-flank hydrothermal upflow zone: Mineral, chemical, and isotopic constraints from hole 896A. *Proceedings of the Ocean Drilling Program, Scientific Results* **148**, 119-150.

Tipper E.T., Galy A. and Bickle M.J. (2006) Riverine evidence for a fractionated reservoir of Ca and Mg on the continents: Implications for the oceanic Ca cycle. *Earth Planet. Sci. Lett.* **247**, 267–279.

Tomašových A. (2004) Postmortem durability and population dynamics affecting the fidelity of brachiopod size-frequency distributions. *Palaios* **19**, 477-496.

Tyrrell T., Zeebe R.E. (2004): History of carbonate ion concentration over the last 100 million years. *Geochim. Cosmochim. Acta* **68**, 3521-3530.

van Geldern R., Joachimski M.M., Daly J., Jansen U., Alvarez F., Yolkin E.A. and Ma X.-P. (2006) Carbon, oxygen and strontium isotope records of Devonian brachiopod shell calcite. *Paleogeo. Paleoclim. Paleoeco.* **240**, 47-67.

Veizer J. (1983) Chemical diagenesis of carbonates: theory and application of trace element technique, in: M.A. Arthur, T.F. Anderson, I.R. Kaplan, J. Veizer, L. Land (Eds.), Stable Isotopes in Sedimentary Geology: Society of Economic Paleontologists and Mineralogists, Short Course, vol. 10, 1983, pp. III/1–III/100.

Veizer J., Ala D., Azmy K., Bruckschen P., Buhl D., Bruhn F., Carden G.A.F., Diener A., Ebneth S., Godderis Y., Jasper T., Korte Ch., Pawellek F., Podlaha O. and Strauss H. (1999) $^{87}Sr/^{86}Sr$, $\delta^{13}C$ and $\delta^{18}O$ evolution of Phanerozoic seawater. *Chem. Geol.* **161**, 59–88.

Veizer J. and Mackenzie F.T. (2003) The chemical composition of ancient ocean. In *Evolution of Sedimentary Rocks* (ed. F.T. Mackenzie) Vol. 7, Treatise on geochemistry (eds. H.D. Holland and K.K. Turkenian) Elsevier-Pergamon, Oxford, 2003, pp. 369-407.

Voigt S., Gale A.S., Flögel S. (2004) Midlatitude shelf seas in the Cenomanian-Turonian greenhouse world: Temperature evolution and North Atlantic circulation. *Paleoceanography* **19**, PA4020, doi:10.1029/2004PA001015.

Wallmann K. (2001) Controls on the Cretaceous and Cenozoic evolution of seawater composition, atmospheric CO_2 and climate. *Geochim. Cosmochim. Acta* **65**, 3005-3025.

Wallmann K. (2004) Impact of atmospheric CO_2 and galactic cosmic radiation on Phanerozoic climate change and the marine $\delta^{18}O$ record. *Geochem. Geophys. Geosyst.* **5** Q06004, doi: 10.1029/2003GC000683.

Wiegand B.A., Chadwick O.A., Vitousek P.M. and Wooden J.L. (2005) Ca cycling and isotopic fluxes in forested ecosystems in Hawaii. *Geophys. Res. Lett.* **32**, L11404, doi: 10.1029/2005GL022746.

Yang W., DePaolo D., Ingram L., Owens T. (2006) Stable Ca, H and O Isotopes in the Modern Death Valley Hydrological System, California. *EOS Trans. AGU,* **87**, Fall Meet. Suppl., Abstract H11I-07.

Zhu P. and Macdougall J.D. (1998) Calcium isotopes in the marine environment and the oceanic calcium cycle. *Geochim. Cosmochim. Acta* **62**, 1691-1698.

Zimmermann H. (2000) Tertiary seawater chemistry-Implications from fluid inclusions in primary marine halite. *Am. J. Sci.* **300**, 723-767.

Auxiliary material for the 'Paper 2'

A.3.1 Automated Calcium Isotope Analysis

We developed a fully automated analytical protocol for the calcium isotope measurements where samples loaded in the mass spectrometer were heated to an ionization temperature of about 1400 °C using an automatic sequence with a built-in program for the sample heating (Table A.3.1). The target ion beam intensity for ^{40}Ca signal was 130 pA (13000 mV), which was usually reached within ~30 min. The sample heating sequence was followed by an automated data acquisition routine. The calcium isotope peaks (masses 40 to 48) were measured in two steps (Farkaš et al., 2007), including ^{41}K that was monitored for possible isobaric interferences of ^{40}K on ^{40}Ca. An individual Ca isotope measurement consisted of 108 cycles (9 blocks of 12 cycles each), with an integration time of 16-s per cycle followed by a 3-s waiting time. Defocused baselines measurements were collected for 30 s at the beginning of each block. A total analytical time of this fully automated Ca isotope technique was ~150 min per sample (30 min for sample heating plus 120 min for data acquisition).

Table A.3.1.

Automatic sequence for the sample heating and data acquisition designed for the Thermo Electron Triton mass spectrometer

Line	Time (min:sec)	Valve	Filament	Function	Target (°C, mV)	Slope (mA/min)	Action
1	00:00	Closed	Ionization	Filament Temp.	1200 °C	260	None
2	10:00	Open	Ionization	Ion Current (^{40}Ca)	5 mV	120	Auto Focus
3	16:35	Open	Ionization	Ion Current (^{40}Ca)	100 mV	100	Auto Focus
4	19:00	Open	Ionization	Ion Current (^{40}Ca)	1000 mV	80	None
5	20:00	Open	Evaporation	Ion Current (^{40}Ca)	2000 mV	40	None
6	21:00	Open	Evaporation	Ion Current (^{40}Ca)	4000 mV	25	Auto Focus
7	23:40	Open	Evaporation	Ion Current (^{40}Ca)	8000 mV	20	None
8	24:40	Open	Evaporation	Ion Current (^{40}Ca)	13000 mV	20	Auto Focus
9	27:10	Open	Evaporation	Ion Current (^{40}Ca)	13000 mV	40	Auto Focus
10	29:50	Open	Evaporation	Ion Current (^{40}Ca)	13000 mV	40	None
11	30:50		End				Data Acquisition

A.3.2 Simulating Phanerozoic evolution of calcium seawater concentrations and isotopic composition

Calcium model

Calcium (Ca) is released into the ocean through hydrothermal circulation systems at mid-ocean ridges (F_{HY}^{Ca}), dolomitization of carbonates deposited on the continental shelf (F_{DOLO}^{Ca}) and via continental weathering of carbonate (F_{WC}^{Ca}), silicate (F_{WS}^{Ca}) and evaporite (F_{WE}^{Ca}) rocks. It is removed from seawater through carbonate burial on the continental shelf (F_{BCS}^{Ca}), pelagic carbonate deposition at the deep-sea floor (F_{BCP}^{Ca}), evaporite accumulation (F_{BE}^{Ca}) and the alteration of oceanic crust (F_{ALT}^{Ca}). All of these Ca fluxes are considered in the model:

$$\frac{dCa}{dt} = F_{HY}^{Ca} + F_{DOLO}^{Ca} + F_{WC}^{Ca} + F_{WS}^{Ca} + F_{WE}^{Ca} - F_{BCP}^{Ca} - F_{BCS}^{Ca} - F_{BE}^{Ca} - F_{ALT}^{Ca}$$

The corresponding flux equations for carbonate and silicate weathering and for hydrothermal Ca release are taken from Wallmann (2001 and 2004). Ca fluxes induced by burial and weathering of evaporites are derived from data given in Hay et al. (2006) assuming that evaporites contain on average 20 wt-% Ca sulfates (Hansen and Wallmann, 2003).

Since the field evidence for Phanerozoic trends in dolomite accumulation remains controversial (Holland, 2005), we use the much better constrained Mg/Ca seawater record (Ries, 2004) to define Ca release and Mg uptake through dolomitization (F_{DOLO}^{Ca}):

$$F_{DOLO}^{Ca} = k_{DOLO} \cdot \left(\left.\frac{Mg}{Ca}\right|_{MOD} - \left.\frac{Mg}{Ca}\right|_{DAT} \right)$$

The rate of dolomitization is set proportional to the divergence between the modeled and observed Mg/Ca seawater ratios (cf. Fig. 3.7). With this parameterization, F_{DOLO}^{Ca} is automatically adjusted to minimize the difference between the two ratios for each time step.

The kinetic constant k_{DOLO} is set to a large value (100 Tmol yr^{-1}) so that the Mg/Ca ratio calculated in the model (MOD) closely tracks the ratio documented in the geological record (DAT). Dolomitization thereby compensated effectively for any divergence between calculated and observed ratios.

Ca bound in carbonates formed during the low-temperature alteration of oceanic crust may originate from both seawater and hydrothermal fluids (Teagle et al., 1996). Carbonates formed under open conditions may contain a large fraction of seawater Ca while closed conditions favor the precipitation of hydrothermal Ca leached from the basaltic crust (Alt et al., 1996). Here, we postulate that the contribution of seawater Ca to carbonate precipitation in altered oceanic crust depends also on the concentration of Ca in seawater (CCa). Considering that alteration is inhibited by the deposition of pelagic carbonate sediments on ridge flanks (Wallmann, 2004), the uptake of seawater Ca in authigenic carbonates (F_{ALT}^{Ca}) is defined as:

$$F_{ALT}^{Ca} = \frac{CCa}{CCa + k_{ALT}} \cdot \frac{CO}{CO(0)} \cdot f_{SP} \cdot F_{ALT}(0)$$

where k_{ALT} is a Monod constant (10 mM Ca), CO is the mass of pelagic and authigenic carbonates deposited onto and within oceanic crust, CO(0) is the modern carbonate mass (1000 x 10^{+18} Mol), f_{SP} is the spreading and subduction rate normalized to the modern value and $F_{ALT}(0)$ is the modern rate of $CaCO_3$ precipitation (1.5 Tmol yr^{-1}) within altered crust. The parameter f_{SP} is calculated from the Phanerozoic $^{87}Sr/^{86}Sr$ record of Veizer et al. (1999) as described in Wallmann (2004) for the equivalent parameter f_{VO}. With this approach, alteration provides negative feedback on dissolved Ca because high Ca concentrations in the ocean promote the fixation of seawater Ca in authigenic carbonates. The release of Ca to seawater by hydrothermal ocean crust alteration, F_{HY}^{Ca}, is assumed to be proportional to the spreading rate, f_{SP} (Wallmann, 2001).

Biogenic carbonate is deposited on the continental shelf and at the deep-sea floor as outlined in Wallmann (2004). Burial of pelagic carbonates is initiated during the Mesozoic and depends on the saturation state of the deep ocean with respect to calcite. The calcite saturation horizon is maintained close to its modern level at 3500 m water depth over the

entire model period through carbonate compensation since possible changes in saturation depth are only poorly constrained (Ridgwell and Zeebe, 2005).

Table A.3.2.

Calcium fluxes applied in the model; see Wallmann (2001) for further definitions.

Flux	Description	Equation/Fluxes (in Tmol yr^{-1})
F_{HY}^{Ca}	Hydrothermal Ca release	$F_{HY}^{Ca} = 4.5 \cdot f_{SP}$
F_{WS}^{Ca}	Ca release during silicate weathering	$F_{WS}^{Ca} = f_B(CO_2) \cdot f_D^{0.65} \cdot f_{ER}^{0.5} \cdot \left(F_{WS,Ca}^{VO}(Q) \cdot + F_{WS,Ca}^{S}(Q)\right)$
F_{WC}^{Ca}	Ca release during carbonate weathering	$F_{WC}^{Ca} = 0.83 \cdot f_{BB}(CO_2) \cdot f_D \cdot f_{LA} \cdot f_{ER}^{0.5} \cdot k_{WC} \cdot CC$
F_{ALT}^{Ca}	Ca uptake during alteration of oceanic crust	$F_{ALT}^{Ca} = \frac{CCa}{CCa + k_{ALT}} \cdot \frac{CO}{CO(0)} \cdot f_{SP} \cdot F_{ALT}(0)$
F_{BC}^{Ca}	Carbonate burial flux	$F_{BC}^{Ca} = 100 \cdot (\frac{Ca \cdot CO_3}{K_{SP}} - 1)$
F_{DOLO}^{Ca}	Ca release via dolomitization	$F_{DOLO}^{Ca} = k_{DOLO} \cdot \left(\frac{Mg}{Ca}\Big\|_{MOD} - \frac{Mg}{Ca}\Big\|_{DAT} \right)$

Magnesium model

Magnesium (Mg) is released into the ocean through continental weathering of carbonates (F_{WC}^{Mg}) and silicate rocks (F_{WS}^{Mg}). It is removed from seawater via carbonate burial (F_{BC}^{Mg}), hydrothermal circulation systems at mid-ocean ridges (F_{HY}^{Mg}) and dolomitization of carbonates deposited on the continental shelf (F_{DOLO}^{Mg}). All of these Mg fluxes are considered in the model:

$$\frac{dMg}{dt} = F_{WC}^{Mg} + F_{WS}^{Mg} - F_{HY}^{Mg} - F_{DOLO}^{Mg} - F_{BC}^{Mg}$$

The corresponding flux equations for carbonate and silicate weathering, hydrothermal Mg uptake and Mg burial in marine carbonates are taken from Hansen and Wallmann (2003). The Mg uptake during dolomitization is set equal to the corresponding Ca release ($F_{DOLO}^{Mg} = F_{DOLO}^{Ca}$).

Calcium isotope model

Calcium has six naturally occurring stable isotopes with atomic masses and abundances of ^{40}Ca (96.941 %), ^{42}Ca (0.647 %), ^{43}Ca (0.135 %), ^{44}Ca (2.086 %), ^{46}Ca (0.004 %) and ^{48}Ca (0.187 %). The mole fraction of ^{44}Ca is thus given as:

$$\Phi = \frac{^{44}Ca}{^{40}Ca + ^{42}Ca + ^{43}Ca + ^{44}Ca + ^{46}Ca + ^{48}Ca}$$

Neglecting isotopic fractionation among the minor Ca isotopes ^{42}Ca, ^{43}Ca, ^{46}Ca and ^{48}Ca, the equation can be simplified to:

$$\Phi = \frac{^{44}Ca}{^{40}Ca + ^{44}Ca + 0.973} = \frac{^{44}Ca}{Ca}$$

The mole fraction of the ^{44}Ca isotope (Φ_{Ca}) is related to the commonly used isotopic ratio

$$R = \frac{^{44}Ca}{^{40}Ca}$$

as:

$$\Phi = \frac{R}{1.01 + R}$$

and the ratio relates to the mol fraction as:

$$R = \frac{1.01 \cdot \Phi}{1 - \Phi}$$

The $\delta^{44}Ca$ value is defined as:

$$\delta^{44}Ca = \left(\frac{R^{Sample}}{R^{Standard}} - 1 \right) \cdot 1000$$

The standard used in this study is the NIST SRM 915a $CaCO_3$. Thus, the $^{44}Ca/Ca$ mole fraction calculated in the model is related to the $\delta^{44}Ca$ (NIST) as:

$$\delta^{44}Ca\,(NIST) = \left(\frac{1.01 \cdot \Phi}{R^{NIST} \cdot (1 - \Phi)} - 1 \right) \cdot 1000$$

and

$$\Phi = 1 - \frac{1010}{1010 + R^{NIST} \cdot (1000 + \delta^{44}Ca^{NIST})}$$

In the Ca isotope model, a characteristic isotopic signature is assigned to each Ca flux to calculate the mass balances of ^{44}Ca in seawater:

$$\frac{dCa}{dt} = \Phi_{HY} \cdot F_{HY}^{Ca} + \Phi_{DOLO} \cdot F_{DOLO} + \Phi_{WC} \cdot F_{WC}^{Ca} + \Phi_{WS} \cdot F_{WS}^{Ca} + \Phi_{WE} \cdot F_{WE}^{Ca} - \Phi_{CARB} \cdot \left(F_{BCP}^{Ca} + F_{BCP}^{Ca} + F_{ALT}^{Ca} \right) - \Phi_{BE} \cdot F_{BE}^{Ca}$$

Fixed $^{44}Ca/Ca$ mole fractions (Φ) were applied for the hydrothermal Ca input into the ocean (Φ_{HY}) and the Ca released into the ocean via silicate and evaporite weathering

(Φ_{WS} and Φ_{WE}). The corresponding $\delta^{44}Ca$ values are listed in Table A.3.2. Since the isotopic composition of carbonates changes through time, we applied a time dependent mole fraction for this major Ca flux into the ocean (Φ_{WC}). Following Garrels and Mackenzie (1971), we assumed that carbonate rocks have an average renewal time of 200 Ma and calculated the isotopic composition of weathering carbonates by a corresponding running mean through the carbonate fossils dataset presented in this paper (cf. Fig. 3.8).

The isotopic composition of Ca released from carbonates during dolomitization depends on the changing isotopic composition of marine carbonates which is related to the time-dependent mole fraction of ^{44}Ca in seawater (Φ_{SW}):

$$\Phi_{DOLO} = \frac{\alpha_{DOLO} \cdot \Phi_{SW}}{\alpha_{DOLO} \cdot \Phi_{SW} + 1 - \Phi_{SW}}$$

The isotopic fractionation between seawater and dolomite is expressed using a fractionation factor α_{DOLO} defined as:

$$\alpha_{DOLO} = \frac{R_{DOLO}}{R_{SW}}$$

where R_{DOLO} and R_{SW} are the isotope ratios in marine carbonates and seawater, respectively.

The composition of marine carbonates is related to the metabolic mechanisms of calcifying organisms, the isotopic composition of seawater, to mineralogy and the carbonate anion concentration in the surface ocean. Since the fractionation mechanisms involved in the formation of biogenic carbonates are poorly known, we used an inverse approach to determine the fractionation factor α_{CARB} from the $\delta^{44}Ca^{SW}$ database presented in this paper.

$$\alpha_{CARB} = \frac{R_{CARB}}{R_{SW}} = k_{CARB} \cdot \left(\partial^{44}Ca^{SW}{}_{MOD} - \partial^{44}Ca^{SW}{}_{DAT}\right)$$

The fractionation factor is set proportional to the divergence between the modeled and observed $\delta^{44}Ca^{SW}$ values. With this parameterization, $\alpha_{cc/sw}$ is automatically adjusted to minimize the difference between the two values for each time step. The kinetic constant k_{CARB} is set to a large value (50) so that the $\delta^{44}Ca^{SW}$ values calculated in the model (MOD) closely track the values documented in the geological record (DAT).

Table A.3.3.

$\delta^{44/40}Ca$ values (in ‰ and relative to NIST SRM 915a) and fractionation factors ($\alpha_{cc/sw}$) applied in the model.

Symbol	Description	Value
$\delta^{44}Ca^{SW}(Q)$	Ca in modern seawater	+1.88
$\delta^{44}Ca^{HY}$	Ca in hydrothermal solutions	+0.7
$\delta^{44}Ca^{WS}$	Ca released from weathering silicate rocks	+0.9
$\delta^{44}Ca^{WE}$	Ca released during evaporite weathering	+1.7
α_{DOLO}	Ca released during dolomitization	0.9982
α_{BE}	Ca buried in marine evaporites	0.9998

Table A.3.4. Trace element (Mn, Sr) and isotope ($\delta^{13}C$, $\delta^{18}O$, $^{87}Sr/^{86}Sr$ and $\delta^{44/40}Ca$) composition of modern and the Phanerozoic brachiopods. Numerical ages are given in million years based on geological time scale of GTS 89 (Harland et al., 1990) and GTS 04 (Gradstein et al., 2004).

Sample ID	Period	Country	Location	Stage	Age GTS 89	Age GTS 04	Mn (ppm)	Sr (ppm)	$\delta^{13}C$ [a] (‰)	$\delta^{18}O$ [a] (‰)	$^{87}Sr/^{86}Sr$ [a]	$\delta^{44/40}Ca$ [b] (‰)
	Recent time *(Ottawa-Carleton Ca isotope data)*											
Y342L	Modern	USA	San Juan Island, NW Pacific	N/A	0.0	0.0	16	1085				1.07
D519L	Modern	USA	San Juan Island, NW Pacific	N/A	0.0	0.0	13	1120				1.09
	Recent time *(IFM GEOMAR Ca isotope data)*											
SJI1	Modern	USA	San Juan Island, NW Pacific	N/A	0.0	0.0						0.92
SJI2	Modern	USA	San Juan Island, NW Pacific	N/A	0.0	0.0						0.97
BP-Mad	Modern	Spain	Madeira	N/A	0.0	0.0						1.05
CrRck	Modern	N. Zealand	South Island, New Zealand	N/A	0.0	0.0						0.82
316282	Modern	Australia	Osprey Reef, Coral Sea	N/A	0.0	0.0						1.19
	Cretaceous period *(IFM GEOMAR Ca isotope data)*											
C-Kr1	Cretaceous	Germany	Kronsmoor	Maastrichtian	74.3	71.0						0.95
C-Ma2	Cretaceous	G. Britain	St. Margarets	Turonian	88.3	89.0	641	419	2.9	-2.0		0.93
C-Sh10	Cretaceous	G. Britain	Lewes, Shoreham	Turonian	88.6	89.5			2.9	-1.5		0.77
C-NP9	Cretaceous	G. Britain	Lewes, New Pit	Turonian	89.7	91.9			2.5	-1.9		0.85
C-Gb5	Cretaceous	G. Britain	Glyndebourne	Turonian	89.7	92.0			4.2	-1.7		0.94
C-HW13	Cretaceous	G. Britain	Eastbourne	Turonian	90.2	93.0	14	427	3.4	-1.6		0.79
C-E31a	Cretaceous	G. Britain	Eastbourne	Cenomanian	91.0	94.0	69	354	6.9	-1.8		1.04
C-HW3	Cretaceous	G. Britain	Eastbourne	Cenomanian	91.1	94.1	98	327	5.0	-1.5		1.19
C-D2	Cretaceous	G. Britain	Dover	Cenomanian	91.9	94.9	46	693	2.8	-1.0		0.87
C-S105	Cretaceous	G. Britain	Southerham	Cenomanian	92.0	95.0	54	782	2.7	-0.7		0.82
C-S73	Cretaceous	G. Britain	Southerham	Cenomanian	92.1	95.1	38	378	2.9	-0.6		0.72
C-S36	Cretaceous	G. Britain	Southerham	Cenomanian	93.5	96.4	43	391	2.3	-0.9		0.82
C-S35	Cretaceous	G. Britain	Southerham	Cenomanian	93.7	96.5	51	472	2.2	-0.7		0.69
	Jurassic period *(Ottawa-Carleton Ca isotope data)*											
J-U2/3-25	Jurassic	Germany	Ursental	Kimmeridgian	152.5	151.5	33	392				0.68
J-U2/3-17	Jurassic	Germany	Ursental	Kimmeridgian	152.5	151.5	9	412				0.69
J-G5-39	Jurassic	Germany	Geisingen	Kimmeridgian	154.0	155.0	3	1280				0.66
J-G5-27	Jurassic	Germany	Geisingen	Kimmeridgian	154.0	155.0	2	1318				0.59
	Triassic period *(Ottawa-Carleton Ca isotope data)*											
Tr4	Triassic	Austria	Weissloferbach	Rhaetian	208.6	201.2	72	1197	1.2	-1.1	0.707710	0.46
Tr11	Triassic	Austria	Weissloferbach	Rhaetian	208.6	201.2	169	977	1.2	-1.2	0.707721	0.59
Tr19	Triassic	Austria	Weissloferbach	Rhaetian	208.8	201.7	81	1003	1.5	-2.0	0.707709	0.48
Tr27	Triassic	Austria	Weissloferbach	Rhaetian	208.9	202.0	262	1158	1.8	-1.5	0.707763	0.73
Tr30	Triassic	Austria	Weissloferbach	Rhaetian	209.0	202.3	162	981	2.2	-1.7		0.70
Tr35	Triassic	Austria	Weissloferbach	Rhaetian	209.1	202.5	265	2645	1.8	-2.8	0.707809	0.32
Tr37	Triassic	Austria	Weissloferbach	Rhaetian	209.2	202.8	225	1324	1.6	-0.8	0.707842	0.39
Tr134	Triassic	Italy	St. Cassian / Cortina d'Ampezzo	Carnian	232.2	225.2	141	599	2.5	-2.0	0.707572	0.73
Tr137	Triassic	Italy	St. Cassian / Cortina d'Ampezzo	Carnian	233.1	226.1	169	571	2.7	-1.2		0.61
Tr141	Triassic	Italy	St. Cassian / Cortina d'Ampezzo	Carnian	233.8	226.8	257	1156	2.7	-3.5	0.707573	0.66
Tr143	Triassic	Italy	St. Cassian / Cortina d'Ampezzo	Carnian	234.1	227.1	205	1139	1.6	-3.4	0.707584	0.49
Tr144	Triassic	Hungary	Köveskál	Carnian	234.4	227.4					0.707583	0.90
Tr145	Triassic	Italy	St. Cassian / Cortina d'Ampezzo	Carnian	234.4	227.4	195	1349	1.6	-3.1	0.707566	0.42
Tr155	Triassic	Germany	Gähnheim	Ladinian	236.5	231.0	117	1238			0.707769	0.34
Tr156	Triassic	Germany	Gerichtstetten	Ladinian	236.6	231.2	498	681	-0.7	-4.4	0.707781	0.62
Tr157	Triassic	Germany	Gähnheim	Ladinian	236.6	231.2	577	872	-0.3	-2.4	0.707798	0.63
Tr167	Triassic	Germany	Zwingelhausen (Backnang)	Ladinian	237.8	233.6	393	970	-0.1	-4.0		0.46

(Continued)

Table A.3.4. (Continued)

Sample ID	Period	Country	Location	Stage	Age GTS 89	Age GTS 04	Mn (ppm)	Sr (ppm)	$\delta^{13}C$ (‰)	$\delta^{18}O$ (‰)	$^{87}Sr/^{86}Sr$	$\delta^{44/40}Ca$ (‰)
Tr178	Triassic	Germany	Gähnheim	Ladinian	238.2	234.4	299	986	1.0	-4.2	0.707774	0.62
Tr207	Triassic	Germany	Neidenfels	Anisian	239.6	237.5	155	943	0.5	-3.7	0.707772	0.72
Tr215	Triassic	Germany	Neidenfels	Anisian	239.7	238.0	108	509	0.1	-6.2		0.76
Tr229	Triassic	Germany	Laibach	Anisian	240.3	241.0	348	1334	1.8	-5.5	0.707929	0.42
	Permian period *(Ottawa-Carleton Ca isotope data)*											
P3	Permian	China	Chongquing Zhongliang Section	Changxingian	245.1	251.1		342	4.0	-2.9	0.707069	1.02
P4	Permian	China	Chongquing Zhongliang Section	Changxingian	245.1	251.1	23	683	3.7	-3.9	0.707048	0.48
P12	Permian	China	Chejiaba near Guangyuan	Changxingian	245.6	251.7	69	1842	-1.7	-6.3	0.707237	1.03
P16	Permian	China	Meishan D	Changxingian	245.7	251.8	36	1371	3.1	-7.7	0.707070	0.50
P20	Permian	China	Chongquing Zhongliang Section	Changxingian	246.6	252.9	26	1393	3.8	-5.7	0.707019	0.66
P22	Permian	China	Chongquing Zhongliang Section	Changxingian	246.9	253.2	72	1585	3.1	-5.9	0.707009	0.45
P23	Permian	China	Chongquing Zhongliang Section	Changxingian	246.9	253.2	109	1016			0.707035	0.82
P27	Permian	Chin a	Chongquing Zhongliang Section	Changxingian	247.2	253.6	121	787	2.9	-4.5	0.707035	0.42
P30	Permian	China	Shangsi Section near Guangyuan	Maokouan	250.0	256.9		1225	2.4	-4.2	0.706985	0.40
P35	Permian	China	Laibin, Guanxi Province	Maokouan	256.0	263.9	225	922	2.9	-3.7	0.706917	0.75
P47	Permian	China	Tonkeng, Xinshao County/ Hunan	Quixian	256.0	263.9	34	1347	2.3	-9.3	0.707651	0.42
P50	Permian	China	Laibin 4	Kungurian	256.1	264.0	30	770	2.4	-4.6		0.37
P60	Permian	China	Xiangliangbei village, Jian county	Quixian	258.0	266.0	87	746	3.4	-6.5	0.707128	0.48
P65	Permian	China	Laibin 3	Kungutian	259.0	267.0	33	1014	2.7	-7.7	0.707349	0.52
P84	Permian	China	Longyin Puan County/Guizhou	Sakmarian	275.5	284.0		714	2.2	-7.2	0.707850	0.81
P86	Permian	China	Laibin, Guanxi Province	Quixian	280.0	288.7	274	647	4.5	-6.8	0.707614	0.82
P92	Permian	Russia	Usolka	Asselian	284.6	293.4	118	401	4.9	-3.5	0.707798	1.15
P93	Permian	China	Guanjiayu, Dongshan, Taiyuan	Asselian	284.7	293.5	82	546	4.0	-6.8	0.708236	0.93
P99	Permian	China	Longyin Puan County/Guizhou	Mapingian	286.0	294.9	121	1014	3.5	-5.6	0.707740	0.63
P100	Permian	China	Longyin Puan County/Guizhou	Asselian	286.0	294.9	35	803	3.8	-6.8	0.707811	0.68
	Carboniferous period *(Ottawa-Carleton Ca isotope data)*											
C5	Carboniferous	Russia	Moscow Basin	Noginskian	291.0	300.0		612	4.4	-2.8		0.75
C12	Carboniferous	Russia	Moscow Basin	Pavl.-Posad.	293.3	302.2		765	3.5	-0.9	0.708176	0.63
C23	Carboniferous	Russia	Moscow Basin	Kashirsky	295.1	304.0	11	501	6.3	-3.0	0.708277	0.90
C25	Carboniferous	Russia	Moscow Basin	Kasimovian	295.5	304.2			4.7	-3.3	0.708240	0.82
C28	Carboniferous	Russia	Moscow Basin	Drogomilovsk.	297.3	304.8		455	3.6	-3.0	0.708198	0.86
C38	Carboniferous	Russia	Moscow Basin	Khamovnich.	299.6	305.7	134	819	2.7	-4.2	0.708259	0.83
C43	Carboniferous	Russia	Moscow Basin	Krevyakinsky	302.4	306.8	62	1030	-0.4	-4.4	0.708289	0.80
C44	Carboniferous	Russia	Moscow Basin	Myachkovsk.	303.0	307.0	19	656	5.6	-2.7	0.708253	0.78
C49	Carboniferous	Russia	Moscow Basin	Myachkovsk.	303.4	307.2	70	689	2.2	-3.4		1.08
C50	Carboniferous	Russia	Moscow Basin	Myachkovsk.	303.4	307.2		479	6.0	-2.5	0.708231	1.13
C58	Carboniferous	Russia	Moscow Basin	Myachkovsk.	303.8	307.5		519	5.0	-2.6	0.708234	0.80
C70	Carboniferous	Russia	Moscow Basin	Myachkovsk.	305.0	308.2		361	5.6	-2.6	0.708259	0.82
C74	Carboniferous	Russia	Moscow Basin	Podolskian	305.4	308.5			2.4	-3.7	0.708283	1.02
C89	Carboniferous	Russia	Moscow Basin	Kashirsky	308.2	310.1		972	5.1	-2.9	0.708281	0.82
C93	Carboniferous	Russia	Moscow Basin	Kashirskian	308.8	310.5			4.7	-2.8	0.708269	0.80
C107	Carboniferous	Russia	Moscow Basin	Tsnian	309.2	310.7			4.8	-2.9	0.708261	0.92
C109	Carboniferous	Russia	Moscow Basin	Tsnian	309.2	310.7			5.8	-2.6	0.708266	0.85
C110	Carboniferous	Russia	Moscow Basin	Kashirsky	309.2	310.7		844	3.7	-3.1	0.708344	0.95
C120	Carboniferous	Russia	Moscow Basin	Vereiskian	310.8	311.7		532	5.3	-3.4		0.87
C123	Carboniferous	Ukraine	Donetsk Basin	Krevyakinsk.	311.2	311.9	80	331	4.4	-5.3	0.708244	1.16
C139	Carboniferous	Ukraine	Donetsk Basin	Cheremshan.	313.8	313.3	299	613	4.4	-2.4		0.81
C148	Carboniferous	Ukraine	Donetsk Basin	Cheremshan.	315.2	314.0	58	323	6.0	-4.3	0.708253	0.44

(Continued)

Table A.3.4. (Continued)

Sample ID	Period	Country	Location	Stage	Age GTS 89	Age GTS 04	Mn (ppm)	Sr (ppm)	$\delta^{13}C$ (‰)	$\delta^{18}O$ (‰)	$^{87}Sr/^{86}Sr$	$\delta^{44/40}Ca$ (‰)
C158	Carboniferous	Ukraine	Donetsk Basin	Cheremshan.	316.8	314.9	89	470	4.9	-2.3		0.93
C181	Carboniferous	Ukraine	Donetsk Basin	Chokierian	326.3	320.8	66	536	4.4	-1.0	0.708132	0.99
C182	Carboniferous	Ukraine	Donetsk Basin	Chokierian	326.5	320.9	113	632	2.1	-2.5	0.708133	0.93
C184	Carboniferous	Ukraine	Donetsk Basin	Chokierian	327.3	321.6	101	693	2.4	-2.8	0.708152	0.97
C187	Carboniferous	Ukraine	Donetsk Basin	Chokierian	327.3	321.6	25	478	3.8	-2.5		0.74
C190	Carboniferous	Ukraine	Donetsk Basin	Chokierian	327.5	321.7	622	693	2.1	-5.1		0.76
C198	Carboniferous	Russia	Moscow Basin	Stschovian	330.5	324.1			2.8	-3.5	0.707850	0.65
C201	Carboniferous	Ukraine	Donetsk Basin	Pendl./Arns.	331.0	324.5	61	1105	1.3	-8.2		0.90
C206	Carboniferous	Russia	Moscow Basin	Tarusskian	331.8	325.1	252	1046	0.5	-5.0		0.46
C207	Carboniferous	Russia	Moscow Basin	Tarusskian	332.0	325.3	317	1135	0.1	-4.5		0.33
C211	Carboniferous	Ukraine	Donetsk Basin	Pendleian	332.5	325.7	103	1369	1.3	-3.4		0.37
C217	Carboniferous	Ukraine	Donetsk Basin	Brigan./Pendl.	330.0	326.1	131	1298	3.0	-5.0	0.707828	0.34
C221	Carboniferous	Ukraine	Donetsk Basin	Brigantian	333.4	326.6	29	1470	2.0	-4.9		0.21
C224	Carboniferous	Ukraine	Donetsk Basin	Brigantian	333.8	327.0	339	817	3.3	-5.8	0.707938	0.74
C233	Carboniferous	Ukraine	Donetsk Basin	Brigantian	334.2	327.5	45	723	1.1	-6.2	0.707875	0.41
C236	Carboniferous	Ukraine	Donetsk Basin	Brigantian	334.4	327.7	58	631	4.0	-4.5	0.707827	0.72
C237	Carboniferous	Ukraine	Donetsk Basin	Brigantian	334.5	327.8	44	1255	4.3	-4.7	0.707827	0.52
C242	Carboniferous	Belgium	Tumhout	Brigantian	335.3	328.8			-0.9	-8.5	0.707864	0.53
C245	Carboniferous	Belgium	Gravenvoeren	Brigantian	335.5	329.0	234	606	0.9	-7.2	0.707788	0.67
C246	Carboniferous	Russia	Moscow Basin	Mickhailovs.	335.5	329.0		1573	2.3	-3.3	0.707813	0.51
C251	Carboniferous	Belgium	Gravenvoeren	Brigantian	335.8	329.3		437	5.8	-7.0	0.707744	0.62
C253	Carboniferous	Belgium	Halen	Brigantian	335.9	329.4			1.3	-6.1	0.707797	0.58
C269	Carboniferous	Belgium	Tumhout	Asbian	336.9	330.6	20	641	3.2	-7.2	0.707795	0.75
C280	Carboniferous	Belgium	Gravenvoeren	Asbian	337.7	331.5	53	935	-3.3	-5.9	0.707607	0.68
C282	Carboniferous	Belgium	Halen	Asbian	337.8	331.6	38	515	3.3	-2.7	0.707654	0.63
C283	Carboniferous	Belgium	Halen	Asbian	337.8	331.6			7.4	-3.3	0.707630	0.81
C284	Carboniferous	Belgium	Halen	Asbian	338.0	331.8	22	628	6.7	-2.0	0.707641	0.80
C294	Carboniferous	Ukraine	Donetsk Basin	Asbian	338.8	332.8	13	2047	1.5	-3.9	0.707633	0.70
C304	Carboniferous	Russia	Moscow Basin	Aleksinskian	339.4	333.4		1104	3.4	-3.3	0.707796	0.69
C311	Carboniferous	Ireland	Sligo-Ireland	Holkerian	340.0	334.1		555	3.7	-3.4	0.707627	0.72
C317	Carboniferous	Belgium	E Sagard 1/70	Holkerian	340.3	334.5	29	879	3.5	-6.2	0.707678	0.60
C319	Carboniferous	Belgium	Gravenvoeren	Holkerian	340.5	334.7	25	349	4.2	-2.4	0.707598	0.48
C331	Carboniferous	Belgium	Gravenvoeren	Holkerian	341.8	336.2	94	369	3.2	-5.2	0.707718	0.87
C339	Carboniferous	Belgium	Lives	Holkerian	342.3	336.8	155	638	2.5	-6.7	0.707748	0.67
C350	Carboniferous	Belgium	Halen	Arundian	343.1	337.7	126	370	4.4	-1.5	0.707684	0.67
C354	Carboniferous	Belgium	Halen	Arundian	343.2	337.8	26	556	6.3	-2.2	0.707655	0.81
C367	Carboniferous	Belgium	Gravenvoeren	Arundian	343.6	338.3	67	416	1.8	-4.3	0.707660	0.70
C373	Carboniferous	Belgium	Halen	Arundian	343.8	338.5	335	710	2.9	-6.7	0.707686	0.75
C374	Carboniferous	Belgium	Salet	Arundian	344.2	338.9	18	453	1.4	-4.4	0.707619	0.50
C378	Carboniferous	Belgium	Tumhout	Chadian	345.0	339.9	48	610	3.0	-7.1	0.707986	0.62
C395	Carboniferous	Belgium	Tumhout	Chadian	347.2	342.4	27	507	5.3	-6.2	0.707735	0.58
C396	Carboniferous	Belgium	E Sagard 1/70	Arun.-Chad.	347.3	342.5	1980	1502	4.5	-5.0	0.707710	-0.11
C397	Carboniferous	Belgium	E Sagard 1/70	Arun.-Chad.	347.9	343.2	603	1691	3.8	-5.1	0.707726	-0.03
C404	Carboniferous	Belgium	E Sagard 1/70	Ivorian	349.7	345.2	307	1247	3.0	-7.3	0.707864	0.20
C409	Carboniferous	Belgium	Tournais 1	Ivorian	349.9	345.4		463	1.6	-3.5	0.707935	0.54
C413	Carboniferous	Belgium	Tournais 2	Ivorian	351.4	347.0	48	1121	1.4	-4.6	0.707910	0.23
C414	Carboniferous	Belgium	Tournais 2	Ivorian	351.5	347.2	17	914	2.5	-3.4	0.707907	0.64
C417	Carboniferous	Belgium	Tournais 2	Ivorian	351.9	347.6		783	1.5	-4.9	0.707937	0.13

(Continued)

Table A.3.4. (Continued)

Sample ID	Period	Country	Location	Stage	Age GTS 89	Age GTS 04	Mn (ppm)	Sr (ppm)	$\delta^{13}C$ (‰)	$\delta^{18}O$ (‰)	$^{87}Sr/^{86}Sr$	$\delta^{44/40}Ca$ (‰)
C426	Carboniferous	Belgium	Yvoir	Ivorian	353.1	348.9		303	6.4	-5.5	0.707991	0.37
C430	Carboniferous	Belgium	E Sagard 1/70	Hastarian	354.2	350.1	199	559	3.4	-3.5	0.707961	0.53
C431	Carboniferous	Belgium	E Sagard 1/70	Hastarian	354.3	350.2	44	955	3.9	-2.7	0.707943	0.63
C433	Carboniferous	Belgium	E Sagard 1/70	Hastarian	354.4	350.3	222	644	2.6	-3.1	0.708003	0.58
C436	Carboniferous	Belgium	Yvoir	Hastarian	354.7	350.6	43	698			0.708154	0.47
C439	Carboniferous		Rocher Bayard	Hastarian	355.9	351.9	23	695	3.7	-6.7	0.708111	0.56
C444	Carboniferous		Rocher Bayard	Hastarian	356.1	352.1	1	849	3.4	-5.3	0.708087	0.35
C445	Carboniferous		E Dranske 2/70	Hastarian	356.3	352.3	1	1037	2.4	-4.8	0.708085	0.44
C450	Carboniferous	G. Britain	Cardiff	Hastarian	357.2	353.3			3.6	-5.8		0.52
C458	Carboniferous	Belgium	Aneseremme	Hastarian	360.4	356.7		722	0.8	-7.0	0.708158	0.40
C459	Carboniferous	Belgium	Aneseremme	Hastarian	360.9	357.3	11	55	1.3	-5.8	0.708188	0.39
C460	Carboniferous	Belgium	Aneseremme	Hastarian	361.6	358.0	12	466	1.0	-6.0	0.708225	0.49
C462	Carboniferous	Belgium	Aneseremme	Hastarian	362.2	358.7	10	901	2.3	-5.7	0.708194	0.44
	Devonian period *(Ottawa-Carleton Ca isotope data)*											
D7	Devonian	Germany	Neuenkirchen	Famennian	366.2	372.2	67	2038	0.5	-5.7	0.708099	0.39
D14	Devonian	Germany	Sagard	Famennian	366.4	372.9	43	1033	0.3	-6.8	0.708075	0.31
D23	Devonian	Germany	Sagard	Famennian	366.6	373.6	150	1358	0.9	-6.6	0.708092	0.40
D24	Devonian	Germany	Aachen	Famennian	366.7	373.9	38	1135	1.8	-7.8	0.708063	0.40
D26	Devonian	Germany	Aachen	Famennian	366.8	374.3	118	938	1.9	-6.8	0.708078	0.38
D33	Devonian	Germany	Sagard	Frasnian	367.0	375.0	129	1332	-0.6	-6.3	0.708059	0.40
D35	Devonian	Germany	Aachen	Frasnian	367.6	375.6	95	1015	0.2	-7.5	0.708096	0.34
D41	Devonian	Germany	Aachen	Frasnian	367.8	375.8	62	1041	-0.5	-8.7	0.708090	0.22
	Devonian period *(IFM GEOMAR Ca isotope data)*											
YA 40-01	Devonian	Russia	Siberia	Famennian	365.6	370.0	53	1498	1.5	-5.4	0.708099	0.20
SY 07-01	Devonian	China	South China	Famennian	366.1	371.8	18	1637	1.3	-5.5	0.708076	0.23
YA 28-01	Devonian	Russia	Siberia	Famennian	366.7	373.9	12	1574	2.9	-5.5		0.23
YA 27-02	Devonian	Russia	Siberia	Famennian	366.8	374.3			3.2	-4.1		0.19
YA 26-01	Devonian	Russia	Siberia	Famennian	366.8	374.3			2.7	-4.4		0.27
YA 26-02	Devonian	Russia	Siberia	Famennian	366.8	374.3	22	1564	3.3	-5.0		0.32
YA 25-01	Devonian	Russia	Siberia	Famennian	366.9	374.6	18	1542	3.8	-4.3	0.708060	0.24
YA 25-03	Devonian	Russia	Siberia	Famennian	366.9	374.6			3.6	-4.7		0.18
YA 24-01	Devonian	Russia	Siberia	Famennian	366.9	374.6			3.2	-3.9		0.26
YA 12-04	Devonian	Russia	Siberia	Frasnian	367.3	375.3	59	1583	-0.4	-5.2	0.708041	0.22
YA 08-02	Devonian	Russia	Siberia	Frasnian	367.5	375.5	60	1495	-0.4	-5.4		0.18
BS 01-04	Devonian	USA	Iowa	Frasnian	368.9	376.9	10	1378	2.2	-4.8		0.26
HG 34-01	Devonian	USA	Iowa	Frasnian	369.6	377.6	23	1736	-0.1	-5.5		0.16
HG 11-01	Devonian	USA	Iowa	Frasnian	370.1	378.1	4	1452	0.6	-5.2		0.30
HG 10-03	Devonian	USA	Iowa	Frasnian	370.2	378.2	6	1399	0.2	-4.9		0.34
HG 08-03	Devonian	USA	Iowa	Frasnian	370.2	378.2	8	1378	0.0	-4.9		0.25
WQ 03-02	Devonian	USA	Iowa	Frasnian	373.6	381.6	12	527	1.0	-5.7		0.47
HQ 01-01	Devonian	USA	Iowa	Frasnian	374.9	382.9	21	715	1.2	-5.7		0.53
HQ 02-02	Devonian	USA	Iowa	Frasnian	375.0	383.0	41	1148	0.2	-5.0		0.51
BQ 54-02	Devonian	USA	Iowa	Givetian	377.7	386.2	14	627	1.3	-4.8		0.47
BQ 49-01	Devonian	USA	Iowa	Givetian	377.7	386.2	45	877	1.4	-6.3		0.47
BQ 48-01	Devonian	USA	Iowa	Givetian	377.7	386.2			0.8	-6.4		0.39
BQ 48-02	Devonian	USA	Iowa	Givetian	377.7	386.2			0.8	-5.1		0.33
BQ 38-02	Devonian	USA	Iowa	Givetian	377.8	386.4	96	917	1.6	-5.8		0.46
BQ 36-02	Devonian	USA	Iowa	Givetian	377.8	386.4	70	894	1.3	-6.2		0.42

(Continued)

Table A.3.4. (Continued)

Sample ID	Period	Country	Location	Stage	Age GTS 89	Age GTS 04	Mn (ppm)	Sr (ppm)	$\delta^{13}C$ (‰)	$\delta^{18}O$ (‰)	$^{87}Sr/^{86}Sr$	$\delta^{44/40}Ca$ (‰)
BQ 35-02	Devonian	USA	Iowa	Givetian	377.8	386.4	94	947	0.5	-6.7		0.41
BQ 25-02	Devonian	USA	Iowa	Givetian	377.8	386.4	57	794	1.2	-5.4		0.42
MRK I 28-03	Devonian	Morocco	Anti-Atlas	Givetian	379.5	389.3	6	866	1.8	-3.1		0.26
MRK I 19-01	Devonian	Morocco	Anti-Atlas	Eifelian	382.4	393.7	13	1036	0.3	-3.8	0.707851	0.28
STR 16	Devonian	Germany	Eifel Mountains	Eifelian	383.5	395.0	28	1096	2.9	-2.7		0.26
STL 04-09	Devonian	Spain	Cantabrian Mountains	Emsian	386.0	398.1	6	1027	1.0	-2.4	0.707815	0.35
MRK III 13-03	Devonian	Morocco	Anti-Atlas	Emsian	386.4	399.0	12	820	1.7	-2.2		0.31
MRK III 12-03	Devonian	Morocco	Anti-Atlas	Emsian	386.5	399.1	23	701	0.9	-3.9	0.707880	0.44
MRK III 08-05	Devonian	Morocco	Anti-Atlas	Emsian	386.8	399.7	11	1107	1.2	-2.5	0.707887	0.26
ELM 11-01	Devonian	Morocco	Anti-Atlas	Emsian	387.4	401.2	11	896	0.7	-2.7	0.707993	0.31
ELM 04-01	Devonian	Morocco	Anti-Atlas	Emsian	387.7	401.8	12	1046	0.2	-3.2	0.707999	0.23
ELM 04-04	Devonian	Morocco	Anti-Atlas	Emsian	387.7	401.8	10	1189	0.4	-2.9	0.707999	0.24
MRK II 02-01	Devonian	Morocco	Anti-Atlas	Emsian	388.0	402.4	14	904	0.5	-2.3	0.708041	0.29
GUR 05-02	Devonian	Russia	Siberia	Emsian	390.1	407.1	12	1354	2.0	-4.9	0.708217	0.39
LOS 02-07	Devonian	Spain	Cantabrian Mountains	Lochkovian	401.9	413.3	5	1642			0.708602	0.26
LOS 04-05	Devonian	Spain	Cantabrian Mountains	Lochkovian	402.0	413.4						0.29
	Silurian period *(Ottawa-Carleton Ca isotope data)*											
S2	Silurian	Ukraine	Podolia	Pridoli	408.7	416.3	85	1457	-0.1	-5.7	0.708736	0.31
S10	Silurian	Ukraine	Podolia	Pridoli	409.0	416.7	75	1476	0.2	-6.1	0.708728	0.39
S18	Silurian	Lithuania	Taurage-11	Pridoli	409.9	417.9	76	1521	-0.3	-5.5	0.708702	0.61
S19	Silurian	Lithuania	Taurage-11	Pridoli	409.9	417.9	160	1739	-0.3	-5.6	0.708692	0.45
S20	Silurian	Latvia	Kolka 54	Pridoli	410.2	418.3	105	1624	-0.2	-5.5	0.708723	0.35
S23	Silurian	Latvia	Kolka 54	Pridoli	410.5	418.7	48	1744	-0.5	-5.4	0.708693	0.37
S28	Silurian	Ukraine	Podolia	Pridoli	410.5	418.7	51	978	0.1	-5.3	0.708738	0.49
S32	Silurian	Sweden	Gotland	Ludfordian	412.3	419.5	184	1567	4.7	-5.0		0.44
S38	Silurian	Sweden	Gotland	Ludfordian	414.8	420.2	37	1679	0.7	-5.7	0.708688	0.31
S43	Silurian	Sweden	Gotland	Gorstian	416.0	420.6	149	1329	0.0	-5.4	0.708566	0.59
S47	Silurian	Sweden	Gotland	Gorstian	419.6	421.7	208	1509	0.3	-5.6	0.708556	0.42
S48	Silurian	Sweden	Gotland	Gorstian	419.6	421.7	41	1898	-0.2	-5.4	0.708554	0.49
S83	Silurian	G. Britain	Much Wenlock	Homerian	425.1	423.8	158	1882	-0.1	-5.3	0.708441	0.43
S86	Silurian	Sweden	Gotland	Homerian	425.1	423.8	41	1996	2.2	-3.9	0.708435	0.32
S88	Silurian	Sweden	Gotland	Homerian	425.1	423.8	88	1925	1.8	-4.1	0.708446	0.28
S89	Silurian	Sweden	Gotland	Homerian	425.1	423.8	46	1870	1.6	-4.3	0.708431	0.26
S114	Silurian	Sweden	Gotland	Sheinwoodian	426.5	424.9	48	1745	-0.5	-4.2	0.708358	0.31
S119	Silurian	Lithuania	Grauzai-105	Sheinwoodian	427.9	426.0	122	1330	-0.8	-4.6		0.44
S124	Silurian	Sweden	Gotland	Sheinwoodian	428.6	426.6	137	1403	4.4	-5.2	0.708342	0.50
S125	Silurian	Sweden	Gotland	Sheinwoodian	428.6	426.6	156	1487	4.3	-5.0	0.708388	0.51
S126	Silurian	Sweden	Gotland	Sheinwoodian	428.6	426.6	128	1697	4.4	-4.8	0.708405	0.47
S138	Silurian	Sweden	Gotland	Sheinwoodian	429.3	427.1	129	1345	3.7	-4.9		0.65
S152	Silurian	Sweden	Gotland	Telychian	430.7	428.6	131	1674	1.4	-5.3	0.708350	0.39
S164	Silurian	Canada	Anticosti Island	Telychian	431.2	429.5	17	1000	1.8	-3.7	0.708218	0.46
S168	Silurian	Canada	Anticosti Island	Telychian	431.7	430.4	19	1147	0.4	-5.0	0.708215	0.44
S169	Silurian	Canada	Anticosti Island	Telychian	431.7	430.4	29	1067	0.6	-4.9	0.708205	0.41
S176	Silurian	Canada	Anticosti Island	Telychian	432.3	431.5	23	1275	1.6	-4.8		0.27
S181	Silurian	Canada	Anticosti Island	Aeronian	433.0	432.8	22	1389	0.6	-4.6	0.708135	0.39
S186	Silurian	Canada	Anticosti Island	Aeronian	433.9	434.5	28	1474	1.5	-5.1		0.28
S192	Silurian	Canada	Anticosti Island	Aeronian	435.4	437.3	57	1147	1.5	-5.0	0.708087	0.57
S193	Silurian	Canada	Anticosti Island	Aeronian	436.5	439.4	79	1013	1.0	-3.8	0.708103	0.48

(Continued)

Table A.3.4. (Continued)

Sample ID	Period	Country	Location	Stage	Age GTS 89	Age GTS 04	Mn (ppm)	Sr (ppm)	$\delta^{13}C$ (‰)	$\delta^{18}O$ (‰)	$^{87}Sr/^{86}Sr$	$\delta^{44/40}Ca$ (‰)
S194	Silurian	Canada	Anticosti Island	Aeronian	436.5	439.4			0.5	-5.0	0.708091	0.35
S195	Silurian	Canada	Anticosti Island	Aeronian	436.5	439.4	97	1140	1.4	-4.7	0.708071	0.53
S196	Silurian	Canada	Anticosti Island	Aeronian	436.5	439.4	66	997	0.5	-4.0	0.708060	0.55
S202	Silurian	Canada	Anticosti Island	Rhuddanian	438.2	442.5	22	1081	0.0	-3.9		0.54
	Silurian period *(IFM GEOMAR Ca isotope data)*											
1818 Sundre	Silurian	Sweden	Gotland, Klehammarsård 3	Ludfordian	411.2	419.2	85	1457	0.5	-5.3		0.24
255 Hamra	Silurian	Sweden	Gotland, Majstre 1	Ludfordian	411.2	419.2			2.5	-4.8		0.32
2122 Burgsvik	Silurian	Sweden	Gotland, Kulhaken 2	Ludfordian	411.5	419.2			7.8	-3.3		0.24
242 Eke	Silurian	Sweden	Gotland, Bodudd 2	Ludfordian	412.0	419.4			7.8	-4.0		0.29
2042 Hemse	Silurian	Sweden	Gotland, Olsvenne 1	Ludfordian	417.0	420.9			1.8	-4.8		0.24
1214 Hemse	Silurian	Sweden	Gotland, Kodings 3	Ludfordian	417.0	420.9			0.2	-5.8		0.22
1944 Hemse	Silurian	Sweden	Gotland, Rangsarve 1	Gorstian	417.0	420.9			1.0	-5.8		0.25
1093 Hemse	Silurian	Sweden	Gotland, Ajmunde 1	Gorstian	417.0	420.9			0.1	-5.5		0.19
1769 Klinteb.	Silurian	Sweden	Gotland, Botes 1	Homerian	424.0	423.0			0.3	-5.8		0.16
194 Halla	Silurian	Sweden	Gotland, Mulde Tegelbruk 1	Homerian	425.0	423.7			1.9	-4.3		0.14
1719 Fröjel	Silurian	Sweden	Gotland, Klinteenklaven 2	Homerian	425.5	424.1			3.3	-3.7		0.20
623 Slite	Silurian	Sweden	Gotland, Slitebrottet 2	Sheinwoodian	427.0	425.3			-0.6	-4.6		0.18
344 Slite	Silurian	Sweden	Gotland, Oivide 1	Sheinwoodian	427.0	425.3			-0.3	-4.5		0.25
946 Högklint	Silurian	Sweden	Gotland, Häftingsklint 2	Sheinwoodian	429.0	426.9			4.9	-4.5		0.24
1535 U Visby	Silurian	Sweden	Gotland, Storbrut 1	Sheinwoodian	429.9	427.6			3.7	-5.0		0.26
1466 U Visby	Silurian	Sweden	Gotland, Nygardsbäcksprofilen 2	Sheinwoodian	429.9	427.6			2.2	-5.1		0.25
	Ordovician period *(Ottawa-Carleton Ca isotope data)*											
O13	Ordovician	China	South China	Hirnantian	439.3	444.5	1132	769			0.708304	0.38
O14	Ordovician	China	South China	Hirnantian	439.3	444.5	445	1067			0.708121	0.17
O36	Ordovician	USA	Cincinnati	Richmondian	439.8	445.2			-0.4	-4.6	0.707829	0.41
O43	Ordovician	China	South China	Rawthey./Cautl.	440.0	445.5	125	438			0.708091	0.30
O45	Ordovician	USA	Cincinnati	Richmondian	440.2	445.8			0.5	-3.7	0.707823	0.58
O46	Ordovician	USA	Cincinnati	Richmondian	440.2	445.8			0.1	-4.2	0.707847	0.52
O51	Ordovician	USA	Cincinnati	Richmondian	440.5	446.3			-0.3	-4.3	0.707838	0.51
O53	Ordovician	USA	Cincinnati	Richmondian	440.8	446.7			0.0	-4.7	0.707839	0.38
O54	Ordovician	USA	Cincinnati	Richmondian	443.0	450.1			0.6	-5.4	0.707881	0.44
O55	Ordovician	USA	Cincinnati	Richmondian	443.0	450.1			-0.3	-5.2	0.707876	0.31
O59	Ordovician	USA	Cincinnati	Richmondian	443.2	450.3			1.3	-3.5	0.707831	0.45
O64	Ordovician	USA	Cincinnati	Richmondian	445.1	451.2			-2.1	-6.5	0.707935	0.37
O72	Ordovician	USA	Lexington	Soudeleyan	447.3	452.4	138	940	0.5	-6.1		0.30
O74	Ordovician	USA	St. Louis	Soudeleyan	453.3	455.5	26	876	0.3	-6.0	0.708027	0.73
O83	Ordovician	USA	St. Louis	Soudeleyan	454.0	455.8	11	1963	1.6	-5.3		0.54
O89	Ordovician	USA	St. Louis	Soudeleyan	454.6	456.1	0	1058			0.708062	0.45
O91	Ordovician	USA	Lexington	Soudeleyan	456.0	456.8	333	636	-1.2	-5.0	0.708095	0.88
O94	Ordovician	USA	Lexington	Soudeleyan	456.2	456.9	109	1413	0.2	-6.2		0.58
O97	Ordovician	USA	St. Louis	Soudeleyan	457.2	457.5			-1.5	-5.2	0.708184	0.56
O100	Ordovician	USA	Arbuckle Mountains	Harnagian	459.9	458.8	39	878	-0.8	-6.2	0.708361	0.36
O104	Ordovician	USA	Arbuckle Mountains	Harnagian	459.9	458.8	0	905	-0.1	-4.6	0.708154	0.40
O111	Ordovician	USA	Arbuckle Mountains	Harnagian	459.9	458.8	45	866	-0.7	-5.1	0.708146	0.42
O114	Ordovician	USA	Arbuckle Mountains	Llo1	467.8	462.5	247	1384	-0.4	-6.2	0.708644	0.44
O119	Ordovician	China	South China	Lln2	470.7	463.7			0.9	-7.6	0.708834	0.47
O122	Ordovician	USA	Arbuckle Mountains	Lln1	474.4	465.3	265	1757	-2.0	-6.5	0.708782	0.49
O123	Ordovician	USA	Arbuckle Mountains	Lln1	474.4	465.3	304	1777	-1.8	-6.1		0.32

(Continued)

Table A.3.4. (Continued)

Sample ID	Period	Country	Location	Stage	Age GTS 89	Age GTS 04	Mn (ppm)	Sr (ppm)	$\delta^{13}C$ (‰)	$\delta^{18}O$ (‰)	$^{87}Sr/^{86}Sr$	$\delta^{44/40}Ca$ (‰)
O127	Ordovician	USA	Arbuckle Mountains	Llnl	474.4	465.3	426		-2.5	-6.5		0.55
O133	Ordovician	China	South China	Llnl-Arg2	475.9	465.9			-0.6	-6.7	0.708740	0.39
O135	Ordovician	China	South China	Llnl-Arg2	475.9	465.9			-0.9	-7.0		0.51
O136	Ordovician	China	South China	Llnl-Arg2	475.9	465.9			-0.6	-6.4		0.35
O138	Ordovician	China	South China	Llnl-Arg2	475.9	465.9			-2.3	-7.3	0.708734	0.53
O157	Ordovician	Australia	Amadeus Basin	Early Arenig 1	477.5	467.0	168	1168	-1.3	-7.4	0.708762	0.26
O161	Ordovician	Australia	Amadeus Basin	Early Arenig 1	477.5	467.0	320	1169	-1.2	-7.4	0.708785	0.38
O173	Ordovician	Russia	St. Petersburg	Late Arenig 2	477.5	467.0	665	896	-0.5	-5.7		0.73
O178	Ordovician	China	South China	Argl	481.0	469.7					0.709103	0.28
O198	Ordovician	China	South China	Argl	487.5	474.5					0.709106	0.24
O199	Ordovician	China	South China	Argl	487.5	474.5					0.708957	0.41
O201	Ordovician	China	South China	Argl	491.0	477.1			-1.1	-9.8	0.708937	0.46
O224	Ordovician	China	South China	Tremadoc	501.5	483.5					0.709034	0.51

[a] The $^{87}Sr/^{86}Sr$, $\delta^{18}O$ and $\delta^{13}C$ values (but also Mn, Sr) are from Veizer et al. (1999), van Geldern et al. (2006) (IFM-GEOMAR, Devonian data) and Samtleben et al. (2000, 2001) (IFM-GEOMAR, Silurian data) and Voigt et al. (2004) (IFM-GEOMAR, Cretaceous data). All $\delta^{44/40}Ca$ data are normalized to NIST SRM915a $CaCO_3$ standard.
[b] The $\delta^{44/40}Ca$ (SRM915a) data of 7 modern brachiopods measured in Ottawa/Carleton (n = 2) and IFM-GEOMAR (n = 5) are from Gussone et al. (2005) and Farkaš et al. (2007), respectively.

Summary of calcium isotope measurements on the modern and Phanerozoic brachiopods

Period	Total number of analysed samples	Total number of samples analysed at 'Ottawa-Carleton'	Total number of samples analysed at 'IFM-GEOMAR'
Recent	7	2	5
Cretaceous	13	0	13
Jurassic	4	4	0
Triassic	21	21	0
Permian	20	20	0
Carboniferous	83	83	0
Devonian	49	8	41
Silurian	51	35	16
Ordovician	39	39	0
Mesozoic	38	25	13
Paleozoic	242	185	57
Total	287	212	75

Table A.3.5. The compilation of the published calcium isotope data from the Phanerozoic marine carbonates (Heuser et al. 2005; Steuber and Buhl, 2006, Farkaš et al., 2007) and phosphates (Schmitt et al., 2003b; Soudry et al., 2004). All literature data, TIMS and MC-ICP-MS, were recalculated to match the $\delta^{44/40}Ca$ (NIST) notation (in per mill, ‰), allowing a direct comparison with the $\delta^{44/40}Ca$ dataset of the Phanerozoic brachiopods (this study).

Sample ID	Period [a]	Material	Location	Stage	Age [a] (Ma)	$\delta^{44/42}Ca$ [b] (IAPSO)	$\delta^{44/40}Ca$ [c] (IAPSO)	$\delta^{44/42}Ca$ [d] (SRM915a)	$\delta^{44/40}Ca$ (SRM915a)
	Neogene period (TIMS data from Heuser et al., 2005)								
1H-1	Neogene	Foraminifera (*G. trilobus*)	Western Equatorial Pacific	Pleistocene	0.1				0.87
1H-2	Neogene	Foraminifera (*G. trilobus*)	Western Equatorial Pacific	Pleistocene	1.0				1.09
2H-6	Neogene	Foraminifera (*G. trilobus*)	Western Equatorial Pacific	Pleistocene	1.5				1.03
3H-2 (A)	Neogene	Foraminifera (*G. trilobus*)	Western Equatorial Pacific	Late Pliocene	3.0				0.77
3H-2 (B)	Neogene	Foraminifera (*G. trilobus*)	Western Equatorial Pacific	Late Pliocene	3.3				0.84
3H-5 (A)	Neogene	Foraminifera (*G. trilobus*)	Western Equatorial Pacific	Early Pliocene	3.9				0.65
3H-5 (B)	Neogene	Foraminifera (*G. trilobus*)	Western Equatorial Pacific	Late Miocene	6.0				0.89
3H-5 (C)	Neogene	Foraminifera (*G. trilobus*)	Western Equatorial Pacific	Late Miocene	6.2				0.85
5H-2	Neogene	Foraminifera (*G. trilobus*)	Western Equatorial Pacific	Late Miocene	9.0				0.74
5H-6	Neogene	Foraminifera (*G. trilobus*)	Western Equatorial Pacific	Late Miocene	10.4				0.75
6H-5	Neogene	Foraminifera (*G. trilobus*)	Western Equatorial Pacific	Middle Miocene	11.4				0.58
4H-5	Neogene	Foraminifera (*G. trilobus*)	Western Equatorial Pacific	Middle Miocene	11.8				0.62
6H-6	Neogene	Foraminifera (*G. trilobus*)	Western Equatorial Pacific	Middle Miocene	13.1				0.64
7H-2	Neogene	Foraminifera (*G. trilobus*)	Western Equatorial Pacific	Middle Miocene	14.7				0.63
7H-5	Neogene	Foraminifera (*G. trilobus*)	Western Equatorial Pacific	Middle Miocene	15.0				0.49
8H-2	Neogene	Foraminifera (*G. trilobus*)	Western Equatorial Pacific	Middle Miocene	16.2				0.51
11H-1	Neogene	Foraminifera (*G. trilobus*)	Western Equatorial Pacific	Middle Miocene	16.7				0.46
11H-6	Neogene	Foraminifera (*G. trilobus*)	Western Equatorial Pacific	Early Miocene	18.4				0.84
12H-2	Neogene	Foraminifera (*G. trilobus*)	Western Equatorial Pacific	Early Miocene	19.9				0.72
13H-3	Neogene	Foraminifera (*G. trilobus*)	Western Equatorial Pacific	Early Miocene	21.7				0.77
13H-5	Neogene	Foraminifera (*G. trilobus*)	Western Equatorial Pacific	Early Miocene	23.0				0.83
14H-4	Neogene	Foraminifera (*G. trilobus*)	Western Equatorial Pacific	Early Miocene	23.5				0.84
7R-2	Neogene	Foraminifera (*G. bulloides*)	Southern Indian Ocean	Late Pliocene	1.9				0.96
8R-3	Neogene	Foraminifera (*G. bulloides*)	Southern Indian Ocean	Late Pliocene	2.4				1.02
9R-2	Neogene	Foraminifera (*G. bulloides*)	Southern Indian Ocean	Late Pliocene	3.1				0.39
10R-3	Neogene	Foraminifera (*G. bulloides*)	Southern Indian Ocean	Late Pliocene	3.6				0.52
11R-1	Neogene	Foraminifera (*G. bulloides*)	Southern Indian Ocean	Early Pliocene	3.7				0.92
12R-2	Neogene	Foraminifera (*G. bulloides*)	Southern Indian Ocean	Early Pliocene	4.4				0.71
13R-1	Neogene	Foraminifera (*G. bulloides*)	Southern Indian Ocean	Late Miocene	6.6				0.96
13R-4	Neogene	Foraminifera (*G. bulloides*)	Southern Indian Ocean	Late Miocene	7.6				0.87
14R-2	Neogene	Foraminifera (*G. bulloides*)	Southern Indian Ocean	Late Miocene	9.2				0.71
15R-2 (A)	Neogene	Foraminifera (*G. bulloides*)	Southern Indian Ocean	Late Miocene	9.4				0.64
15R-2 (B)	Neogene	Foraminifera (*G. bulloides*)	Southern Indian Ocean	Late Miocene	9.4				0.67
16R-3	Neogene	Foraminifera (*G. bulloides*)	Southern Indian Ocean	Late Miocene	9.6				0.77
17R-5	Neogene	Foraminifera (*G. bulloides*)	Southern Indian Ocean	Late Miocene	9.9				0.80
19R-1	Neogene	Foraminifera (*G. bulloides*)	Southern Indian Ocean	Middle Miocene	11.6				0.75
19R-4	Neogene	Foraminifera (*G. bulloides*)	Southern Indian Ocean	Middle Miocene	11.8				0.71
20R-2	Neogene	Foraminifera (*G. bulloides*)	Southern Indian Ocean	Middle Miocene	12.9				0.63
21R-2	Neogene	Foraminifera (*G. bulloides*)	Southern Indian Ocean	Middle Miocene	14.2				0.71
22R-1	Neogene	Foraminifera (*G. bulloides*)	Southern Indian Ocean	Middle Miocene	15.1				0.48
23R-1	Neogene	Foraminifera (*G. bulloides*)	Southern Indian Ocean	Middle Miocene	16.4				0.65
24R-1	Neogene	Foraminifera (*G. bulloides*)	Southern Indian Ocean	Early Miocene	17.3				0.74
25R-1	Neogene	Foraminifera (*G. bulloides*)	Southern Indian Ocean	Early Miocene	18.5				0.45
26R-1	Neogene	Foraminifera (*G. bulloides*)	Southern Indian Ocean	Early Miocene	20.0				0.49
27R-2	Neogene	Foraminifera (*G. bulloides*)	Southern Indian Ocean	Early Miocene	21.0				0.59

(Continued)

Table A.3.5. (Continued)

Sample ID	Period [a]	Material	Location	Stage	Age [a] (Ma)	$\delta^{44/42}Ca$ [b] (IAPSO)	$\delta^{44/40}Ca$ [c] (IAPSO)	$\delta^{44/42}Ca$ [d] (NIST)	$\delta^{44/40}Ca$ (NIST)
	Neogene period (TIMS data from Schmitt et al., 2003)								
Pho 5682	Neogene	Phosphate	Peru	Pleistocene	0.5		-1.08		0.80
Pho 5553	Neogene	Phosphate	USA, California	Late Miocene	9.0		-1.10		0.78
Pho 5554	Neogene	Phosphate	USA, California	Late Miocene	9.9		-0.98		0.90
OB 53-14	Neogene	Phosphate	USA, North Carolina	Late Miocene	10.8		-1.12		0.76
OB 3-7	Neogene	Phosphate	USA, North Carolina	Middle Miocene	16.8		-1.06		0.82
OB 24-9	Neogene	Phosphate	USA, North Carolina	Early Miocene	17.1		-0.86		1.02
OB 64-20	Neogene	Phosphate	USA, North Carolina	Early Miocene	18.1		-0.88		1.00
GH 8.5R	Neogene	Phosphate	USA, North Carolina	Early Miocene	18.8		-0.91		0.97
FG 41	Neogene	Phosphate	Malta	Early Miocene	19.4		-1.08		0.80
FG 17	Neogene	Phosphate	Malta	Early Miocene	22.0		-0.53		1.35
FG 8	Neogene	Phosphate	Malta	Early Miocene	24.3		-0.76		1.12
	Paleogene and Cretaceous period (MC-ICP-MS data from Soudry et al., 2004)								
1	Paleogene	Phosphate	Israel, Negev	Early Eocene	46.0			0.42	0.84
2	Paleogene	Phosphate	Israel, Negev	Early Eocene	49.0			0.32	0.64
3	Cretaceous	Phosphate	Israel, Negev	Early Maastrichtian	71.0			0.33	0.66
4	Cretaceous	Phosphate	Israel, Negev	Late Campanian	73.0			0.34	0.68
5	Cretaceous	Phosphate	Israel, Negev	Late Campanian	75.0			0.30	0.60
6	Cretaceous	Phosphate	Israel, Negev	Late Campanian	79.0			0.22	0.44
7	Cretaceous	Phosphate	Israel, Negev	Santonian/Campanian	83.0			0.06	0.12
8	Cretaceous	Phosphate	Israel, Negev	Middle Turonian	91.0			-0.09	-0.18
9	Cretaceous	Phosphate	Israel, Negev	Late Cenomanian	94.0			0.02	0.04
10	Cretaceous	Phosphate	Israel, Negev	Late Albian	106.0			-0.06	-0.12
11	Cretaceous	Phosphate	Israel, Negev	Late Aptian	114.0			-0.11	-0.22
	Cretaceous and Jurassic period (TIMS data from Farkaš et al., 2007)								
K2	Cretaceous	Belemnite	Germany	Aptian	124.5				0.52
K11	Cretaceous	Belemnite	Great Britain	Barremian	126.2				0.48
K15	Cretaceous	Belemnite	Great Britain	Barremian	126.3				0.61
K20	Cretaceous	Belemnite	Germany	Barremian	126.6				0.37
K35	Cretaceous	Belemnite	Great Britain	Barremian	127.4				0.42
K41	Cretaceous	Belemnite	Germany	Barremian	127.8				0.37
K45	Cretaceous	Belemnite	Great Britain	Barremian	128.2				0.46
K67	Cretaceous	Belemnite	Great Britain	Barremian	130.5				0.49
K75	Cretaceous	Belemnite	Germany	Hauterivian	133.1				0.47
K92	Cretaceous	Belemnite	Germany	Hauterivian	135.2				0.46
K98	Cretaceous	Belemnite	Germany	Valanginian	136.2				0.34
K110	Cretaceous	Belemnite	Germany	Valanginian	138.1				0.35
K111	Cretaceous	Belemnite	Germany	Valanginian	138.6				0.29
K112	Cretaceous	Belemnite	Germany	Valanginian	140.0				0.33
J16	Jurassic	Belemnite	Russia	Tithonian	147.8				0.31
J53	Jurassic	Belemnite	Russia	Tithonian	149.4				0.28
J67	Jurassic	Belemnite	New Zealand	Kimmeridgian	151.1				0.26
J77	Jurassic	Belemnite	New Zealand	Kimmeridgian	153.6				0.17
U2/3belem	Jurassic	Belemnite	Germany	Kimmeridgian	~ 154				0.23
G3-belem	Jurassic	Belemnite	Germany	Kimmeridgian	~ 154				0.14
G5-belem1	Jurassic	Belemnite	Germany	Kimmeridgian	~ 154				0.08
J94	Jurassic	Belemnite	Russia	Oxfordian	155.7				0.11
J114	Jurassic	Belemnite	Russia	Oxfordian	156.7				0.09

(Continued)

Table A.3.5. (Continued)

Sample ID	Period [a]	Material	Location	Stage	Age [a] (Ma)	$\delta^{44/42}Ca$ [b] (IAPSO)	$\delta^{44/40}Ca$ [c] (IAPSO)	$\delta^{44/42}Ca$ [d] (NIST)	$\delta^{44/40}Ca$ (NIST)
J125	Jurassic	Belemnite	Russia	Callovian	157.4				0.12
J132	Jurassic	Belemnite	Russia	Callovian	157.7				0.28
J138	Jurassic	Belemnite	Russia	Callovian	158.4				0.35
	Cretaceous and Jurassic period (MC-ICP-MS data from Farkaš et al., 2007)								
K20	Cretaceous	Belemnite	Germany	Barremian	126.6	-0.86			0.39
K25	Cretaceous	Belemnite	Germany	Barremian	126.7	-0.89			0.33
K30	Cretaceous	Belemnite	Germany	Barremian	127.1	-0.89			0.33
K35	Cretaceous	Belemnite	Great Britain	Barremian	127.4	-0.91			0.28
K41	Cretaceous	Belemnite	Germany	Barremian	127.8	-0.91			0.28
K45	Cretaceous	Belemnite	Great Britain	Barremian	128.2	-0.83			0.45
K51	Cretaceous	Belemnite	Germany	Barremian	128.3	-0.83			0.45
K67	Cretaceous	Belemnite	Great Britain	Barremian	130.5	-0.85			0.40
K75	Cretaceous	Belemnite	Germany	Hauterivian	133.1	-0.84			0.44
J77	Jurassic	Belemnite	New Zealand	Kimmeridgian	153.6	-0.88			0.35
J94	Jurassic	Belemnite	Russia	Oxfordian	155.7	-0.97			0.17
J109	Jurassic	Belemnite	Russia	Oxfordian	155.9	-0.97			0.17
J114	Jurassic	Belemnite	Russia	Oxfordian	156.7	-1.00			0.11
J119	Jurassic	Belemnite	Russia	Callovian/Oxfordian	157.3	-0.98			0.16
J125	Jurassic	Belemnite	Russia	Callovian	157.4	-0.93			0.24
J132	Jurassic	Belemnite	Russia	Callovian	157.7	-0.93			0.24
J138	Jurassic	Belemnite	Russia	Callovian	158.4	-0.90			0.31
J143	Jurassic	Belemnite	Russia	Callovian	158.7	-0.92			0.27
	Cretaceous and Carboniferous period (MC-ICP-MS data from Steuber and Buhl, 2006)								
X4	Cretaceous	Belemnite	Germany	Campanian	~ 75	-0.85			0.18
H705/11	Cretaceous	Rudist	Austria	Santonian	~ 84	-0.80			0.28
H705/28	Cretaceous	Rudist	Austria	Santonian	~ 84	-0.84			0.20
H705/37	Cretaceous	Rudist	Austria	Santonian	~ 84	-0.84			0.21
H705/40	Cretaceous	Rudist	Austria	Santonian	~ 84	-0.89			0.10
H705/48	Cretaceous	Rudist	Austria	Santonian	~ 84	-0.88			0.13
H705/51	Cretaceous	Rudist	Austria	Santonian	~ 84	-0.88			0.13
E1	Cretaceous	Oyster	Algeria	Cenomanian	~ 95	-1.01			-0.13
E2	Cretaceous	Oyster	Algeria	Cenomanian	~ 95	-1.05			-0.21
3763/1	Cretaceous	Oyster	Algeria	Cenomanian	~ 95	-0.98			-0.07
KO2/9-2	Cretaceous	Bioclast (calcite)	Greece	Cenomanian	~ 95	-0.85			0.18
KO1/33-1	Cretaceous	Bioclast (calcite)	Greece	Cenomanian	~ 95	-0.67			0.54
Ma11/17	Cretaceous	Rudist	France	Barremian	~ 125	-0.90			0.08
Ma11/29	Cretaceous	Rudist	France	Barremian	~ 125	-0.89			0.09
Ma11/43	Cretaceous	Rudist	France	Barremian	~ 125	-0.91			0.05
Ma11/50	Cretaceous	Rudist	France	Barremian	~ 125	-0.94			0.00
Ma11/57	Cretaceous	Rudist	France	Barremian	~ 125	-0.95			-0.02
Ma11/60	Cretaceous	Rudist	France	Barremian	~ 125	-0.91			0.06
Ma11/66	Cretaceous	Rudist	France	Barremian	~ 125	-0.95			-0.02
Ma11/69	Cretaceous	Rudist	France	Barremian	~ 125	-0.91			0.07
Ma11/79	Cretaceous	Rudist	France	Barremian	~ 125	-0.93			0.03
OXY1	Cretaceous	Belemnite	Germany	Barremian	~ 125	-0.83			0.23
OXY2	Cretaceous	Belemnite	Germany	Barremian	~ 125	-0.80			0.27
OXY3	Cretaceous	Belemnite	Germany	Barremian	~ 125	-0.82			0.24
N130/4	Carboniferous	Micrite	Spain	Moscovian	~ 310	-0.39			1.11

(Continued)

Table A.3.5. (Continued)

Sample ID	Period [a]	Material	Location	Stage	Age [a] (Ma)	$\delta^{44/42}Ca$ [b] (IAPSO)	$\delta^{44/40}Ca$ [c] (IAPSO)	$\delta^{44/42}Ca$ [d] (NIST)	$\delta^{44/40}Ca$ (NIST)
Pa50/1	Carboniferous	Micrite	Spain	Moscovian	~ 310	-0.40			1.08
Pa50/2	Carboniferous	Micrite	Spain	Moscovian	~ 310	-0.39			1.11
Pa50/4	Carboniferous	Micrite	Spain	Moscovian	~ 310	-0.37			1.14
NON2/1	Carboniferous	Skeletal calcite (bioclast)	Spain	Moscovian	~ 310	-0.47			0.94
RL-A1/1	Carboniferous	Skeletal calcite (bioclast)	Spain	Moscovian	~ 310	-0.46			0.95
RL-CL3	Carboniferous	Skeletal calcite (bioclast)	Spain	Moscovian	~ 310	-0.48			0.92
C105	Carboniferous	Brachiopod	Great Britain	Visean (?)	~ 330	-0.73			0.42
5106	Carboniferous	Brachiopod	Great Britain	Visean	~ 330	-0.90			0.08

[a] Numerical ages presented here were adopted from the literature, or were estimated based on the stratigraphic position of a sample and therefore should be taken only as rough approximations.
[b] The $\delta^{44/42}Ca$ (IAPSO) values were converted to $\delta^{44/40}Ca$ (SRM915a) using the following relation: $\delta^{44/40}Ca$ (SRM915a) = [2*($\delta^{44/42}Ca$ (IAPSO)) +1.88 ‰]. However, the MC-ICP-MS data of Farkaš et al. (2007) were also corrected for a systematic offset of 0.12 ‰, and thus for these data the conversion was as follows: $\delta^{44/40}Ca$ (NIST) = [2*($\delta^{44/42}Ca$ (IAPSO) + 0.12‰) +1.88 ‰].
[c] The $\delta^{44/40}Ca$ (IAPSO) values were converted to $\delta^{44/40}Ca$ (SRM915a) using the following relation: $\delta^{44/40}Ca$ (SRM915a) = [$\delta^{44/42}Ca$ (IAPSO) +1.88 ‰].
[d] The $\delta^{44/42}Ca$ (SRM915a) values were converted to $\delta^{44/40}Ca$ (SRM915a) using the following relation: $\delta^{44/40}Ca$ (SRM915a) = [2*($\delta^{44/42}Ca$ (SRM915a))].

Summary of the published calcium isotope data from the Phanerozoic marine carbonates and phosphates

Period	Total number of analysed samples: (All literature data)	Total number of analysed samples (Heuser et al., 2005) 'IFM-GEOMAR'	Total number of analysed samples (Schmitt et al., 2003a)	Total number of analysed samples (Soudry et al., 2004)	Total number of analysed samples (Farkaš et al., 2007) 'Ottawa-Boehum'	Total number of analysed samples (Steuber and Buhl, 2006) 'Bochum'
Neogene	56	45	11	0	0	0
Paleogene	2	0	0	2	0	0
Cretaceous	50	0	0	9	17	24
Jurassic	15	0	0	0	15	0
Carboniferous	9	0	0	0	0	9
Cenozoic	58	45	11	2	0	0
Mesozoic	65	0	0	9	32	24
Paleozoic	9	0	0	0	0	9
Total	132	45	11	11	32	33

4 Testing the boron isotope paleo-pH proxy: An example from Middle and Late Jurassic skeletal carbonates

by

Juraj Farkaš [a], John Blenkinsop [b], and Ján Veizer [a]

[a] *University of Ottawa and Ottawa-Carleton Geoscience Centre, Ottawa, K1N 6N5,ON, Canada*

[b] *Carleton University and Ottawa-Carleton Geoscience Centre, Ottawa, K1S 5B6,ON, Canada*

Abstract

The aim of this study is to utilize boron isotopes to assess changes in pH of Jurassic seawater and their implication on the $\delta^{18}O$ based estimates of coeval sea surface temperatures (SSTs). The heavy $\delta^{18}O$ values of the Jurassic (Callovian and Oxfordian) belemnites were originally interpreted as low SSTs, consistent with a coeval cool climate mode suggested by the geological record. Some studies, however, argued that the ^{18}O enrichment of belemnite calcite is rather a reflection of low pH of surface oceans, a hypothesis testable by boron isotope geochemistry due to its sensitivity to pH.

The $\delta^{11}B$ record of the Middle and Late Jurassic (MLJ) belemnites delineates a quasi-systematic variation of about 10‰, which is tentatively explained as a relative variability in seawater pH of about 1 ± 0.2 units, assuming a hypothetical value for the boron isotope composition of Jurassic seawater ($\delta^{11}B_{SW}$) of 22 ± 2‰. The latter value is, however, at odds with the results of geochemical modeling of the oceanic boron cycle, which indicate that the $\delta^{11}B_{SW}$ value during the Jurassic should has been within a range of 30 to 50‰. This expectation is further supported by the published boron isotope data from well-preserved Jurassic brachiopods that suggest Jurassic $\delta^{11}B_{SW}$ of about 39.5 ‰. These results therefore indirectly indicate that the boron isotope systematics of our MLJ belemnites has been compromised by diagenesis.

Consequently, we are unable to utilize the measured $\delta^{11}B$ dataset to evaluate the effect of seawater pH on the $\delta^{18}O$ record of the MLJ belemnites, hence the SSTs estimates. Nevertheless, the present study shows that boron isotope geochemistry of fossil skeletal carbonates is much more prone to diagenetic resetting than are the isotope systems of O, C, S, Sr and Ca. Therefore care must be exercised in the use of boron isotopes for the reconstructions of paleo-seawater pH.

4.1 Introduction

Boron isotopes are commonly used as a tracer of geological and hydrological processes in surficial environments, but their potential as a proxy for pH of past seawater has been recognized only recently. Boron isotope composition of modern marine carbonates

is controlled primarily by seawater pH (Vengosh et al., 1991; Hemming and Hanson, 1992) thus it may potentially be used to reconstruct temporal changes in pH of paleo-seawater. Since pH of the surface oceans is controlled by equilibrium with atmospheric pCO_2 (Zeebe and Wolf-Gladrow, 2001), the $\delta^{11}B$ record may, in turn, provide an additional constraint on the relationship between atmospheric pCO_2 levels and Earth's climate over geological time.

A study covering the last ~ 450,000 years of Vostok ice cores (Hönisch and Hemming, 2005) has demonstrated a tight coupling between the $\delta^{11}B$ values of planktonic foraminifera and atmospheric pCO_2, suggesting that marine $\delta^{11}B$ record can potentially yield atmospheric pCO_2 levels beyond the time frame of ice core archives (Spivack et al., 1993; Sanyal et al., 1995; Gaillardet and Allègre, 1995; Pearson and Palmer, 2000; Palmer and Pearson, 2003; Kasemann et al., 2005; Pelejero et al., 2005).

A complicating issue is that the boron isotope composition of seawater varied with time (Lemarchand et al., 2000; Pagani et al., 2005), which constrains the reliability of pH estimates to the last 15 to 20 Ma, the approximate residence time of boron in modern oceans (Lemarchand et al., 2000). On longer time scales, gradual fluctuations of less than ~0.3‰ Ma^{-1} are to be expected (Lemarchand et al., 2000; Simon et al., 2006) and were documented (Joachmiski et al., 2005). Nevertheless, any systematic and rapid variations in marine $\delta^{11}B$ record, relative to the boron residence time in seawater, are more likely caused by temporal changes in pH than to vagaries of the oceanic boron isotope budget.

The objective of this study is to apply boron isotopes to better understand potential temporal variability of pH for the Jurassic surface oceans. This, in turn, has implications for the $\delta^{18}O$-based estimates of past sea surface temperatures (SSTs) because the oxygen isotope composition of inorganic and biogenic carbonates reflects not only temperature but also pH of a solution (Spero et al., 1997; Zeebe, 1999). Earlier studies based on the Jurassic belemnites (Podlaha 1995; Podlaha et al., 1998; Veizer et al., 1999) yielded heavy $\delta^{18}O$ values for Callovian and Oxfordian samples (Fig. 4.1) and these were originally interpreted as low SSTs, consistent with a coeval cool climate mode (Frakes and Francis, 1988; Frakes et al., 1992; Crowley. 1998; Dromart et al., 2003; Price and Mutterlose, 2004).

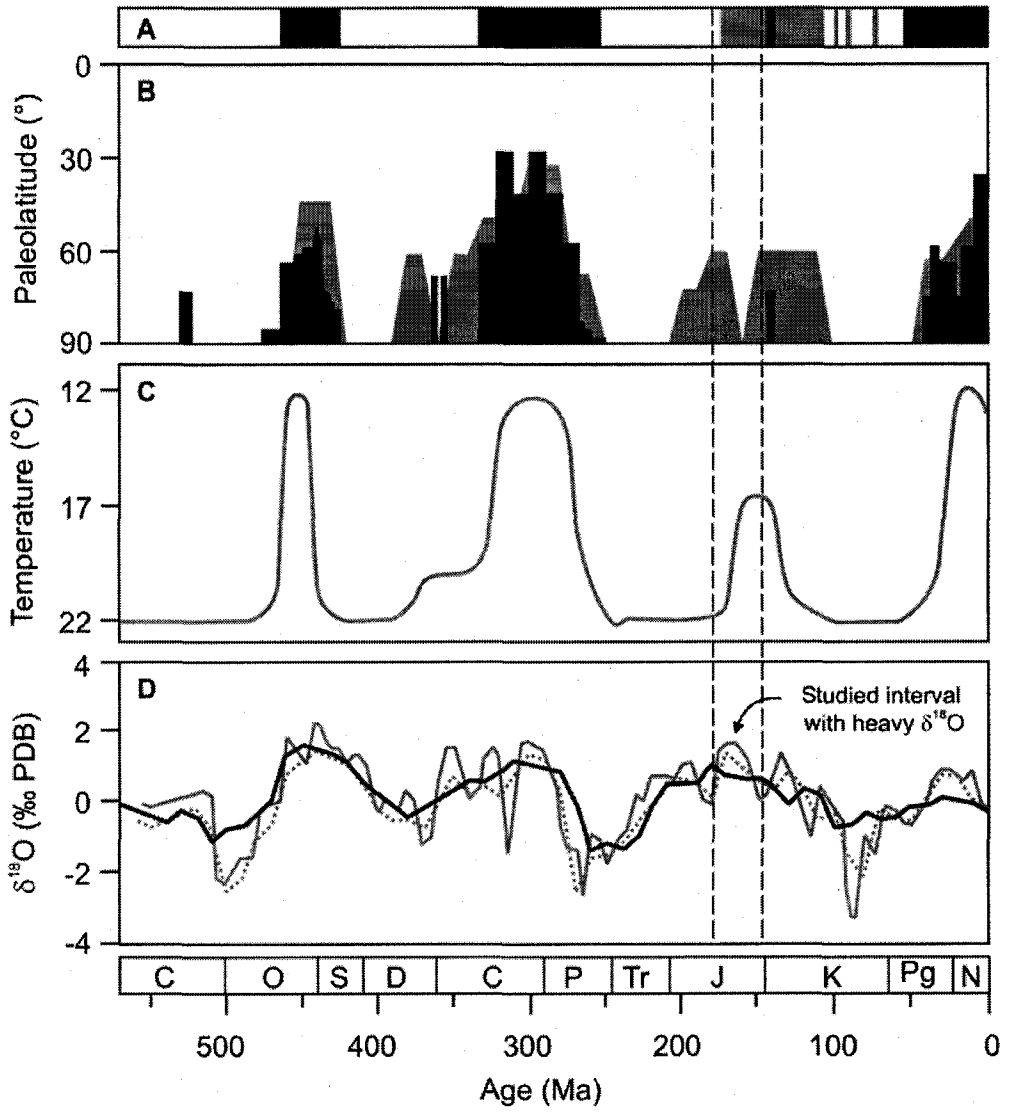

Fig. 4.1. (A) Climate regimes as determined from the sedimentological record (Frakes and Francis, 1988; Frakes et al., 1992; Crowley, 1998). Black intervals represent cool climate modes (icehouses) and the white intervals warm climate modes (greenhouses); gray bars indicate that the Jurassic/Cretaceous climate regime is not considered to be typical icehouse although tillites were recently documented in South Australia dated at ~140 Ma (Alley and Frakes, 2003). (B) Distribution of glacial deposits as a function of paleolatitude; black bars represent tillites and gray bars the frequency of ice rafted debris (modified after Veizer et al., 1999 and Royer et al., 2004; Alley and Frakes, 2003). (C) Estimates of global temperatures based on distribution of climate sensitive deposits and fossils (www.scotese.com/climate.htm). (D) Detrended oxygen isotope record of shallow-marine skeletal carbonates (brachiopod, belemnite and foraminifera data) from Veizer et al. (2000). The black curve represents a running mean with a step of 10 Ma and an averaging window of 50 Ma (10/50), the gray dotted curve has parameters 10/20, and the gray curve 5/10. Vertical dashed lines mark out the Middle/Late Jurassic period with the heavy $\delta^{18}O$ values that was the focus of our study.

Others (Royer et al., 2004; Wallmann, 2004) argued that these heavy $\delta^{18}O$ values are more likely a reflection of lower pH of contemporary seawater, presumably due to higher atmospheric pCO_2 levels (Berner and Kothavala, 2001), because the geological record provides no unequivocal evidence for Mesozoic glacial deposits, such as striated bedrock or tillites. However, there is some evidence for a cooler Late Jurassic/Early Cretaceous climate, such as the occurrences of glendonites and dropstones (Kemper, 1987; Price, 1999; Dromart et al., 2003) and more recently a tillite-bearing sequence dated at ~140 Ma has been described from South Australia (Alley and Frakes, 2003). Thus, constraining pH of Jurassic seawater via boron isotopes may help to clarify this controversy.

4.2 Samples

The detailed descriptions of samples analyzed in this study and their $\delta^{18}O$ datasets are available elsewhere (Podlaha 1995; Podlaha et al., 1998; Veizer et al., 1999; Tomašových, 2004). A total of 33 modern and fossil skeletal carbonates, 28 belemnites, 4 brachiopods and 1 coral were analyzed for their $\delta^{11}B$ values. Larger volume samples (n = 15) were measured also for their boron content. Fossil samples originate from three paleogeographically distinctive localities of the Tethyan realm, Russia (Peski, Ribinsk, Voskresensk), Germany (Geisingen, Ursental), and New Zealand (Kawhia Harbour). They cover the time interval from the Late Callovian (~160 Ma) to the Early Tithonian (~150 Ma) with an average stratigraphic resolution of ≤ 1 Ma. The numerical ages used in this study are based on the geological time scale of Harland et al. (1990) but conversion to the latest time scale of Gradstein et al. (2004) can be made via Gradstein et al. (1994). For comparison, we also collected modern skeletal carbonates, brachiopod (*Terebratalia transversa*) and coral (*Acropora palmata*) at San Juan Island, NW Pacific (Tomašových, 2004) and Belize, respectively.

4.3 Methods

4.3.1 Sample Preparation

Powders from the belemnite and brachiopod skeletons, composed of low-Mg calcite (aragonite for the coral sample), were rinsed with nanopure water (>18 MΩ cm) and ultrasonically cleaned in non-buffered (pH ≈5) quartz-distilled 30% H_2O_2 for at least 12 hours to remove organic matter. Any adsorbed fractions, such as clay particles or soluble salts, were removed by ultrasonication in nanopure water that had been additionally cleaned with a boron specific anion-exchange resin Amberlite™ IRA-743 (Hemming and Hanson, 1992). Washed powders, typically 5 to 10 mg of $CaCO_3$, were dried and weighed into PFA (perfluoroalkoxy) vials, and afterwards dissolved with an excess (~150 µL) of 2N quartz-distilled HCl. Sample solutions were evaporated to dryness at temperatures below 70 °C to avoid potential isotope fractionation due to the volatilization of boron as BCl_3 (Ishikawa and Nakamura, 1990; Klötzli, 1992). Sample size permitting, two aliquots from each sample were prepared, one for boron isotope composition and the other for boron concentration. The latter was determined via isotope dilution, using an aqueous H_3BO_3 spike solution IRMM-610 (Institute of Reference Materials and Measurements) enriched in ^{10}B with measured $^{10}B/^{11}B$ ratio of 18.916 ± 0.040 (2σ, n = 4) and the ^{10}B content of 3.6831 µmol g^{-1}.

The isotope dilution technique was also used for the determination of yields and procedural blanks of boron typical for our analytical procedures. The recovery yields of boron, tested on a sample size of ~20 ng, were close to 100% (99.85 ± 0.5%, n = 2), documenting no loss of boron and thus no isotope fractionation during the sample preparation. Total procedural boron blanks were consistently below 50 pg and therefore negligible as the amount of boron from a sample was in the range of 5 to 10 ng.

4.3.2 Mass spectrometry N-TIMS

Boron isotope abundances were analyzed on a Thermo Finnigan Triton thermal ionization mass spectrometer at Carleton University in the Isotope Geochemistry and Geochronology Research Centre (IGGRC) of the Ottawa-Carleton Geoscience Centre

(OCGC), adopting the method of Hemming and Hanson (1994). Briefly, the boron isotope abundances were measured in a negative-ion mode (N-TIMS), collecting simultaneously $^{10}BO_2^-$ and $^{11}BO_2^-$ ions as masses 42 and 43, respectively. The measured isotope ratio, 43/42, was corrected for the contribution of ^{17}O on mass 43 (see below):

$$43/42_{corrected} = 43/42_{measured} - 0.00076 \quad (4.1)$$

where the $43/42_{corrected}$ represents the ratio of interest, $^{11}B/^{10}B$. The boron isotope composition of natural samples is expressed as a delta notation ($\delta^{11}B$) in parts per thousand (‰) relative to the SRM 951 boric acid standard, applying the following relation:

$$\delta^{11}B_{SRM}\ (‰) = [(^{11}B/^{10}B)_{sample} / (^{11}B/^{10}B)_{SRM} - 1] * 1000 \quad (4.2)$$

For SRM 951, typically 10 ng of boron was mixed with ~0.5 µL of B-free seawater (an ionization promoter), cleaned in boron-specific resin Amberlite™ IRA-743, and loaded onto an outgassed zone refined Re single filament. For carbonate samples and IAPSO seawater no ionization promoter was needed and these solutions were loaded directly onto the Re filament. Solutions containing ~3 ng of boron were over ~5 min evaporated to dryness at 0.5 A and then heated for 30 seconds at 1.2 A (Kasemann et al., 2005). The exposure of filaments loaded with samples ($CaCl_2$) to laboratory air was minimized as $CaCl_2$ is highly hygroscopic and adsorbs moisture from the air causing a potential boron contamination (Foster et al., 2006). The sample wheel was therefore introduced into the mass spectrometer without delay and the ion source housing pumped down immediately.

In the mass spectrometer, the filament current was in ~25 min brought to an operating temperature in a range of 975 ± 20 °C. In the first step the filament current was raised to 1 A at a speed of 0.1 A min^{-1}, followed by a stepwise increase of 0.015 A min^{-1} until the operating temperature was reached. Before data acquisition, a possible isobaric interference from organic matter on mass 42 ($^{12}C^{14}N^{16}O$) was evaluated by monitoring mass

26 ($^{12}C^{14}N$). If the isobaric interference was detected, runs were discarded (ca. 10% of all runs). Ion beam intensity for $^{11}BO_2^-$ was typically in the range 50 to 1000 mV (0.5 to 1000 pA). The data acquisition for a single run comprised 10 blocks of 10 cycles over a period of ~30 min, with defocused baselines collected for 30 sec at the beginning of each block. Acceptable runs showed relative in-run fractionation for the $^{11}B/^{10}B$ ratio of ≤ 0.6‰. Most of the samples, ~ 65 %, were analyzed in duplicate, using the same sample solution, to monitor possible effects of in-run fractionation and other analytical artifacts, such as inconsistent heating routine and/or a minor isobaric interference. In this study, the analytical uncertainty of the reported $\delta^{11}B$ values was calculated as two standard deviations (2σ) that was typically better than ± 1.5‰. The long-term, over 4 months, external reproducibility of the $\delta^{11}B$ measurements was tested via repeat analysis of SRM 951 and the following in-house standards: IAPSO seawater (Ocean Scientific International), present-day coral (*Acropora palmata*), and modern brachiopod (*Terebratalia transversa*).

4.4 Results

Replicate analyses of SRM 951, IAPSO seawater and modern skeletal carbonates are presented in Table 4.1. Expressed as the $\delta^{11}B$ (SRM 951) values, the IAPSO seawater showed heavy isotope enrichment of 39.2 ± 0.7‰ (2σ), and the modern coral and brachiopod have $\delta^{11}B$ signatures of 24.0 ± 1.4‰ and 14.9 ± 1.2‰, respectively. These results are in general agreement with previously published values measured by N-TIMS (Hemming and Hanson, 1992 and 1994) or MC-ICP-MS (Lécuyer et al., 2002). Note, however, that our $\delta^{11}B$ value of modern brachiopod (*Terebratalia transversa*) is about 3‰ lighter compared to the data of Lécuyer et al. (2002) based on the identical species. The difference is likely due to lower pH of the surface ocean waters at our sampling site San Juan Island (Friday Harbor), with measured pH of ~ 7.7 (Tomašových A., personal communication).

Analytical data from fossil belemnite and brachiopod samples, their $\delta^{11}B$ values and boron concentrations, are presented in Table 4.2. A total of 61 boron isotope analyses, 47 natural and 14 spiked ratios, from 31 fossil skeletal carbonates (28 belemnites and 3

brachiopods) were performed. The $\delta^{11}B$ record of the Middle and Late Jurassic (henceforth MLJ) skeletal carbonates, plotted against geological time (Fig. 4.2), showed a temporal variation of about 10‰. The Late Callovian $\delta^{11}B$ values scattered from –1 to 4‰ with a mean of about 1.5‰. The Oxfordian signatures are slightly heavier, with the range of 0.5 to 6‰ and an average of 3‰. Most of the Kimmeridgian values plot around 9‰, with a solitary maximum of 13‰ and a minimum of 4‰. The Early Tithonian signatures decline from 4 to –1.5‰. Overall, the $\delta^{11}B$ record of the MLJ belemnites and brachiopods show a quasi-systematic increase from 1.5 to 9‰, throughout the Callovian, Oxfordian and Kimmeridgian (~159 to 152 Ma), followed by a rapid decline to –1.5‰ in the Early Tithonian (~152 to 150 Ma). The boron concentrations were measured only for 14 larger-volume samples and were low, typically a couple of $\mu g\ g^{-1}$ (Table 4.2).

Table 4.1.

External reproducibility of boron isotope measurements, $^{11}B/^{10}B$ and $\delta^{11}B$, as determined by repeat analyses of SRM 915, IAPSO seawater and modern skeletal carbonates, over a period of four months

No.	SRM 951 (Isotope standard) $^{11}B/^{10}B$	Seawater (IAPSO) $^{11}B/^{10}B$	Coral *(Acropora* sp.*)* $^{11}B/^{10}B$	Brachiopod *(Terebratalia* sp.*)* $^{11}B/^{10}B$
1	4.0074	4.1680	4.1090	4.0686
2	4.0037	4.1673	4.1109	4.0687
3	4.0119	4.1673	4.1069	4.0693
4	4.0115	4.1702	4.1073	4.0733
5	4.0101	4.1671	4.1019	4.0687
6	4.0141	4.1665	4.1070	4.0649
7	4.0121	4.1676	4.1036	4.0702
8	4.0136	4.1660	4.1044	4.0722
9	4.0054	4.1661	4.1025	4.0714
10	4.0092	4.1651	4.1073	4.0672
Mean value	**4.0099**	**4.1671**	**4.1061**	**4.0695**
2σ	0.0069	0.0027	0.0058	0.0049
	$\delta^{11}B$ (SRM 951)	$\delta^{11}B$ (SRM 951)	$\delta^{11}B$ (SRM 951)	$\delta^{11}B$ (SRM 951)
Mean (‰)	**0.00**	**39.21**	**23.99**	**14.85**
2σ	1.73	0.69	1.44	1.23

Table 4.2.

Trace element (B, Fe, Mn, Sr) and isotope ($\delta^{11}B$, $\delta^{18}O$ and $^{87}Sr/^{86}Sr$) composition of the MLJ belemnites and brachiopods

I.D.	Country	Location	Material	Fossil Name	Stage	Age (Ma)	B ($\mu g\ g^{-1}$)	Fe ($\mu g\ g^{-1}$)	Mn ($\mu g\ g^{-1}$)	Sr ($\mu g\ g^{-1}$)	$^{87}Sr/^{86}Sr$	$\delta^{18}O$ (‰)	$\delta^{11}B$ (‰)	2σ	*n*
J143	Russia	Peski	Belemnite	*Pachyteuthis sp.*	Callovian	158.7	1.4	25	13	896	0.706825	-0.1	1.6	2.5	2
J140	Russia	Peski	Belemnite	*Pachyteuthis sp.*	Callovian	158.5	3.0	48	16	865	0.706819	1.3	1.9	1.4	1
J133	Russia	Peski	Belemnite	*Cylindroteuthis sp.*	Callovian	157.7	2.2	261	0	719	-	1.8	-0.8	1.4	1
J127	Russia	Peski	Belemnite	*Pachyteuthis sp.*	Callovian	157.4	1.9	71	0	630	0.706839	1.6	2.2	1.5	2
J119	Russia	Peski	Belemnite	*Pachyteuthis sp.*	Callov./Oxford.	157.3	-	28	4	589	0.706826	1.5	3.2	1.4	1
J118	Russia	Peski	Belemnite	*Pachyteuthis sp.*	Callov./Oxford.	157.1	2.9	126	2	676	0.706838	2.0	3.8	0.5	2
J115	Russia	Peski	Belemnite	*Cylindroteuthis sp.*	Callov./Oxford.	157.0	-	36	0	828	-	0.4	-0.6	1.4	1
J114	Russia	Peski	Belemnite	*Cylindroteuthis sp.*	Oxfordian	156.7	0.9	0	0	591	0.706825	1.2	0.6	0.3	2
J111	Russia	Ribinsk	Belemnite	*Pachyteuthis sp.*	Oxfordian	155.9	-	324	0	700	-	0.1	1.0	1.2	2
J105	Russia	Ribinsk	Belemnite	*Pachyteuthis sp.*	Oxfordian	155.9	-	546	0	764	-	-0.8	0.9	5.7	2
J100	Russia	Ribinsk	Belemnite	*Pachyteuthis sp.*	Oxfordian	155.8	-	420	5	722	-	-0.3	1.8	0.9	2
J95	Russia	Ribinsk	Belemnite	*Pachyteuthis sp.*	Oxfordian	155.7	-	1245	18	883	-	-1.2	5.7	1.9	2
J89	Russia	Ribinsk	Belemnite	*Pachyteuthis sp.*	Oxfordian	155.6	-	125	0	841	0.706897	-0.9	4.0	1.4	1
J87	Russia	Voskresensk	Belemnite	*Acroteuthis sp.*	Oxfordian	155.2	-	640	62	1124	-	1.1	1.5	1.4	1
J81	N. Zealand	Kawhia H.	Belemnite	*Belemnopsis sp.*	Kimmeridgian	154.0	-	165	6	1174	0.706784	1.0	6.7	1.4	1
EK1	Germany	Geisingen	Belemnite	Unidentified	Kimmeridgian	154.0	1.0	35	5	1140	-	-	8.7	1.4	1
EK2	Germany	Geisingen	Belemnite	Unidentified	Kimmeridgian	154.0	1.0	18	4	344	-	-	9.6	1.4	1
EK3	Germany	Geisingen	Brachiopod	*Lacunosella sp.*	Kimmeridgian	154.0	1.4	21	3	378	-	-	9.5	1.4	1
EK4	Germany	Geisingen	Brachiopod	*Lacunosella sp.*	Kimmeridgian	154.0	1.5	11	2	1318	-	-	9.1	1.4	1
J80	N. Zealand	Kawhia H.	Belemnite	*Belemnopsis sp.*	Kimmeridgian	153.9	-	186	1	1053	0.706836	-2.5	8.3	2.1	2
J79	N. Zealand	Kawhia H.	Belemnite	*Belemnopsis sp.*	Kimmeridgian	153.7	0.3	55	10	1410	0.706854	-3.0	7.6	1.6	2
J76	N. Zealand	Kawhia H.	Belemnite	*Belemnopsis sp.*	Kimmeridgian	153.6	-	26	4	1095	0.706862	-2.4	8.8	0.1	2
J74	N. Zealand	Kawhia H.	Belemnite	*Belemnopsis sp.*	Kimmeridgian	152.4	-	28	0	1197	0.706938	-1.1	4.3	0.8	2
J72	N. Zealand	Kawhia H.	Belemnite	*Belemnopsis sp.*	Kimmeridgian	152.2	-	57	7	1023	0.706971	-0.5	8.5	1.4	2
LK1	Germany	Ursental	Belemnite	Unidentified	Kimmeridgian	152.0	0.9	18	9	1279	-	-	8.8	1.4	1
LK2	Germany	Ursental	Brachiopod	*Lacunosella sp.*	Kimmeridgian	152.0	3.7	268	33	392	-	-	13.3	1.4	1
J71	N. Zealand	Kawhia H.	Belemnite	*Belemnopsis sp.*	Kimmeridgian	152.0	0.4	234	18	902	0.706967	-3.4	8.2	0.7	2
J69	N. Zealand	Kawhia H.	Belemnite	*Hibolites sp.*	Tithonian	151.5	-	436	33	918	0.707024	-1.5	4.3	3.8	2
J66	N. Zealand	Kawhia H.	Belemnite	*Hibolites sp.*	Tithonian	151.1	-	1365	125	894	0.707052	-0.7	-0.3	1.4	1
J63	Russia	Voskresensk	Belemnite	*Pachyteuthis sp.*	Tithonian	150.0	-	633	10	1179	-	-1.7	-0.9	1.5	2
J61	Russia	Voskresensk	Belemnite	*Cylindroteuthis sp.*	Tithonian	150.0	-	17	0	1452	-	-0.8	-1.7	1.4	1

Fe, Mn, Sr concentrations and the $\delta^{18}O$ and $^{87}Sr/^{86}Sr$ datasets are from Podlaha (1995), Podlaha et al. (1998) and Farkaš et al. (2007).

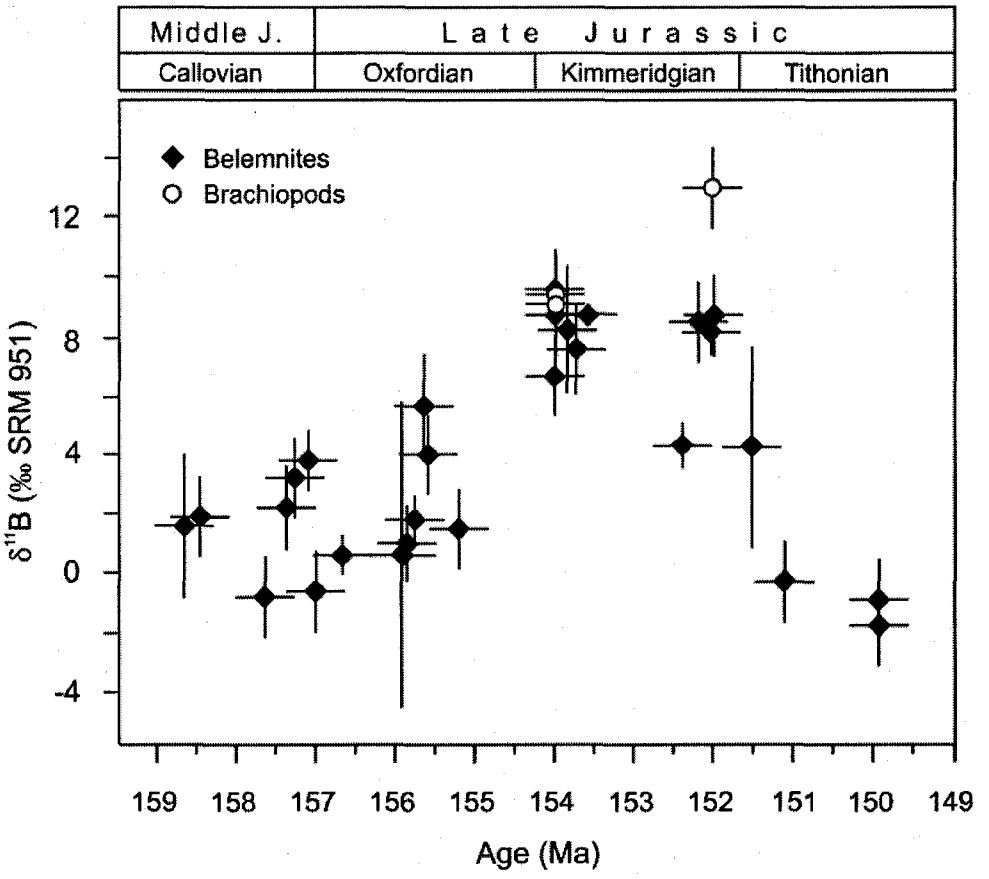

Fig. 4.2. Measured $\delta^{11}B$ values of the MLJ skeletal carbonates (belemnites = black diamonds, brachiopods = open circles) plotted as a function of geological time. Vertical error bars represent two standard deviations (2σ) and horizontal bars indicate an approximate stratigraphic resolution of ± 1 Ma.

4.5 Discussion

In this section we present and discuss two interpretations for the observed $\delta^{11}B$ record of the MLJ skeletal carbonates. Firstly, we address the original question of this study and explore a tentative possibility that the measured $\delta^{11}B$ variations were controlled primarily by temporal changes in pH of Jurassic surface oceans. The second alternative considers an option that the boron isotope data are all signals compromised by secondary processes. Both explanations are critically evaluated in light of other chemical (trace

elements, isotopes) and textural (SEM, CL) data acquired previously for these samples, which are complemented by relevant published data on the boron isotope geochemistry of well-preserved skeletal carbonates. Finally, a conclusion is drawn about the more realistic explanation for our experimental $\delta^{11}B$ dataset.

4.5.1 Paleo-pH estimates from $\delta^{11}B$ record of marine skeletal carbonates

There are two aqueous species of boron in seawater, neutral boric acid $B(OH)_3$ (i.e. H_3BO_3) and charged borate ions $B(OH)_4^-$. The relative abundance of these two species is a function of seawater pH, due to the following chemical equilibrium (Zeebe and Wolf-Gladrow, 2001):

$$B(OH)_3 + H_2O \Leftrightarrow B(OH)_4^- + H^+ \tag{4.3}$$

There is an isotope fractionation between the $B(OH)_3$ and $B(OH)_4^-$ aqueous species, the $\delta^{11}B$ value of borate ions being about 20‰ lighter than that of boric acid. Consequently, if the proportion of $B(OH)_3$ and $B(OH)_4^-$ species changes with pH, their $\delta^{11}B$ values would also change. It is assumed that boron is incorporated into $CaCO_3$ crystal lattice exclusively as $B(OH)_4^-$ ions that are substituting for CO_3^{2-}, and that there is no significant isotope fractionation associated with this process (Zeebe and Wolf-Gladrow, 2001).

Thus, the boron isotope composition of marine carbonates ($\delta^{11}B_{CC}$) can be used to calculate pH of the ambient seawater, providing that the $\delta^{11}B$ value of paleo-seawater ($\delta^{11}B_{SW}$) is known. Having constrained $\delta^{11}B_{CC}$ and $\delta^{11}B_{SW}$, the pH of paleo-seawater can be calculated using the following equation (Zeebe and Wolf-Gladrow, 2001):

$$pH = pK_B - \log [(\delta^{11}B_{CC} - \delta^{11}B_{SW}) / (\delta^{11}B_{SW} - \alpha_{(B3-B4)} * (\delta^{11}B_{CC}) - \varepsilon)] \tag{4.4}$$

where pK_B is the equilibrium constant for boric acid (pK_B = 8.6 at 25 °C), $\alpha_{(B3-B4)}$ is an empirical fractionation factor between dissolved $B(OH)_3$ and $B(OH)_4^-$ species ($\alpha_{(B3-B4)}$ =

1.027 at 25 °C) as determined by experiments on natural and cultured biogenic low-Mg calcites (Sanyal, 1996; Lécuyer et al., 2002), and ε equals $(\alpha_{(B3-B4)} - 1)*1000$.

At present, the $\delta^{11}B_{SW}$ of the Jurassic oceans is unknown or at best only broadly constrained (Lécuyer et al., 2002; see also Simon et al., 2006). Because of this uncertainty, the subsequent discussion will focus solely on relative temporal changes in the boron isotope composition of the MLJ belemnites, assuming scenarios with arbitrary $\delta^{11}B_{SW}$ values of 20, 22 and 24‰. With these hypothetical $\delta^{11}B_{SW}$ the reconstructed pH estimates show a relative variability of about 1 ± 0.2 units (Fig. 4.3 and Table 4.3), with the absolute pH value dependent on the scenario chosen.

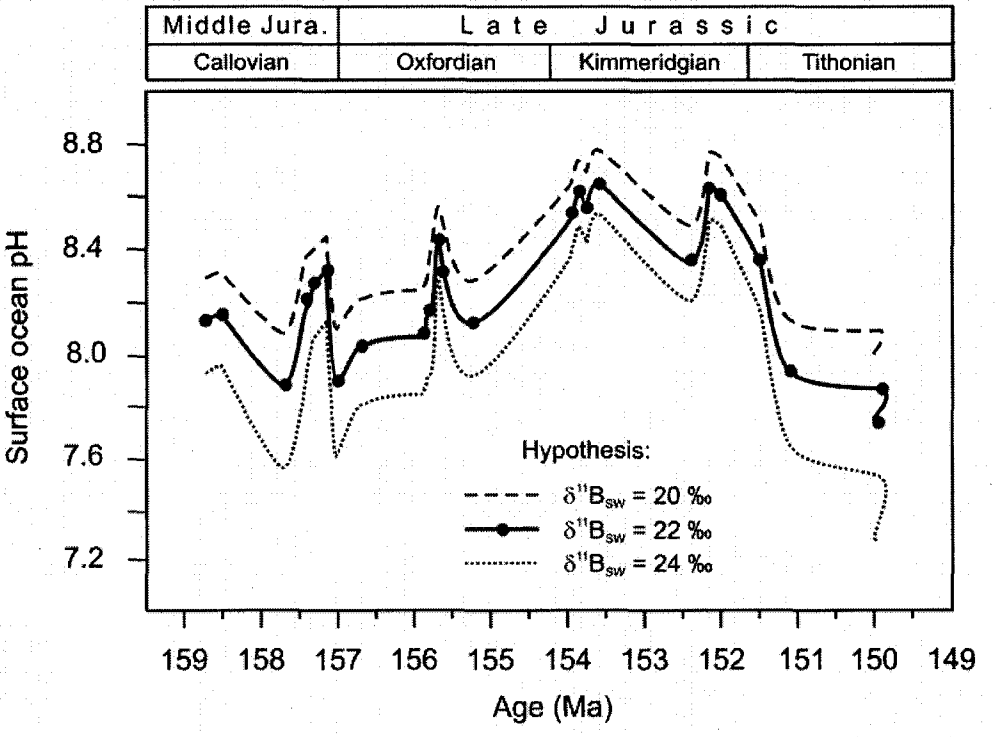

Fig. 4.3. Estimates of paleo-seawater pH variations calculated from the $\delta^{11}B$ record of the MLJ skeletal carbonates (belemnites data only), assuming arbitrary values for $\delta^{11}B_{SW}$ of 20, 22 and 24‰. Note that these $\delta^{11}B_{SW}$ values differ from the hypothesized boron isotope composition of the Jurassic seawater by Lécuyer et al. (2002) (see also Simon et al., 2006), which is assumed to have been close to its modern counterpart, around 39.5‰. We did not investigate this possibility because any combination of our boron isotope data with $\delta^{11}B_{SW}$ in excess of ~30‰ yields unreasonable paleo-seawater pH estimates.

Table 4.3.

The hypothetical pH estimates of the MLJ surface oceans (pH_{MODEL}) calculated from the boron isotope composition of the belemnites ($\delta^{11}B_{CC}$) and the $\delta^{18}O$ based paleo-temperature estimates (SST) corrected for the effect of changing pH (ΔSST)

				Scenario 1 ($\delta^{11}B_{SW}$ = 24 ‰)			Scenario 2 ($\delta^{11}B_{SW}$ = 22 ‰)			Scenario 3 ($\delta^{11}B_{SW}$ = 20 ‰)		
Age (Ma)	$\delta^{11}B_{CC}$ (‰)	$\delta^{18}O_{CC}$ (‰) [a]	SST (°C) [b]	pH_{MODEL}	ΔpH [c]	ΔSST (°C) [d]	pH_{MODEL}	ΔpH	ΔSST (°C)	pH_{MODEL}	ΔpH	ΔSST (°C)
158.7	1.6	0.8	8.97	7.92	0.18	1.25	8.11	-0.01	-0.09	8.27	-0.17	-1.17
158.5	1.9	1.4	6.81	7.95	0.15	1.02	8.14	-0.04	-0.26	8.29	-0.19	-1.32
157.7	-0.8	1.5	6.46	7.54	0.56	3.79	7.86	0.24	1.61	8.07	0.03	0.19
157.4	2.2	1.3	7.17	7.98	0.12	0.80	8.16	-0.06	-0.44	8.32	-0.22	-1.47
157.3	3.2	1.3	7.17	8.08	0.02	0.13	8.24	-0.14	-0.98	8.39	-0.29	-1.96
157.1	3.8	1.2	7.52	8.13	-0.03	-0.23	8.29	-0.19	-1.29	8.43	-0.33	-2.24
157.0	-0.6	0.1	11.60	7.59	0.51	3.50	7.89	0.21	1.45	8.09	0.01	0.06
156.7	0.6	0.2	11.22	7.79	0.31	2.12	8.02	0.08	0.55	8.19	-0.09	-0.64
155.9	1.0	-0.3	13.17	7.84	0.26	1.75	8.06	0.04	0.29	8.23	-0.13	-0.86
155.9	0.9	-0.4	13.56	7.83	0.27	1.84	8.05	0.05	0.35	8.22	-0.12	-0.80
155.8	1.8	-0.7	14.77	7.94	0.16	1.10	8.13	-0.03	-0.21	8.29	-0.19	-1.27
155.7	5.7	-0.9	15.59	8.28	-0.18	-1.26	8.42	-0.32	-2.20	8.55	-0.45	-3.09
155.6	4.0	0.4	10.46	8.15	-0.05	-0.35	8.30	-0.20	-1.39	8.44	-0.34	-2.33
155.2	1.5	0.8	8.97	7.90	0.20	1.33	8.10	0.00	-0.03	8.26	-0.16	-1.12
154.0	6.7	-2.4	22.05	8.36	-0.26	-1.75	8.49	-0.39	-2.66	8.62	-0.52	-3.53
153.9	8.3	-2.7	23.41	8.47	-0.37	-2.49	8.59	-0.49	-3.37	8.72	-0.62	-4.25
153.7	7.6	-2.4	22.05	8.42	-0.32	-2.17	8.55	-0.45	-3.06	8.68	-0.58	-3.93
153.6	8.8	-1.6	18.53	8.50	-0.40	-2.72	8.63	-0.53	-3.59	8.76	-0.66	-4.47
152.4	4.3	-1.4	17.68	8.18	-0.08	-0.52	8.33	-0.23	-1.54	8.46	-0.36	-2.46
152.2	8.5	-1.3	17.25	8.48	-0.38	-2.58	8.61	-0.51	-3.46	8.74	-0.64	-4.34
152.0	8.2	-1.2	16.83	8.46	-0.36	-2.45	8.59	-0.49	-3.33	8.72	-0.62	-4.20
151.5	4.3	-1.0	16.00	8.18	-0.08	-0.52	8.33	-0.23	-1.54	8.46	-0.36	-2.46
151.1	-0.3	-1.1	16.42	7.64	0.46	3.11	7.92	0.18	1.21	8.12	-0.02	-0.12
150.0	-0.9	-1.4	17.68	7.52	0.58	3.95	7.85	0.25	1.70	8.06	0.04	0.25
150.0	-1.7	-1.4	17.68	7.29	0.81	5.53	7.74	0.36	2.47	7.98	0.12	0.79

[a] The averaged $\delta^{18}O$ (PDB) values of the belemnites ($\delta^{18}O_{CC}$), as given by moving average of 7 data points; original $\delta^{18}O$ data are from Podlaha et al. (1998).

[b] SSTs were calculated as: $SST\ (°C) = 16.0 - 4.14*(\delta^{18}O_{CC} - \delta^{18}O_{SW}) + 0.13*(\delta^{18}O_{CC} - \delta^{18}O_{SW})^2$ (Arthur and Anderson, 1983). The oxygen isotope composition of the MLJ seawater ($\delta^{18}O_{SW}$) was assumed to have a value of -1‰ (SMOW) (cf. Podlaha et al., 1998).

[c] ΔpH represents a difference between the pH of modern (pH = 8.1) and past surface oceans, the latter calculated from the $\delta^{11}B$ belemnite record (see Eq. 4.4).

[d] ΔSST is the SST correction due to changing pH (see Eq. 4.5).

Variations in the paleo-seawater pH of about 1 unit would have an effect on $\delta^{18}O$ signatures of belemnite calcite, as the oxygen isotope composition of a calcite reflects the average oxygen isotope composition of the total dissolved inorganic carbonate species (Σ DIC = $H_2CO_3 + HCO_3^- + CO_3^{2-}$) in a solution, which varies with pH (Spero et al., 1997; Zeebe, 1999; Zeebe and Wolf-Gladrow, 2001). Thus, any change in seawater pH affects not only the boron isotope composition of calcite but also its $\delta^{18}O$ signatures, causing a negative coupling between $\delta^{18}O$ and $\delta^{11}B$ values. Indeed, there are indications of a general anti-correlation between $\delta^{18}O$ and $\delta^{11}B$ signatures of the studied MLJ belemnites (Fig. 4.4) that is particularly obvious for a time interval from ~159 to 152 Ma (R^2 = 0.47, p = 0.001, n = 22). This may reflect the influence of seawater pH on the oxygen and boron isotope compositions of the MLJ belemnites.

Therefore, we calculated the pH-correction for the SSTs estimates (Table 4.3 and Fig. 4.4) using the following relation (Zeebe, 2001):

$$\Delta SST\ (°C) = \Delta pH * b * s \qquad (4.5)$$

where ΔSST is the pH-correction of SST, ΔpH represents the pH difference between modern ocean (pH = 8.1) and its ancient counterpart, b is a linear coefficient of paleo-temperature equation (-4.80°C per ‰), and the parameter s equals -1.42‰ pH^{-1}, which is the slope of the $\delta^{18}O$ of calcite as a function of pH of a solution (Zeebe, 1999 and 2001).

Despite the observed pattern of negative correlation between $\delta^{18}O$ and $\delta^{11}B$, the modeled pH changes have only a marginal impact on the $\delta^{18}O$-based SSTs trends (Fig. 4.4). If true, this would suggest that the effect of seawater pH on the oxygen isotope composition of belemnite calcite played only a minor role, indicating that the observed ^{18}O enrichment in the MLJ samples would primarily arise from relatively cool SSTs of the contemporary oceans.

The downfall of this interpretation is that it needs to assume significantly light boron isotope composition of Jurassic seawater of about 22 ± 2‰, in order to maintain seawater pH in a sensible range (i.e. close to 8).

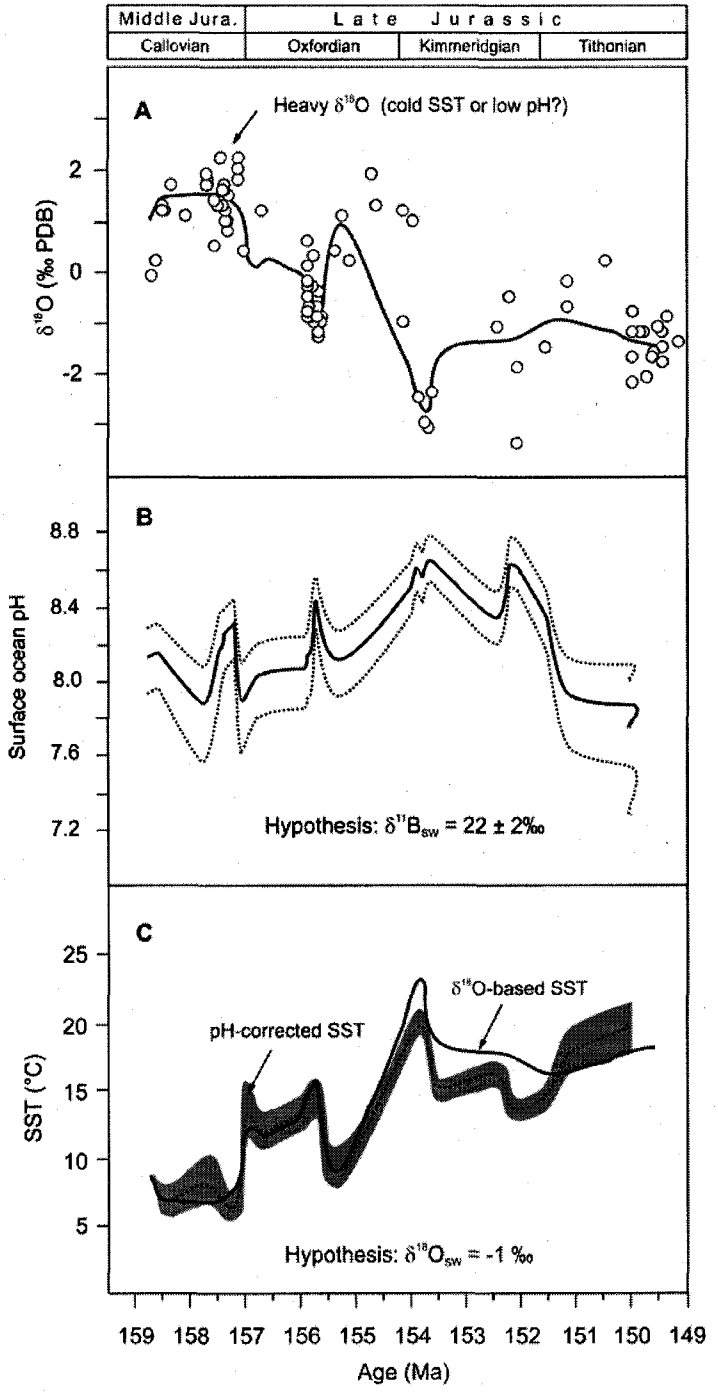

Fig. 4.4. (A) The oxygen isotope composition of the MLJ belemnites (data from Podlaha et al., 1998). The solid line represents a 7 point moving average. (B) Estimates of pH of the MLJ surface oceans, as calculated from the $\delta^{11}B$ values of the MLJ belemnites. Note the statistically significant negative correlation between $\delta^{18}O$ and pH (i.e. $\delta^{11}B$) for the time interval from ~159 to 152 Ma (R^2 = 0.47, p = 0.001, n = 22). (C) The SST estimates calculated from the averaged oxygen isotope compositions ($\delta^{18}O$, PDB) of the MLJ belemnites (solid line), and the pH-corrected SSTs (dashed line with gray band).

This $\delta^{11}B_{SW}$ value is however at odds with the estimates of Lécuyer et al. (2002) who concluded, based on the analysis of Callovian and Oxfordian brachiopods, that the boron isotope composition of Jurassic seawater was close to it modern counterpart, hence around

39.5‰. Moreover, the results of geochemical modeling of Joachmiski et al. (2005) and Sime et al. (2006) also suggest that the $\delta^{11}B_{SW}$ value of Phanerozoic oceans should have fluctuated within a range 30 to 50‰. These studies therefore indicate that the $\delta^{11}B_{SW}$ value of 22 ± 2‰ is likely an unrealistic estimate, which indirectly suggest that the boron isotope systematics of our MLJ belemnites could have been altered by secondary processes.

4.5.2 Diagenesis and preservation of primary isotope signatures

The degree of preservation of the studied MLJ belemnites was examined in detail by Podlaha (1995) and Podlaha et al. (1998) using conventional techniques, such as optical screening (microscopy, CL, SEM) and trace element chemistry (Sr, Mn and Fe). Visual inspection of belemnite rostra confirmed that primary ultrastructure of non-luminescent concentrically oriented low-Mg calcite prisms was well preserved. These were separated by domains of luminescent diagenetic calcite, constituting up to 10 vol % of the rostra (Veizer, 1974). Only non-luminescent calcite layers were therefore sampled by micro-drilling for further geochemical investigations. The trace element contents of these sampled domains were within the ranges for modern biogenic low-Mg calcites (Table 4.2) (Veizer, 1983; Brand et al., 2003), with strontium concentrations around 900 μg g^{-1} (range 344 to 1452 μg g^{-1}) and manganese typically below 50 μg g^{-1} (< 1 to 125 μg g^{-1}). The isotope studies of oxygen, carbon (Podlaha et al., 1998; Veizer et al., 1999), sulfur (Kampschulte, 2001; Kampschulte and Strauss, 2004), strontium (Podlaha, 1995; Veizer et al., 1999) and calcium (Farkaš et al., 2007) carried out on the same samples are also consistent with good preservation of the samples and with retention of the original isotope signatures. The coherency of strontium isotope signals (Table 4.2) with studies of other authors (e.g. Jones and Jenkyns, 2001) further supports this proposition.

On the other hand, the relatively low boron concentrations and $\delta^{11}B$ values of the MLJ belemnites (Table 4.2), compared to modern skeletal carbonates and/or fossil brachiopods (Fig. 4.5) (Hemming and Hanson, 1992 and 1994; Lécuyer et al., 2002) indicate that diagenetic processes may have affected the boron isotope systematics in our samples while having only a negligible impact on the O, C, S, Ca and Sr isotope systems and the trace element compositions (Sr, Mn, Fe).

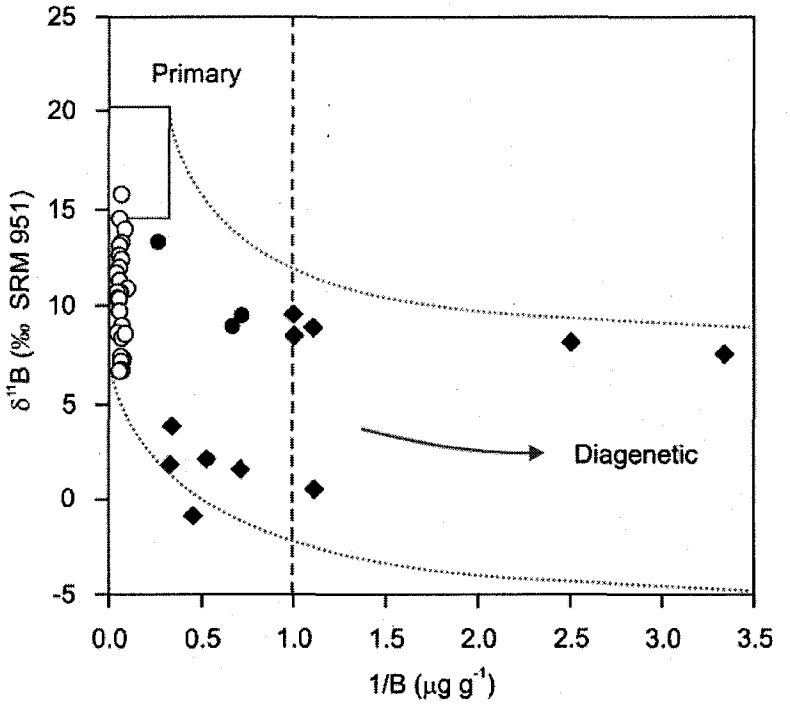

Fig. 4.5. The boron isotope composition ($\delta^{11}B$) of modern and fossil skeletal carbonates as a function of boron concentration (1/B in μg g^{-1}); the open rectangle indicates a range of $\delta^{11}B$ and 1/B values typical of modern biogenic carbonates (Vengosh et al., 1991; Hemming and Hanson, 1992; Lécuyer et al., 2002), open circles represent data from well-preserved Paleozoic brachiopods (Joachimski et al., 2005). Our data from the MLJ skeletal carbonates are represented by black circles (brachiopods) and black diamonds (belemnites). The vertical dashed line at ~ 1 μg g^{-1} of boron shows a theoretical threshold between well-preserved and diagenetically altered signals, which is based on a lower limit of boron content in certain modern skeletal carbonates, such as gastropods that contain only 1 to 3 μg g^{-1} of boron (Vengosh et al., 1991). The arrow and dotted lines show a general trend of progressive diagenetic alteration.

To further explore this possibility we analyzed boron contents and $\delta^{11}B$ values of the Kimmeridgian brachiopods and belemnites collected from the same stratigraphic horizons at two localities in Germany, the Early Kimmeridgian at Geisingen and the Late Kimmeridgian at Ursental (Table 4.2, samples EK1 to EK4, and LK1,2). These samples therefore experienced identical post-depositional histories and their $\delta^{11}B$ values yielded near-identical isotope compositions (Fig. 4.6b), which are however significantly different from the $\delta^{11}B$ signatures of well-preserved coeval brachiopods (Lécuyer et al., 2002) (Fig. 4.6a). This

comparison therefore provides convincing evidence that the boron isotope systematics of the studied MLJ belemnites has been compromised by diagenesis and that the measured $\delta^{11}B$ record represent secondary signal.

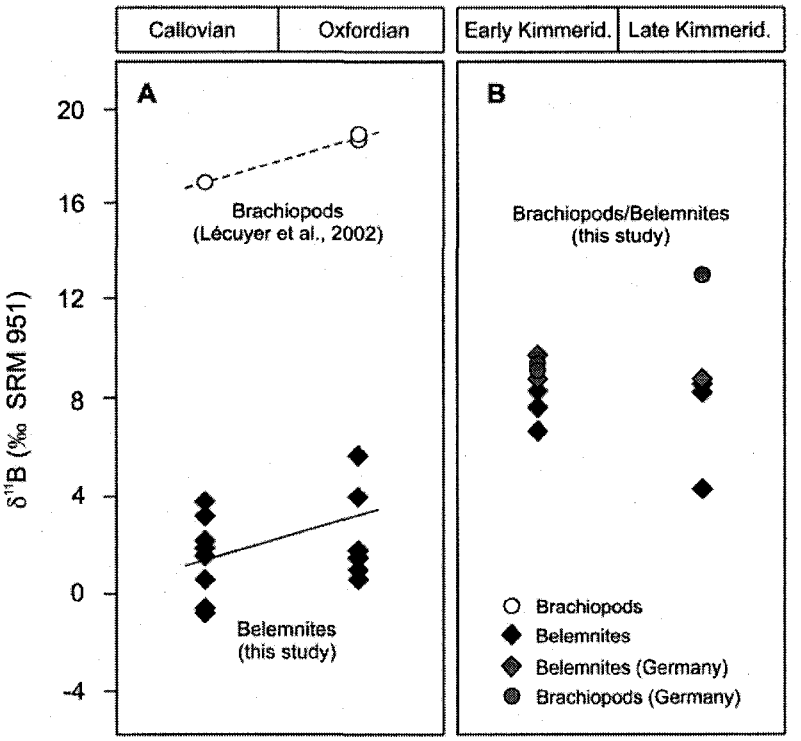

Fig. 4.6. (A) The boron isotope composition of the Callovian and Oxfordian marine skeletal carbonates. Open circles are brachiopod data from Lécuyer et al. (2002) and black diamonds the $\delta^{11}B$ values from our belemnite samples. (B) The comparison of the $\delta^{11}B$ values of the Kimmeridgian belemnites (gray diamonds) and brachiopods (gray circles) collected from the same stratigraphic horizons in Germany (Geisingen and Ursental) (for details see Table 4.2, samples EK 1 to 4 and LK1 and LK2).

4.6 Conclusions

The primary objective of this study was to constrain pH variations of the Jurassic surface oceans using the boron isotope composition of belemnite calcite as a proxy. Knowledge of seawater pH is important for realistic interpretation of oxygen isotope data in terms of paleo-temperatures. The $\delta^{18}O$ values of the Jurassic (Callovian and Oxfordian)

belemnites were originally interpreted as a reflection of cool SSTs (Podlaha et al., 1998; Veizer et al., 2000). Some authors (Royer et al., 2004; Wallmann, 2004), however, argued that the ^{18}O enrichment is rather a result of lower pH of the contemporary seawater due apparently to elevated levels of atmospheric CO_2 (Berner and Kothavala, 2001), a hypothesis potentially testable by boron isotopes due to their sensitivity to pH.

The $\delta^{11}B$ record of the MLJ belemnites shows a quasi-systematic variation with an overall magnitude of about 10‰. We first present a tentative explanation for the experimental $\delta^{11}B$ record that is based on a relative variability in seawater pH of about 1 ± 0.2 units, assuming a hypothetical value for the boron isotope composition of Jurassic seawater ($\delta^{11}B_{SW}$) of 22 ± 2‰. However, considering the boron isotope data of Lécuyer et al. (2002) and the geochemical modeling of Joachmiski et al. (2005) and Sime et al. (2006) this interpretation seems unlikely, because the above studies suggest that the $\delta^{11}B_{SW}$ value during the Jurassic should have been considerably heavier, at least 30‰.

Yet, any combination of our boron isotope data with $\delta^{11}B_{SW}$ in excess of ~30‰ yields unreasonable pH estimates of paleo-seawater, which indirectly indicates that the boron isotope systematics of the MLJ belemnites has most likely been compromised by diagenesis. This possibility was confirmed by comparing the boron isotope data of coeval belemnites and brachiopods that show near-identical $\delta^{11}B$ signatures, which are however significantly lighter than the published $\delta^{11}B$ data from well-preserved coeval brachiopods (Lécuyer et al., 2002) and/or modern skeletal carbonates. Consequently, we are unable to utilize the measured $\delta^{11}B$ dataset to assess the effect seawater pH on the $\delta^{18}O$ record of the MLJ belemnites and to evaluate whether the ^{18}O enrichment of belemnite calcite is due to cooler SSTs or rather lower pH of surface oceans.

Nevertheless, the present study show that boron isotope geochemistry of skeletal carbonates is much more prone to diagenetic alteration than are the isotope systems of O, C, S, Sr and Ca. Therefore care should be exercised in the use of boron isotopes in fossil skeletal carbonates for reconstructions of paleo-seawater pH and boron concentrations should also be reported to buttress the pristine character of isotope signatures.

Acknowledgements

This study was funded by the Natural Sciences and Engineering Research Council of Canada (NSERC) grants to JV. Assistance with the mass spectrometry and laboratory work of L.A. Spencer, B. Cousens and S. Carr from the Ottawa-Carleton Geoscience Centre (OCGC) and the Isotope Geochemistry and Geochronology Research Centre (IGGRC) is greatly acknowledged.

References

Alley N.F. and Frakes L.A. (2003) First known Cretaceous glaciation: Livingston Tillite Member of the Cadna-owie Formation, South Australia. *Aust. J. Earth Sci.* **50** 139–144.

Arthur M.A. and Anderson T.F., Stable isotopes of oxygen and carbon and their applications to sedimentological and paleoenvironmetal problems, in Arthur M.A., Anderson T.F., Kaplan I.R., Veizer J. and Land L.S. (Eds.), Stable isotopes in sedimentary geochemistry: Society of Economic Paleontologists and Mineralogists Short Course, Vol. 10, 1983, pp. 1–151.

Berner R.A. and Kothavala Z. (2001) GEOCARB III: A revised model of atmospheric CO_2 over Phanerozoic time. *Am. J. Sci.* **301** 182–204.

Brand U., Logan A., Hiller N. and Richardson J. (2003) Geochemistry of modern brachiopods: applications and implications for oceanography and paleoceanography. *Chem. Geol.* **198** 305–334.

Crowley T.J., Significance of tectonic boundary conditions for paleoclimate simulations, in: T.J. Crowley, K. Burke (Eds.), Tectonic Boundary Conditions for Climate Reconstructions, New York, Oxford University Press, 1998.

Dromart G., Garcia J.-P., Picard S., Atrops F., Lécuyer C. and Sheppard S.M.F. (2003) Ice age at the Middle-Late Jurassic transition? *Earth Planet. Sci. Lett.* **213** 205–220.

Farkaš J., Buhl D., Blenkinsop J. and Veizer J. (2007) Evolution of the oceanic calcium cycle during the late Mesozoic: Evidence from $\delta^{44/40}Ca$ of marine skeletal carbonates. *Earth Planet. Sci. Lett.* **253** 96–111.

Foster G.L., Yunyan N., Haley B. and Elliott T. (2006) Accurate and precise isotopic measurement of sub-nanogram sized samples of foraminifera hosted boron by total evaporation NTIMS. *Chem. Geol.* **230** 161–174.

Frakes L.A. and Francis J.E. (1988) A guide to Phanerozoic cold polar climates from high latitude ice-rafting in the Cretaceous. *Nature* **333** 547–549.

Frakes L.A., Francis J.E. and Syktus J.I., Climate Modes of the Phanerozoic: the history of the earth's climate over past 600 million years. Cambridge Univ. Press, Cambridge, 1992, pp. 271.

Gaillardet J. and Allègre C.J. (1995) Boron isotopic composition of corals: Seawater or diagenesis record? *Earth Planet. Sci. Lett.* **136** 665–676.

Gradstein F. M., Agterberg F. P., Ogg J.G., Hardenbol J., van Veen P., Thierry T. and Huang Z. (1994) A Mesozoic time scale. *J. Geophys. Res.* **99** 24051–24074.

Gradstein F.M., Ogg J.G., Smith A.G., Agterberg F.P., Bleeker W., Cooper R.A., Davydov V., Gibbard P., Hinnov L., House M.R., Lourens L., Luterbacher H.-P., McArthur J., Melchin M.J., Robb L.J., Shergold J., Villeneuve M., Wardlaw B.R., Ali J., Brinkhuis H., Hilgen F.J., Hooker J., Howarth R.J., Knoll A.H., Laskar J., Monechi S., Powell J., Plumb K.A., Raffi I., Röhl U., Sanfilippo A., Schmitz B., Shackleton N.J., Shields G.A., Strauss H., Van Dam J., Veizer J., van Kolfschoten Th. and Wilson D., A Geologic time scale, Cambridge Univ. Press, Cambridge, 2004.

Harland W.B., Armstrong R.L., Cox A.V., Craig L.E., Smith A.G. and Smith D.G., A Geologic Time Scale, Cambridge Univ. Press, Cambridge, 1990.

Hemming N.G. and Hanson G.N. (1992) Boron isotopic composition and concentration in modern marine carbonates. *Geochim. Cosmochim. Acta* **56** 537–543.

Hemming N.G. and Hanson G.N. (1994) A procedure for the isotopic analysis of boron by negative thermal ionization mass spectrometry. *Chem. Geol.* **114** 147–156.

Hönish B., Hemming N.G., Grottoli A.G., Amat A., Hanson G.N. and Bijma J. (2004) Assessing scleractinian corals as recorders for paleo-pH: Empirical calibration and vital effects. *Geochim. Cosmochim. Acta* **68** 3675–3685.

Hönisch B. and Hemming N.G. (2005) Surface ocean pH response to variations in pCO_2 through two full glacial cycles. *Earth Planet. Sci. Lett.* **236** 305–314.

Ishikawa T. and Nakamura E. (1990) Suppression of Boron Volatilization from a Hydrofluoric Acid Solution Using a Boron-Mannitol Complex. *Anal. Chem.* **62** 2612–2616.

Joachimski M.M., Simon L., van Geldern R. and Lécuyer Ch. (2005) Boron isotope geochemistry of Paleozoic brachiopod calcite: Implications for a secular change in the

boron isotope geochemistry of seawater over Phanerozoic. *Geochim. Cosmochim. Acta* **69** 4035–4044.

Jones Ch.-E. and Jenkyns H.C. (2001) Seawater strontium isotopes, oceanic anoxic events, and seafloor hydrothermal activity in the Jurassic and Cretaceous. *Am. J. Sci.* **301** 112–149.

Kampschulte A., Sulfur Isotope Investigations of Structurally Substituted Sulfate of Phanerozoic Carbonates: Implications for Chemical Evolution of Seawater, Doctoral dissertation (in German), Ruhr University Bochum, 2001.

Kampschulte A. and Strauss H. (2004) The sulfur isotopic evolution of Phanerozoic seawater based on the analysis of structurally substituted sulfate in carbonates. *Chem. Geol.* **204** 255–286.

Kasemann S.A., Hawkesworth Ch.J., Pravec A.R., Fallick A.E. and Pearson P.N. (2005) Boron and calcium isotope composition in Neoproterozoic carbonate rocks from Namibia: evidence for extreme environmental change. *Earth Planet. Sci. Lett.* **231** 73–86.

Kemper E. (1987) Das Klima der Kreide-Zeit. *Geologische Jahrbuch*, A96, 5–185.

Klötzli U.S. (1992) Negative thermal ionization mass spectrometry: a new approach to boron isotope geochemistry. *Chem. Geol.* **101** 111–122.

Lécuyer Ch., Grandjean P., Reynard B., Albarède F. and Telouk P. (2002) $^{11}B/^{10}B$ analysis of geological materials by ICP-MS Plasma 54: Application to the boron fractionation between brachiopod calcite and seawater. *Chem. Geol.* **186** 45–55.

Lemarchand D., Gaillardet J., Lewin É. and Allègre C.J. (2000) The influence of rivers on marine boron isotopes and implications for reconstructing past ocean pH. *Nature* **408** 951–436.

Pagani M., Lemarchand D., Spivack A. and Gaillardet J. (2005) A critical evaluation of the boron isotope-pH proxy: The accuracy of ancient ocean pH estimates. *Geochim. Cosmochim. Acta* **69** 953–961.

Palmer M.R. and Pearson P.N. (2003) A 23,000-Year Record of Surface Water pH and pCO_2 in the Western Equatorial Pacific Ocean. *Science* **300** 480–482.

Pearson P.N. and Palmer M.R. (2000) Atmospheric carbon dioxide concentrations over the past 60 million years. *Nature* **406** 695–699.

Pelejero C., Calvo E., McCulloch M.T., Marshall J.F., Gagan M.K., Lough J.M. and Opdyke B.N. (2005) Preindustrial to Modern Interdecadal Variability in Coral Reef pH. *Science* **309** 2204–2207.

Podlaha O.G., Model calculations on the basis of high-resolution isotope stratigraphy (Sr,C,O) of the Jurassic and Lower Cretaceous (Bajoc-Apt.) period. Doctoral dissertation (in German), Ruhr University Bochum, 1995.

Podlaha O.G., Mutterlose J. and Veizer J. (1998) Preservation of $\delta^{18}O$ and $\delta^{13}C$ in belemnite rostra from the Jurassic/early Cretaceous successions. *Am. J. Sci.* **298** 324–347.

Price G.D. (1999) The evidence and implications of polar-ice during the Mesozoic. *Earth-Science Reviews*, **48** 183–210.

Price G.D. and Mutterlose J. (2004) Isotopic signals from late Jurassic–early Cretaceous (Volgian–Valanginian) sub-Arctic belemnites, Yatria River, Western Siberia. *J. Geol. Soc.* **161** 959–968.

Royer D.L., Berner R.A., Montañez I.P., Tabor N.J. and Beerling D.J. (2004) CO_2 as a primary driver of Phanerozoic climate, *GSA Today* **14** 4–10.

Sanyal A., Hemming N.G., Hanson G.N. and Broecker W.S. (1995) Evidence for a higher pH in the glacial ocean from boron isotopes in foraminifera. *Nature* **373** 234–236.

Sanyal A., Hemming N.G., Broecker W.S., Lea D.W., Spero H.J. and Hanson G.N. (1996) Oceanic pH control on the boron isotopic composition of foraminifera: Evidence from cultured experiments. *Paleoceanography* **11** 513–414.

Simon L., Lécuyer Ch., Maréchal Ch. and Coltice N. (2006) Modelling the geochemical cycle of boron: Implications for the long-term $\delta^{11}B$ evolution of seawater and oceanic crust. *Chem. Geol.* **225** 61–76.

Spero H.J., Bijma J., Lea D.W. and Bemis B.E. (1997) Effect of seawater carbonate concentration on foraminiferal carbon and oxygen isotopes. *Nature* **390** 497–500.

Spivack A.J., You Ch.F. and Smith H.J. (1993) Foraminiferal boron isotope ratios as a proxy for surface ocean pH over the past 21 Myr. *Nature* **363** 149–151.

Tomašových A. (2004) Postmortem durability and population dynamics affecting the fidelity of brachiopod size-frequency distribution. *Palaios* **19** 477–496.

Veizer J. (1974) Chemical diagenesis of belemnites shells and possible consequences for paleotemperature determination, *N. Jb. Geol. Pal.*, A64, **147** 91–111.

Veizer J., Chemical diagenesis of carbonates: theory and application of trace element technique, in: M.A. Arthur, T.F. Anderson, I.R. Kaplan, J. Veizer, L. Land (Eds.), Stable Isotopes in Sedimentary Geology: Society of Economic Paleontologists and Mineralogists, Short Course, vol. 10, 1983, pp. III/1–III/100.

Veizer J., Ala D., Azmy K., Bruckschen P., Buhl D., Bruhn F., Carden G.A.F., Diener A., Ebneth S., Godderis Y., Jasper T., Korte Ch., Pawellek F., Podlaha O. and Strauss H.

(1999) $^{87}Sr/^{86}Sr$, $\delta^{13}C$ and $\delta^{18}O$ evolution of Phanerozoic seawater. *Chem. Geol.* **161** 59–88.

Veizer J., Godderis Y. and François L.M. (2000) Evidence for decoupling of atmospheric CO_2 and global climate during the Phanerozoic eon. *Nature* **408** 698–701.

Vengosh A., Kolodny Y., Starinsky A., Chivas A.R. and McCulloch M.T. (1991) Coprecipitation and isotopic fractionation of boron in modern biogenic carbonates. *Geochim. Cosmochim. Acta* **55** 2901–2910.

Wallmann K. (2004) Impact of atmospheric CO_2 and galactic cosmic radiation on Phanerozoic climate change and the marine $\delta^{18}O$ record. *Geochem. Geophys. Geosyst.* **5**, Q06004 doi:10.1029/2003GC000683.

Zeebe R.E. (1999) An explanation of the effect of seawater carbonate concentration on foraminiferal oxygen isotopes. *Geochim. Cosmochim. Acta* **63** 2001–2007.

Zeebe R.E. (2001) Seawater pH and isotopic paleotemperatures of Cretaceous oceans. *Palaeogeo. Palaeoclim. Palaeoeco.* **170** 49–57.

Zeebe R.E. and Wolf-Gladrow D.A., CO_2 in seawater: Equilibrium, kinetics, isotopes, Elsevier Oceanography Series, 65, Elsevier, Amsterdam, 2001, pp. 346.

5 Appendix: Laboratory procedures and additional data

A.5.1 Methodology for Ca isotope analysis

A.5.1.1 Sample dissolution and ion exchange chemistry

Cleaned carbonate powders were dissolved in adjusted volume of 2 N HCl so the concentration of Ca in the solution was 0.4 μg per μL. For the Ca isotope analysis 25 μL (10 μg of Ca) were pipetted into PFA vial and mixed with 65 μL of the Ca double spike solution. The mixtures were dried down and redissolved in 10 μL of 2.5 N HCl. These solution were loaded onto PFA micro-columns filled with 250 μL of cation exchange resin BioRad AG50W-X12 (Fig. A.5.1). Additional 1600 μL of 2.5 N HCl was used to rinse the sample into the resin. Following the elution of 1600 μL (Mg, Na, and K), the Ca fraction was collected with additional 1500 μL of 2.5 N HCl into the new PFA vial. After the elution of the Ca fraction, the resin was cleaned with 5000 μL of 6N HCl and pre-conditioned with additional 1500 μL of 2.5N HCl.

The ion exchange chemistry for the separation of Ca from the sample matrix was used only for the seawater and belemnite samples. Later, however, it was realized that effect of carbonate matrix has no significant influence on the measured Ca isotope composition in skeletal carbonates and therefore the ion exchange chemistry was not applied to brachiopod samples that were analyzed during the later stages of the project.

The influence of carbonate matrix was tested by comparing the Ca isotope composition of two aliquots of the same carbonate sample (modern and fossil brachiopod). The first aliquot was prepared by direct dissolution of the sample in 2.5 N HCl and therefore contained the Ca fraction and the carbonate matrix. The second aliquot was passed through the cation exchange column and should represent only the Ca fraction devoid of other cations. The repeat measurements of the Ca isotope composition of the two aliquots were identical within the analytical error suggesting negligible effect of carbonate matrix on the measured Ca isotope composition.

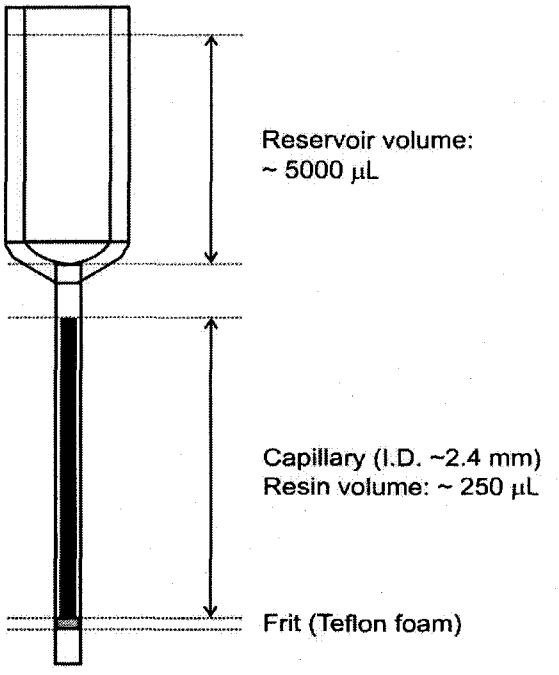

Fig. A.5.1. Schematic view of a PFE Teflon micro-column filled with cation exchange resin BioRad AG50W-X12 that was used for a quantitative separation of Ca from other cations, such as Mg, K and Sr.

A.5.1.2 Calibration of ion exchange columns

The PFA micro-columns were calibrated by collecting discrete volumes of a calibration solution into polyethylene tubes. The calibration solution was a mixture of Ca, Sr, Mg and K, dissolved in 2.5 N HCl, with cation concentrations resembling those in natural carbonates. Approximately 3000 µL of 2.5 N HCl were passed through the column and collected in 75 discrete steps of 40 µL each. The concentrations of Ca, Sr, Mg and K of individual elution steps were analyzed by conventional ICP-OES technique and the elemental elution curves are plotted in Fig. A.5.2.

A.5.1.3 Total procedural Ca blank

The Ca blank was determined by conventional isotope dilution technique applying the ^{48}Ca single spike solution as a tracer. The total procedural Ca blank was consistently below 15 ng, representing a cumulative contribution of Ca from multiple sources such as H_2O, H_2O_2, HCl, ion exchange resin, and loading procedure (Re filament and HNO_3). The

amount of Ca supplied from the sample was on average 10 μg and therefore the contribution of Ca from the blank was negligible (< 0.15%).

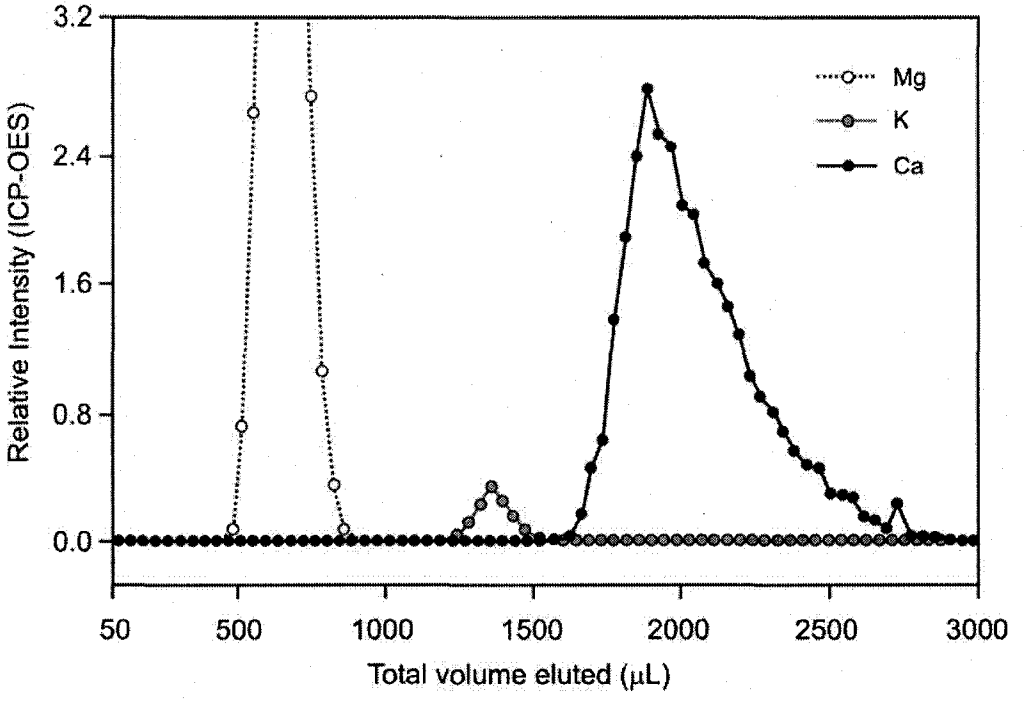

Fig. A.5.2. Typical elemental elution curve for a PFA Teflon micro-column, showing that the Ca fraction is efficiently separated from Mg and K. The Sr fraction is not displayed as the first signal of Sr commonly starts at a volume of about 3000 μL. The intensities of the elements in cuts were determined by conventional ICP-OES. The following wavelengths (nm) were used: Mg (280.270), K (766.491), Ca (396.847), and Sr (407.771).

A.5.1.4 Double spike technique

A precise measurement of the Ca isotopes abundances in natural samples is possible due to a double spike technique, which allows for the correction of isotope fractionation introduced during the process of chemical preparation and isotope analysis. The Ca isotope double spike used in this study was prepared from two individual single spike solutions made from isotopically enriched carbonates Ca43-NX and Ca48-RT from Oak Ridge National Laboratory. The Ca43-NX and Ca48-RT carbonates were precisely weighed (±0.003 mg, 2σ) and dissolved in adjusted volume of 3.5% HNO_3 so the concentration of Ca

in the single spike solution would be close to 5 μg per 1000 μL. The Ca isotope compositions of the ^{43}Ca and ^{48}Ca single spike solutions were determined by TIMS and showed only minor (<0.5%) deviations from the certified values (Table A.5.3). The isotope abundances (%) of ^{40}Ca, ^{42}Ca, ^{43}Ca, ^{44}Ca and ^{48}Ca, as presented in Table A.5.3, were determined by total evaporation technique using a cumulative counting of intensities of individual Ca isotope ion beams.

Table A.5.3.

Measured and certified isotope compositions and abundances (atom. %) of the ^{43}Ca and ^{48}Ca single spike solutions. The ratios represent a mean value of 6 repetitive analyses.

	^{43}Ca Spike (Ca43-NX)		**^{48}Ca Spike (Ca48-RT)**	
	Measured	Certified	Measured	Certified
Isotope Ratios	Mean value, (2σ)	Mean	Mean value, (2σ)	Mean
$^{40}Ca/^{43}Ca$	0.12736 ± 0.00157	0.12070	NA	NA
$^{42}Ca/^{43}Ca$	0.00959 ± 0.00157	0.00929	NA	NA
$^{44}Ca/^{43}Ca$	0.06058 ± 0.00194	0.06029	NA	NA
$^{48}Ca/^{43}Ca$	0.00108 ± 0.00001	0.00107	NA	NA
$^{40}Ca/^{44}Ca$	2.10286 ± 0.08117	2.00198	NA	NA
$^{42}Ca/^{44}Ca$	0.15831 ± 0.00519	0.15415	NA	NA
$^{40}Ca/^{48}Ca$	NA	NA	0.02299 ± 0.00034	0.02147
$^{42}Ca/^{48}Ca$	NA	NA	0.00025 ± 0.00001	0.00025
$^{43}Ca/^{48}Ca$	NA	NA	0.00005 ± 0.00001	0.00010
$^{44}Ca/^{48}Ca$	NA	NA	0.00076 ± 0.00001	0.00074
$^{40}Ca/^{44}Ca$	NA	NA	30.3022 ± 0.18020	29.1667
$^{42}Ca/^{44}Ca$	NA	NA	0.33190 ± 0.00280	0.33333

	^{43}Ca Spike (Ca43-NX)		**^{48}Ca Spike (Ca48-RT)**	
	Measured	Certified	Measured	Certified
Isotope Abundance	Atom. %, (2σ)	Atom. %	Atom. %, (2σ)	Atom. %)
^{40}Ca	10.616 ± 0.120	10.130	2.239 ± 0.049	2.100
^{42}Ca	0.800 ± 0.002	0.780	0.025 ± 0.001	0.024
^{43}Ca	83.468 ± 0.002	83.930	0.005 ± 0.001	0.010
^{44}Ca	5.023 ± 0.017	5.060	0.074 ± 0.001	0.072
^{46}Ca	(0.001) [a]	0.001	(0.010) [a]	0.010
^{48}Ca	0.091 ± 0.001	0.090	97.647 ± 0.050	97.800
Total	99.999	99.991	100.000	100.016

[a] The abundances of ^{46}Ca could not be measured precisely due to its extremely low natural occurrence and these were therefore assumed to be 0.001% (for ^{43}Ca-spike) and 0.010% (for ^{48}Ca-spike), as stated on their certificates.

The ^{43}Ca and ^{48}Ca single spike solutions were weighed and mixed in such a way that the $^{43}Ca/^{48}Ca$ ratio in the double spike solution would be close to that of terrestrial materials between 0.7215 and 0.7310 (Russell et al., 1978). The Ca isotope compositions of the double spike solution was determined by TIMS and yielded the $^{43}Ca/^{48}Ca$ ratio of 0.7221 ± 0.0004, 2σ, n = 8. The measured Ca isotope abundances of the double spike are presented in Table A.5.4.

Table A.5.4.

The Ca isotope composition of the ^{43}Ca-^{48}Ca double spike solution as determined by repetitive measurement (n = 9) performed on the same solution. The $^{43}Ca/^{48}Ca$ ratio of double spike is compared to natural $^{43}Ca/^{48}Ca$, which is representative of bulk terrestrial Ca.

	^{43}Ca-^{43}Ca double spike	**Bulk terrestrial Ca**
Isotope Ratios	Mean value, (2σ)	Mean value, (2σ)
$^{40}Ca/^{48}Ca$	0.11710 ± 0.00252	
$^{42}Ca/^{48}Ca$	0.00719 ± 0.00003	
$^{43}Ca/^{48}Ca$	0.72206 ± 0.00011	0.72215± 0.00050 [a]
$^{44}Ca/^{48}Ca$	0.04432 ± 0.00001	
$^{40}Ca/^{44}Ca$	2.65332 ± 0.01033	
$^{42}Ca/^{44}Ca$	0.16221 ± 0.00029	

[a] Data from Russell et al. (1978)

In order to minimize a possible contamination from pipette tips the $^{43}Ca/^{48}Ca$ double spike was kept in a sealed PFA bottle equipped with a special tube that allowed a drop-wise addition of the double spike to a sample. Approximately 65 μL (8 drops) of $^{43}Ca/^{48}Ca$ double spike was added to 25 μL of sample solution (0.4 μg of Ca per μL). As a result the $^{40}Ca/^{48}Ca$ ratio (sample to spike ratio) of the mixture was close to 50. The double spike was added to a sample prior to cation exchange chemistry so potential isotope fractionation caused by incomplete recovery of Ca from the columns can be corrected.

A set of experiments was performed in order to test effect of variable sample to spike ratio on the measured Ca isotope composition. The standard solution of SRM915a was spiked with three different amounts of double spike yielding $^{40}Ca/^{48}Ca$ ratios of 30, 50 and 100. The measured $^{44}Ca/^{40}Ca$ are plotted as a function of $^{40}Ca/^{48}Ca$ in Fig. A.5.3. Results

suggest that overspiked sample with $^{40}Ca/^{48}Ca$ ratio of about 30 showed a tendency towards isotopically heavier values, while an underspiked sample with $^{40}Ca/^{48}Ca$ ratio close to 100 yielded isotopically lighter values. As a consequence all samples analyzed in this study were carefully double spiked so their $^{40}Ca/^{48}Ca$ ratios were close to 50 or 60 ('normal' in Fig. A.5.3), thus minimizing the effect of variable sample to spike ratio on the measured $^{44}Ca/^{40}Ca$.

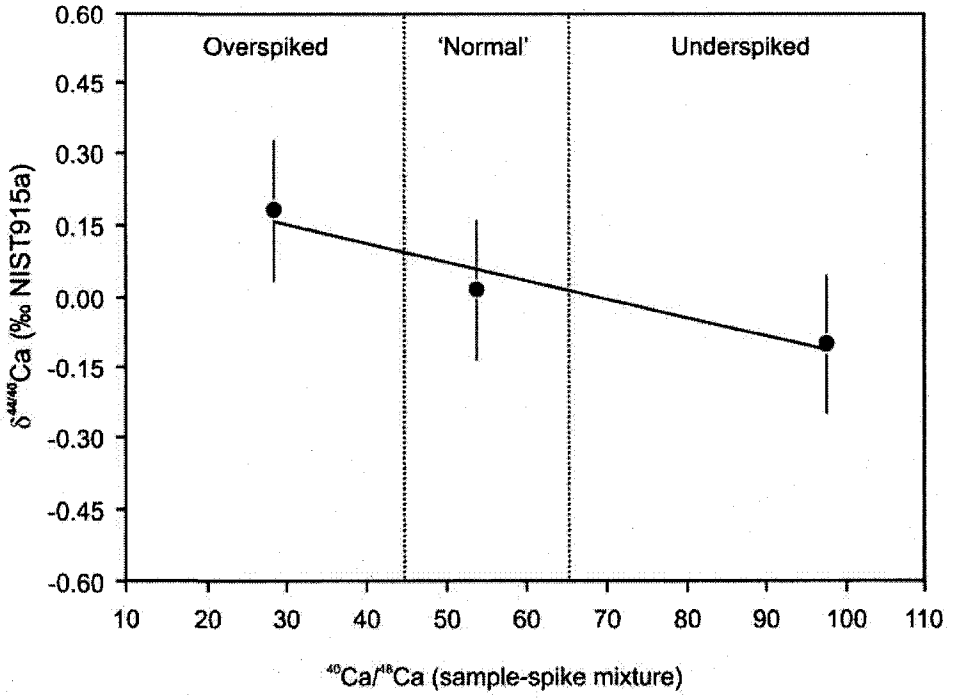

Fig. A.5.3. The $\delta^{44/40}Ca$ of spiked samples as a function of variable sample to spike ratio, the latter represented by $^{40}Ca/^{48}Ca$ ratio in a sample-spike mixture. Dotted lines define an area of the optimal, i.e. 'normal', double spiking that was used for the isotope analysis of natural samples. Each point (solid circle) represents a mean value of two measurements from the same solution and vertical bars indicate 2σ external reproducibility of ± 0.15‰. The solid line represents the liner regression fitted to the data.

A.5.1.5 Iterative double spike correction algorithm

The original $^{44}Ca/^{40}Ca$ ratio of a sample was calculated from the measured $^{40}Ca/^{48}Ca$, $^{43}Ca/^{48}Ca$ and $^{44}Ca/^{48}Ca$ ratios in a sample-spike mixture applying an iterative routine based

on algorithm with an exponential fractionation term adopted from Heuser et al. (2002). The iterative algorithm function 'CaCalcRussell' used for the correction of the added $^{43}Ca/^{48}Ca$ double spike and calculation of the original sample $^{44}Ca/^{40}Ca$ ratio (PureSample_4440_recalc) was programmed in Visual Basic for MS Excel (see below):

```
Function CaCalcRussell
(Mix_4348 As Double, Mix_4448 As Double, Mix_4048 As Double)

'Dimensioning of variables
Dim MixCalc_4348 As Double
Dim MixCalc_4448 As Double
Dim MixCalc_4048 As Double
Dim MixCalc_4440 As Double
Dim Spike_4348 As Double
Dim Spike_4448 As Double
Dim Spike_4048 As Double
Dim Spike_4440 As Double
Dim PureSample_4348 As Double
Dim PureSample_4448 As Double
Dim PureSample_4048 As Double
Dim PureSample_4440 As Double
Dim PureSample_4348_recalc As Double
Dim PureSample_4448_recalc As Double
Dim PureSample_4048_recalc As Double
Dim PureSample_4440_recalc As Double
Dim beta As Double
Dim fu As Double
Dim Q40 As Double
Dim Qmean As Double
Dim DeltaQ As Double
Dim Q4840 As Double
Dim Q4844 As Double
Dim Krit As Double

'Criteria for ending of Iteration
Krit = 0.000000001
Dim Counter As Single

'Russell-Values
PureSample_4448 = 11.27268628
```

```
PureSample_4348 = 0.731146432
PureSample_4048 = 531.5409762
PureSample_4440 = 0.021207558

'Spike-Values for normalization

Spike_4348 = 0.72205607
Spike_4448 = 0.04431731
Spike_4048 = 0.11710032
Spike_4440 = 0.37693225

'Loop counter for break Iteration
Counter = 0

'Iteration
Do
Q4844 = (Mix_4448 - Spike_4448) / (PureSample_4448 - Mix_4448)
Q4840 = (Mix_4048 - Spike_4048) / (PureSample_4048 - Mix_4048)
Qmean = (Q4844 + Q4840) / 2
DeltaQ = Q4844 - Q4840
MixCalc_4348 = (Spike_4348 + Qmean * PureSample_4348) / (1 + Qmean)
beta = Log(MixCalc_4348 / Mix_4348) / Log(43 / 48)
MixCalc_4048 = Mix_4048 * (40 / 48) ^ beta
MixCalc_4448 = Mix_4448 * (44 / 48) ^ beta
MixCalc_4440 = MixCalc_4448 / MixCalc_4048
Q40 = Qmean * PureSample_4048 / Spike_4048
PureSample_4440_recalc = (1 + 1 / Q40) * MixCalc_4440 - (1 / Q40) *
Spike_4440
fu = Log(PureSample_4440_recalc / PureSample_4440) / Log(44 / 40)
PureSample_4448_recalc = PureSample_4448 * (44 / 48) ^ fu
PureSample_4348_recalc = PureSample_4348 * (43 / 48) ^ fu
PureSample_4048_recalc = PureSample_4048 * (40 / 48) ^ fu
Mix_4448 = MixCalc_4448
Mix_4348 = MixCalc_4348
Mix_4048 = MixCalc_4048
PureSample_4448 = PureSample_4448_recalc
PureSample_4348 = PureSample_4348_recalc
PureSample_4048 = PureSample_4048_recalc
PureSample_4440 = PureSample_4440_recalc
Counter = Counter + 1

'Ende Iteration bei Erfuellung eines der Kriterien
```

```
Loop Until Abs(DeltaQ) < Krit Or Counter = 50

If Counter = 10 Then MsgBox "game over"

CaCalcRussell = PureSample_4440_recalc

End Function
```

The above function '`CaCalcRussell`' is adopted from Heuser et al. (2002), however, the isotope composition of the $^{43}Ca/^{48}Ca$ double spike defined as '`Spike-Values for normalization`' was updated to reflect the composition of our double spike solution (cf. Table A.5.4).

The calculated $^{44}Ca/^{40}Ca$ ratio in the original sample '`PureSample_4440_recalc`' was converted to delta notation ($\delta^{44/40}Ca$) in a permil (‰) relative to the NIST SRM 915a $CaCO_3$ standard using the following relation:

$$\delta^{44/40}Ca_{NIST} = \left(\frac{^{44}Ca/^{40}Ca_{SAMPLE}}{^{44}Ca/^{40}Ca_{NIST}} - 1 \right) \cdot 1000$$

where the $^{44}Ca/^{40}Ca_{NIST}$ ratio is equal to 0.021538 ± 0.000003 (2σ) as determined by a repeat analysis of the NIST SRM 915a $CaCO_3$ standard (see section A.5.1.8; Table A.5.7).

A.5.1.6 Mass spectrometry TIMS

The calcium isotope composition of standards (SRM 915a and IAPSO seawater) and skeletal carbonates was determined on a multi-collector thermal ionization mass spectrometer (TIMS) Thermo Electron Triton at Carleton University in the Isotope Geochemistry and Geochronology Research Centre (IGGRC).

For the TIMS measurements, the evaporated samples containing about 10 μg of Ca were redissolved in 10 μL of 5% HNO_3. From this solution 3 μL (~3 μg of Ca) were loaded as calcium nitrate solution directly onto a double filament assembly, with an outgassed

zone-refined Re as the filament material. The solution was slowly, over 10 minutes, dried at a filament current of 0.5 A, then heated at 1.5 A for 1 minute and finally taken to dull red at about 2.2 A for half a minute (Tuttas and Schwieters, 2002). The reaction of the $Ca(NO_3)_2$ with Re and O_2 must lead to precipitation of high-mass Ca compounds on the filament as the in-run mass fractionation (the instrumental fractionation) for the $^{44}Ca/^{40}Ca$ ratio was minimal, typically bellow ± 0.03‰ (2σ), but the external reproducibility was high up to ±0.5‰ (2σ). The external reproducibility of the $^{44}Ca/^{40}Ca$ ratio was, however, significantly improved to less than ± 0.15‰ after the application of the $^{43}Ca/^{48}Ca$ double spike and the iterative double spike correction algorithm.

Calcium isotope measurements were performed on a multi-collector TIMS Thermo Electron Triton. The instrument was operated in a positive ionization mode with the acceleration voltage of 10 000 V and 10^{11} Ω resistor for the Faraday cups. The setup of nine moveable Faradays cups for the Ca isotope analysis is displayed in Fig. A.5.4 and Table A.5.5. The complete Ca isotope mass range from ^{40}Ca to ^{48}Ca was measured in two sequences. The first sequence collected peaks from ^{40}Ca to ^{44}Ca with ^{42}Ca on the central cup and also monitored ^{41}K for a possible isobaric interference of ^{40}K on ^{40}Ca ($^{40}K/^{41}K = 1.7384 \times 10^{-3}$). The second sequence registered isotope peaks from ^{44}Ca to ^{48}Ca with ^{46}Ca on the central cup.

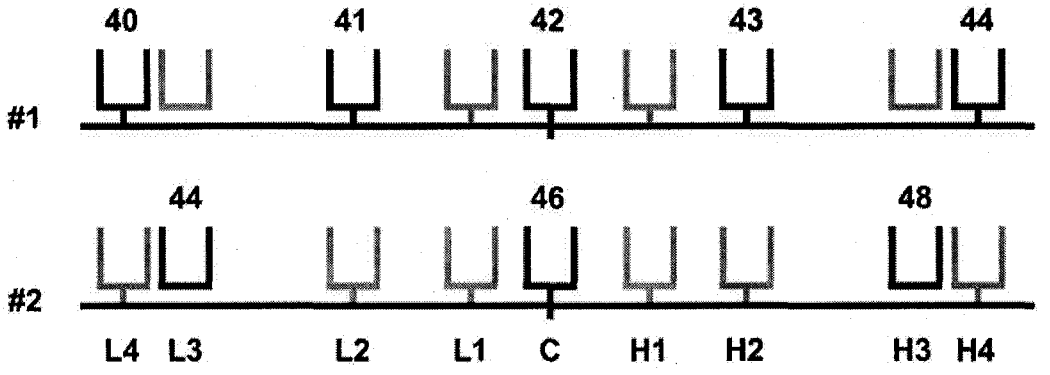

Fig. A.5.4. The configuration of Faraday cups used for the Ca isotope analysis on Thermo Electron Triton mass spectrometer. In the first sequence (#1) masses 40 to 44 are collected, including ^{40}Ca, ^{41}K, ^{42}Ca, ^{43}Ca, and ^{44}Ca. In the second sequence (#2) isotope peaks of ^{44}Ca, ^{46}Ca and ^{48}Ca are registered.

Table A.5.5.

The position of the cups for the Ca isotope analysis

Cup	Target position (in mm)	Isotope peak (mass)	
	Distance from the central (C) cup	First sequence	Second sequence
H4	+69.01	^{44}Ca	-
H3	+59.19	-	^{48}Ca
H2	+32.57	^{43}Ca	-
H1	+15.44	-	-
C	0.00	^{42}Ca	^{46}Ca
L1	-13.12	-	-
L2	-32.49	^{41}K	-
L3	-59.50	-	^{44}Ca
L4	-69.25	^{40}Ca	-

The sample filament was heated automatically to 260 mA at a rate of 15 mA per minute, and simultaneously the ionization filament was brought to 2650 mA with a rate of 150 mA per minute, corresponding to an ionization temperature of about 1300 °C. The beam valve was opened and the ^{40}Ca peak focused and centered. A manual stepwise heating of the ionization filament continued until reaching a target beam intensity for ^{40}Ca of about 100 pA (10 000 mV), which corresponded to the ionization filament current of about 2900 mA and temperature 1400 °C.

Prior to data collection, the vacuum in the ion source and analyzer was below 1.5 x 10^{-7} and 3 x 10^{-9} mbar, respectively. Defocused baseline measurements collected for 30 seconds were carried out at the beginning of measurement and also before each block. Checks of the baselines and peaks showed that there were no reflected ions or electrons perturbing measurements, especially during the second step when the large ^{40}Ca signal does not fall into a cup. During the initial stages of the project the individual Ca isotope measurement consisted of 100 cycles (10 blocks of 10 cycles each), but later it was extended to 108 cycles (9 blocks of 12 cycles each) in order to apply the *Virtal amplifier* rotation correction. Each cycle consisted of a 16-second integration time, followed by a 3-second waiting time. A total analytical time for an individual measurement was approximately 120 minutes, including the 25-minute heating routine.

A.5.1.7 Automated Ca isotope analysis

A fully automated analytical protocol for the calcium isotope measurement was developed in the later stages of the thesis project. Samples loaded in the mass spectrometer were heated to an ionization temperature of about 1400 °C using an automatic sequence with a build in program for the sample heating (Table A.5.6). The target ion beam intensity for ^{40}Ca signal was 130 pA (13000 mV), which was usually reached within ~30 min. The sample heating sequence was followed by an automated data acquisition routine. The Ca isotope peaks (masses 40 to 48) were measured in two steps (Fig. A.5.4 and Table A.5.5). An individual Ca isotope measurement consisted of 108 cycles (9 blocks of 12 cycles each). Defocused baselines measurements were collected for 30 s at the beginning of each block. A total analytical time of this fully automated Ca isotope technique was ~150 min per sample (30 min for sample heating plus 120 min for data acquisition).

Table A.5.6.

Automatic sequence for the sample heating and data acquisition designed for the Thermo Electron Triton mass spectrometer

Line	Time (min:sec)	Valve	Filament [a]	Function	Target (°C, mV)	Slope (mA/min)	Action
1	00:00	Closed	Ionization	Filament Temp.	1200 °C	260	None
2	10:00	Open	Ionization	Ion Current (^{40}Ca)	5 mV	120	Auto Focus
3	16:35	Open	Ionization	Ion Current (^{40}Ca)	100 mV	100	Auto Focus
4	19:00	Open	Ionization	Ion Current (^{40}Ca)	1000 mV	80	None
5	20:00	Open	Evaporation	Ion Current (^{40}Ca)	2000 mV	40	None
6	21:00	Open	Evaporation	Ion Current (^{40}Ca)	4000 mV	25	Auto Focus
7	23:40	Open	Evaporation	Ion Current (^{40}Ca)	8000 mV	20	None
8	24:40	Open	Evaporation	Ion Current (^{40}Ca)	13000 mV	20	Auto Focus
9	27:10	Open	Evaporation	Ion Current (^{40}Ca)	13000 mV	40	Auto Focus
10	29:50	Open	Evaporation	Ion Current (^{40}Ca)	13000 mV	40	None
11	30:50		End				Data Acquisition

[a] Evaporation filament represents a 'sample' filament.

A.5.1.8 Long term reproducibility of Ca isotope measurements

A long-term reproducibility of the Ca isotope measurements was evaluated by a repeat analysis of the NIST SRM 915a $CaCO_3$ standard over a period of one year (from December 2005 to December 2006). A total of 30 measurements of the NIST SRM 915a standard were carried out and the results are presented in Table A.5.7. The measured $^{44}Ca/^{40}Ca$ ratios showed a long-term mean of 0.021538 ± 0.000003 (2σ, n = 30), which was also used for normalization of the $\delta^{44/40}Ca$ values. The $\delta^{44/40}Ca$ values of the NIST SRM 915a varied between –0.10 and +0.17 ‰ with the average of 0.01 ± 0.13 ‰. The given statistical uncertainty represents two standard deviations (2σ) of all measured $\delta^{44/40}Ca$ values.

Table A.5.7.

Database of $\delta^{44/40}Ca$ values of the NIST SRM 915a $CaCO_3$ standard as measured over a period of one year (from December 2005 to December 2006). The long-term external reproducibility is expressed as two standard deviations (2σ) calculated from 30 individual measurements from the same solution.

Analysis No.	Date	$^{40}Ca/^{44}Ca$	$^{44}Ca/^{40}Ca$	$\delta^{44/40}Ca_{NIST}$ (‰)
1	December, 2005	46.426223	0.0215396	0.08
2	December, 2005	46.431662	0.0215370	-0.04
3	December, 2005	46.426560	0.0215394	0.07
4	January, 2006	46.431628	0.0215370	-0.04
5	January, 2006	46.433839	0.0215360	-0.08
6	February, 2006	46.429234	0.0215382	0.02
7	February, 2006	46.427201	0.0215391	0.06
8	February, 2006	46.434521	0.0215357	-0.10
9	February, 2006	46.431669	0.0215370	-0.04
10	May, 2006	46.428534	0.0215385	0.03
11	May, 2006	46.429760	0.0215379	0.01
12	June, 2006	46.422170	0.0215414	0.17
13	June, 2006	46.432658	0.0215366	-0.06
14	June, 2006	46.427650	0.0215389	0.05
15	June, 2006	46.428090	0.0215387	0.04
16	June, 2006	46.427650	0.0215389	0.05
17	June, 2006	46.428618	0.0215384	0.03
18	June, 2006	46.431248	0.0215372	-0.03
19	July, 2006	46.426567	0.0215394	0.07
20	July, 2006	46.432827	0.0215365	-0.06
21	July, 2006	46.432320	0.0215367	-0.05
22	July, 2006	46.425442	0.0215399	0.10
23	July, 2006	46.430810	0.0215374	-0.02
24	August, 2006	46.426539	0.0215394	0.07
25	August, 2006	46.425393	0.0215399	0.10
26	August, 2006	46.432159	0.0215368	-0.05
27	August, 2006	46.431945	0.0215369	-0.04
28	August, 2006	46.429249	0.0215381	0.02
29	August, 2006	46.431426	0.0215371	-0.03
30	December, 2006	46.429345	0.0215381	0.01
	Mean value	**46.429431**	**0.0215381**	**0.01**
	2σ	0.005851	0.0000027	0.13

A.5.2 Methodology for B isotope analysis

A.5.2.1 Sample dissolution

Sample preparation and clean chemistry protocols for the B isotope analysis used in this study were adopted with slight modifications from Hemming and Hanson (1994).

Approximately 5 to 10 mg of carbonate powder washed in H_2O and H_2O_2 were weighed into PFA vial and dissolved with an excess (~150 μL) of 2N HCl. Sample solutions were evaporated at temperatures strictly below 70°C to avoid potential isotope fractionation due to the volatilization of B as BCl_3 (Klötzli, 1992; Ishikawa and Nakamura, 1990). Sample size permitting, two aliquots from each sample were prepared, one for the analysis of natural B isotope composition and the other for the determination of B concentrations by isotope dilution technique.

A.5.2.2 Total procedural B blank

The isotope dilution technique was also used for the determination of B yields and blanks. A spike material IRMM-610 (Table A.5.8) enriched in ^{10}B was used as a tracer for the isotope dilution. The recovery yields of B, tested on a sample size of ~20 ng, were close to 100% (~99.85±0.5%), documenting no loss of B and therefore no isotope fractionation during the sample preparation. Total procedural B blanks were consistently below 50 pg and thus negligible, as the amount of B from a sample was in the range of 5 to 10 ng.

Table A.5.8.

Certified and measured B isotope composition of the IRMM-610 spike material (H_3BO_3 solution), as determined by a repeat analysis of the same spike solution.

IRMM-610 spike	Measured (n = 4), (mean, 2σ)	Certified (mean, 2σ)
$^{10}B/^{11}B$ (^{17}O corrected)	18.916 ± 0.040	18.802 ± 0.020

A.5.2.3 Mass spectrometry N-TIMS

Boron isotope compositions of standards (SRM 951 and IAPSO seawater) and skeletal carbonates (belemnites and coral) were determined on a multi-collector thermal ionization mass spectrometer Thermo Electron Triton operated in a negative ionization mode (N-TIMS), adopting the method of Hemming and Hanson (1994).

For the SRM 951 standard, approximately 10 ng of B were mixed with 0.5 µL of B-free seawater that acted as an ionization promoter. The B-free seawater was prepared by cleaning the IAPSO seawater with the B-specific resin Amberlite® IRA-743, using a batch technique. For carbonate samples no ionization promoter was needed and therefore these solutions were loaded directly onto outgassed zone-refined Re single filament. Solutions, containing ~3 ng of B, were slowly over ~5 min evaporated to dryness at 0.5 A, and then heated for 30 seconds at 1.2 A (Kasemann et al., 2005). The exposure of filaments loaded with the samples ($CaCl_2$) to laboratory air was minimized as $CaCl_2$ is highly hygroscopic and adsorbs moisture from the air causing potential B contamination (Foster et al., 2006). The sample wheel was, therefore, immediately introduced into the mass spectrometer and the air in the ion source housing pumped down.

The B isotope analyses were performed on a multi-collector thermal ionization mass spectrometer Thermo Electron Triton. The instrument was operated in a negative ionization mode (N-TIMS), and B isotopes were measured as $^{10}BO_2^-$ and $^{11}BO_2^-$ ions corresponding to masses 42 and 43, respectively. The measured isotope ratio, 43/42, was corrected for the contribution of ^{17}O on the mass 43 using the following relation:

$$43/42_{corrected} = 43/42_{measured} - 0.00076$$

where $43/42_{corrected}$ represents the ratio of interest $^{11}B/^{10}B$. The setup of the Faraday cups for the B isotope analysis is presented in Fig. A.5.5 and Table A.5.9. Masses 43 and 42 were registered in one sequence using cups L1 and L2, respectively.

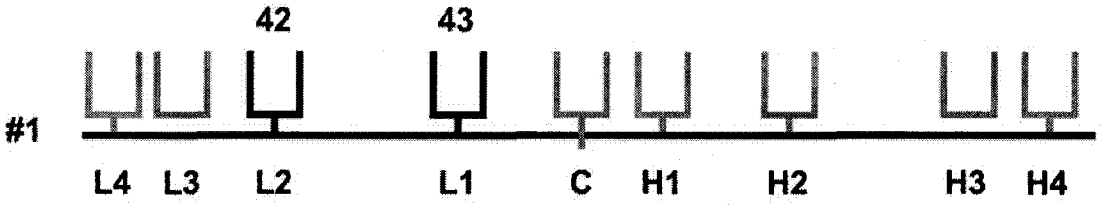

Fig. A.5.5. The configuration of Faraday cups used for the B isotope analysis. Masses 42 and 43, representing negatively charged $^{10}BO_2$ and $^{11}BO_2$ ion peaks, were collected in a single sequence (#1).

Table A.5.9.

The position of the cups for the B isotope analysis

Cup	Target position (in mm) Distance from the central (C) cup	Isotope peak (mass) Sequence (#1)
H4	+55.73	-
H3	+45.31	-
H2	+36.23	-
H1	+26.48	-
C	0.00	-
L1	-26.45	$^{11}BO_2$ (43)
L2	-56.50	$^{10}BO_2$ (42)
L3	-65.43	-
L4	-85.37	-

The operating vacuum in the ion source and analyzer was below 1.5 x 10^{-7} and 2 x 10^{-9} mbar, respectively. The sample filament was gradually, within 25 minutes, brought to an operating temperature of 975 ± 20 °C. In the first step the filament current was raised to 1000 mA at a rate of 100 mA per minute, followed by a stepwise increase of 15 mA per minute until reaching the operating temperature. Ion beam intensities for $^{11}BO_2^-$ peak were typically from about 1 to 10 pA. The data acquisition for a single run comprised 10 blocks of 10 cycles with a 16-second integration time and 3-second waiting time. Defocused baselines were collected for 30 seconds at the beginning of each block. A total analytical time for a single measurement was about 55 minutes, 25 minutes for filament heating and 30 minutes for data acquisition. Acceptable runs showed relative in-run fractionation for the

$^{11}B/^{10}B$ ratio of less than 0.6‰. Most of the samples (approx. two-thirds) were analyzed in duplicate, using the same sample solution, to eliminate the effect of in-run fractionation and other analytical artifacts, such as inconsistent heating routine and/or minor isobaric interferences.

Before data acquisition, possible isobaric interferences from organic matter on mass 42 ($^{12}C^{14}N^{16}O$) were evaluated by monitoring mass 26 ($^{12}C^{14}N$). If isobaric interferences on mass 26 were detected, runs were discarded. Typically, the intensity of the $^{12}C^{14}N$ peak was decreased below the detection limit of < 1 mV (for Faraday cups) after a sample was several times ultrasonically cleaned in H_2O_2.

A.5.2.4 Long term reproducibility of B isotope measurements

The long-term, over a period of four months, reproducibility of boron isotope measurements was evaluated based on repeat analysis of SRM 951 standard and additional in-house standards, the IAPSO seawater, modern coral *Acropora palmate* and brachiopod (*Terebratalia* sp.). The boron isotope composition of natural samples is expressed as a delta notation ($\delta^{11}B$) in parts per thousand (‰) relative to the SRM 951 boric acid standard:

$$\delta^{11}B_{SRM} = \left(\frac{^{11}B/^{10}B_{SAMPLE}}{^{11}B/^{10}B_{SRM}} - 1 \right) \cdot 1000$$

where the $^{11}B/^{10}B_{SRM}$ normalization ratio is equal to 4.0100 ± 0.0069 (2σ, n = 10). The mean $\delta^{11}B$ values of the SRM 951, IAPSO, modern coral and brachiopod yielded 0.00 ± 1.73, 39.21 ± 0.69 and 23.99 ± 1.44 and 14.85 ± 1.23 ‰, respectively (Table A.5.10). The given analytical uncertainties represent two standard deviations (2σ).

Table A.5.10.

External reproducibility of boron isotope measurements, $^{11}B/^{10}B$ and $\delta^{11}B$, as determined by repeat analyses of SRM 951, IAPSO seawater and modern skeletal carbonates, over a period of four months

No.	SRM 951 (Isotope standard) $^{11}B/^{10}B$	Seawater (IAPSO) $^{11}B/^{10}B$	Coral *(Acropora* sp.*)* $^{11}B/^{10}B$	Brachiopod *(Terebratalia* sp.*)* $^{11}B/^{10}B$
1	4.0074	4.1680	4.1090	4.0686
2	4.0037	4.1673	4.1109	4.0687
3	4.0119	4.1673	4.1069	4.0693
4	4.0115	4.1702	4.1073	4.0733
5	4.0101	4.1671	4.1019	4.0687
6	4.0141	4.1665	4.1070	4.0649
7	4.0121	4.1676	4.1036	4.0702
8	4.0136	4.1660	4.1044	4.0722
9	4.0054	4.1661	4.1025	4.0714
10	4.0092	4.1651	4.1073	4.0672
Mean value	**4.0099**	**4.1671**	**4.1061**	**4.0695**
2σ	0.0069	0.0027	0.0058	0.0049
	$\delta^{11}B$ (SRM 951)	$\delta^{11}B$ (SRM 951)	$\delta^{11}B$ (SRM 951)	$\delta^{11}B$ (SRM 951)
Mean (‰)	**0.00**	**39.21**	**23.99**	**14.85**
2σ	1.73	0.69	1.44	1.23

References

Hippler D., Villa I., Nägler Th.F. and Kramers J. (2004) A ghost haunts mass spectrometry: Real isotope fractionation or analytical paradox? *Geochim. Cosmochim. Acta* **68/11** (Suppl. 1), A215.

Hemming N.G. and Hanson G.N. (1992) Boron isotopic composition and concentration in modern marine carbonates. *Geochim. Cosmochim. Acta* **56**, 537–543.

Hemming N.G. and Hanson G.N. (1994) A procedure for the isotopic analysis of boron by negative thermal ionization mass spectrometry. *Chem. Geol.* **114** 147–156.

Tuttas D. and Schwieters J., Advances in high precision isotope ratio measurements of calcium using TIMS, Triton – Thermo Electron Application Flash Report No. T4. 2002.

Klötzli U.S. (1992) Negative thermal ionization mass spectrometry: a new approach to boron isotope geochemistry, *Chem. Geol.* **101,** 111–122.

Ishikawa T. and Nakamura E. (1990) Suppression of Boron Volatilization from a Hydrofluoric Acid Solution Using a Boron-Mannitol Complex, *Anal. Chem.* **62**, 2612–2616.

Kasemann S.A., Hawkesworth Ch.J., Pravec A.R., Fallick A.E. and Pearson P.N. (2005) Boron and calcium isotope composition in Neoproterozoic carbonate rocks from Namibia: evidence for extreme environmental change, *Earth Planet. Sci. Lett.* **231**, 73–86.

Foster G.L., Yunyan N., Haley B. and Elliott T. (2006) Accurate and precise isotopic measurement of sub-nanogram sized samples of foraminifera hosted boron by total evaporation NTIMS, *Chem. Geol.* **230,** 161–174.

Russell W.A., Papanastassiou D.A. and Tomberllo T.A. (1978) Ca isotope fractionation on the Earth and other solar system materials. *Geochim. Cosmochim. Acta* **42**, 1075–1090.